

https://dspace.org/

Physico-chemical characterisation of a one hundred thousand year old ochre processing toolkit from Blombos Cave, South Africa

Mphuthi, Dikeledi Salamina

2016

http://hdl.handle.net/10539/21690

Mphuthi, Dikeledi Salamina (2016) Physico-chemical characterisation of a one hundred thousand year old ochre processing toolkit from Blombos Cave, South Africa, University of Witwatersrand, Johannesburg, <http://wiredspace.wits.ac.za/handle/10539/21690>

Downloaded from a DSpace repository. https://dspace.org/

Physico-chemical characterisation of a one hundred thousand year old ochre processing toolkit from Blombos Cave, South Africa



A Masters Dissertation submitted to the faculty of Science, University of the Witwatersrand in fulfillment of the requirements for the Masters` degree

DIKELEDI S. MPHUTHI

Johannesburg 2016

DECLARATION

I declare that this research is my own, unaided work. It is being submitted for the Degree of Master of Science at the University of the Witwatersrand, Johannesburg. It has not been submitted before for any degree or examination at any other University.



……

(Signature of Candidate)

…22nd ……..Day of.....July 2016.....

Supervisors:

Prof Ewa Cukrowska (WITS University, School of Chemistry)

Prof Christopher Henshilwood (WITS University, Evolutionary Studies Institute; University of Bergen, Institute for Archaeology, History, Culture and Religion)

Co-supervisor:

Luke Chimuka (WITS University, School of Chemistry)

ABSTRACT

The Middle Stone Age (MSA) levels (c. 100 – 72 ka) (thousand years) at Blombos Cave, South Africa, contain buried remnants of human existence and their activities (these include ochre-stained shell beads, processed ochre pieces, bone tools, stone tools, and ochre processing toolkits). A preliminary study on the occupation layers at Blombos Cave was done in order to chemically and physically characterise the sediment deposits. The interpretation of the information preserved in these sediments, as a result of human activities, was achieved by using the following characterisation techniques: FT-IR, ICP-OES/MS, CHNS analysis as well as pH and EC measurements.

Fluctuations in the bio-essential trace elements (K, P, Mg, Ca, S, Fe, Al, Cr, Na, Cu and C) and in the markers of *in situ* burning (P, K, C, Ca and Mg) through the MSA levels suggested a non-contiunous anthropogenic occupation of the cave. Further, the dark coloured layers were indicative of periods when heavy human activities, such as fire use, were encoutered. These layers were characterised by high levels of P, K, C, Ca and Mg, also elevated pH and EC levels were observed. The calcite origin for these sediment deposits was confirmed to be pyrogenic. The layers found to contain large bone, ochre and shell densities (with no evidence of fire use) had high levels of Fe, P high Ca and low EC. The calcite origin for these sediment deposits was geogenic. Biogenic calcite was only observed in the more recent CA and CC layers.

Substantial amounts of ochre assemblages were recovered from the MSA levels at Blombos Cave. Among these was an ochre processing toolkit recovered from the CP layer (c.100 ka). Ochre is abundant in African archaeological sites after 165 ka and is likely to have played a symbolic role in the lives of prehistoric people. It contains an iron-oxide mineral as well as accessory minerals. When mixed with a binder (such as fat or water) ochre can be used as a pigment. A large number of fragmented bone remains were found in the M1 and M2 levels. It is suggested that the majority of the fragmentation occurred while the bones were in a fresh state; implying marrow extraction by the site occupants. The exploitation of bone

marrow was crucial in order to extract the fat and use it as a binder during the pigment production. Some of the broken and marrow-extracted bones were heated and used as fuel during seasons when wood was scarce while the other bones were deliberately engraved for symbolic intent.

The characterisation of the ochre processing toolkit was achieved by mineralogical analysis and elemental fingerprinting. FT-IR analysis revealed that the general matrix of the ochre samples comprised of hematite (Fe_2O_3) or goethite (α-FeO(OH)) as the main chromophores and clay minerals (such as kaolinite ($Al_2Si_2O_5(OH)_4$), muscovite [$(KF)_2(Al_2O_3)_3(SiO_2)_6(H_2O)$] and illite [$K(Al_4Si_2O_9(OH)_3)$]), calcite ($CaCO_3$) and quartz ($SiO_2$) as the main accessory minerals. PXRD analysis confirmed Fe_2O_3, $Al_2Si_2O_5$ $(OH)_4$, [$K(Al_4Si_2O_9(OH)_3)$] and SiO_2 to be the predominant mineral phases in the ochre, implying this specific type of ochre was preferred during the production of the pigment. Fe_2O_3 contributed the red hue and the aluminosilicates their clayey properties making them good extenders of the pigment.

Multivariate statistics and Fe ratios made it possible to identify elements important for differentiating the ochre recovered from the CP layer. Analysis of variance (ANOVA one-way) showed a statistically significant difference between the ochre residues in terms of trace elemental profiling. The variance suggested different geological origins for the ochre.
FT-IR was used as a screening technique for any organic residues associated with the toolkit and GC-MS was used to identify the preserved organic residues. These were mostly lipids and terpenes. The identified bio-molecular markers; stearic acid and dehydroabietic acid were exploited to give insight on the origin of the residues. Stearic acid suggested the use of animal fat while dehydroabietic acid implied the use of a resin (potentially as a binder in the pigment).

The characterisation investigations revealed that the prehistoric populations at Blombos Cave specifically sourced hematite and aluminosilicate- containing ochre pigments in order to fulfil their social and cultural demands. The MSA site

occupants' chemical understanding of these materials suggested they were technologically advanced.

Keywords: Blombos Cave, MSA levels, ochre, mineralogical analysis and elemental fingerprinting.

DEDICATION

To my loving parents, Mr and Mrs Mphuthi, thank you for always believing in me.

ACKNOWLEDGEMENTS

I would like to express my sincere gratitude to Prof Ewa Cukrowska, Prof Christopher Henshilwood, and Prof Luke Chimuka for having given me the opportunity to work under their supervision. Their complete support and guidance has led to the successful completion of my research as well as their constructive criticism and comments on the various drafts of the dissertation.

I would like to thank Dr Karen van Niekerk for providing me with the samples that made it possible to carry out this interesting research.

I would also like to express my sincere appreciation to the late Dr Stanley Moyo for his mentorship and advice throughout my research and for his assistance with the use of most instruments especially ED- XRF and FT-IR.

I would like to thank all the members of the Environmental Analytical Chemistry Research group who helped me cope with all the challenges I have come across through my studies, they made my work in the lab pleasurable through their limitless help and support.

In particular, I would like to thank Lehlononolo Serithi for his constant support, encouragement and patience.

I would also like to thank my friend, Ontibile Molefe, who kept me going even when times were tough.

Some analysis would have not been possible if it was not for Prof D. Billing would allowing us access to use PXRD instrument in his lab and Mr Hlengi Nyoni at University of Johannesburg for GC-MS analysis.

My studies would have not been possible if it was not for the National Research Foundation (NRF) for providing the entire funding for my studies and living expenses.

To the one who made it all possible, my Lord and King, Christ Jesus, who is the author and perfector of my faith. Without whom none of this would have been possible. Thank you.

CONTENTS PAGE

DECLARATION i

ABSTRACT ii

DEDICATION v

ACKNOWLEDGEMENTS vi

CONTENTS PAGE vii

LIST OF FIGURES xi

LIST OF TABLES xvi

ABBREVIATIONS AND ACRONYMS xviii

CHAPTER ONE 1

Introduction 1

1.1 Background on the southern African Middle Stone Age 2

1.2 Blombos Cave stratigraphy and ages of the deposits 4

1.2.1 The ochre processing workshop in the M3 phase 7

1.3 Description of the research problem investigated 7

1.4 Motivations 8

CHAPTER TWO 9

Literature review 9

2.1 Blombos Cave and its link to complex cognition in the Middle Stone Age 10

2.1.1 Bifacially worked stone points 10

2.1.2 Bone tools 12

2.1.3 Perforated Nassarius kraussianus shells 13

2.2 Subsistence at MSA sites 15

2.3 Evidence of fire use at MSA sites 16

2.4 Microarchaeological analysis: identifying and interpreting prehistoric combustion features in sediments 18

2.4.1 Micromorphology 18
2.4.2 Micro- Fourier Transform Infrared Spectroscopy 18
2.5 Multi-elemental characterisation of anthropogenic sediments 21
2.6 Ochre and its application at MSA sites 23
2.6.1 Grindstone and hammerstone tools associated with ochre processing 25
2.6.2 Ethnographically recorded uses of ochre 27
2.7 Characterisation, differentiation and provenance of ochre 29
2.7.1Elemental fingerprinting 29
2.7.2 Mineralogical composition analysis 32
2.8 Organic residue analysis in archaeology 34
2.8.1 Gas chromatography coupled to a mass spectrometer 34
CHAPTER THREE 36
Research objectives 36
3.1 General aim 37
3.2 Specific aims 37
3.3 Key questions 38
3.4 Hypothesis 38
CHAPTER FOUR 39
Sampling methods 39
4.1 Site description 40
4.2 Excavation strategies 41
4.2.1 Excavation coordinate system 41
4.2.2. Excavation and recording of depositional features, artifacts and deposit surfaces 43
4.3 Recovery of the ochre processing toolkit and the associated artifacts 43
4.4 Description of the sediment samples 45
CHAPTER FIVE 47
Materials and Methods 47

5.1 Equipment 48
5.1.1 pH and electrical conductivity measurements 48
5.1.2 Analytical balances 48
5.2 Sample preparation methods 49
5.2.1 Microwave assisted digestion 49
5.2.2 Sample preparation for organic analysis 51
5.3 Instrumental techniques used for characterisation 53
5.3.1 Inductively coupled plasma-optical emission spectrometer (ICP-OES) 53
5.3.2 Inductively coupled plasma-mass spectrometer (ICP-MS) 56
5.3.3 X-Ray Fluorescence (XRF) spectrometry 57
5.3.4 Carbon, hydrogen, nitrogen and sulphur micro analyser (CHNS) 61
5.3.5 Fourier Transform Infrared Spectroscopy (FT-IR) 61
5.3.6 Powder X-ray diffraction 64
5.3.7 Gas chromatography- Mass Spectrometry (GC-MS) 66
5.4 Chemicals 68
5.4.1 Solution preparation for digestion 68
5.4.2 Solutions and procedures for ultrasonic assisted extraction 69
5.5 Quality assurance 70
5.5.1 Analytical figures of merit 71
5.6 Statistical data analysis 71
5.6.1 Multivariate statistics 71
CHAPTER SIX 75
Results and discussion 75
6.1 Physico-chemical characterisation of Blombos Cave sediments profile: A preliminary study 76
6.1.1 Soil pH and electrical conductivity measurements of the sediments 76
6.1.2 Identification of human occupation and activity areas by CHNS analysis 80

6.1.3 Identification of human occupation and activity areas by multi-element characterisation 81
6.1.4 Differentiating between calcite origins using FT-IR spectroscopic analysis ... 91
6.1.5 Conclusion 93
6.2 Physico-chemical characterisation of a 100 ka ochre processing toolkit 93
6.2.1 Geochemical characterisation, differentiation and provenance of ochre 94
6.3 Organic residue analysis 116
6.3.1 FT-IR as a screening technique for organic residue identification 116
6.3.2 GC-MS in organic residue analysis 119
CHAPTER SEVEN 124
Overall conclusion and future research 124
7.1 Overall conclusion 125
7.2 Future research 126
List of conferences, seminar presentations and publications 127
REFERENCES 128
APPENDIX 158
Appendix A- Sample preparation 158
Appendix B Analytical figures of merit for ICP-OES data 162
Appendix C 1 FT-IR analysis of sediments 163
Appendix C2 Grinding curve 185
Appendix D FT-IR analysis of ochre 186
Appendix E ED-XRF results 201
Appendix F GC-MS in organic residue analysis 207

LIST OF FIGURES

Chapter 1 Introduction

Figure 1.1 (a) Interior, (b) exterior view of Blombos Cave, Southern Cape (Henshilwood, 2012) (Image: Magnus Haaland)……4

Figure 1.2 South section of Blombos Cave showing layers, phases, and ages. The ochre-processing toolkit came from layer CP in the M3 phase and is shown *in situ*. (Henshilwood *et al.*, 2011)**……..**5

Chapter 2 Literature review

Figure 2.1 Still Bay bifacial points (Henshilwood *et al.*, 2001b; Villa *et al.*, 2009)……..11

Figure 2.2 (a) Bone point from the MSA levels at Peers Cave (d'Errico and Henshilwood 2007); (b–g) bone tools from the Still Bay levels at Blombos Cave; (b–e) bone awls; (f–g) bone points; (h–i) engraved lines on tools c and Henshilwood *et al.*, 2001a; d'Errico and Henshilwood 2007); (j) engraved bone fragment (d'Errico *et al.*, 2001)…….12

Figure 2.3 Perforated N. kraussianus from the MSA phases M1 and M2 at Blombos Cave (Vanhaeren *et al.*, 2013)……14

Figure 2.4 (a) Knotting with floating shells, (b) continuous stringing with the same orientation of N. kraussianus, (c) knotting with floating pairs of dorsally joining shells, (d) braiding with two strings, (e) knotting with floating pairs of ventrally joining shells, (f, g) continuous stringing with alternate orientation of N. kraussianus (Vanhaeren *et al.*, 2013)…….15

Figure 2.5 (a) μ- FT-IR spectra for geogenic calcite (chalky limestone) illustrate that peak sharpening occurs with grinding, leaving peak positions unchanged. A single specimen was ground and re-pressed. With grinding, the ν3 peak sharpens more than ν2, which sharpens more than ν4. Peak areas also increase slightly with grinding. (b) Peak intensity ratios (defined as ν4 /ν2) and FWHM ratios (defined as ν 2 / ν4). The trend with increased grinding is denoted with an arrow (Poduska et al., 2011……..21

Figure 2.6 Ochre samples exhibiting a variety of colours (Rifkin, 2012)……24

Figure 2.7 The extraction of the ochre powder from different mineral sources: a) grinding a hard haematite nodule b) grinding a soft yellow limonite fragment; c) grinding a soft water-worn grey shale chunk; d) extracting ochre powder from a red ochre chunk (Rifkin, 2012)…….26

Figure 2.8 Close-up view of the engraved pattern on the ochre piece (Henshilwood *et al.*, 2009 a, b).....27

Chapter 4 Sampling methods

Figure 4.1 Geographic location of Blombos Cave on the southern Cape coast of South Africa (Image by: Magnus Haaland)……...40

Figure 4.2 Blombos Cave site map (Image adapted from: Haaland, 2012)…….42

Figure 4.3 Blombos Cave excavation grid system: (a) Square meter grid, (b) Quadrate coordinate system (Image adapted from: Haaland, 2012)…….42

Figure 4.4 (a) ochre-processing container (abalone shell) shown *in situ* and (b) thin orange CPA layer (yellow arrow) with sandy CP layer above (Henshilwood *et al.*, 2011) (Image by: Henshilwood and Moéll Pedersen)…….44

Figure 4.5 Red pigment exposed after removal of quartzite cobble from shell (Henshilwood *et al.*, 2011)(Image by: Henshilwood and Moéll Pedersen)……...44

Figure 4.6 *In situ* CP layer toolkit (Image by: Magnus Haaland)…….45

Chapter 5 Methods and materials

Figure 5.1 (a) Schematic of the MAE system and the vessel design (b) Anton Paar Multiwave 3000 microwave sample preparation system (Image (a) adapted from: Anton Paar, 2009)…….51

Figure 5.2 Indirect sonication system (a) closed and (b) open showing water bath……53

Figure 5.3 Schematic diagram showing the major components of the ICP-OES and the general set up of the system (Image adapted from: Arcinus, 2000)…….54

Figure 5.4 Schematic of a quadrupole ICP-MS (Image adapted from Makiese, 2012)……..57

Figure 5.5 XRF principle and energy diagram (Image adapted from: Settle, 1997)……..58
Figure 5.6 Schematic diagrams of WD XRF and ED XRF instruments. (a) WD XRF relies on diffraction crystals to separate the X-rays from the sample; (b) ED XRF has a solid state SiLi detector that converts X-ray photons into pulses that are processed electronically (Image adapted from Settle, 1997)……...59
Figure 5.7 Handheld Bruker Handheld Tracer lll SD ED XRF instrument showing the system set-up……60
Figure 5.8 Vibrational modes of a nonlinear triatomic molecule. Arrows indicate motion in the plane of the paper, + is towards and – away from the observer. (a) symmetric stretching, (b) asymmetric stretching, (c) out-of-plane wagging, (d) out-of-plane twisting, (e) in-plane scissoring, (f) in-plane rocking. (Image adapted from Pollard *et al.*, 2006)……...63
Figure 5.9 FT-IR spectrometer layout (Image adapted from: Introduction to spectroscopy 4th ed. by Pavia, Lampman, Kriz and Vyvyan)……...63
Figure 5.10 Illustration of Bragg's law……65
Figure 5.11 Schematic of gas chromatograph (left) (Image adapted from: Settle 1997); GC system interfaced with an MS detector (right) (University of Johannesburg)……67

Chapter 6 Results and discussion

Figure 6.1 pH and EC measurements for the sediment profile……77
Figure 6.2 EC ranges for typical sediment matrices (Image adapted from: College of agriculture and life sciences, Virginia state university)……79
Figure 6.3 Carbon content for the occupation layers of the M2 and M3 phases..81
Figure 6.4 Variations in major, minor and trace elemental content down the profile depth at Blombos Cave……..85
Figure 6.5 Variations in trace elemental content down the profile depth at Blombos Cave……86
Figure 6.6 Transmission IR spectrum showing hematite (green) embedded in the accessory minerals, quartz (purple) and illite (blue). Representative sample is BBC CP H6c L20 514 (red)……..96

Figure 6.7 Transmission IR spectrum showing hematite (red) embedded in the accessory minerals, quartz (light blue), kaolinite (purple) and illite (dark blue) Representative sample is BBC CPA G6d ochre fragments (green)……...97
Figure 6.8 Transmission IR spectrum showing goethite (orange) embedded in the accessory minerals, quartz (black), kaolinite (dark blue), illite (light blue) Representative sample is BBC CP H6c L1 416 (red)……98
Figure 6.9 Diffraction pattern for the group one ochre sample CP H6c L20 514 (K: kaolinite; H: hematite; C: calcite; G: goethite; Q: quartz; I: illite)……..99
Figure 6.10 Diffraction pattern for the group two ochre sample CPA G6d ochre fragments. (K: kaolinite; Q: quartz; I: illite, H: hematite)……...100
Figure 6.11 Diffraction pattern for the group three ochre sample BBC CP H6c L1 416. (K: kaolinite; Q: quartz; I: Illite; G: goethite)……100
Figure 6.12 Dendogram showing the clustering of related ochre samples from the CP layer……107
Figure 6.13 Scree plot of the variance % for the trace elemental data…… 110
Figure 6.14 PC bi-plot showing principle component 2 vs principle component 3 for the trace elemental data set…….111
Figure 6.15 Transmission IR spectra show a) minerals; calcite (blue) and quartz (red) with representative sample CP H6c Mastic O1 442 S1 (yellow)**,** b) minerals; calcite (green) and quartz (red) with representative sample CP H6c L24 520 (purple)…….116

Appendix

Figures C1-C43 FT-IR spectra for the sediments from Blombos Cave**.....**161-182
Figure C44 Grinding curve example of a calcite……183
Figures D1-D13 FT-IR spectra for the ochre from the CP layer ……184-189
Figure D14 FT-IR frequency chart…….190
Figures D15-23 PXRD diffraction patterns for CP layer ochre**.....**193-197
Figure E1 BBC CP H6C L1 416 ED-XRF spectrogram…….198
Figure E2 BBC CP G6D O1 476 ED-XRF spectrogram……**...**198
Figure E3 BBC CP H6C L16 453 ED-XRF spectrogram……...199
Figure E4 BBC CP H6C L30 529 ED-XRF spectrogram……...199

Figure E5 BBC CP H6C OCHRE FLAKE ED-XRF spectrogram…….200
Figure E6 BBC CP H6C L35 534 ED-XRF spectrogram……...200
Figure E7 BBC CP H6C 506 ED-XRF spectrogram……..201
Figure F1 TIC chromatogram for CP H6c L24 520……...208
Figure F2 TIC chromatogram for CP H6c mastic O1 441 S1……209

LIST OF TABLES

Chapter 4 Sampling methods

Table 4.1 List of BBC sediments analysed during the study…….....46

Chapter 5 Materials and methods

Table 5.1 Microwave assisted digestion power programme…….....51

Table 5.2 Operating conditions for the ICP-OES…….55

Table 5.3 Operating conditions for GC-MS……..68

Table 5.4 Frequently used solutions for complete dissolution of the matrices….69

Table 5.5 Extraction conditions for GC-MS analysis……...70

Chapter 6 Results and discussion

Table 6.1 Bio-essential elements considered in the interpretation of human activities at Blombos Cave…….82

Table 6.2 Percentage distribution of ochre raw material categories by frequency and mass across the MSA phases at Blombos Cave……..86

Table 6.3 Classification of the sediments according to calcite origin and the distribution of major elements in the sediments……90

Table 6.4 FT-IR and PXRD mineralogical characterisation of the material associated with the ochre processing toolkit……..93

Table 6.5 Classification of the ochre according to their chromophores and accessory minerals…….95

Table 6.6 ICP-OES elemental data for the ochre samples from the CP layer (presented as mean ± SD $x10^3$ mg kg^{-1})…….103

Table 6.7 Major and trace elements identified using ED-XRF…….....104

Table 6.8 Concentrations of the major and trace elements detected by ED-XRF in ochre from the CP layer (values in mg kg^{-1})……...105

Table 6.9 Pearson's correlation matrix showing the coefficient values (r) for the major and trace elements……..109

Table 6.10 ANOVA results for trace elemental data for the CP layer ochre…..112

Table 6.11 Samples selected by FT-IR for organic residue analysis and the commonly preserved organic residues…….115
Table 6.12 Classification of organic residues identified by GC-MS……..118
Appendix
Table A1 Actual weights of sediment samples……156-157
Table A2 Actual weights of ochre samples…….157
Table A3 Toolkit pieces, spatial references and descriptions……..158-159
Table B1 Limit of detection values for ochre from CP layer……..160
Table D1 IR correlation chart for inorganic minerals……...190-192
Table E1 Fe-normalized and the $\log_{10}$ transformed trace elemental data……..202
Table E2 Fe-normalized and the $\log_{10}$ transformed major elemental data ..…..203
Table F1 Compounds identified by GC-MS for screened samples…….204-207

ABBREVIATIONS AND ACRONYMS

ANOVA: analysis of variance

B.P: Before Present

BBC: Blombos Cave

ED-XRF: energy dispersive X-ray fluorescence

ESA: Early Stone Age

ESR: electron spin resonance

EXAFS: extended X-ray absorption fine structure

FT-IR: Fourier-transform infrared

GC-MS: Gas chromatography mass spectrometry

HCA: hierarchal cluster analysis

I.C.P-A.E.S: inductively coupled plasma - atomic emission spectrometry

ICP-MS: inductively coupled plasma - mass spectroscopy

ICP-OES: inductively coupled plasma optical emission spectroscopy

LSA: Late Stone Age

MAE: microwave assisted extraction

MSA: Middle Stone Age

NAA: neutron activation analysis

OSL: optically stimulated luminescence

PCA: principle component analysis

PIXE: particle induced X-ray emission

PXRD: powdered X-ray diffraction

REE: rare earth elements

RSD: relative standard deviation

SEM-EDS: Scanning electron microscopy energy dispersive x-ray spectrometer

TIC: total ion current

Tk: toolkit

TL: thermoluminescence

UAE: ultrasound assisted extraction

XRD: X-ray diffraction

XRF: X-ray fluorescence spectroscopy

CHAPTER ONE

Introduction

This introductory chapter serves to give a background on the southern African Middle Stone Age (MSA) period, highlighting two important techno-traditions (Still Bay and the Howieson's Poort) which portray the technological and behavioural innovation of *Homo sapiens*. Further an overview of Blombos Cave, the crux of this research, is given. This is expounded by a detailed description of the stratigraphy of the MSA site and a brief background of the artifacts recovered. The chapter is concluded by the statement of the problem as well as the motivations for this study.

1.1 Background on the southern African Middle Stone Age

The southern African archaeological Stone Age sequence is divided into three major periods: Early Stone Age (ESA), Middle Stone Age (MSA) and Later Stone Age (LSA). The MSA highlights a period in prehistory between the ESA and LSA which lasted from about 280 to 30 thousand years ago (ka) (Jacobs *et al.*, 2008). Anatomical and genetic evidence suggests that during this time modern humans (*Homo sapiens*) had emerged (Jacobs *et al.*, 2008) and characteristic forms of human behaviour such as abstract thinking were developing. This period consists of a range of different local and regional techno-complexes and sub-stages. These are mainly defined by stone tool typology and technology (Haaland, 2012).

It was in 1929 that two South African archaeologists Goodwin and van Riet Lowe introduced the term "Middle Stone Age" with an aim to describe stone tool industries (technologically different from those of the ESA and LSA periods) in the south African MSA assemblages (Haaland, 2012). The MSA assemblages display a significant variation in stone tool-making traditions but are generally influenced by prepared core technologies, blades and blade cores, complex flake and point production and notched pieces (McBrearty and Brooks, 2000; Mourre *et al.*, 2010; Lombard, 2012). It is said that some of these stone tools were hafted so they represent the earliest evidence of regular manufacture and use of compound adhesives and composite technology (Lombard, 2006a; Wadley *et al.*, 2009; Lombard, 2011). As a result the southern African MSA period marks an increase in technological innovation and the progression of more complex social behaviours (McBrearty and Brooks, 2000; Henshilwood *et al.*, 2009; 2011).

Still Bay (c. 75–72 ka) and Howiesons Poort (c. 65–59 ka) are notable and distinct southern African MSA techno-traditions (Lombard, 2005; Wadley, 2007; Jacobs *et al.*, 2008; Henshilwood and Dubreuil 2011). These industries bear great modernization which depicts early technological advancements of *Homo sapiens*. These advances in technology are highlighted by the heat treated, pressure flaked bifacial stone points at Still Bay (Henshilwood *et al.*, 2001b; Villa *et al.*, 2009)

and the backed stone segments mounted on arrows launched by bow (Wurz, 1999; Wadley and Mohapi, 2008; Lombard and Phillipson, 2010) at Howiesons Poort. It is also the discovery of associated bone points and tools (Henshilwood *et al*., 2001), engraved ochres and ostrich egg shells (Henshilwood *et al.*, 2002; Texier *et al.*, 2010; Mackay and Welz, 2008), and shell beads (Henshilwood *et al.*, 2004) which validates the interpretation of these periods as bearing evidence of symbolically mediated behaviour.

The phrase "symbolically mediated behaviour" encompasses the concept of "modern human behaviour". This refers to behaviour that is facilitated by socially created patterns of symbolic thinking, actions, and communication. This allows for the exchange of material and information as well as cultural continuity between and across generations and co-existing communities (Henshilwood *et al.*, 2003a). In other words modern human behaviour is the symbolic thought intended to accomplish some organised behavioural outcome. According to McBrearty and Brooks (2000), there are four features that are distinctive of modern human behaviour: abstract thinking, the ability to plan and organize, "behavioural, economic and technological innovativeness," and symbolic behaviour. Many of these aspects of modern human behaviour can be broken down into more specific categories, including art, personal embellishment and technological advancement.

There are a number of archaeological sites, geographically confined to southern Africa, which are known to contain the above mentioned MSA assemblages (i.e. Still Bay and Howiesons Poort assemblages) such as Diepkloof Rock Shelter, Blombos Cave, Sibudu, Klasies River and many others. However in this study we focus on one site, Blombos Cave (Figure 1.1). At Blombos Cave, the Still Bay bifacial points are found *in situ*; meanwhile the site lacks any evidence of Howiesons Poort-like assemblages. As a result Still Bay assemblages are incorporated into the MSA levels at Blombos Cave (i.e. Still Bay is a MSA sub-stage). Blombos Cave, on the coastal belt of the southern Cape, is located 20 km west of the town of Still Bay, South Africa. The site features in many debates concerning the origin of modern human behaviour. Blombos Cave has well-preserved faunal and cultural material in the MSA levels. It is the permeation of

the calcium carbonate ($CaCO_3$) rich ground waters through the roof and walls of the cave that has created an alkaline environment best suited for the preservation of bone and shell, predominantly near hearths and ash deposits. The good organic preservation at Blombos meant the Still Bay artifacts lay in food remains, including bone and marine shell (Henshilwood *et al.*, 2001b).

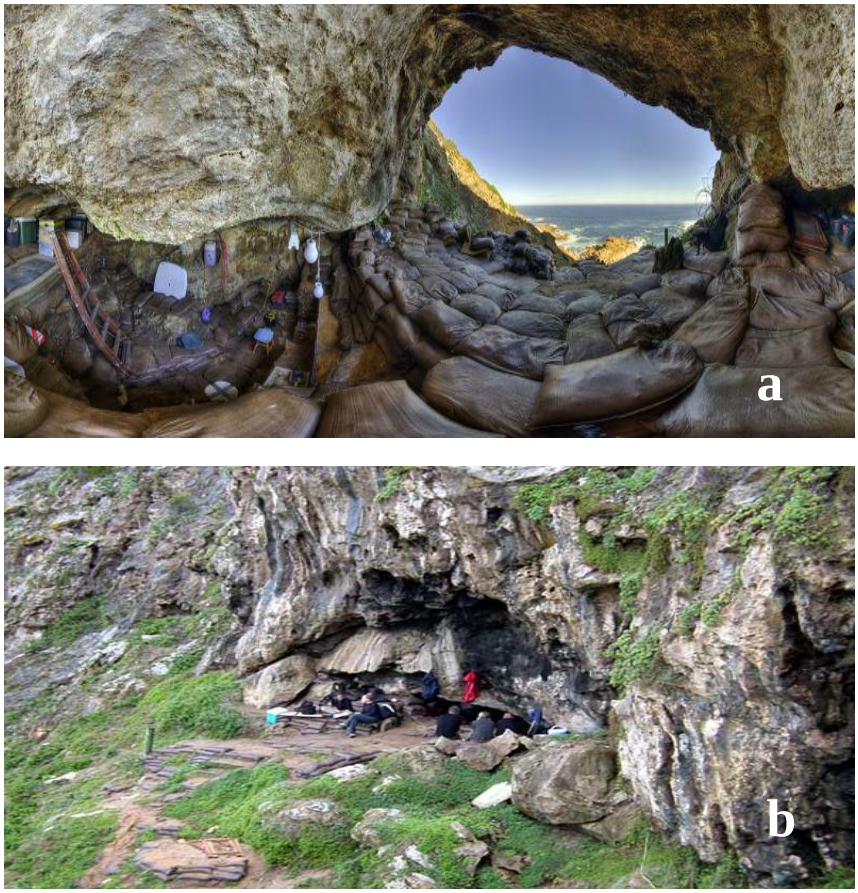


Figure 1.1 (a) Interior, (b) exterior view of Blombos Cave, Southern Cape (Henshilwood, 2012) (Image: Magnus Haaland)

1.2 Blombos Cave stratigraphy and ages of the deposits

The profile of the cave consists of MSA and LSA layers, with the former constituting the major section of the sediments. Blombos Cave Hiatus or DUN is a layer of sterile yellow dune sand roughly 5–50 cm thick. This sand blew into the

unoccupied cave during the lowered sea levels at 70 ka, and the layer sits above the M1 phase, separating the LSA and MSA levels. This provides visible evidence that the LSA occupation did not disturb the underlying MSA deposits (Henshilwood, 2005). The LSA deposits are less than 2 ka with clear burnt layers that preserve their original hearth-like structures.

The matrix of the MSA levels consists of geogenic aeolian, marine-derived dune sand, blown in through the cave entrance, limestone, as well as wind-borne halites. The anthropogenic deposits consist of marine shell, bone, charcoal and ash, lithic materials mainly quartz, quartzite and silcrete and humic material. The MSA levels are classified into three phases, namely the M1, M2 upper, M2 lower and M3 phases, while the layers are classified alphabetically ranging from CA to CP according to age (Figure 1.2).

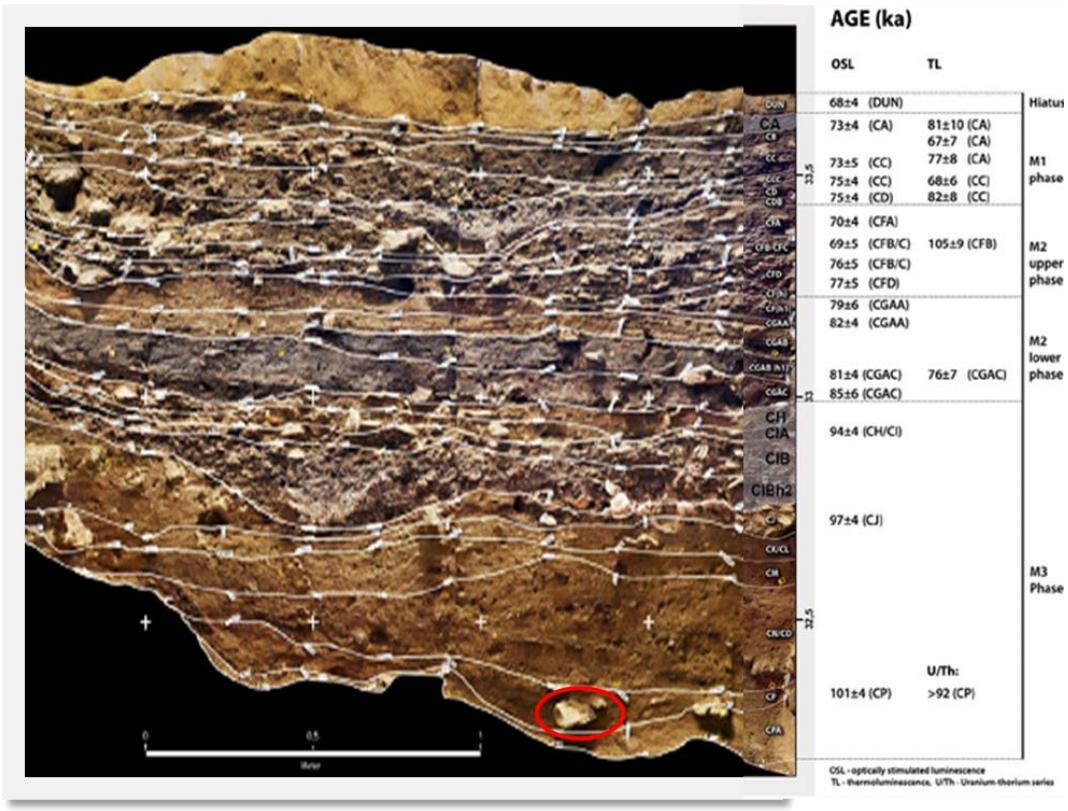


Figure 1.2 South section of Blombos Cave showing layers, phases, and ages. The ochre-processing toolkits (Tk1) from layer CP in the M3 phase is shown *in situ*. (Image: Magnus Haaland)

The single-grain optically stimulated luminescence (OSL) was mostly used to determine the time of deposition of the artifact-bearing deposits at Blombos Cave. Other methods, such as thermoluminescence (TL) (Tribolo *et al.* 2006), uranium-thorium (U/Th) (Henshilwood *et al.,* 2011) and electron spin resonance (ESR) (Henshilwood, 2012) have also been employed to date the cave deposits.

A phase is defined as a chronologically limited cultural unit within a local culture sequence. Each phase is made up of a number of different layers with similar diagnostic traits that sets it apart from other phases. The term layer describes a single unit that gathers through natural or human deposition, or both. Layers may vary from those above or below and are identified with regard to the texture or composition or even both, as well as colour, thickness and features (Henshilwood *et al.*, 2001b).
The five uppermost layers (CA, CB, CC, CD and CDB) below the Hiatus make up the M1 phase. This phase constitutes of artifacts including the Still Bay type bifacial stone points, bone tools, marine shell beads, and engraved ochre.

The underlying four layers, typified by carbonized deposits, large hearths, and shellfish, represent the M2 phase. The upper part of the M2 phase contains most of the bone tools (Grine and Henshilwood, 2002b), probably used as awls and projectile points, as well as a human premolar crown (Henshilwood *et al.*, 2001b). The M1 and the upper M2 phases have an age of c. 77 – 72 ka , the lower M2 phase is dated at c. 85 ka and the M3 at c. 100 ka (Henshilwood *et al.,* 2011). The lower M2 phase represents a period of short-lived occupation and does not contain artifacts associated with the Still Bay, it does however contain a few basin hearths, a very large hearth in the CGAC layer, small quantities of blades, flakes and cores in silcrete, quartz, and quartzite and some small ochre pieces. The upper M2 phase on the other hand contains markers (bifacial foliate points) associated with the Still Bay and the implication made is that the age of 76.8±3.1 ka for the CF level (Figure 1.2) (Jacobs *et al.*, 2006) should be regarded as the terminus post quem for the Still Bay levels at Blombos Cave (Henshilwood *et al.*, 2009).

1.2.1 The ochre processing workshop in the M3 phase

The M3 phase is dominated by shellfish deposits, lithics mainly in quartzite and a high density of modified ochre pieces. Among the recovered archaeological artifacts, ochre constitutes as some of the major finds (Henshilwood *et al.*, 2009). The 2008 excavation led to the recovery of a 100 ka ochre-processing workshop from the M3 phase, comprising of a toolkit (detailed description in section 4.4). The analysis of the toolkit revealed that a liquefied pigment rich mixture was produced and stored in a Haliotis midae (abalone) shell and that ochre, bone, charcoal, grindstones, and hammerstones all formed a part of the toolki (Henshilwood *et al.*, 2011).

The toolkit was found *in situ* in the CP layer together with a few other archaeological remains. It may appear as though the site was used primarily as a workshop and was neglected shortly after the compounds were made. Later on dune sand blew into the cave burying the toolkits into a preserved state. The recovery of the toolkit at Blombos Cave adds evidence for early technological and behavioural developments associated with *Homo sapiens* (Henshilwood *et al.*, 2011).

1.3 Description of the research problem investigated

Pigments have been used by humankind for many years to paint representations of their environments, depict significant social symbols, to decorate and enhance the appearance of their surroundings or themselves. Early pigments were mineral based implying that *Homo sapiens* were utilizing materials that were readily available in the immediate environment. Mineral based pigments have the advantage of being chemically stable and require little processing (i.e. grinding and mixing with a binding medium) before they could be used.

The *in situ* discovery and subsequent analysis of the ochre processing toolkit at c.100 ka from Blombos Cave provides evidence of early technological, symbolic and behavioural developments associated with *Homo sapiens.* The toolkit

documents their ability to deliberately plan, produce, and collect a pigmented compound and to make use of containers.

1.4 Motivation

Sediments preserve information about prehistoric activities. These were characterised with an aim to determine the degree to which past human activities left detectable chemical residues in the sediments.

Ferruginous rocks (ochre) are the most commonly used and commonly available mineral pigments. Knowledge of their composition and methods of preparation/processing and application can improve our understanding on how the past humans were technologically and symbolically advanced.

In this research trace elemental analysis of the ochre recovered from the site was done to establish chemical signatures that are characteristic of a particular source. The origins of these materials offer insight regarding possible trade routes and socio-cultural interactions between different cultures.

A mineralogical study of the ochre from Blombos Cave was carried out in order to better understand the application of the ochre in the manufacture of this first known pigmented compound.

Understanding past pigment production processes leads to inferences concerning technical skills of early humans and their social position within civilization.

Lastly, analysis of organic residues which have been absorbed into the structural matrix of archaeological materials, can provide information about past artifact function and diet. Hence residue analysis was done.

CHAPTER TWO

Literature review

This chapter commences with an in-depth literature review of Blombos Cave and its link to complex cognition in the MSA. Here symbolic evidence (recovered from the cave deposits) of modern human behaviour is given. Focus is placed on the MSA assemblages and use of ochre at the MSA site. Ochre differentiation and provenance using a variety of analytical techniques is included, this entails examples highlighting work already done.

The concept of fire use at MSA sites is briefly discussed and this is exemplified by Blombos Cave hearths. The notion of microarchaeology, a tool used to identify and interpret prehistoric combustion features in sediments, is introduced. This is expounded by examples on work previously done. The chapter is concluded by a concise review on organic residue analysis.

2.1 Blombos Cave and its link to complex cognition in the Middle Stone Age

During the last twenty years, archaeological research on the MSA has increased. The revived interest in this period of the African Stone Age sequence is most likely a reflection of the realisation amongst researchers that the southern African MSA represents an exceptionally formative period in human prehistory. The MSA represents the evolutionary era during which: (a) early humans developed mental capabilities comparable to the cognitive variations seen in present day humans; and (b) the period when humans first developed symbolic behaviour and syntactical language (Henshilwood and Dubreuil, 2009; 2011).

Blombos Cave MSA (c. 100 – 72 ka) deposits provide some of the first evidence of advanced human behaviour and debuts in talks regarding the early cognitive developments of *Homo sapiens*. This evidence includes Still Bay bifacial points, ochre-stained perforated marine shell beads (Henshilwood *et al.*, 2004; d'Errico *et al.*, 2005; Vanhaeren *et al.*, 2013), formal bone tools (d'Errico and Henshilwood, 2007), engraved patterns on ochre (Henshilwood *et al.*, 2009) and the production of a pigmented compound at c. 100 ka (Henshilwood *et al.*, 2011).

2.1.1 Bifacially worked stone points

The 73 ± 3 ka M1 phase at Blombos Cave contains, among other artifacts, high densities of the bifacially worked stone points. The upper M2 phase also contains the bifacial points, although in lesser quantities than in M1. Bifacially worked points are the fossiles directeurs of the Still Bay techno-complex and are commonly referred to as "lance-heads" or "laurel leaf-shaped" stone points (Goodwin and Van Riet Lowe 1929). Still Bay points have bifacially retouched sides, are elliptic to lanceolate shaped and most often they have two pointed apices (Figure 2.1). The M1 and upper M2 MSA phases at Blombos highlight the c. 75–71 ka Still Bay techno-tradition period in the prehistory of southern Africa. During this period both the technological and behavioural collections of early *Homo sapiens* had drastically increased to embrace innovative technologies

(Henshilwood, 2012) for example the use of heat treated, pressure flaked bifacial stone points (Henshilwood *et al.*, 2001b; Villa., 2009; Mourre *et al.*, 2010).
Figure 2.1 shows the pressure flaked Still Bay points at Blombos Cave. These are made from silcrete, quartzite, and quartz.



Figure 2.1 Still Bay bifacial points (Henshilwood *et al.*, 2001b; Villa *et al.*, 2009)

A study of these bifacial points has shown that some were used as spear points for hunting and that others served as multifunctional tools (Lombard, 2007a). Roughly half of the silcrete points were heat treated before being finished off with flaking using hard-hammer, soft-hammer and pressure-flaking techniques. This is the earliest known use of pressure-flaking (Mourre *et al.*, 2010). Heat treatment was done because silcrete in its raw form is difficult to knap hence heating was used on the southern Cape silcrete to improve its flaking qualities (Brown *et al.*, 2008). Certain artifacts that have been recovered were made from raw materials that were not local such as the silcrete (sourced 30 km north of Blombos in the Riversdale region) (Roberts, 2003), suggesting that the inhabitants of the cave were travelling great distances to acquire particularly preferred materials.
Still Bay bifacials may also have played a symbolic role (Henshilwood *et al.* 2001b; Henshilwood and Marean, 2003). Burkitt (1928) interpreted the Still Bay

as marking the arrival of *Homo sapiens* on the subcontinent. These bifacials represent a high level of technical skill in the MSA, and the method of manufacture was certainly in accoradnace with people whose culture was influenced by symbols (Henshilwood and Marean, 2003; Minichillo, 2005).

2.1.2 Bone tools

The recovery of bone tools shows technological innovation in the Still Bay levels at Blombos Cave. Bone tools (Figure 2.2), which are often perceived as a characteristic marker in the Eurasian transition to modern cognitive behaviour, are rare at MSA sites. More than thirty formal bone artifacts have been recovered from the Still Bay levels at Blombos Cave, including awls and points (Henshilwood and Sealy, 1997; d'Errico and Henshilwood, 2007).



Figure 2.2 (a) Bone point from the MSA levels at Peers Cave (d'Errico and Henshilwood 2007); (b–g) bone tools from the Still Bay levels at Blombos Cave; (b–e) bone awls; (f–g) bone points; (h–i) engraved lines on tools c and Henshilwood *et al.*, 2001a; d'Errico and Henshilwood 2007); (j) engraved bone fragment (d'Errico *et al.*, 2001)

The majority were awls made on long-bone shaft fragments, further manufactured by scraping and then used to pierce soft material such as leather, or small shells to make beads (d'Errico *et al.*,2005).

The points were treated differently to awls. The high polish on these points bears no obvious application but it rather seems to have been a technique that gives a distinct appearance to these artifacts. These may have formed part of a material culture exchange system among groups to maintain or enhance social relations (Henshilwood and van Niekerk, 2013). Blombos Cave bone tools provide comprehensive evidence for systematic bone tool manufacture and use.

At Blombos Cave at least two bone fragments, c. 75–72 ka (Still Bay levels), have possible engravings. The symbolic marking on a bone is a feature that is likely to support a symbolic interpretation. Microscopic analysis of the bone fragments marked with eight parallel lines signifies that the lines were deliberately engraved for symbolic intent (d'Errico *et al.*, 2001).

2.1.3 Perforated Nassarius kraussianus shells

The presence of personal ornaments has led to a strong argument for early behavioural modernity in the Upper Palaeolithic (Wadley 2001a; Henshilwood *et al.* 2004; d'Errico *et al.* 2005). Marine shell beads are known from Middle Palaeolithic sites in North Africa and the Levant (Cremaschi *et al.* 1998; Wrinn and Rink 2003; Vanhaeren *et al.* 2006; Bouzouggar *et al.* 2007; d'Errico *et al.* 2009), dated at c. 100–60 ka. The oldest beads from southern Africa are Nassarius kraussianus (N. kraussianus) (more than seventy) shell beads (Figure 2.3). These were identified and recovered from the Still Bay levels at Blombos Cave. These shells were pierced using a bone tool to create an opening and then they were strung, perhaps on a cord or sinew and worn as a personal embellishment. The frequent rubbing of the beads against each other and against the cord containing them, resulted in distinct use-wear facets on each bead that are absent on these shells in their natural environment. These use-wear patterns are what define the shells as beads (Henshilwood and van Niekerk, 2013).

The display of personal ornaments during the Still Bay phase was not peculiar. Distinct assemblages of beads depicting wear patterns and colouring specific to that group were recovered from various levels within the site. This pattern proposes that a substantial amount of individuals may have worn beads, either on themselves or attached to a garment (Henshilwood and van Niekerk, 2013).

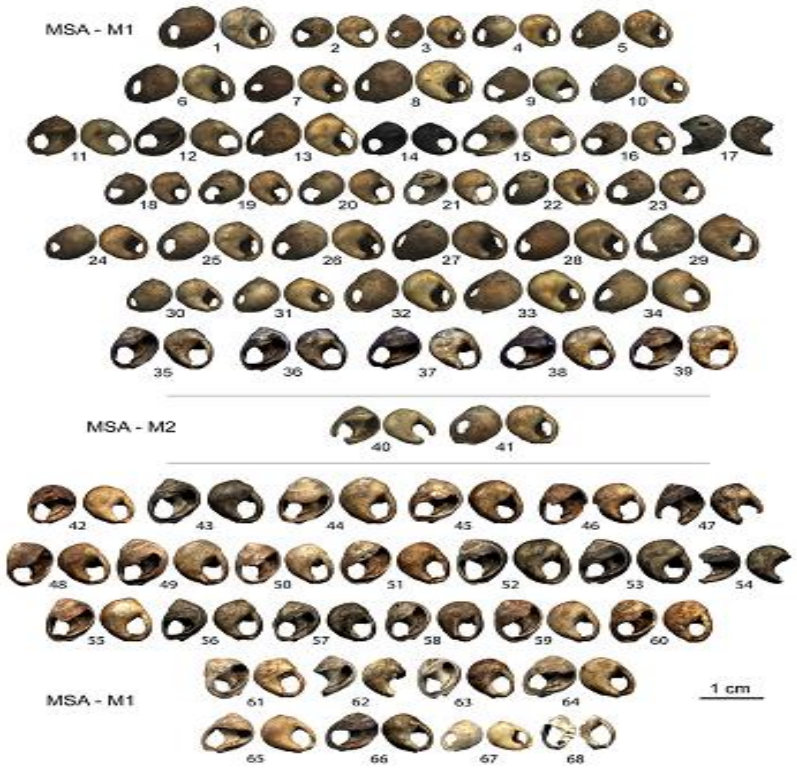


Figure 2.3 Perforated N.kraussianus from the MSA phases M1 and M2 at Blombos Cave (Vanhaeren *et al.*, 2013).

Personal adornments have featured as a key item in discussions regarding the origin of behavioural modernity (e.g. Henshilwood, 2012). The wearing of beads is a behaviour associated with exhibiting on the physical body an item that can portray symbolic meaning that is understood by members of the same cultural group hence the early existence of bead use is usually regarded as evidence for the presence of complex communication systems (Henshilwood and Dubreuil, 2009). Figure 2.4 illustrates how the beads were arranged and strung during their use and wear by the MSA people.

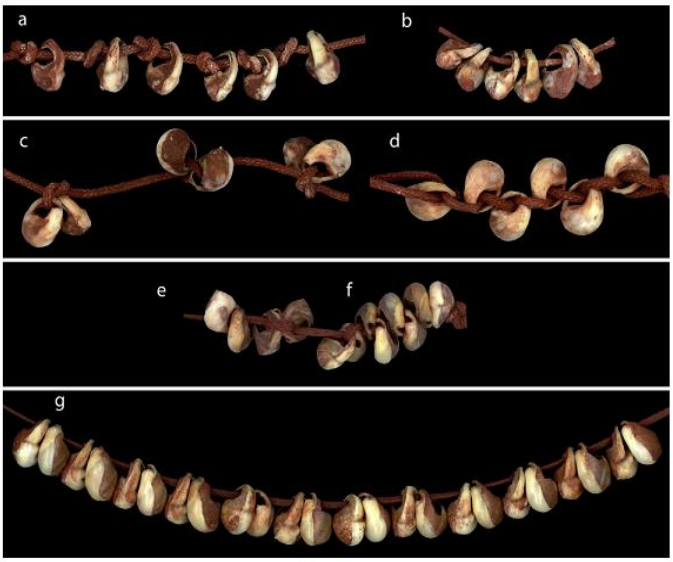


Figure 2.4 (a) Knotting with floating shells, (b) continuous stringing with the same orientation of N. kraussianus, (c) knotting with floating pairs of dorsally joining shells, (d) braiding with two strings, (e) knotting with floating pairs of ventrally joining shells, (f, g) continuous stringing with alternate orientation of N. kraussianus (Vanhaeren *et al.*, 2013)

2.2 Subsistence at MSA sites

Blombos Cave has a great variety of terrestrial and marine faunal remains which are consistently found throughout the Still Bay occupation units. These remains include: fish (van Niekerk, 2011), shellfish, birds, tortoise and ostrich egg shell (Henshilwood *et al.*, 2001b) and a broad range of mammals of various sizes (Henshilwood *et al.*, 2001b; Thompson and Henshilwood, 2011). This shows that the MSA people practiced a survival strategy that involved a wide range of animals.The great amount of shell fish recovered from the Still Bay units at Blombos Cave shows that people were regularly collecting them at the shore and bringing them to the cave for consumption. However, in terms of density, the abundance of shellfish in the Still Bay layers (M1 phase) at Blombos Cave was less (17.5 kg m^{-3}) compared to the other MSA layers (for example the shell midden c.100 ka M3 phase had a shell density of 68.4 kg m^{-3}). This implies that

there was great exploitation of shellfish in the earlier occupation phases at Blombos (Henshilwood *et al.,* 2001b).

The variations observed in shellfish procurement through the MSA phases at Blombos Cave can be accounted for by the changing climate conditions and retreating sea levels. These factors have led to the alteration of the cave's proximity to the coastline and the sea level temperatures (Jacobs *et al.,* 2006; Chase, 2010; Compton, 2011; Blome *et al.,* 2012). So at some point during the Still Bay occupation units, the environmental conditions drastically changed and the coastal line retreated, the shellfish became inaccessible hence the hunting of terrestrial animals became more common. The stronger members of the society became more devoted to big-game hunting and preferred the larger animals. This depicted a shift in subsistence from resources that are easily caught and collected to those that would yield high return.

Tortoises became highly-ranked resources as big-game hunting became more popular during Still Bay times. One can infer that human behaviour in the MSA was flexible, responding to changes in the environment and resource accessibility. The humans were able to adapt to new means of survival and restructuring of social roles (Thompson and Henshilwood, 2014a).

2.3 Evidence of fire use at MSA sites

The best evidence for the use of fire is the occurrence of well conserved hearths; these are the remnants of a domestic fire feature that retain some or most of its original structural or compositional elements (e.g. organic matter and overlying ash) (Dibble *et al.,* 2009).These well preserved hearths are often found in a round or oval shape with an upper layer composed of light coloured minerals, a lower layer loaded with charcoal and a substrate of reddened sediment (Schiegl *et al.*, 1996). Hearths may represent the remnants of (1) short-lived activities (Berna and Goldberg, 2008; Goldberg *et al.,* 2012), forming in a matter of minutes or hours; (2) a central activity in a permanent or semi-permanent occupation of a site,

persisting for months when well-maintained (Mallol *et al.*, 2007); or (3) repeated resourceful use of the same space over many years.

The LSA deposits at Blombos Cave are not as deep as the MSA, and are more immensely bedded and undistorted. Also the burned layers in the LSA deposits tend to be thicker and appear to preserve their original hearth-like structures (Henshilwood, 2005).

In the M1 phase, the deposit is dispersed with numerous small basin-shaped ash and carbon hearths with a diameter of up to 0.5 m. Carbonized sand and organic partings of a few millimetres thick act as visual markers for the separation of discrete occupation layers. The partings are made up of dune sand mixed with plant material, possibly used for bedding or fuel, animal dung and other organic material that has become compressed and burnt and are generally dark in colour (Henshilwood, 2006).

In the upper M2 phase, the CFB/ CFC layer is a very shell dense layer and in some areas this unit contains large quantities of decomposing roof spall and large hearths. The lowermost layer CGA in the lower M2 phase is sandy and less shelly but contains many hearths (Henshilwood, 2006).
In the M3 phase, the CI layer is the thickest, most dense midden with shell, bone and stone excavated at Blombos Cave and contains extensive compact *in situ* hearths and ash deposits (Henshilwood *et al.*, 2001).

Hearths are a deliberate transport of wood or plant material to the cave for the purpose of burning to produce light or heat. The actual function of hearths is often not discernible, and is probably not easily classified; they could be used for cooking, heating, or even for light or protection. These hearths could have served any one of these purposes and most likely served several of these purposes at any one time during their use (Goldberg *et al.*, 2009).

2.4 Microarchaeological analysis: identifying and interpreting prehistoric combustion features in sediments

Microarchaeological analyses are essential for documenting the composition, preservation, and function of hearths and other burned residues. These techniques focus on the characterisation of sediments.

2.4.1 Micromorphology

This is one of a number of analytical approaches that fall under microarchaeological analysis (Weiner, 2010), and can be used to identify the by-products of burning and determine whether these by-products are *in situ* or have been reworked by human activity or natural processes (Karkanas *et al.*, 2007). Micromorphology has improved the knowledge of researchers on the identification of ash remains and their preservation conditions in a number of controversial cases (Schiegl *et al.*, 1996; Weiner *et al.*, 1998; Goldberg *et al.*, 2001).

Goldberg *et al.* (2009) performed micromorphological analysis of sediments from the MSA site of Sibudu Cave, KwaZulu-Natal, South Africa, and the analysis provided evidence of site formation processes of predominantly anthropogenic deposits. This approach allowed for a detailed interpretation of individual anthropogenic activities, including the construction of hearths and bedding and the maintenance of occupational surfaces through the sweep out of hearths and the repeated burning of bedding.

It can be said that anthropogenic deposits contain microscopic information about past human lifestyles with equal or even greater value than other macroscopic facets of the archaeological record typically studied, such as bones, lithics, and plants (Courty, 2001; Goldberg and Macphail, 2006; Berna *et al.*, 2007).

2.4.2 Micro- Fourier Transform Infrared Spectroscopy

Micro-FT-IR spectroscopy (μ-FT-IR) is an analytical technique that is to determine the mineralogical composition of archaeological sediments. It is also

used to identify changes to the crystal structure of materials that result from heating. However the difficulty with infrared (IR) spectroscopy is that the interpretation of the spectra is often complicated, especially when mixtures of minerals are present.

Minerals in archaeological sites can be produced in four different ways, namely geogenic, authigenic, biogenic and anthropogenic. Geogenic minerals are derived from some geological source such as the breakdown products of igneous rocks. Authigenic minerals are those that form *in situ* in the sediments as a result of changing chemical environments. Biogenic minerals are produced by organisms. Anthropogenic minerals are the products of human activities. Most of these are formed at high temperatures and can be referred to as pyrogenic minerals (Weiner, 2010).

By separating the effect of particle size and atomic disorder contributions to peak width by repetitive grinding of the sample, μ-FT-IR can also be used to differentiate between well-ordered geogenic calcite; less well ordered pyrogenic calcite and poorly ordered calcite. This is of much importance in many archaeological sites as calcite is often a major component of the sediments in the archaeological sites. Biogenic calcite is not common in archaeological contexts but may be present in the form of shell remains and earthworm deposits (Canti, 1998, 2007).

IR spectroscopy can reveal subtle differences in the degree of local disorder among different sources of crystalline calcite quickly and easily by decoupling two competing contributions to spectral peaks: particle-size-dependent optical absorption and local atomic order. This method is particularly powerful because no direct measurement of particle size is required and because the analysis strategy can be readily generalized for use with other infrared-active solid materials. Generally solid materials possess optical phonons that correspond to intra-unit cell vibrational modes. When probed with IR light, they lead to absorption peaks whose frequencies each vary slightly depending on the specimen

size, shape, and the polarization of the incident light (Mayerhöfer, 2004). Thus, the phonon mode may be manifested as a broad and complex IR absorption peak due to phonon-optical coupling (polariton) contributions from bulk, surface, transverse and longitudinal optical modes.

The calcite specimens are typically hand-ground and dispersed in an IR-transparent matrix like potassium bromide (KBr) this is the norm for assessing polymorph and atomic-level structural information in the context of archaeology, geology, and materials science. (Gebauer *et al.*, 2008; Weiner, 2010). When a calcite-KBr pellet is reground multiple times, each grinding reduces particle sizes and homogenizes the distribution of calcite within the KBr mixture.

Calcite has three symmetry-allowed phonon modes in the mid-infrared range: 713 cm^{-1} (ν 4, in-plane CO_3 bend), 874 cm^{-1}(ν2, out-of-plane CO_3 bend), and 1420 cm^{-1} (ν3, asymmetric CO_3 stretch) (White, 1974). As a specimen is subjected to more grinding, IR peaks sharpen to yield both higher intensities and smaller full width half-maximum (FWHM) values, but the mode frequencies remain constant (Figure 2.5a). A specimen can be reground and re-pressed repeatedly before the FWHM reaches a limiting value. The limiting values, as well as the starting widths, vary among different sources of calcite specimens. Importantly, a comparison of peak width and height ratios of the ν 2 and ν 4 bending modes for all calcites (Figure 2.5b) shows a strong inverse correlation.

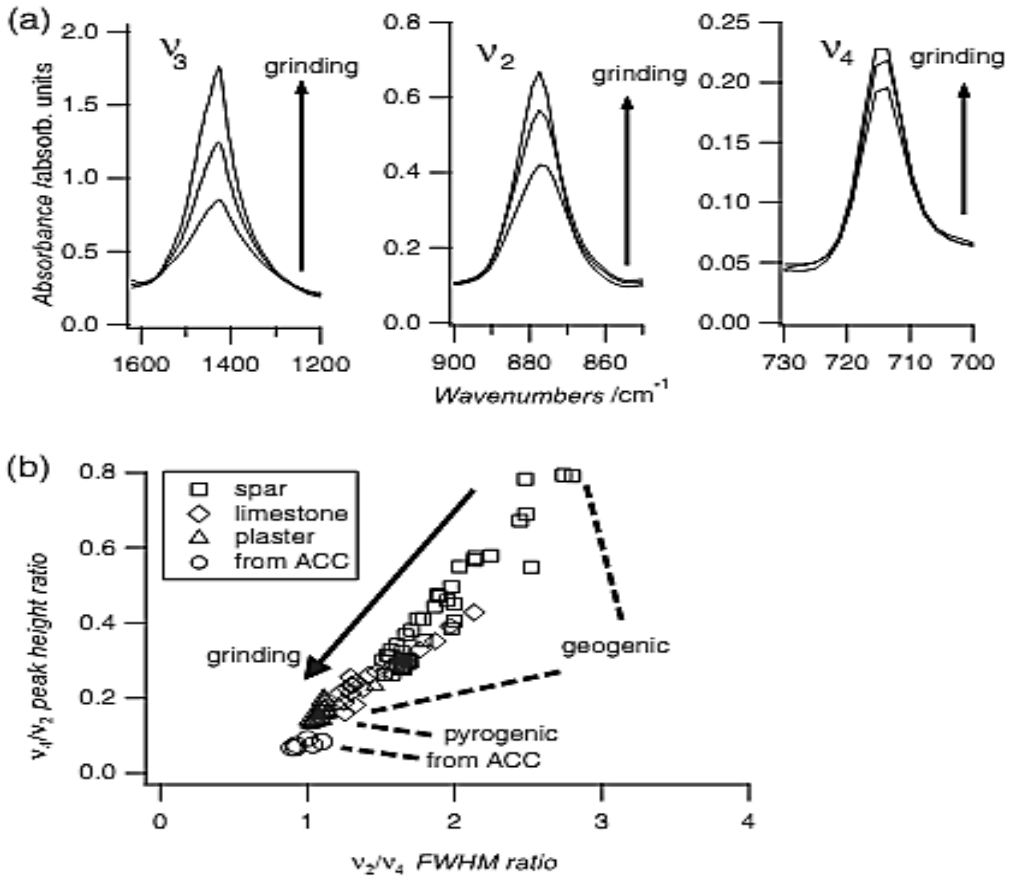


Figure 2.5 (a) μ- FT-IR spectra for geogenic calcite (chalky limestone) illustrate that peak sharpening occurs with grinding, leaving peak positions unchanged. A single specimen was ground and re-pressed. With grinding, the ν3 peak sharpens more than ν2, which sharpens more than ν4. Peak areas also increase slightly with grinding. (b) Peak intensity ratios (defined as ν4 /ν2) and FWHM ratios (defined as ν 2 / ν4). The trend with increased grinding is denoted with an arrow. (Poduska *et al.*, 2011).

2.5 Multi-elemental characterisation of anthropogenic sediments

The concept of using phosphorus as an indicator of past human occupation was introduced by Arrhenius (1963). Its principal application is in sediment chemistry in archaeology, where phosphorus quantities in sediments are measured (Nunez

and Vinberg, 1990; Quine, 1995; Leonardi *et al.*, 1999). Phosphorus analysis has been a commonly used method in archaeology because the technique is robust, and phosphorus is abundant in organic matter, which is one of the most common human additions to sediments (Middleton, 2004).

The chemistry of phosphorus is highly complex and it can form a large number of compounds (Parker, 1993). Phosphorus is an important element in living systems—in proteins, energy transfer (metabolism and photosynthesis), nerve and muscle function, nucleic acids, the skeletons of animals and the reproductive organs of plants—as well as in inorganic systems, particularly minerals (Severson and Shacklette, 1988; Parker, 1993).

There are numerous pathways by which human activities can lead to phosphorus enrichment in anthropogenic sediments, including burning organic materials (e.g., in hearths), the disposal of plant and animal tissue as organic waste, processing plant and animal tissue during food preparation, the storage of organic material (food as well as other materials), the processing of non-food organic materials (e.g. wood and bone) and the processing of inorganic materials (e.g. chipped stone tools) (Middleton, 2004). Phosphorus is such an effective indicator of human occupation and activity due to the many potential sources.

However, the technique has its limitations; phosphorus concentrations alone cannot distinguish between the different phosphorus-enriching activities. The determination of additional elements, by using other techniques, makes it possible to differentiate between distinct sources of phosphorus enrichment. Hence multi-elemental characterisation techniques such as the ICP-OES/MS were introduced. These techniques first featured in the 1960's (Cook and Heizer 1962, 1965) and they enable the differentiation between the chemical residues of different activities.

During multi-elemental characterisation, the concentrations of the elemental composition of the sediment samples are firstly obtained then the samples are numerically classified to identify chemically similar groups. The sample groups

are then matched to the ethnoarchaeologically defined patterns of enrichment with specific elements, associated with specific activities.

Many human activities are seasonal based, and as a result the composition of an occupation unit may change over time. Therefore, chemical activity signatures may overlap as a result of changes in the composition of the occupation unit over time (Middleton, 2004).

In situ burning is normally characterised by very high concentrations of phosphorus, potassium, calcium and iron. Wood ash on the other hand is characterised by very high concentrations of phosphorus, potassium and calcium, and somewhat high concentrations of other elements. Food preparation areas are characterised by high phosphorous and calcium. General activity areas or occupation units are characterised by high alkaline earths, while middens have high phosphorus and calcium concentrations (Middleton, 2004). In his study Middleton (2004) used a mild acid to extract chemical traces or residues from anthropogenic sediments. A multi-elemental characterisation of the traces was done to identify and differentiate the activities that occurred on the sediments.

2.6 Ochre and its application at MSA sites

Ochre is a coloured earth pigment, composed of a mixture of clay, quartz, and iron oxides or oxy-hydroxides, such as hematite or goethite. The meaning of this term has been extended in archaeology to refer to any category of rocks containing iron oxides (or oxy-hydroxides), with a reddish or yellowish streak (Henshilwood *et al.*, 2009; Hodgskiss, 2010).

The highly prized material is the earliest known pigment to be used by humans and its application is indicative of human advancement as it extends back to earlier hominids (Wreschner, 1980).

In mixtures, ochre usually binds quartz grains together (Jercher *et al.*, 1998; Bernatchez, 2008). Organic and inorganic inclusions often occur in ochre which

can even alter its colour (Ruan *et al.,* 2002; Bikiaris *et al.,* 1999; Hradil *et al.,* 2003; Hodgskiss, 2013).

There seems to have been a demand for colouring material during the MSA and great quantities have been found at some southern African sites (Wadley *et al.,* 2004), for example at Blombos Cave (Henshilwood *et al.,* 2002, 2009); Hollow Rock Shelter (Evans, 1994; Högberg and Larsson, 2011); Dale Rose Parlour (Schirmer, 1975); Sibudu (Wadley, 2009; Wadley *et al.,* 2009); and Diepkloof (Rigaud *et al.,* 2006). Ochre exhibits a range of colours from light yellow to blood red (Figure 2.6) (Robertson *et al.,* 1976). Ochre can also be found along more doubtful colouring materials, grey and white for instance. The colour depends on the proportions in which the iron-oxide chromophores and iron hydroxides are present, the matrix composition and on the particle size distribution (Mortimore *et al.,* 2004).



Figure 2.6 Ochre samples exhibiting a variety of colours (Rifkin, 2012)

Ochre is mainly composed of the following forms namely, goethite (α-FeOOH), hematite (α-Fe_2O_3), and magnetite (Fe_3O_4), including maghemite (γ-Fe_2O_3) and lepidocrocite (γ-FeOOH). These forms of iron oxide or oxy-hydroxide are often found embedded in various matrices which include white minerals such as chalk ($CaCO_3$), kaolin ($Al_2Si_2O_5(OH)_4$), quartz (SiO_2), gypsum ($CaSO_4.2H_2O$) and talc ($Mg_3Si_4O_{10}(OH)_2$) (Montagner *et al.,* 2013). Yellow ochre consists mainly of

goethite/oxy-hydroxides iron oxides, while red ochre comprises of hematite as the main chromophore (Bikiaris *et al.*, 1999; Elias *et al.*, 2006).

Evidence of ochre occurrence and its use in southern Africa improved greatly in the second part of the MSA period (Dayet *et al*., 2013). At most MSA sites ochre is present after c. 100 ka (Watts, 1998, 2009, 2010; Wurz, 2000; Barham, 2001; Wadley, 2001a). At the Pinnacle Point site near Mossel Bay, ochre was being used at 165 ka (Marean *et al.*, 2007; Watts, 2010). At Blombos Cave at 100 ka, ochre was processed and combined with fat, crushed fatty bone, quartz chips and charcoal to produce a pigmented compound that may have been used as paint or a cosmetic (Henshilwood *et al.*, 2011). The ability of one to source, combine, and store substances that could either enhance technology or social practices signifies a target in the evolution of complex human reasoning.

2.6.1 Grindstone and hammerstone tools associated with ochre processing

There is evidence of ochre residues on some stone tools recovered from the M3 phase at Blombos Cave. These stones were mainly used as grinding and crushing tools, and their particular use at Blombos Cave, was to grind ochre into a powder (Figure 2.7).

Archaeologists often attribute the use of ochre to enhanced mental abilities and symbolism. Although a link between the visible use of ochre, cognition and symbolism has not yet been clearly demonstrated, it can be argued that by understanding ochre processing technologies one can determine the skill, knowledge and mental abilities required to execute those activities (Rifkin, 2012).

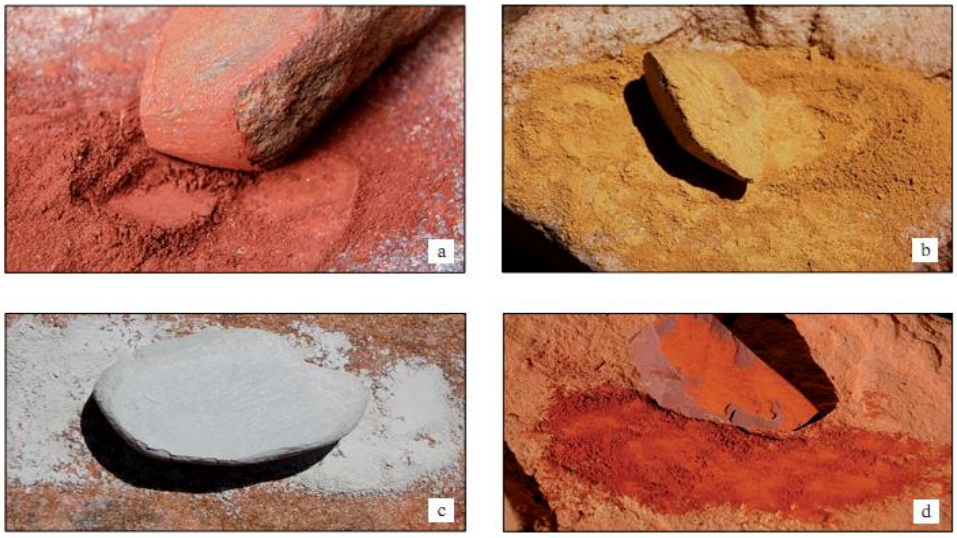


Figure 2.7 The extraction of the ochre powder from different mineral sources: a) grinding a hard haematite nodule b) grinding a soft yellow limonite fragment; c) grinding a soft water-worn grey shale chunk; d) extracting ochre powder from a red ochre chunk (Rifkin, 2012)

The discovery of two engraved ochre pieces at Blombos Cave depicts early evidence for the symbolic use of colourants (d'Errico *et al.*, 2012). The larger ochre piece had a crosshatched design engraved inside several broken boundary lines and the piece was found in the upper M2 phase dating back to c. 77 ka.

Incised ochre pieces bear evidence of being utilized where other striations were created by deliberate grinding or scraping to produce an ochreous powder which is widely assumed to have been used as a pigment (Henshilwood *et al.*, 2001a). It seems likely that ochre was purposefully brought into the cave for a specific reason because the nearest source is approximately within a 50 km radius of the site in the outcrops of Bokkeveld Group deposits (which is mostly shale and siltstone; Henshilwood *et al.*, 2001a. About 32 km inland from the cave chemical weathering of the outcrops has yielded extensive yellow and red ochre deposits (Rogers, 1988). As a result of continual Cenozoic marine transgressions the coastal zone outcrops have become less weathered and less ocherous (Rogers, 1988).

The amount of ochre from Blombos Cave is greater than that documented for most MSA sites in southern Africa (Henshilwood *et al.*, 2001a). Figure 2.8 depicts red shale; this flat fragment has a facet on one edge that shows evidence of grinding followed by scraping. On one main surface there is a collection of deliberately incised conjoining lines that form a pattern.

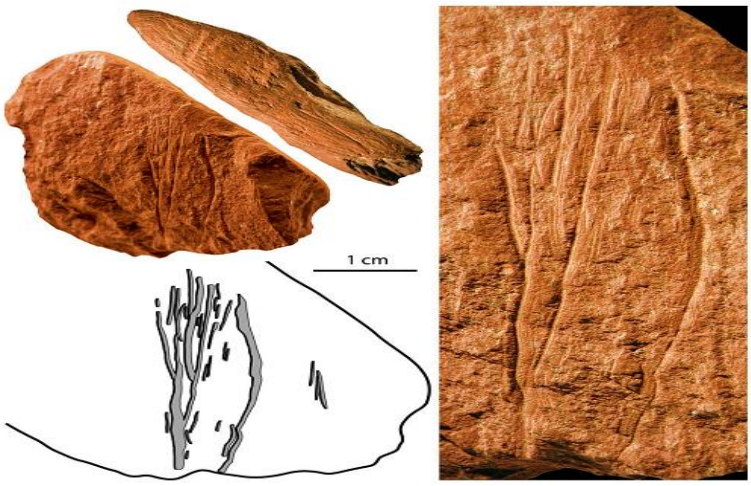


Figure 2.8 Close-up view of the engraved pattern on the ochre piece (Henshilwood *et al.*, 2009 a, b)

2.6.2 Ethnographically recorded uses of ochre

Ochre pigments are still important materials in many cultures and are used for both ceremonial and burial purposes and play an important role for cultural expression. While some of the cultural uses of ochre are known solely based on the use of raw minerals and artifacts found in archaeological sites, very little is known about the procurement and processing of ochre by MSA humans. It is possible that they preferred particular sources of ochre for specific characteristics of the ochre, and that ochre was traded along ancient exchange means (Popelka-Filcoff *et al.*, 2007).

The possible uses of ochre include:

- Body paint: red ochre is reportedly the most widely used earth pigment applied to human bodies and artifacts as a symbolic sign in many cultural ceremonies (Watts 2002; Rifkin 2012). Ochre paint is also often used for ritual purposes (Bleek and Lloyd, 1911). The 100 ka ochre-processing

workshop at Blombos provides evidence of the production of a pigmented mixture that could have been used for body painting purposes (Henshilwood *et al.*, 2011).

Red ochre powder for cosmetic use: the Ovahimba women (of Northern Namibia) are known for covering their bodies, hair and personal attire with a red ochre-based substance. The pigment is known as otjise and is comprised of a mixture of dairy-derived butterfat and red (otjiserundu) ochre powder (Rifkin, 2012). The otjise is also applied by men when they are to be wed (Galton, 1853).

- Medicinal use of ochre: ochre in medicine is reported from the ethnographic record where ochre would be moistened and applied to sores or mixed with cold ash and used in the treatment of burns (Velo, 1984; 1986). Ingestion of clay minerals and other non-food substances is termed geophagy. Clay minerals are ingested for a number of reasons, namely; to resolve ionic imbalances (Jones and Hanson, 1985), for essential mineral supplementation (Rifkin, 2012), to stabilize the digestive tract pH (Kreulen, 1985), to suppress intestinal parasites (Knezevich, 1998) and to detoxify the body against enterotoxins (Lozano, 1998; Reynolds *et al.*, 1998; Rifkin, 2011).

- As an aggregate in hafting adhesives: the use of ochre powder in hafting adhesives has been recorded in the MSA, LSA and Middle and Upper Palaeolithic contexts and more recent past. An explanation for why ochre would have been used in the process of hafting tools seems to come from experimental work conducted by Allain and Rigaud (1986). Their work shows that an adhesive recipe using mastic, wax or resin requires an inert powder such as ochre for at least two reasons. First, the ochre acts as an emulsifier because wax and resin would not mix well and, secondly, ochre allows for the hardening of the mastic when it dries. The reason why a filler is used in adhesive recipes is because pure resins are too hard when they are heated alone and they would not resist high impact pressure (Rots, 2002).

2.7 Characterisation, differentiation and provenance of ochre

The geochemical characterisation of ochre can be achieved by determining the matrix, chromophore and elemental composition.

2.7.1Elemental fingerprinting

Elemental characterisation studies are fundamental to understanding ochre geochemistry and are the foundation for possible ochre sourcing in the future (Popelka-Filcoff *et al.,* 2008). The elemental analysis of ochre is becoming more common as a method for patterns of resource use, trade and exchange (Popelka-Filcoff *et al.*, 2005; Smith *et al.,* 1998; Stafford *et al.*, 2003).

Identifying the unique trace element "fingerprint" of ochre artifacts and of extant sources of ochre can facilitate the matching of human-transported pigments to the locations at which they were collected in antiquity (Popelka-Filcoff, 2006).

Ochre is a heterogeneous material compared to other raw material types, it is therefore essential to also apply multivariate and discriminant statistics (see section 5.3) to differentiate the geochemical groups within the sample. MacDonald *et al.* (2011) conducted a study which focussed on assessing the range of geochemical groups within assemblages of archaeological ochre, and determined whether the geochemistry of the ochre satisfies the provenance postulate which states: the geochemical variability between different sources of materials must be greater than the internal variability within any one source (Glascock and Neff, 2003; Weigand *et al.,* 1977). If the provenance postulate is satisfied, then elemental analysis may be used to source the artifacts (Popelka-Filcoff *et al.*, 2006).

Elemental analysis involves obtaining elemental concentration data on major, minor and trace elements and to explore trends among them through application of multivariate statistics.

2.7.1.1 Energy dispersive X-ray fluorescence

ED-XRF as a non-destructive technique is well suited for the major elemental analysis of high value archaeological collections. The technique is employed in

the identification of major and minor elements present in solid samples. It is used for observing the distribution of individual elements within a defined 2-D area. Its main disadvantage is that a large amount of sample is required for determination of the minor elements and it is in capable of distinguishing between the ferrous (Fe^{2+}) and ferric iron (Fe^{3+}) in mineral samples.The technique generally has a poor limit of detection (Rephacholi, 1994 and Downer, 2008).

In a study to examine the variation in the major, minor and trace element patterns of ochre from iron-oxide sources in south eastern Missouri, Popelka-Filcoff *et al.* (2007) used ED-XRF and instrumental neutron activation analysis (INAA) to better understand the differences that may occur within and between sources. Jercher *et al.* (1998) used X-ray diffraction (XRD) with the Rietveld refinement and XRF to determine the mineralogy and elemental composition of modern Aboriginal ochre.

2.7.1.2 Scanning electron microscopy

SEM is a non-destructive technique used to observe grain morphologies and surface textures of sedimentary or rocky samples. It is especially useful for viewing clay-sized sedimentary components. When coupled to an energy dispersive x-ray spectrometer (EDS) basic elemental composition can be determined. SEM-EDS is often used in the mineralogical investigation of archaeological problems, including the characterisation and provenance of geological raw materials (Freestone and Middleton, 1987).

It is an excellent tool that has been found to be useful in the analysis of archaeological potteries (Goldstein *et al.*, 2003). Genestar *et al.* (2005) used Fourier Transform Infrared (FT-IR) spectroscopy and SEM-EDS to characterise and differentiate natural earths (ochre, siennas and umbers). They concluded that SEM-EDS is probably the best technique for characterising green earths and umbers, since they do not show significant differences in their matrix. So the presence of elements such as manganese, magnesium or chromium is useful for identifying the earth pigment and establishing its origin. In their work on the origin and geochemical characterisation of red ochres, Iriarte *et al.* (2009) used XRD, SEM–EDS and inductively-coupled plasma mass spectrometry (ICP-MS) to determine geochemical signatures of different ochre samples from outcrops

inside Tito Bustillo Cave (Ribadesella, Asturias) and the Monte Castillo Caves (Puente Viesgo, Cantabria).

2.7.1.3 Instrumental neutron activation analysis

INAA is non-destructive popular trace elemental technique used for provenance studies because of its capability to determine several rare earth elements and many trace elements with good accuracy and precision (Tsolakidou and Kilikoglou, 2002). INAA was used in the preliminary chemical characterisation in 44 ceramic samples from São Paulo II archaeological site by Ribeiro *et al.* (2011). Another study by Popelka-Filcoff *et al.* (2008) involves the use of INAA on ochre limited to geological sources from the western Tucson basin, Arizona and the subsequent multivariate analysis of the data.

2.7.1.4 Inductively-coupled plasma mass spectrometry and inductively-coupled plasma optical emission spectrometry

ICP-MS and OES are techniques used for the analysis of trace elements. They both depict high sensitivity however; ICP-MS has a lower detection limit than ICP-OES. The techniques are destructive as the solid matrix needs to be liquefied before analysis. Trace element analysis is mainly based on transition metals and rare earth elements (REE) and these are diagnostic for differentiating geological sources of ochre (Popelka-Filcoff *et al.*, 2008). Trace element fingerprinting entails obtaining precise measurements of a few dozen elements whose concentrations are less than 1000 ppm (Glascock, 1992) and which ideally have remained immobile from their source in the weathering environment. The concentrations of these trace elements are often source specific and can be used to distinguish among ochre deposits.

ICP-MS has been greatly employed in provenance studies, however researchers are leaning more towards the recently developed laser ablation Inductively-coupled plasma mass spectrometry (LA ICP-MS). Laser ablation completely eliminates the need for sample digestion thus allowing for a minimally destructive analysis of rare pigment artifacts which remain completely preserved for museum display or future research (Zipkin *et al.*, 2014). In the recent years, several studies

including Russ *et al.* (2012) and Bu *et al.* (2013) have employed LA ICP-MS to measure the trace element composition of ochre pigments. Zipkin *et al.* (2014) used LA ICP-MS to distinguish between three sources of ochreous rocks from northern Malawi.

2.7.2 Mineralogical composition analysis

2.7.2.1 X-ray diffraction

XRD is a non-destructive crucial technique for the identification of mineralogical phases of the ochre and is one of the most widely-used techniques for pigment identification in artifacts (Filippakis *et al.,* 1979). A study by Tankersley *et al.* (1995) showed that XRD could be used successfully to determine that ochre from the Hell Gap site in Wyoming was acquired from the Powars II ochre mine (Stafford *et al.,* 2003).The mineralogical composition of yellow and red ochre pigments from Alentejo—Terras rossas, Portugal was determined by XRD analysis. The EVA code was used for the identification of the phases and hematite was found to be the main chromophore mineral and calcite was commonly identified (Gil *et al.,* 2007). Dayet *et al*. (2015) used the degree of cristallinity of the illite phases as a provenance proxy for Diepkloof ochre.

2.7.2.2 Fourier Transform Infrared Spectroscopy

FT-IR is popular in studies involving the characterisation and provenance of pigments such as ochre. IR spectroscopy provides complementary information to Raman, often providing information on materials that are poor Raman scatterers. FT-IR has been used successfully to analyse both inorganic and organic archaeological material (Prinsloo, Wadley and Lombard, 2014). For inorganic samples like ochre, FT-IR is used to determine the mineral composition. The technique identifies a substance with an amorphous or slightly crystalline structure which is the major component of the inorganic material. Additionally IR spectroscopy can distinguish numerous varieties of yellow, brown, and red inorganic materials (Balakhnina *et al.,* 2011). In their 2011 publication Balakhnina *et al.* (2011), reported on some characteristic lines present in the vibrational spectra of most ochre pigments, these include the line with frequency

466 cm^{-1} which corresponds to quartz vibrations; at 914 cm^{-1}, Al–O–H vibrations, the doublet at 1008–1032 cm^{-1} indicates Si–O–Al and Si–O–Si stretching vibrations and play an important role in identifying ochre components. The lines at 3150 cm^{-1} (FeOOH) and 3436 cm^{-1} (H_2O) are said to be characteristic of all types of ochre. FT-IR is a good technique to indicate the presence of binders in ochre/pigment compounds. This is achieved by taking the vibrational spectrum of the dry pigment powder as the reference spectrum. If a binding media is present in a pigment compound, the interaction between the pigment powder and the binder should cause a shift in the spectrum. This shift is then accounted for by the formation of new functional groups.

FT-IR (among other techniques), was used for the multi-technique characterisation and provenance study of the pigments used in the San rock art in South Africa (Bonneau, Pearce and Pollard, 2012).

There are a number of infrared sampling techniques applicable to archaeological samples. Transmission spectra using KBr discs can be used if grinding of small samples is permitted. Specular Reflectance measurements using an infrared microscope can be carried out on untreated samples. This method has some disadvantages namely; the spectra contain a mixture of reflectance bands at the same time and poor signal-to-noise ratios (Claybourn, 2003) making them difficult to interpret. The use of a micro-attenuated total reflection (ATR) attachment can overcome this problem. It improves the signal-to-noise ratio so the spectra obtained are similar to the transmission spectra and easy to interpret (Goodall, 2007).

2.8 Organic residue analysis in archaeology

Organic molecules associated with archaeological artifacts have been identified primarily through the use of mass spectrometric methods (Charrié–Duhaut *et al.*, 2009).

2.8.1 Gas chromatography coupled to a mass spectrometer

Gas chromatography is a technique commonly used for separating volatile components of mixtures. The separated components are then identified and quantified (Littlewood, 1970). Gas chromatography coupled to a mass spectrometer (GC-MS) is an analytical technique used for the identification and quantification of organic compounds (such as lipids, proteins, plant resins, polysaccharides and a variety of plant extracts) in a given sample based on their mass ratios.

In an archaeological context, GC-MS is commonly used to identify trace organic compounds from archaeological material such as ceramics; stone tools; grindstones; sediments and cooking slabs. The identified organic compounds are then classified respectively, whether they derive from animal and plant tissue (Kedrowski *et al.,* 2009). Different plants and animals produce different types and quantities of organic compounds.

Extracting organic compounds from archaeological material is necessary before GC-MS analysis can be done. This is performed by adding a solvent such as methanol, chloroform, cyclohexane, acetone, acetonitrile or water (or a combination of several of these solvents) to the sample and extracting using an appropriate technique. A number of extraction techniques can be used depending on the sample type and compounds to be extracted. For organic compounds in archaeological samples, microwave assisted extraction (MAE) or ultrasonic assisted extraction (UAE) techniques can be used.

Different classes of organic compounds will be absorbed by different solvents. For example, dodecanoic acid (lauric acid) has a high affinity for methanol and a low affinity for water. The most feasible way is to try a range of solvents with different polarities. An optional step in the extraction process would be to firstly

grind the archaeological sample with a mortar and pestle and then add the specific solvent this maximizes the contact between the residue and the solvent.

In the study by Scott *et al.* (2002) of rock art in California a more comprehensive characterisation is achieved by combining XRF for elemental data, XRD for mineralogical characterisation and FT-IR to confirm the mineralogy of the amorphous material. GC-MS was also used to look for organic binders/resins in the pigment.

Previously, only a few studies have focussed on the procurement and use of mineral pigments by indigenous cultures in southern Africa. This study serves as an extension of the work previously done and also provides a formal mineralogical and geochemical characterization of the sediments and ochre materials from Blombos Cave.

CHAPTER THREE

Research objectives

This chapter outlines the aims and objectives of the research study. These objectives were used to focus the research so that the desired results would be obtained.

3.1 General aim

The general aim of this multi-disciplinary research was to execute a comprehensive physico-chemical characterisation of a c. 100 ka year old ochre processing toolkit at Blombos Cave, by using a combination of non-destructive and destructive analytical techniques in order to enhance our understanding of how ochre materials were selected and processed (thermally or mechanically) by MSA inhabitants at Blombos Cave.

3.2 Specific aims

To characterise of the sediment deposits at Blombos Cave by:

- multi-elemental analysis using the ICP-OES/MS and using the concentrations of P, K, Mg and other elements to infer human occupation and specific anthropogenic activities.
- mineralogical characterisation using FT-IR and differentiating between the sources of calcite using grinding curves.
- measuring the pH and electrical conductivity(EC) to correlate how the pH and electrical conductivity (salinity) vary with the depth of the profile.

To characterise and differentiate the ochre from the toolkit by:

- elemental fingerprinting using the ED-XRF and ICP-OES.
- using PXRD and FT-IR to give the mineral composition and mineral phases.
- using statistical analysis to study grouping patterns between the ochre samples.

To do an organic residual analysis of the ochre by:

- using FT-IR as a screening technique for any organic residues.
- using GC-MS to identify and quantify any preserved organic residues.

3.3 Key questions

This research wished to address the following questions concerning the exploitation of the toolkit (c. 100 ka) highlighting the period of the southern African MSA.

1. Can the physico-chemical characterisation study provide substantial information on the past lifestyle of the site occupants and the chronological variation present at the site?
2. Do each of the ochre samples from the site have a distinct chemical signature?
3. Can the mineral composition and/or mineral phase of the ochre be used to understand the crucial role of ochre during the pigment production?
4. Will the differentiation and sourcing of the ochre conclude on the transportation of the mineral, the exchange itineraries and socio-cultural interactions between members of different cultures?
5. Can any organic residues be identified?
6. Is there a possibility that these residues could have been used as binders/resins during the pigment production?

3.4 Hypothesis

A physico-chemical characterisation of the toolkit and its surroundings (i.e. Blombos Cave sediments) can provide insight on the technological, symbolic (engraved ochre, shell beads etc.) and social (transportation and exchanging of minerals) developments of early humans at the site.

CHAPTER FOUR

Sampling methods

This chapter entails a review of the strategies implemented during the excavation of the archaeological material from the MSA levels at Blombos Cave. Descriptive details on the ochre processing toolkit and the associated artifacts are also contained.

4.1 Site description

The study area was Blombos Cave. The cave (Figure 4.1) is located approximately 100 m from the Indian Ocean, and is about 35 m above sea level.

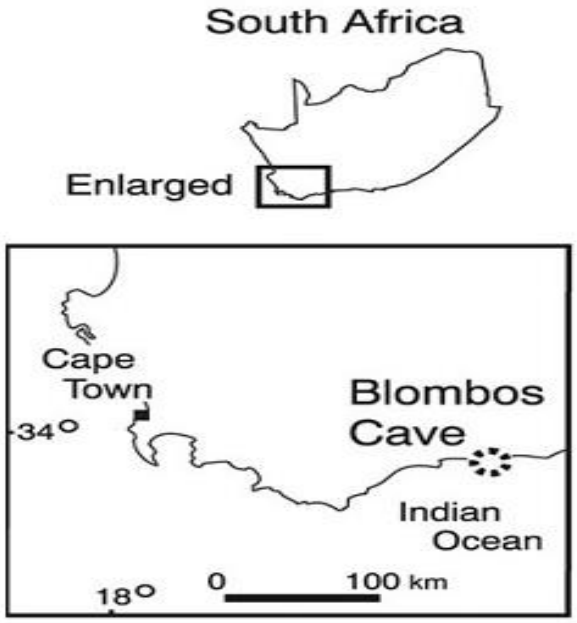


Figure 4.1 Geographic location of Blombos Cave on the southern Cape coast of South Africa (Image by: Magnus Haaland)

Blombos Cave is situated in an ancient wave-cut cliff formed in calcified sediments of the Bredasdorp Group. The cave was discovered by Professor Christopher Henshilwood in 1991 and has since been excavated from 1997 – 2014 under his direction.

The interior of the cave consists of a single main chamber with an interior cave floor of about 39 m² behind the drip line. Located west of the cave's main chamber are anthropogenic deposits extending inwardly for 3-5 m. However, in this segment of the cave, the ceiling lowers to a point where it falls in level with the surface, inhibiting entrance to the deposit beneath. North-east of the cave's main chamber, the deposits develop into a low laying ante-chamber of unknown extent due to the sand filling it.

The outer talus of cave forms a gradually sloping platform of about 23 m². This talus slope extends 4-5 m south then the ground abruptly drops down towards the shoreline which lies 35 m below the cave entrance. The talus mainly comprises of MSA deposit, rock fall and unconsolidated sediments. Further, this talus is steadied by 14 m² of enormous, uncovered blocks. At some point during the early occupation of the site these blocks had fallen from the rock face above in a manner that permitted the site preservation, sediment stabilisation and sediment accumulation in front of the cave's drip line (Haaland, 2012).

4.2 Excavation strategies

Excavations of the MSA levels were done by a team of archaeologists under the leadership of Henshilwood. As of 1999 the stratigraphic and spatial information, including MSA phase, layer, square, sub-square and precise artifact locations have been recorded during the site excavations.

4.2.1 Excavation coordinate system

A local coordinate system was established when Blombos Cave was first excavated. This coordinate system is based on a square meter grid which is aligned according to the north-south axis of the cave. The cave mouth is defined as south. The square meter grid forms an alpha-numerical coordinate system, starting from A1 with values increasing in the south-eastern direction (grey axes on Figure 4.2).

Each square meter is spatially referenced by the planar coordinates of its north-western corner (e.g. 'A1' on Figure 4.3a). During excavation, the square meter grid is further subdivided into four 0.5 m² quadrates. The quadrates are named a, b, c and d, further all excavated material is given a spatial reference combining the square meter grid (e.g. A1) and the quadrate reference (e.g. 'b') a typical example would be A1b. Objects excavated within the quadrates are spatially recorded using the local quadrate coordinate system (0, 0 – 50, 50 cm), and the origin of this system is placed in the quadrate's north-west corner (e.g. 0, 0 on Figure 4.3b).

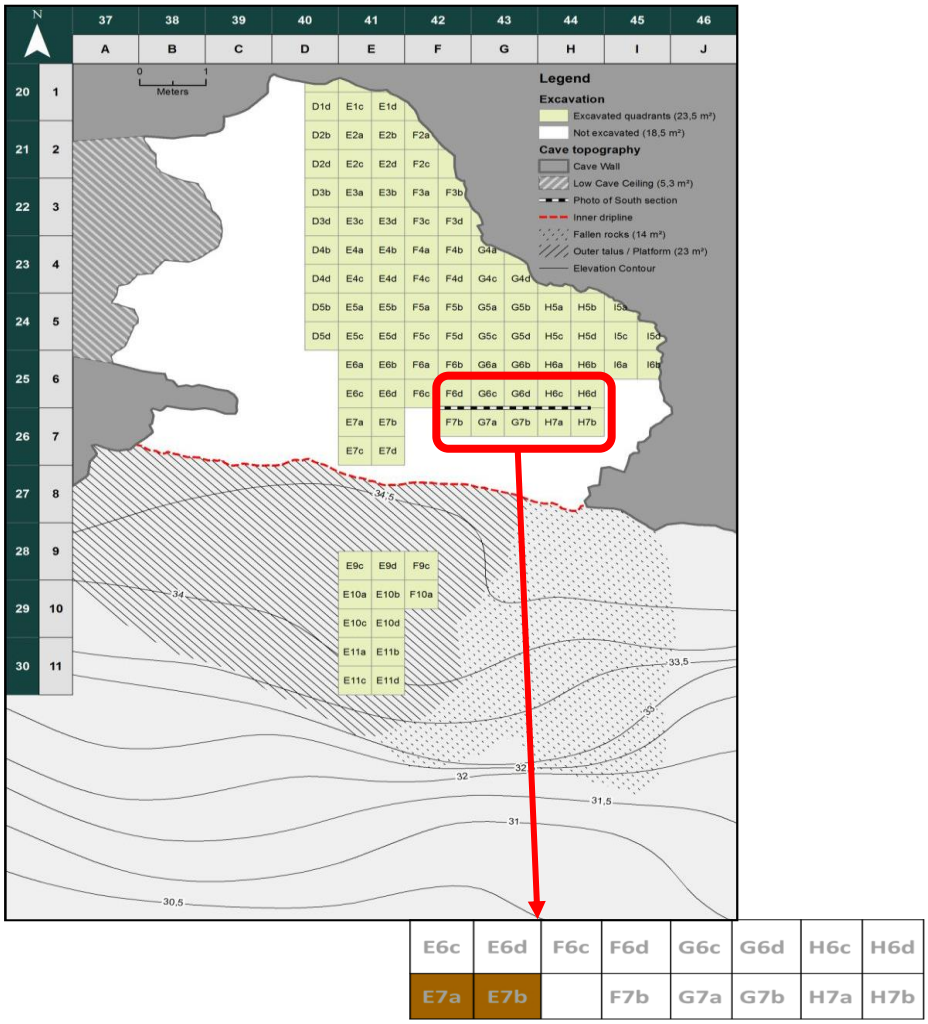


Figure 4.2 Blombos Cave site map showing the excavated quadrates (Image adapted from: Haaland, 2012)

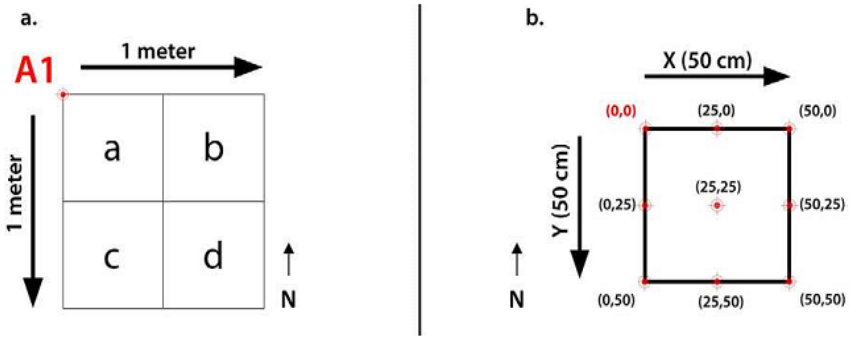


Figure 4.3 Blombos Cave excavation grid system: (a) Square meter grid, (b) Quadrate coordinate system (Image adapted from: Haaland, 2012)

4.2.2. Excavation and recording of depositional features, artifacts and deposit surfaces

The archaeological deposits at Blombos Cave were excavated quadrate by quadrate. The recording procedure for documenting the spatial distribution of archaeological artifacts and features at Blombos Cave has changed through time. However, recently a Trimble VX Spatial Station has been applied in the excavation process, allowing the digital recording of individual 3D location of archaeological features, artifacts and surfaces with very high precision (1/1000 of a cm) and accuracy (±2 mm).

During excavation, deposit volumes are measured and bulk sediment samples are taken from each stratigraphic unit in each quadrate. All non-plotted material (deposit/sediment) is recovered in buckets by quadrate and unit and kept separate for sieving through a nested 3.0-1.5 mm sieve. The remaining, sieved material is then washed and dried and put in plastic bags labelled coarse fraction (from 3 mm sieve) and fine fraction (1.5 mm sieve) respectively. The fractions are later sorted into major categories (lithic artifacts, bones, ostrich egg shell, ochre, shell fish) in the field laboratory, and prepared for further analysis in the main laboratory (Haaland, 2012).

4.3 Recovery of the ochre processing toolkit and the associated artifacts

The toolkit was recovered from the CP layer with its contents intact for later analysis in the laboratory. Loose and compacted sediments were sampled from the CP layer and the orange coloured CPA layer which lies directly below the CP layer (Figure 4.4).

The recovery of the artifacts related to the toolkit was photographed at the various phases during their excavation. The artifacts were not washed but were immediately placed in labelled plastic bags. Each artifact was taken to the laboratory for examination on the Leica Z6APO stereomicroscope. This

microscope is equipped with a digital camera to record any natural and anthropogenic traces of modification, including pigment residues.

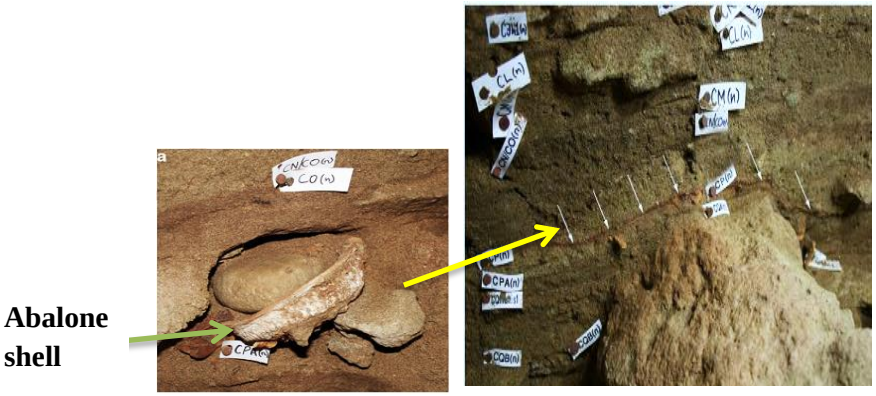


Figure 4.4 (a) ochre-processing container (abalone shell) shown *in situ* and (b) thin orange CPA layer (yellow arrow) with sandy CP layer above (Henshilwood *et al.*, 2011) (Image by: Henshilwood and Moéll Pedersen)

The toolkit (Tk1) contained a number of artifacts which were located both above and below the Haliotis midae (abalone shell).
The removal of the quartzite cobble from the shell aperture revealed a thick red pigment compound on the shell nacre, overlain by aeolian sand (Figure 4.5).



Figure 4.5 Red pigment exposed after removal of quartzite cobble from shell (Henshilwood *et al.*, 2011) (Image by: Henshilwood and Moéll Pedersen)

Microscopic and chemical analysis of the red compound revealed that it was made up of micro-flakes of two ferruginous siltstones (ochre), namely FS1 and FS2. These are predominantly present inside the shell, with small quantities present in the CP unit matrix. FS1 and FS2 are composed of quartz, hematite, muscovite/illite, and goethite but differ in their petrographic structure and elemental composition. Also the red compound was made up of fragments of crushed trabecular (spongy) bone which, once rich in fat and marrow, may have acted as a binder in the compound. Lastly the pigment compound contained of charcoal fragments, quartz and quartzite micro-flakes coated with ochre.

Figure 4.6 shows an overview of the *in situ* CP layer ochre processing toolkit.



Figure 4.6 *In situ* CP layer toolkit (Image by: Magnus Haaland)

Table A3 (in appendix A) entails a descriptive list of these pieces.

4.4 Description of the sediment samples

Table 4.1 lists the sediment samples analysed in this study. The samples were named according to the layer as well as the section/square from which they were sampled. Here the site is referred to as BBC, short for Blombos Cave.

Table 4.1 List of BBC sediment samples analysed during the study

Site	Square	Unit	Site	Square	Unit
BBC	E6d	CA	BBC	F6d	CGAC
BBC	H7b	CA	BBC	H6c	CGAC
BBC	F7b	CB	BBC	G7b	CH
BBC	H7a	CB	BBC	H6c	CH
BBC	H7b	CC	BBC	H6d	CH/CI
BBC	F7b	CC	BBC	F6d	CIA
BBC	G7b	CCC	BBC	H6d	CIA
BBC	H6d	CCC	BBC	F6d	CIB
BBC	H7a	CD	BBC	H6c	CIB
BBC	F6d	CD	BBC	G6c	CIBh2
BBC	H6d	CDB	BBC	H6d	CIBh2
BBC	G6c	CDB	BBC	G6c	CJ
BBC	F6d	CFA	BBC	H6d	CJ
BBC	H6d	CFA	BBC	F6d	CK/CL
BBC	F6d	CFB/CFC	BBC	H6c	CK/CL
BBC	H6c	CFB/CFC	BBC	F6d	CM
BBC	G7a	CFD	BBC	H6c	CM
BBC	F6d	CFD	BBC	F6d	CN/CO
BBC	F6d	CGAA	BBC	H6c	CN/CO
BBC	H6d	CGAA	BBC	F6d	CP
BBC	F6d	CGAB	BBC	H6d	CP
BBC	H6c	CGAB	BBC	H6c	CP
BBC	F6d	CGAB(h1)	BBC		
BBC	H7a	CGAB(h1)	BBC		

CHAPTER FIVE

Materials and Methods

The purpose of this chapter is to provide detail on the analytical techniques used to achieve the research objectives outlined in third chapter.

The major experimental protocol of the research was subdivided into the following activities:

<u>The physico-chemical characterisation of Blombos Cave stratigraphy as a preliminary background study</u>

- Measure the pH and electrical conductivity of the sediment deposits
- Characterise the sediments using these techniques: ICP-OES/MS, Carbon, hydrogen, nitrogen and sulphur (CHNS) analyser and FT-IR

<u>The physico-chemical characterisation of a 100 000 year old toolkit from the CP layer</u>

- Characterise the ochre using the following techniques: ICP-OES, ED XRF, PXRD, FT-IR, Raman spectroscopy and GC-MS
- Apply multivariate statistical methods on elemental data to differentiate ochre samples

Sediment samples from two different quadrates of each stratigraphic unit throughout the MSA levels at Blombos Cave were collected. Only two quadrates from each layer were analysed due to the restricted availability of the samples.

A total of 31 ochre samples recovered from the CP layer were analysed in this study. Samples were ground to powder using an alumina vessel and ball in a mixer mill. This was done after crushing the raw ochre into smaller pieces using a rock hammer. The resulting powders were thoroughly mixed in order to ensure homogeneity before analysis. Five methods of analysis were employed for characterising the ochre. These are FT-IR, PXRD, ED-XRF, ICP-OES and GC-MS. The choice of the method of analysis was determined by the amount of the available sample and whether the method is destructive or not. Samples with minimum quantities were analysed using FT-IR and ED-XRF only, while samples present in larger amounts were subjected to FT-IR, ED-XRF, PXRD and ICP-OES analyes. Ochre pieces bearing any engravings were examined intact using non-invasive ED-XRF in order to preserve them. Organic residue analysis (using FT-IR GC-MS) was employed on samples suspected to have been man-made (for example, mastic lumps which formed part of the toolkit).

5.1 Equipment

5.1.1 pH and electrical conductivity measurements

The Aqua Read GPS Aquameter with the coupled pH electrode and EC sensor was used. The sediment samples (5 g) were dissolved in 10 ml of deionised water. The solutions were stirred and allowed to reach equilibrium before the measurements were taken. For the calibration of the pH electrode, the Metrohm ion analysis (Metrohm Ltd. Switzerland) buffer solutions were used: pH 4, 7 and 9.

5.1.2 Analytical balances

An analytical balance (Precisa 180A, Switzerland), with a precision of 10^{-4} g, was used for all the weighing.

5.2 Sample preparation methods

Producing a good chemical analysis, particularly of difficult materials such as those often encountered in archaeology, often poses as a challenge. Accurate procedures need to be implemented for the preparation of samples for inorganic trace elemental and organic residual analysis. Some of the important reasons for sample preparation include:

- To degrade and solubilize the matrix, to release all metals/elements for analysis.
- To extract metals/elements from the sample matrix into a solvent more suited to the analytical method to be used.
- To concentrate metals/elements present at very low levels to bring them into a concentration range suitable for analysis.
- To separate an analyte/s from other species that might interfere in the analysis.
- To dilute the matrix sufficiently so that the effect of the matrix on the analysis will be constant and measurable.
- To separate different chemical forms of the analytes for individual determination of the species present.

5.2.1 Microwave assisted digestion

Microwave assisted digestion was used for degradation and solubilisation of the matrix, to release all elements for analysis. To ensure complete dissolution of the sample, a suitable digestion method must be selected. The choice of method depends on the sample type, the elements being determined and the analytical technique used for analysis.

5.2.1.1 Principle

Microwaves are electromagnetic radiation in the frequency range 0.3 to 300 GHz and here they are irradiated to chemical reactions. Microwaves are between the radio frequency and the infrared regions of the electromagnetic spectrum. To avoid interference with communication networks, all microwave heaters are

designed to work at either 2.45 or 0.9 GHz. In the liquid and solid states, molecules do not rotate freely in the microwave field and respond to the radiation differently, and this is where microwave heating comes in. The mechanism of microwave heating is different from that of conventional heating. In conventional heating, thermal energy is transferred from the source to the object through conduction and convection. In microwave heating, electromagnetic energy is transformed into heat through ionic conduction and dipole rotation. Ionic conduction refers to the movement of ions in a solution under an electromagnetic field. The friction between the solution and the ions generates heat. Dipole rotation is the reorientation of dipoles under microwave radiation. A polarized molecule rotates to align itself with the electromagnetic field at a rate of 4.9×10^9 times per second. The larger the dipole moment of a molecule, the more vigorous is the oscillation in the microwave field.

Microwave digestion can either occur in a closed or open system. Digesting a sample in a closed system in a microwave oven has several advantages over open container dissolution methods. Firstly the containers are fabricated of high-temperature polymers, which are less likely to contain metal contaminants than are glass or ceramic beakers or crucibles. The sealed container eliminates the chance of airborne dust contamination. The sealed, pressurized containers reduce evaporation, so that less acid digestion solution is required, reducing blanks. The sealed container also eliminates losses of more volatile metal species, which can be a problem in open container sample dissolution, especially in dry ashing. The electronic controls on modern microwave digesters allow very reproducible digestion conditions. Finally, automated systems reduce the need for operator attention.

5.2.1.2 Instrumentation

The samples were digested using a closed system; the Multiwave 3000 SOLV Anton Paar microwave sample preparation with Rotor 6MF 100* (Österreich, Austria) (Figure 5.1).

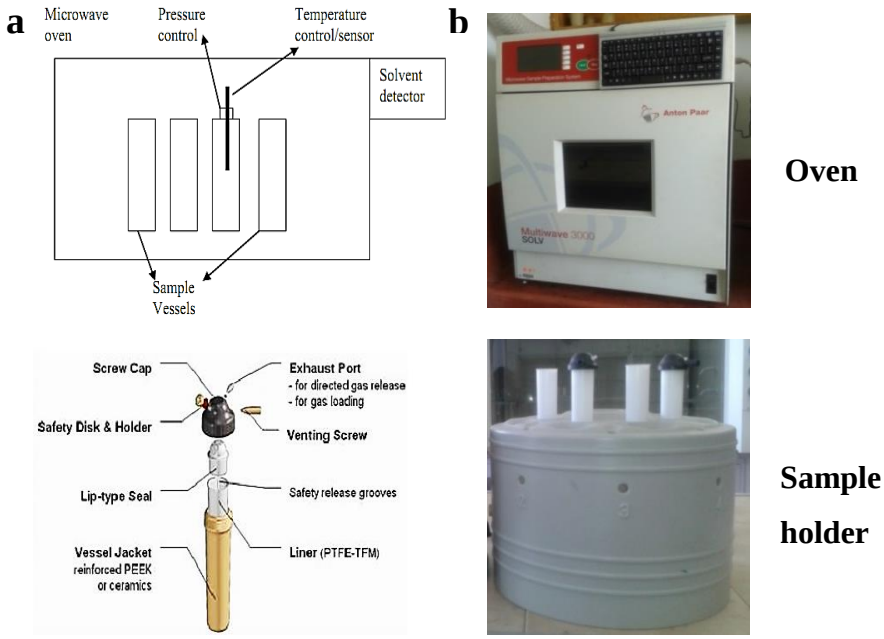


Figure 5.1 (a) Schematic of the MAE system and the vessel design (b) Anton Paar Multiwave 3000 microwave sample preparation system (Image (a) adapted from: Anton Paar, 2009)

The microwave power was programmed as indicated in Table 5.1. Temperature range was from 0 to 300 ^{o}C.

Table 5.1 Microwave assisted digestion power programme

	Power[W]	**Ramp [min]**	**Hold [min]**
Phase 1	500	15	15
Phase 2	400	5	15
Phase 3	0	0	10

5.2.2 Sample preparation for organic analysis

All organic molecules have an affinity for the sample matrix to one degree or another; else the organic molecules would not be present in the sample. That is why the first task in any analysis is to isolate the analytes from the bulk of the sample. During the extraction process it is necessary to overcome the interaction

between the analyte and the sample substrate. Extraction of organics from solid substrates is a process in which solutes desorb from the matrix and then dissolve into the solvent. Extraction efficiency is influenced by three related factors: solubility, mass transfer, and matrix effects. The solubility of an analyte depends largely on the type of the solvent. For a selected solvent, its solubility is affected by temperature and pressure. Mass transfer refers to the analyte being carried from the core of the matrix to the solvent. It involves the solvent penetrating into the matrix and removing the solutes from the adsorbed sites. Mass transfer is dependent on the diffusion coefficient as well as on the particle size and structure of the matrix. Matrix effects are the least comprehended of the three factors. A highly soluble compound can be non-extractable because it is deeply penetrated in the matrix pores, or is strongly bound to its surface. The selection of a solvent greatly depends on the nature of the analytes and the matrix (Mitra, 2003).

5.2.2.1 Ultrasonic assisted extraction

Ultrasonic assisted extraction (UAE) also known as sonication is used in the extraction of semi volatile organics from solid matrices. The technique uses ultrasonic vibration to ensure intimate contact between the sample and the solvent. Sonication is relatively fast, but the extraction efficiency is not as high as some of the other techniques (Kotronarou *et al.*, 1992). Ultrasonic instruments take standard alternating current frequency and magnify it from 50 or 60 Hz (cycles per second). Standard laboratory ultrasonic instruments run at 20,000 to 23,000 Hz (i.e., 20-23 kHz). Sonication can be either direct or indirect. Direct sonication uses a specially designed inert tool called a horn or probe (formally known as a sonotrode). This is placed in the sample-solvent mixture. In indirect sonication the sample-solvent mixture is placed in a container which is then placed in a sonic bath and energy transferred to the sample.

In this study indirect sonication was done using the ElmaTranssonic 460 (Elma, Singen, Germany) (Figure 5.2) to aid in the extraction of organic compounds in the ochre and mastic lump samples.



Figure 5.2 Indirect sonication system (a) closed and (b) open showing water bath

5.3 Instrumental techniques used for characterisation

All the techniques used for the quantification and characterisation of the sediment deposits and ochre at Blombos cave ochre are described below.

5.3.1 Inductively coupled plasma-optical emission spectrometer (ICP-OES)

ICP-OES is a multi-elemental destructive technique used to measure the concentrations of the total metals and trace elements present in a liquid sample or leachates. The sample solution is exposed to an inductively coupled argon plasma discharge. The volatile components of the sample are then driven off and the analyte is converted into gaseous phase atoms or ions in excited states. The light emitted by the excited atoms or ions is measured.

Main advantages:

- Simultaneous multi elemental determinations are possible
- The high temperature of the plasma discharge allows for the elimination of multiple interferences
- Low limits of detection are possible

Main disadvantages:

- Cost of running the instrument is high
- Solid samples need to be dissolved before analysis

5.3.1.1 Principle

ICP-OES operates on the principle of promoting atoms to higher electronic energy levels when they are heated to higher temperatures. The plasma temperature (6000-8000K) is enough to ionize most atoms. As the excited species return back to ground electronic state, the absorbed energy is released as an-element specific radiation. A transfer optic feeds this radiation into the optical system. The optical radiation is diffracted into its spectral components in the optical system with an intensity which is measured by semiconductor detectors and processed by incorporated software. The intensity of the emitted radiation is proportional to the concentration of the element in the sample.

5.3.1.2 Instrumentation and procedure

The main components of ICP-OES are the sample introduction system comprising of a peristaltic pump, nebulizer, spray chamber and drain assembly; the gas supply, ICP torch and the plasma; a source for production of stable radio frequency; transfer optics and optical spectrometer; detectors and computer (Smith, 1990) (Figure 5.3).

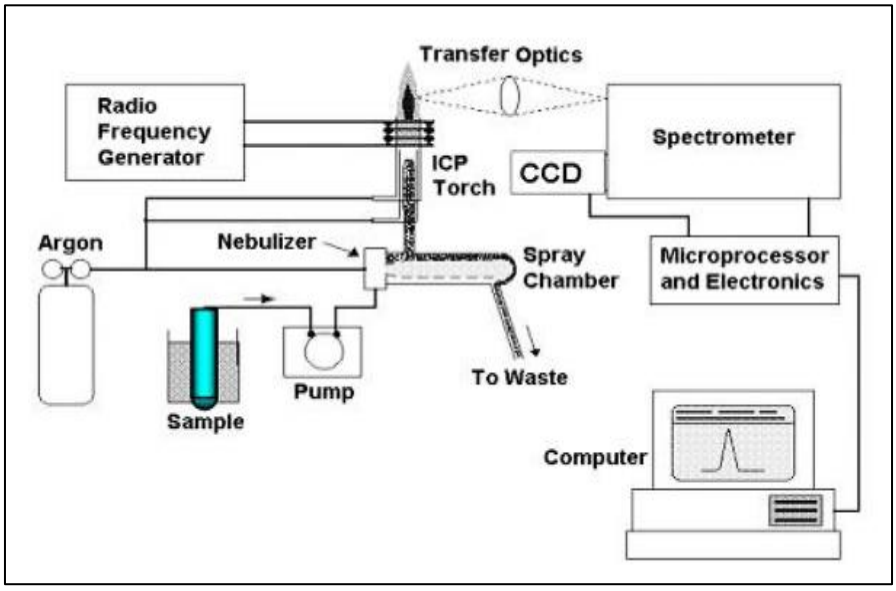


Figure 5.3 Schematic diagram showing the major components of the ICP-OES and the general set up of the system (Image adapted from: Arcinus, 2000)

The sample is pumped into the instrument as a stream of liquid by the peristaltic pump and it gets converted into an aerosol once inside the instrument through a process called nebulization. The sample is then entrained in the plasma support gas flow, which is typically Argon. As soon as the sample reaches the plasma, it immediately collides with the electrons and charged ions in the plasma and is itself broken down into charged ions. This is followed by the break-up of the various molecules in the sample into their respective atoms which then lose electrons and recombine repeatedly in the plasma, giving off radiation at the characteristic wavelengths of the elements involved. The radiations are sorted by wavelength in the spectrometer and the electronic signal of these radiations is converted into concentration information that the analyst can use.

Table 5.2 Operating conditions for the ICP-OES

Parameter	**Setting**
RF Power	1400 W
Coolant Gas Flow	14.00 mL min^{-1}
Auxiliary Gas Flow	1.00 mL min^{-1}
Nebulizer Gas Flow	1.00 mL min^{-1}
Sample Pump Flow	2.00 mL min^{-1}
Sample Aspiration Rate	2.00 mL min^{-1}
Replicates	3
Plasma Torch	Quartz
Spray Chamber	Single pass
Nebulizer	Cross flow
Processing Mode	Area

The Spectro Genesis End-on-plasma (Spectro analytical instruments (Pty) Ltd, Johannesburg, South Africa). ICP-OES was used for total major, minor and trace elemental determination.

5.3.2 Inductively coupled plasma-mass spectrometer (ICP-MS)

ICP-MS/OES have multi-elemental capability which gives them an advantage over other analytical techniques. These techniques also have the potential of coupling to various separation and sample preparation techniques. It is said that while ICP-OES is reliable, vigorous and suitable for routine analysis, ICP-MS is even better in terms of detection limit and therefore a more appropriate research tool for trace level analyses.

ICP-MS has exceptional properties such as high sensitivity (with limit of detection as low as 10^{-6} to 10^{-9} mg L^{-1}), relative salt tolerance and compound-independent element response.

The technique nonetheless does have its limitations, and these include:

- Matrix effects, which are more common and severe than for ICP-OES
- Solutions need to be diluted as high solids concentrations may plug the orifice
- Running costs of the instrument are extremely high
- Analyte elements must have an ionization potential less than that of argon, 15.8eV

5.3.2.1 Principle

ICP-MS is based on the same principle as the ICP-OES. In this technique after the aerosol produced in the nebulizer has been vaporized, atomized and ionized by the plasma, the ions are extracted from the hot plasma through an interface and into a quadrupole mass spectrometer (Figure 5.4). A system of electronic lenses are used to focus the ion beam before entrance into the quadrupole mass filter where the target isotopes are selected according to their mass to charge ratio and quantified by an appropriate detector.

The Agilent 7700 series ICP-MS (Agilent technologies, California, USA) was used for the trace elemental determination in the sediment samples.

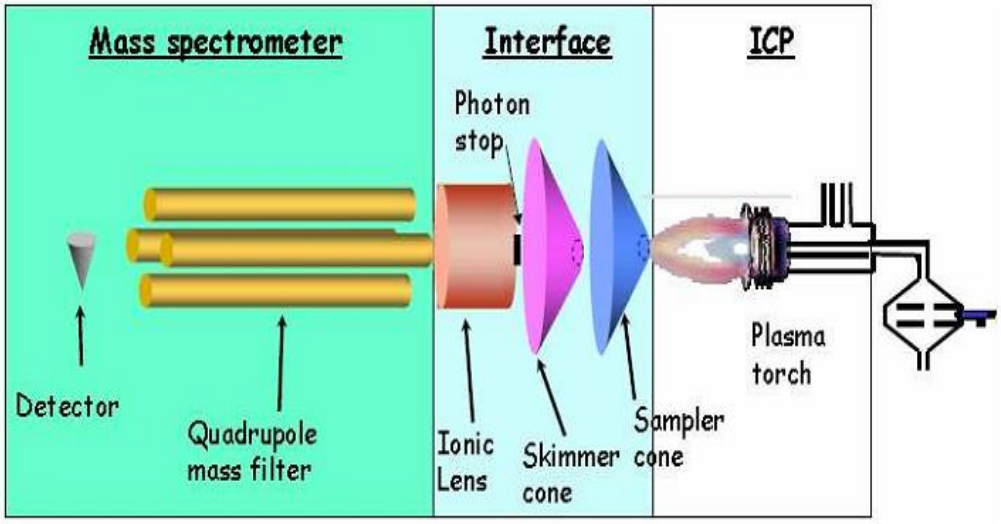


Figure 5.4 Schematic of a quadrupole ICP-MS (Image adapted from Makiese, 2012)

5.3.3 X-Ray Fluorescence (XRF) spectrometry

XRF is a technique that allows for qualitative identification and quantitative determination of the elemental composition of a variety of solid samples. There is minimal sample preparation involved as well as non-destructive methodology. A qualitative spectrum on an XRF instrument can be obtained within 5 minutes to provide gross elemental composition. Limitations to the technique include matrix interferences which can prevent the detection of some elements.

5.3.3.1 Principle

XRF is based on the detection of emitted X-ray radiation from excited atoms. This technique is a two -step process that begins with the removal of an inner shell electron of an atom. The resulting vacancy is filled by an outer shell electron. The second step is the transition from the outer shell electron orbital to an inner shell electron orbital. The transition is accompanied by the emission of an X-ray photon. The fluorescent photon is characteristic of the element and is equal to the difference in energy between the two electron energy levels. Since the energy difference is always the same for given energy levels, the element can be identified by measuring the energy of the emitted photon. In turn, the intensity of the emitted photon determines the concentration of the element. This emission

process is limited to the X-ray region of the electromagnetic spectrum that ranged from 0.1 to over 120 eV or 11 to 0.1 nm. The photon energies detected are designated as K, L or M X-rays, depending on the energy level being filled. For example, a K shell vacancy filled by an L level electron results in the emission of a K**α** X-ray (Figure 5.5).

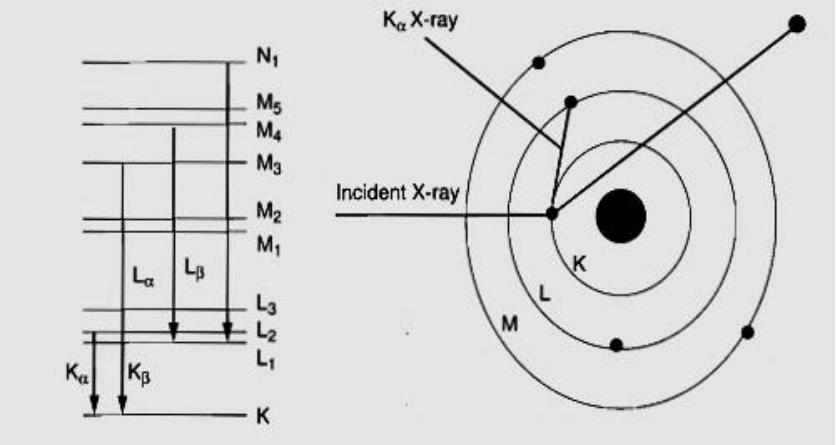


Figure 5.5 XRF principle and energy diagram (Image adapted from: Settle, 1997)

There are many X-ray lines as there are inner shell electrons. However, the most analytically useful and most intense lines are the K shell electrons for elements from boron through cerium, whereas the L and M lines are used for the remainder of the periodic table. The energy or wavelength of the emitted X-ray determined the element while the intensity of the X-ray emission defined the concentration of that element.

There are two ways in which the X-rays are detected: energy dispersive X-ray (ED XRF) spectrometers and wavelength dispersive X-ray (WD XRF) spectrometers. Figure 5.6 provides a schematic that illustrates each approach.

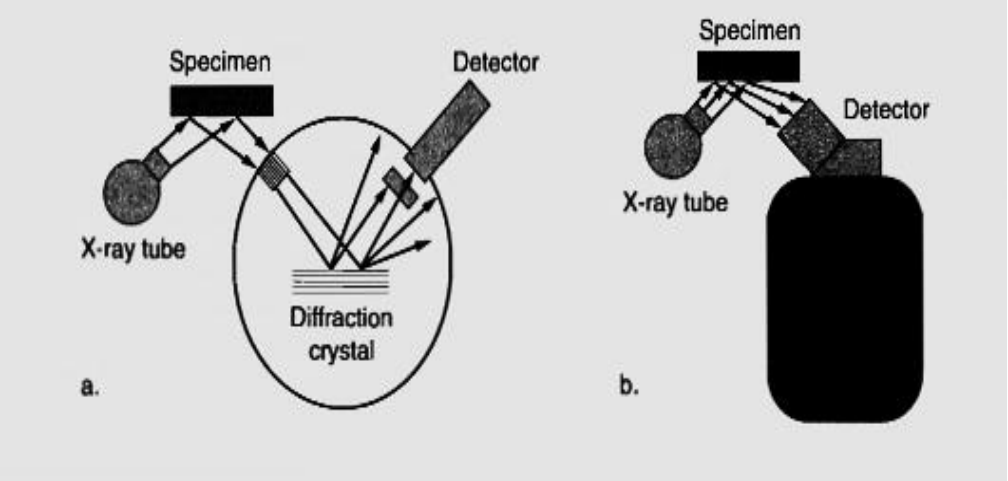


Figure 5.6 Schematic diagrams of WD XRF and ED XRF instruments. (a) WD XRF relies on diffraction crystals to separate the X-rays from the sample, (b) ED XRF has a solid state SiLi detector that converts X-ray photons into pulses that are processed electronically (Image adapted from Settle, 1997)

In both cases the process begins with excitation and a number of sources are used. The source of excitation also differentiates the various X-ray techniques. The most conventional and primary excitation sources are X-ray tubes. The dispersion of emitted X-rays allows the different X-ray energies to be measured and intensities to be determined.

The planes of a crystal are used to disperse the emitted X-ray photons from the specimen based on Bragg's law:

$$n\lambda = 2d \sin\Theta \qquad (5.1)$$

where n is an integer, λ is the wavelength of the photon, d is the lattice spacing and Θ is the angle of incidence of the radiation. The d values of the typical crystals used in WD XRF range from 0.14 to 8nm. The smaller d values are for natural crystals such as Lithium, fluoride and germanium. The larger d values are obtained with synthetic crystals. The WD XRF system is a sequential measurement where the instrument must step through the 2Θ values of the goniometer. This provides higher spectral resolution and better sensitivity than

ED XRF system. The ED XRF collects all the X-ray photons simultaneously onto the detector and hence has the advantage of detecting all the elements simultaneously, which means the analysis can be rapid and no elements are missing. The drawback however, is that the overall resolution of the ED XRF system is not as good as the WD XRF.

There are three basic detectors used in XRF instrumentation; gas ionization, scintillation and solid state semiconductors. The first two are found in WD XRF systems, while solid state semiconductors (lithium drifted silicon (Si(Li)) wafer are found in ED XRF systems. The X-ray strikes the Si(Li) detector and generates a series of pulses that correspond to the X-ray energy. The pulse height is proportional to the X-ray energy. The concentration of the element is determined by counting the pulses.

ED XRF system was used for determining the major elemental composition of the ochre samples. For this study a Bruker Handheld Tracer lll SD ED XRF (Figure 5.7) instrument was employed. The operating conditions were as follows: spectrometer was equipped with a 4-watt, miniature (<15 mm diameter and <75 mm long) X-ray tube containing a Rh target and titanium and sulphur filter. The X-ray tube was operated at 40 keV and 10.00 µA.



Figure 5.7 Handheld Bruker Handheld Tracer lll SD ED XRF instrument showing the system set-up

5.3.4 Carbon, hydrogen, nitrogen and sulphur micro analyser (CHNS)

This technique used to determine the elemental composition of a sample. High temperature combustion is used as a way of removing the elements from material. The products of combustion are CO_2, H_2O, N_2 and SO_x, depending on the elemental composition of the compound analysed. A LECO-932 CHNS analyser from LECO Corporation (Michigan, USA) was used to determine the amount of organic carbon and sulphur in selected soil samples. The samples (~2 mg) are weighed into tin boats, which are then compressed into capsules and taken to sample loading and then dropped into the furnace. The sample is combusted in the heated oxygen rich environment. Programmable control of the direct oxygen jet injection during high temperature combustion guarantees complete combustion. The gaseous combustion products are purified, separated into their components by special adsorption traps, and sequentially analysed using a detector. In this study a thermo conductivity detector (TCD) was used.

5.3.5 Fourier Transform Infrared Spectroscopy (FT-IR)

FT-IR is a non-destructive method used for the identification of all types of organic and many types of inorganic compounds. The technique assists in the determination of functional groups in organic materials and the molecular composition of surfaces. The technique is mainly applied in the identification of compounds by matching the spectra of unknown compounds with reference spectra (fingerprinting) also in the identification of functional groups in unknown substances. Any sample type can be analysed with the technique with little preparation required. Often solid samples need to be ground and mixed with a transparent matrix (such as KBr) or dissolved in a suitable solvent (CCl_4 and CS_2). The limitations of the technique include:

- Minimal elemental information is given for most samples
- Background solvent or solid matrix must be relatively transparent in the spectral region of interest
- Molecule must be active in the infrared radiation (IR) region

5.3.6.1 Principle of IR

IR spectroscopy is the absorption measurement of different IR frequencies by a sample positioned in the path of an IR beam. The main goal of IR spectroscopic analysis is to determine the chemical functional groups in the sample. Different functional groups absorb characteristic frequencies of IR radiation. IR spectroscopy is an important and popular tool for structural elucidation and compound identification.

IR is basically heat, and arises from relatively low-energy transitions between molecular vibrational and rotational energy states. It is usually referred to in units known as wave number, rather than wavelength. Wave number ($\tilde{\nu}$) is the number of waves per cm, and is the reciprocal wavelength (λ). The most analytically useful region of the IR spectrum is 4000–650 cm^{-1} wavenumbers. In this region, most organic compounds produce a unique absorption spectrum, and hence it is called the ‘‘fingerprint region’’. This part of the electromagnetic spectrum corresponds to the energy associated with molecular vibrations, and the absorption of IR is the result of the exact matching of the frequency of the radiation with the energy associated with a particular mode of vibration of a molecular group. At any temperature above absolute zero, all molecules are constantly vibrating. Even a simple diatomic (e.g., O_2) or triatomic (e.g., H_2O) molecule has a large number of possible vibrational modes, corresponding to the stretching and bending of the various bonds. Stretching of a bond implies that the distance between the two bonded atoms is continuously varying. Bending vibrations imply a change of bond angle between two bonds, and can involve scissoring, rocking, wagging, and twisting (Figure 5.8).

Most commercial instruments separate and measure IR radiation using dispersive spectrometers or Fourier transform spectrometers. Fourier transform spectrometers have superior speed and sensitivity and have also been applied to many areas that are very difficult to analyze by dispersive instruments. All frequencies are examined simultaneously in Fourier transform infrared (FT-IR) spectroscopy. A simplified optical layout of a typical FT-IR spectrometer is illustrated in Figure 5.9.

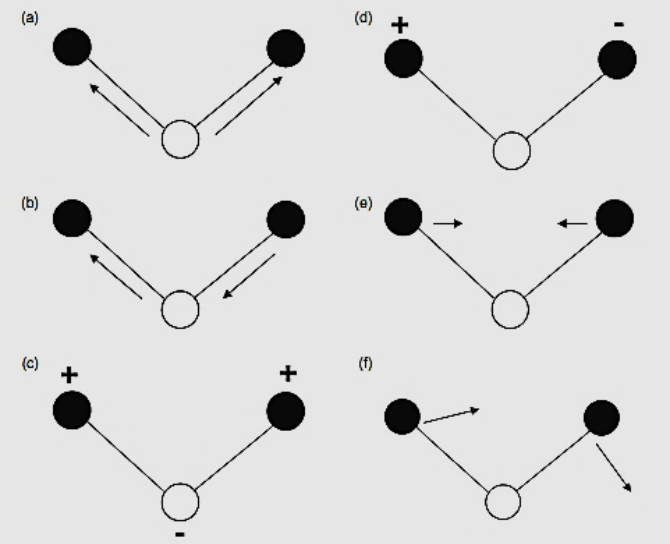


Figure 5.8 Vibrational modes of a nonlinear triatomic molecule. Arrows indicate motion in the plane of the paper, + is towards and – away from the observer. (a) symmetric stretching, (b) asymmetric stretching, (c) out-of-plane wagging, (d) out-of-plane twisting, (e) in-plane scissoring, (f) in-plane rocking. (Image adapted from Pollard *et al.*, 2006).

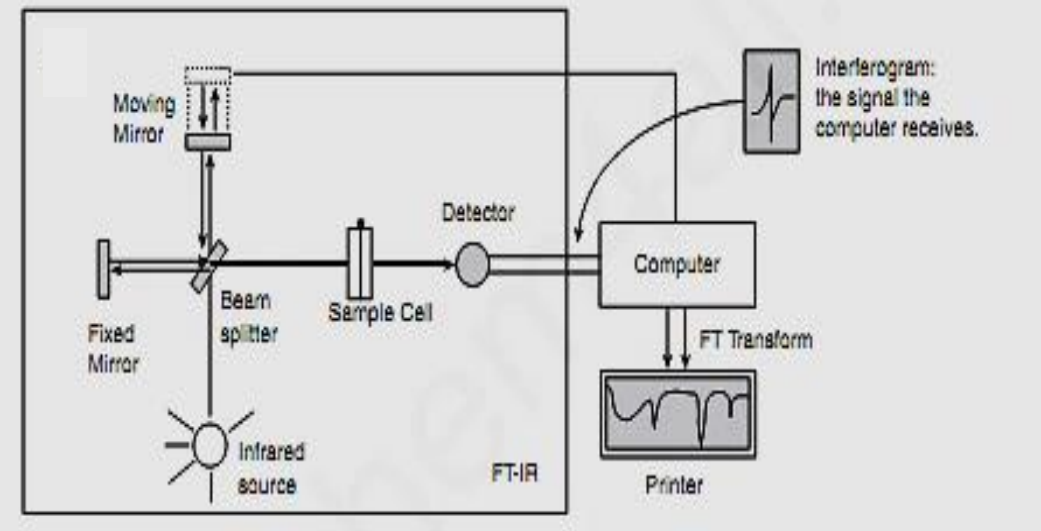


Figure 5.9 FT-IR spectrometer layout (Image adapted from: Introduction to spectroscopy 4th ed. by Pavia, Lampman, Kriz and Vyvyan, 2008)

The interferometer, which divides radiant beams, generates an optical path difference between the beams, and then recombines them in order to produce

repetitive interference signals measured as a function of optical path difference by a detector. As its name implies, the interferometer produces interference signals (called an interferogram), which contain infrared spectral information generated after passing through a sample. A mathematical operation known as Fourier transformation converts the interferogram to the final IR spectrum (showing intensity versus frequency).

FT-IR spectra were recorded in the frequency range of 4000-400 cm^{-1}using a Thermo Scientific Nicolet iS5 FT-IR Spectrometer (Thermo Fisher Scientific, Inc. (NYSE:TMO). KBr was used as a carrier for mounting the sample in the beam. The KBr (50 mg) was homogenized together with 10 µg of the sample using a pestle and mortar. The homogenized mixture was then pressed into a transparent pellet using a PIKE Technologies (Madison, USA) pellet press using the 7 mm die set. The iD1 Transmission accessory was used with the samples mounted in pellet holders. Acquired FT-IR spectra were compared to the standards spectra found on Omnic software minerals library (Thermo Scientific, USA) and the Steve Weiner library (http://wws.weismann.ac.il/Structural_Biology/Weiner/microarchaeology).

5.3.6 Powder X-ray diffraction

X-ray powder diffraction (XRD) is a versatile non-destructive analytical technique widely used to characterise unknown crystal structures, identify and quantify mineral phases, recognise amorphous materials in partially crystalline mixtures and identify three-dimensional micro-structural properties as well as quantitatively determine different phases in multi-phase mixtures by peak ratio calculations (Louër and Mittemeijer, 2000). XRD analysis is divided into two classes; single-crystal X-ray diffraction (SCXRD) and powder X-ray diffraction (PXRD). SCXRD is often used to determine the molecular structure of new material, while PXRD is used for phase identification and quantitative phase analysis. It can also be configured for many applications including variable temperature studies, texture and stress analysis and reflectometry. In this study PXRD was used to determine the phases of the ochre minerals.

5.3.8.1 Principle

The operative equation in XRD is the Bragg law (equation 5.1) and is illustrated in Figure 5.10.

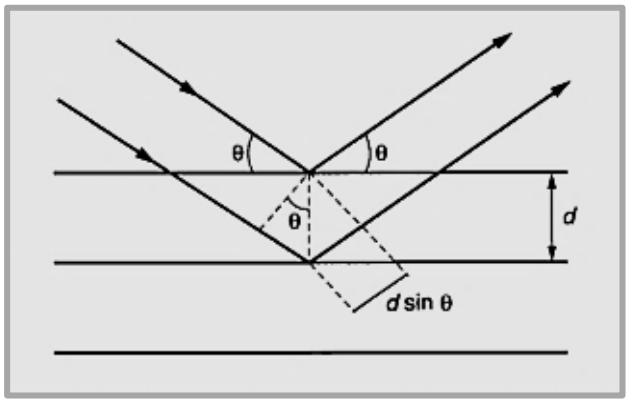


Figure 5.10 Illustration of Bragg's law

When the path length in the crystal (2d sinΘ) is a multiple of the wavelength then constructuve interference occurs and the diffracted intensity is obtained. In general the d spacing is a function of the lattice parameters (a.b.c) and angles (**α**,**β**,**γ**) defining the unit cell, and the Miller indices (h,k,l) denoting a particular relfection. It is the geometry of the crystal that determines the positions of the peaks in the diffraction pattern, so the more symmetric the mineral is, the fewer the peaks in the diffraction pattern. The intesities of the peaks are determined by rhe type and arrangement of the atoms within the crystal lattice.

The radiation used in a typical diffraction measurement contains several wavelengths denoted K$\boldsymbol{\alpha}_1$, K$\boldsymbol{\alpha}_2$, K**β** which are characteristic of the material producing the X-rays. The shorter the wavelength the more energetic and penetrating the radiation. Longer wavelengths spread out the peaks in the diffraction pattern, overcoming the line overlapping problem. Solid material can be either described as amorphous, that means the atoms are arranged randomly or as crystalline, where atoms are arranged in regular, repeating planes that form a three-dimensional structure. When a focussed X-ray beam interacts with these planes of atoms, part of the beam is transmitted, part is absorbed by the sample, part is refracted, and part is scattered (diffracted). The direction and intensity of

the diffracted beams depends on the orientation of the crystal lattice with respect to the incident beam. Thus X-rays are diffracted by each material (mineral) differently, based on what atoms make up the crystal lattice and their spatial distribution or arrangement in space. When an X-ray beam hits a sample and diffraction occurs, the distances between the planes of the atoms that constitute the sample can be measured by applying Bragg's Law.

5.3.8.2 Instrumentation

A basic powder diffraction system consists of an X-ray source, two circle goniometer (Θ and 2Θ cricles), sample stage, detector and a computer for instrument control and data analysis. In this research a D2 Bruker Powdered X-ray Diffractometer (Karlsruhe, German), using Cu Kα radiation (1.5418 Å) was used for the minerlogical composition. Rietveld refinement was also employed to estimate the average crystallite size of the minerals. The Eva code was used to identify the phases. The ochre samples were ground to powder and flatly packed on a sample holder before analysis. The scans were run for ten minutes for each sample.

5.3.7 Gas chromatography- Mass Spectrometry (GC-MS)

Gas chromatography (GC) is a technique used to perform dynamic separation and identification of all types of volatile organic compounds and several inorganic permanent gases. GC involves the partitioning of gaseous solutes between an inert mobile phase and a stationary liquid/solid phase. The major components of a GC include; the carrier gas, the injection port, the column, the detector and the data acquisition system which consist of an electrometer and an integrating device.

The carrier gas carries the sample through the system. The gas is usually helium, nitrogen, hydrogen, air or a mixture of argon and methane. Choice of gas used depends on the application and type of detector used. For example the flame ionization detector (FID) requires a flame so it uses hydrogen and air to support the combustion. The injection port or GC inlet is the next major component of the GC system. The purpose of the GC inlet is to introduce the sample into the carrier gas stream. Several types of inlets and sample introduction techniques are available; however the most common type involves the injection of 1-3 μL of a

liquid sample into a heated inlet. The injection can either be manual or automated. The column is responsible for the separation of the components in the sample mixture and the narrow the diameter the greater the column's separation efficiency or peak sharpness.

In this study a mass selective detector was used. In this detector the molecules are bombarded with electrons producing ion fragments that pass into the mass filter. The ions are filtered based on their mass/charge ratio. GC-MS provides excellent qualitative identification of the components by matching the compounds mass spectrum with spectra included in the libraries that are part of the system. To use GC-MS the organic components must be in solution for injection into the gas chromatograph. The solvent must be volatile and organic.
An Agilent technology 7890A (GC system with an auto sampler) interfaced with a LECO® GC X GC TOFMS Pegusus 4D system (LECO Corporation Michigan, USA) (Right on Figure 5.11), was used to identify and quantify unknown semi-volatile and volatile organic compounds in the complex mineral matrices.

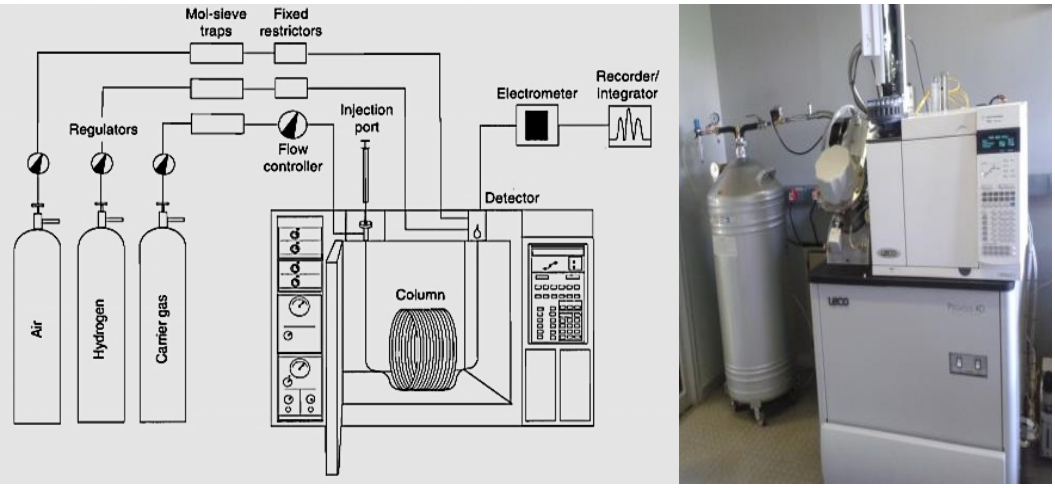


Figure 5.11 Schematic of gas chromatograph (left) (Image adapted from: Settle 1997); GC system interfaced with an MS detector (right) (University of Johannesburg)

The operating conditions and parameters are shown below in Table 5.3.

Table 5.3 Operating conditions for GC-MS

Component	Parameters
Column	RXi-5Si MS fused silica column (Restek chromatography products, USA)
Length	30 m
Inner diameter	0.25 mm
Thickness of stationary phase	0.25 µm
Temperature range	-60 to 350 ^{o}C
Carrier gas	Helium
GC inlet	Split mode
Injection volume	1 µL
Flow rate	1 ml/min
Run time	20 min
Temperature range	50 to 250 ^{o}C

5.4 Chemicals

The following solvents were used to extract the organic compounds from the ochre and roof spall samples: hexane, methanol, chloroform and dichloromethane (Sigma-Aldrich, Johannesburg, South Africa). The following acids were used for the disruption of the soil and ochre matrices during the microwave assisted digestion procedure: HCl, HNO_3, HF and H_3BO_3. Analytical grade reagents mostly from Merck (Darmstadt, Germany) were used. Deionized water was prepared from the Millipore instrument (Massachusetts, USA).

5.4.1 Solution preparation for digestion

Table 5.4 lists the commonly used solutions for wet digestion

Table 5.4 Frequently used solutions for complete dissolution of the matrices

Reagents	Sample Type
Water	Soluble salts
Dilte acids	Dry-ashed sample residues, easily oxidized metals and alloys, salts
Concentrated acids (HNO_3)	Less radily oxidized metals and alloys, steels, metal oxides
Concentated acid with added oxidizing agent	Metals, alloys, soils, particulates from the air, refractory minerals, vegetable matter
Hydrofluoric acid	Silicates and other rock samples

(Extracted from: Mitra, S. Sample preparation techniques in analytical chemistry)

A sample mass of 0.250 g was weighed into the vessel liner then an Aqua-Regia solution of HNO_3: HCl (ratio of 1:3) was used [i.e. 9 ml of HCl (32%): 3 ml of HNO_3 (65%)] with 1 ml of HF (40%). The vessel liner caps were then replaced and the vessels placed in the jacket then mounted onto the rotor. The vessels were allowed to cool down and taken out. Boric acid (4% v/v) was prepared by dissolving 40 g of boric acid (H_3BO_3) with hot deionised water in 1000 ml volumetric flask and diluted to the mark.

To complex with the excess fluoride ions, 6 ml of the boric acid was added. The samples were then filtered and poured into 50 ml centrifuge tubes and brought to volume with deionised water. Analysis was done using ICP-OES/MS.

5.4.2 Solutions and procedures for ultrasonic assisted extraction

The extractable organic compounds present in the sample matrices (together with their polarities) were not known, hence a range of solvents with different polarities were used. The solvents used are listed below in their order of increasing polarity:

Methanol> chloroform> dichloromethane> hexane

The samples were weighed into weighing bottles then the corresponding volume of the solvent was pipetted. The bottles containing the solutions were then placed

into a beaker half filled with deionised water then located in the ultrasonic extraction bath for the duration of the extraction (in 15 minute intervals). The extracts were then filtered using hydrophilic or hydrophobic syringe filtering disks. The resulting filtrates were placed in 1.5 ml auto samplers and the caps were sealed with parafilm to avoid the evaporation of the solvents. The extraction conditions are shown in Table 5.5.

Table 5.5 Extraction conditions for GC-MS analysis

Sample Mass (g)	Solvent	Solvent volume (ml)	Extraction time (min)
0.150	Hexane	2	60
0.150	Chloroform	2	60
0.150	Methanol	2	60
0.150	Dichloromethane	2	60

5.5 Quality assurance

A number of factors were taken into account to ensure good quality results. For the identification and determination of organic compounds on the GC-MS weighing bottles were thoroughly cleaned with soap and deionised water and dried. They were then rinsed twice with the respective organic solvent. For microwave assisted digestion, glassware and Teflon tubes were cleaned with soap, rinsed with tap water and deionised water and dried. Samples and reagents were weighed on the analytical balance and the mass was read to 3 decimals places. High precision micro-pipettes were used for preparation of solutions. Blank samples were used to check for any possible contamination. Extractions were done in triplicates and each extract was also analysed in triplicates. For trace elemental analysis three blank samples were prepared and analysed with the rest of the samples. Samples were analysed in triplicates to assess the repeatability and reproducibility of the analysis.

5.5.1 Analytical figures of merit

5.5.1.1 Method of limit of detection

The Limit of detection (LOD) is the lowest analyte concentration which can be detected by the instrument used (Armbruster *et al.*, 2008). This was calculated using the following formula (Hutter, 2011):

$$\text{LOD} = 3 \times \text{standard deviation of the blank sample} \quad (5.2)$$

5.6 Statistical data analysis

5.6.1 Multivariate statistics

Multivariate statistical treatment of elemental data allows an understanding of the variance within the sample set and calculates probabilities for sample grouping (Popelka-Filcoff *et al.*, 2007). Data on major, minor and trace elements for the ochre samples were obtained to explore geochemical trends among the samples, through application of multivariate statistics with an aim to distinguish the sources.

5.6.1.1 Cluster analysis

Cluster analysis is frequently employed as an initial method to discern possible patterning or clustering in the elemental data. The term cluster analysis covers many methods used for classification of samples into meaningful groups. Clustering routines strive to classify the samples into chemically-related groups. These cluster routines are designed such that members of a group are alike and differ from members of other groups in the data set and are usually based on Euclidean distance (Popelka-Filcoff, 2006). Hierarchical cluster analysis forms clusters of related samples (Bishop and Neff, 1989). Similar samples are grouped together then the groups are linked together by similarity, and then grouping the remaining samples until all samples are related to each other through a dendrogram. This “tree-like” structure allows a one-dimensional visualization of how the samples are related to each other and to other clusters. Typical methods

for grouping samples include calculating the dissimilarity between objects by the squared Euclidean distance among others.

$$d\frac{2}{jk} = \frac{1}{n}\sum_{i=1}^{n}[Cij - Cik]^2 \qquad (5.3)$$

Squared Euclidean distance is defined above (equation 5.3), where the distance squared between samples j and k is calculated from the concentrations (C) of j and k. The value n represents the number of elements used in the analysis and behaves as a scaling factor (Glascock, Braswell and Cobean, 1998).

A clustering algorithm, or linkage, can be calculated by several methods, with the most common methods being single linkage, complete linkage, average linkage cluster analysis and Ward's method (Baxter, 1994). Single linkage combines samples by finding the two most similar samples in the data matrix. Complete linkage forms groups by combining a sample into a group where the sample is similar with all members of the group at some predetermined level. Average linkage is a combination of single and complete linkage, where samples are placed due to their similarity to members of the group as well as similarity to other samples in the matrix. Ward's method linkage finds the solution for the minimum variance in clusters (Aldenferder and Blashfield, 1984). Results of cluster analysis are generally plotted as a dendrogram, with linkage distance on the abscissa and the samples on the ordinate. Branches link the samples together to visually show group associations (Popelka-Filcoff, 2006).

5.6.1.2 Principle component analysis (PCA)

Principal components analysis (PCA) has three main functions: 1) to remove correlation between variables in the data set, 2) to transform data into a new set of axes that preserves the Euclidian distance between samples and where data variance can be observed, and 3) to reduce the number of variables necessary to describe most of the variance in the data (Glascock, 1992; Glascock, Braswell and Cobean, 1998; Baxter, 1995; Dunteman, 1989). The use of PCA assumes that the data has some structure and that this structure can be modelled. It also presumes

that the reduction of dimensions can lead to data interpretation without significant loss of information. In addition, the use of PCA in this study has a fundamental assumption that group separation has a chemical origin. If elements are correlated (e.g. rare earth elements), transformation into PC space allows a way to differentiate the elements and visually identify any groups (Baxter, 1994). The reduction of variables (elements) in PC space is important as a few principal components can be used to explain the same data in a few dimensions which is easier to conceptualize than 30 or more elemental variables measured in this study (Baxter, 1994). Displaying the samples in principal component (PC) space helps to identify patterns or groups within the data. Principal components are essentially linear transforms of the variables that maximize the geometric distance between samples. The first PC describes the maximum variance; the second PC describes the remaining variance after removing the first PC and is orthogonal to the first PC, and so on throughout the number of PCs in the data set (Bishop and Neff, 1989).

The equations describing the transformation are:

$$P1 = a_{11}X + a_{21}Y + a_{31}Z + ... + a_{i1}Q \quad (5.4)$$
$$P2 = a_{12}X + a_{22}Y + a_{32}Z + ... + a_{j2}Q$$

Where the coefficients aij are used as the linear transform to arrive at the PC values in PC space, and X, Y, Z represent the elements (variables). The coefficients can then be applied to any sample, and then the sample can be plotted as a point in a graph of PC2 vs PC1 (Baxter, 1994). Another advantage of PCA is that the analysis maintains the original variation in the data set (Neff and Glascock, 1995).

5.6.1.3 Pearson's linear correlation

Pearson's correlation test is done in order to determine whether a relationship exists between two quantitative variables of a sample; i.e. if they can be correlated.

The type of correlation is classified by observing the effect of one variable on the other. For example if one variable increases what happens to the other variable.

- In a positive correlation, while the one variable increases the other variable also increases.
- In a negative correlation, when the one variable increases – the other variable decreases.
- In a no correlation situation the one variable will increase while the other variable neither increases nor decreases.

The Pearson's correlation coefficient is a statistical measure of the strength of the linearity between two quantitative variables. In a sample, the coefficient is denoted by r and is calculated as follows:

$$r(x,y) = \frac{n\sum(xy) - (\sum x)(\sum y)}{\sqrt{[n\sum x^2 - (\sum x)^2][n\sum y^2 - (\sum y)^2]}} \quad (5.5)$$

Where r has the following constraint:

$$-1 \leq r \leq 1$$

Also, any positive values denote positive linear correlation, whereas negative values denote negative linear correlation and a value of 0 denotes no linear correlation. The closer the value is to 1 or –1, the stronger the linear correlation.

CHAPTER SIX

Results and discussion

This chapter commences with the results obtained from the physico-chemical characterisation of Blombos Cave sediments profile. The findings for this investigation are discussed with relevant aid from literature and conclusive deductions are made. Results from the characterisation of the 100 ka ochre processing toolkit conclude this chapter. Covered in these results is the geochemical, elemental and organic residue analysis of the toolkit as well as the statistical treatment of the elemental data. The findings are discussed and with the aid of literature, conclusions are made. The techniques used in this study included pH and EC measurements, CHNS analysis, FT-IR, ICP-OES/MS, ED-XRF, PXRD and GC-MS.

6.1 Physico-chemical characterisation of Blombos Cave sediments profile: A preliminary study

Humans inhabit a site then leave buried remains of their existence and of their activities (ash, plants, animal remains, bone, stone tools, and manufacturing by-products). After burial these remains are affected by weathering and diagenetic processes then over time become part of the sediment matrix. This results in the alteration of the composition of sediments. The chemical composition of sediments at sites where there was human occupation preserves information on changes brought by the human activities. (Groenman van Waateringe and Robinson, 1988; Retallack and Wright, 1990; Retallack, 2000).

A physico-chemical characterisation of the sediments from Blombos Cave was done as a preliminary study. The primary objective for this investigation was to determine the degree to which past human activities leave detectable chemical residues in the sediments. Physico-chemical techniques (such as multi-element analysis) were used for the identification and interpretation of human activity areas within the sediments profile at the prehistoric site.

6.1.1 Soil pH and electrical conductivity measurements of the sediments

The pH and electrical conductivity (EC) measurements for the sediments are illustrated in Figure 6.1.

The sediment pH for the site varied upon moving down the profile depth, with values ranging from 7.4 to 9.4. According to Braadbaart, Poole and van Brussel (2009) relative alkaline conditions exist for example in shell-rich soils, pyroclastic layers of volcanic ash, and ash from ancient hearths especially where wood, bone, peat and cow dung had been used as a fuel.

The layers from the M1 phase had low pH values (7.4-8.4) when compared to the rest of the profile. Although this phase endured heavy human activity during the Still Bay industry, the shell density (17.5 kg m^{-3}) was found to be the lowest of all the MSA phases in the profile thus the less alkaline pH.

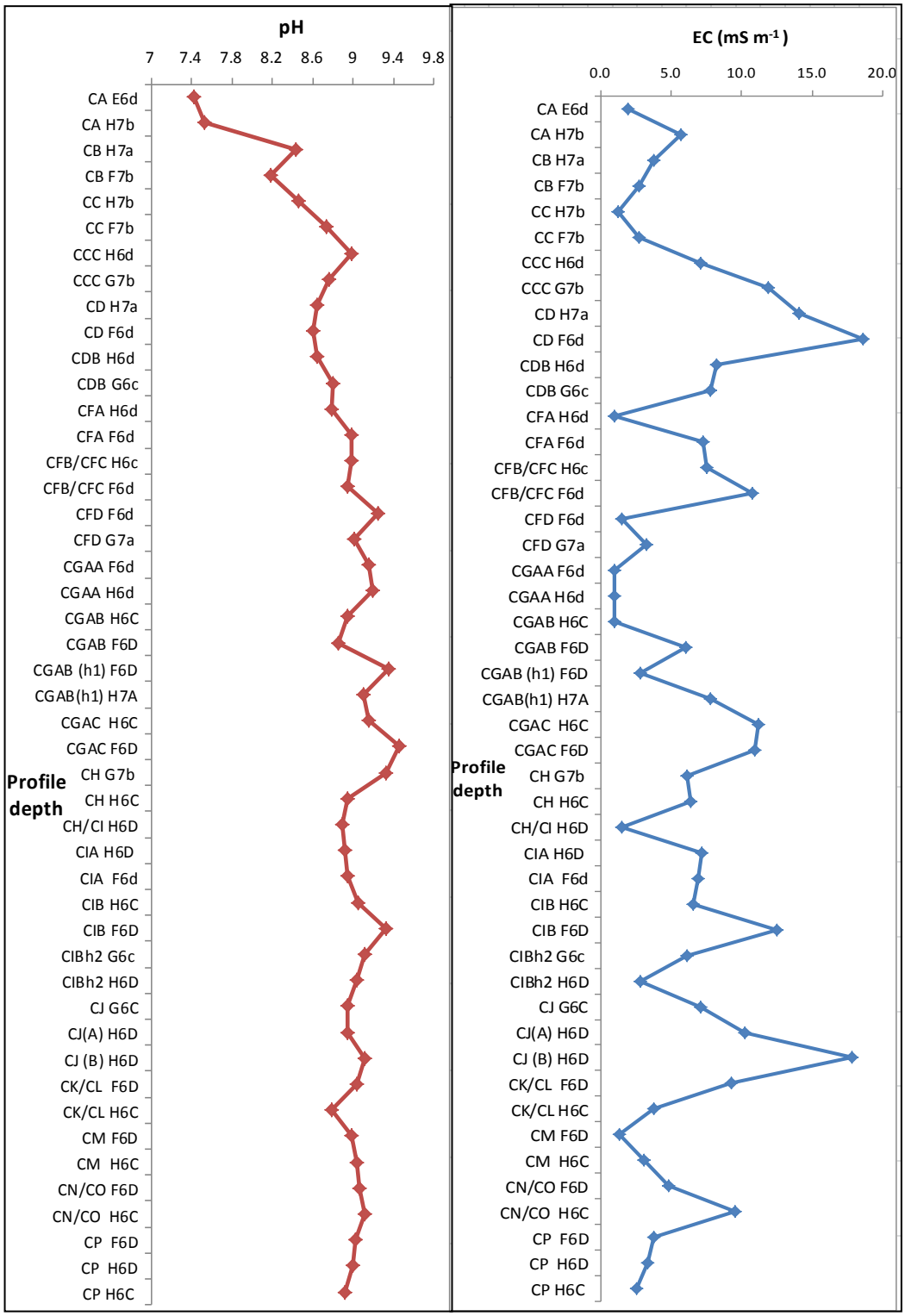


Figure 6.1 pH and EC measurements for the sediment profile

Moving down to the lower layers, the pH tended to increase steadily. Since the M2 phase was typified by large hearths as well as great shell quantities, it consequently followed that the soil pH will peak (9.4). pH levels decrease slightly when continuing down to the M3 phase. This part of the profile was rich in shell and ochre remains with a few hearths. The elevated pH (9.3) for the M3 phase was unsurprisingly due to the hearth from the CIB layer. The CK/CL layer had the lowest pH value for this phase.

Sediment pH at an archaeological site provides means of evaluating the preservation potential of artifacts. Highly acidic (low pH) soil causes the breakdown of organic materials like hide and bone. Hence the absence of these artifacts could be due to poor preservation conditions. Contrary, in highly alkaline sediments (for example the M3 phase) artifacts such as bone and shell remains are well preserved. Blombos Cave's formation is of calcarenite dune implying it is calcium carbonate ($CaCO_3$) rich hence the sediment matrix is naturally alkaline. However, heavy human occupation and other factors have caused an increase in the pH. For example snail shells or valves are largely present in the archaeological deposits at Blombos Cave. The $CaCO_3$ in these valves forms a matrix that is able to neutralize hydronium ions (H^+) in the sediments, in this way the pH of the sediments is buffered. As a result this produces ideal conditions for the preservation of bone and dental remains in the shell- containing deposits (Weiner, 2010). Also the presence of wood ash and charcoal elevates pH values in sediments (Weide, 1966).

There exists a direct correlation between the pH and the EC for the occupation layers at Blombos Cave (evident in Figure 6.1). For example, the CK/CL layer which had the lowest pH also had the lowest EC when compared to the other layers of the M3 phase, ditto for the CA layer of the M1 phase. The concentration of the cations in the sediments strongly influences pH because as the cation content increases, the pH increases (i.e. increase in alkalinity) (Birkeland, 1999). Prolonged or intense occupation results in the release of more cations to the sediment matrix, hence the pH of dense or intensely occupied sites, tends to be

higher (Carr, 1982). Generally the pH and EC for the darker coloured layers (for example GCAC) was high.

Electrical conductivity (EC) is useful in measuring the amount of dissolved salts in the sediments. Alkaline and calcareous sediments are dominated by the presence of exchangeable Ca^{2+}, K^{+}, Mg^{2+} and Na^{+}. The accumulation of these soluble salts (generally from heavy human activity such as fire use) results in a high soil EC (Holliday, 2004). The soluble nature of K makes it susceptible to leaching resulting in a lack of potassium (K) (commonly known as potash deficiency) in certain layers. Sodium (Na) was present in very low quantities throughout the layers, this can also be attributed to leaching which may have occurred over the years (Middleton and Price, 1996).

Figure 6.2 shows the different EC ranges used to classify sediment types.

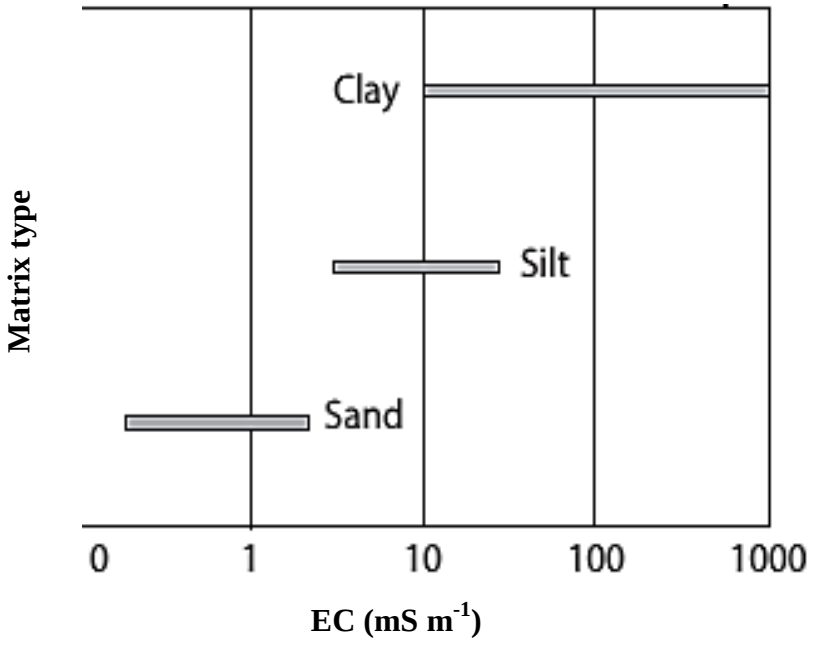


Figure 6.2 EC ranges for typical sediment matrices (Image adapted from: College of agriculture and life sciences, Virginia state university).

Sandy sediments have a low conductivity, silts have a medium conductivity, and clays have a high conductivity. This implies that EC is strongly correlated with the particle size and texture of the sediments. The EC values for the layers ranged

from 1.0 to 18.6 mS m^{-1}. This very well suggests that the layers were sand (for example CGAA), silt (CIA) and mixtures of silt and clay (CDB). According to Datnoff *et al.* (2007) potash deficiency is common in lime-rich ($CaCO_3$) sediments with low clay content so in relation to Figure 6.2 such sediments are sandy or silty and have a low EC.

When performing sediment analysis it is imperative to consider the complexity of these systems. Elements may exist in different ways within sediments matrices, for example as minerals or complexes with organic matter. Hence one needs to account for the vast chemical behaviours of different elements in the sediment matrix due to the pH, redox potential and electrical conductivity (Bohn *et al.*, 1985).

6.1.2 Identification of human occupation and activity areas by CHNS analysis

The total C content was determined for selected occupation layers from the M2 and M3 phases. These layers were specifically analysed because they contained large amounts of shell, bone, hearth and ash deposits, which are good sources of excess C in the soil. The C content from each of the selected layers is shown in Figure 6.3.

The overall C levels were higher for the layer from the M2 phase (CFD, CGAB and CGAC) when compared to those from the M3 phase (CJ, CN/CO and CP). The M2 phase is typified by carbonised deposits while the M3 phase is dominated by shell and bone middens. Consequently the M3 phase has a higher shell density (68.4 kg m^{-3}) when compared to the preceding M2 and M1 phases (with shell densities of 31.8 kg m^{-3} and 17.5 kg m^{-3}, respectively). According to Outcalt and Kennard (2008) the increased decomposition activity that occurs after burning activities, results in increased levels of readily decomposable C, increased pH and the conversion of sediment nutrients to soluble forms.

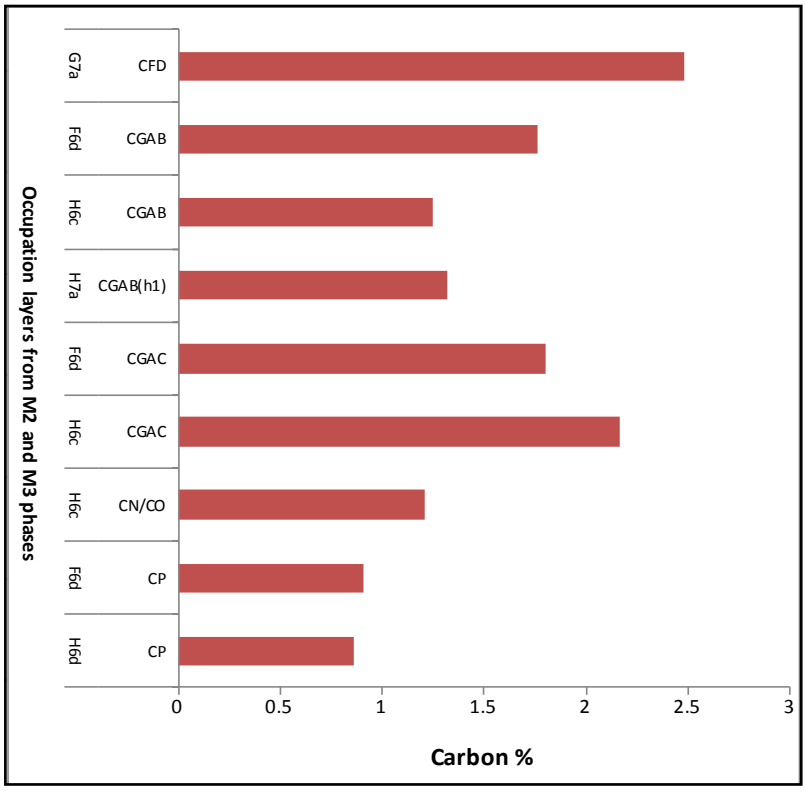


Figure 6.3 Carbon content for the occupation layers of the M2 and M3 phases

Wattez (1988, 1992), reported that different burning intensities can produce colour variations in wood ash. While moderate temperature burning produces yellow or brown-coloured ashes, high temperature heating produces more typical grey or white ashes. This means that the white ashy CFD layer may have resulted from high intensity burning of wood during habitation, thus the increased C levels (Bethell and Màtè, 1989; Rottlander 1983). From Figure 6.3, it can be deduced that the layers which endured heavy burning activities (for example, CGAC, marked by a darker colour) contribute more to the increased levels of C in the soil than those which just contained bone and shell remains (for example, CP).

6.1.3 Identification of human occupation and activity areas by multi-element characterisation

Multi-element analysis of soil and sediment samples has become popular due to the technique's quick and relatively cheap capacity (Wilson, Davidson and

Cresser, 2007). As a result several authors have reported on the use of ICP-OES during archaeological investigations of sediments. This is often done to confirm human occupation and to interpret the use of space by the former occupants of the site (Middleton and Price, 1996; Parnell *et al.*, 2002; Knudson *et al.*, 2004; Sullivan and Kealhofer, 2004; Cook *et al.*, 2005).

ICP-OES/MS were the techniques used for the multi-element analysis of the sediments at Blombos Cave. The analysis gave total concentrations of the major, minor and trace elements. Table 6.1 illustrates the bio-essential major and trace elements used in this study to interpret prehistoric human occupancy and activities at the site.

Table 6.1 Bio-essential major and trace elements considered in the interpretation of human activities at Blombos Cave

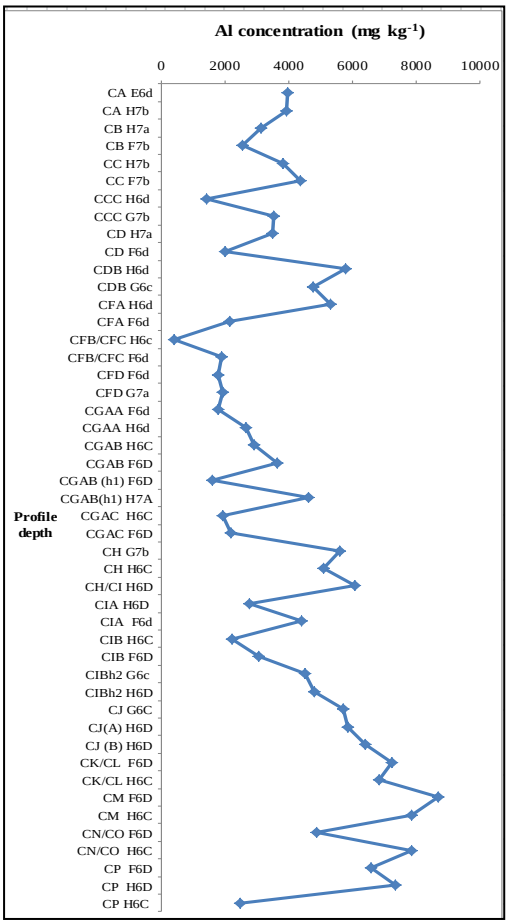
Major and trace elements
Fe (iron)
Al (aluminium)
K (potassium)
Mg (magnesium)
Na (sodium)
Cu (copper)
Pb (lead)
Th (thorium)
Co (cobalt)
V (vanadium)
Cr (chromium)
P (potassium)
C (carbon
S (sulphur)

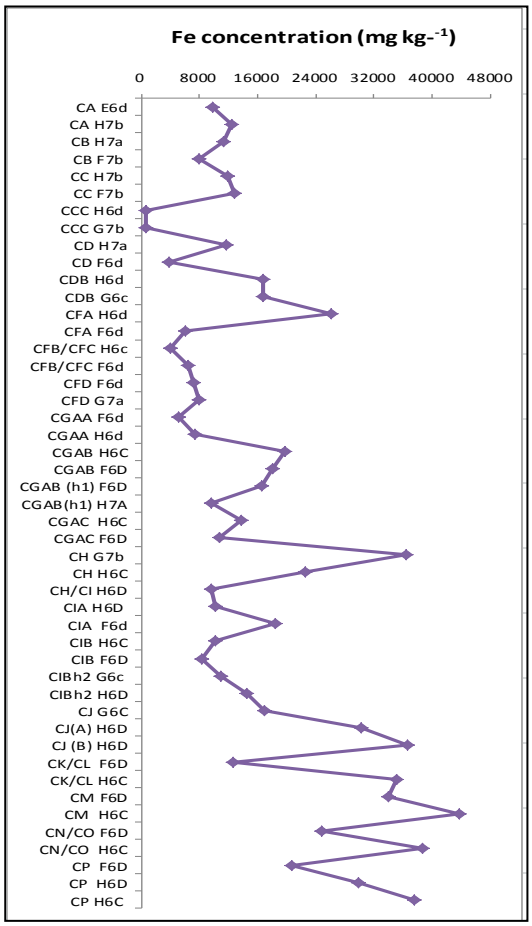
Figures 6.4-6.5 show how the major, minor and trace elemental content varies through the profile depth. Figure 6.4 shows variations for major, minor and trace

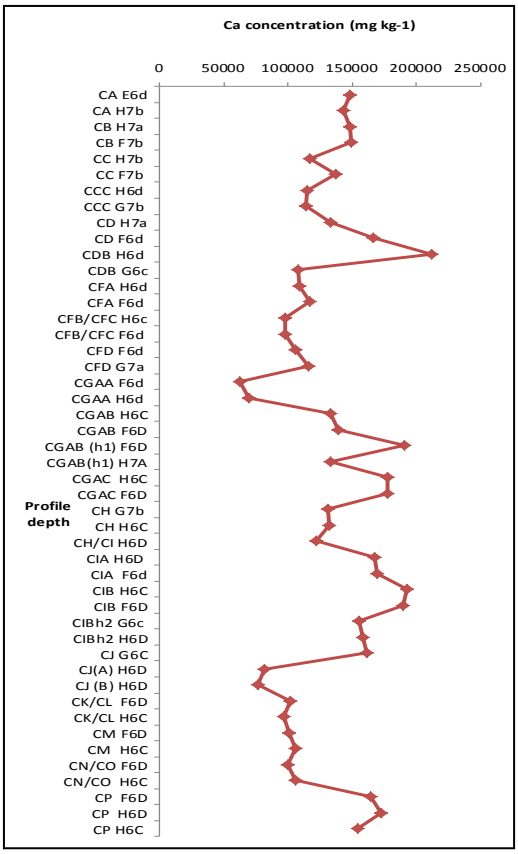
elements detected by the ICP-OES (as mg kg^{-1}) while Figure 6.5 illustrates variations for trace elements detected by ICP-MS (as µg kg^{-1}).

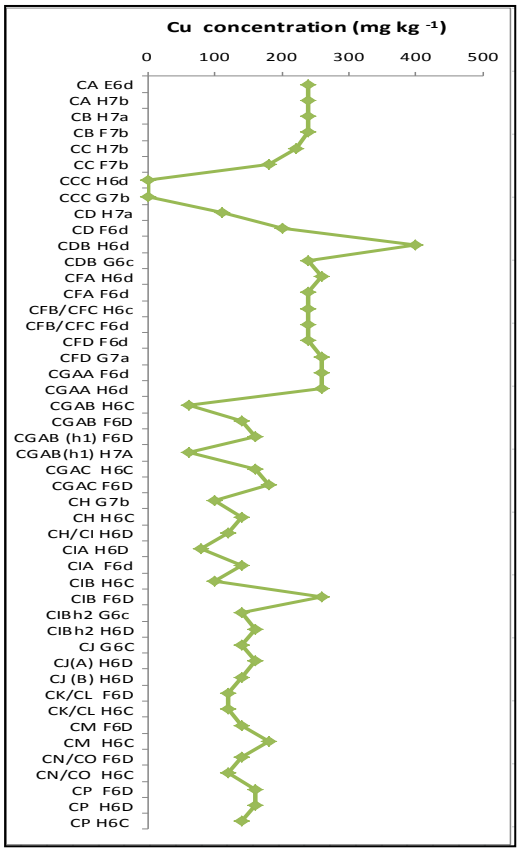
There was a fluctuation in the elemental content when proceeding down the profile depth (as indicated by Figures 6.4 and 6.5). The discussed results are grouped according to the MSA phases, that is the M1, M2 and M3 phase. Figure 1.2 in section 1.2 illustrates the sediments deposit profile at Blombos Cave also highlighting the stratigraphic units which make up the MSA phases.

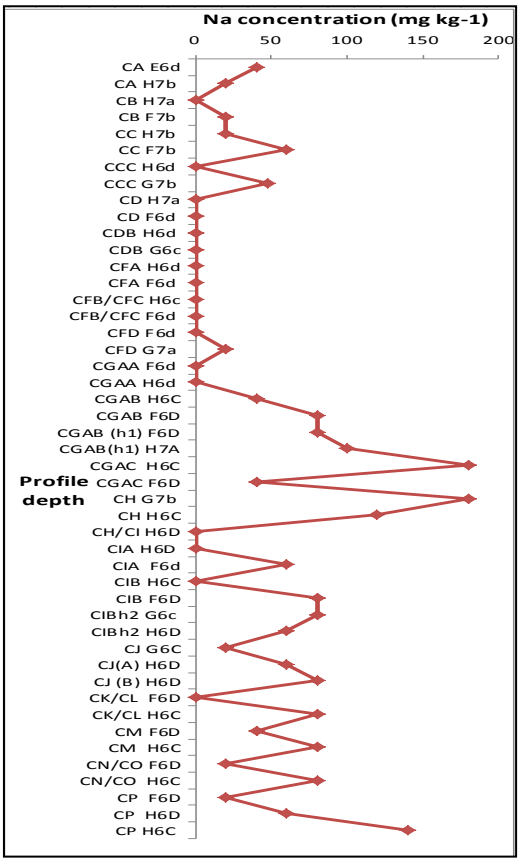
Generally, the Ca content was high through the entire profile this could be due to a number of reasons, namely: heavy human induced activities on the site, calcium rich sediments and bone weathering (Carr, 1982).

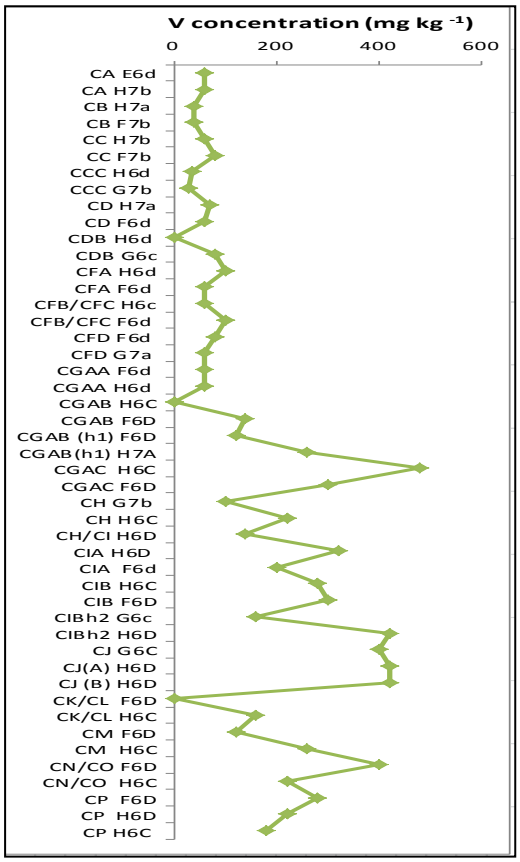





Ca concentration (mg kg-1)
0
50000
100000
150000
200000
250000
Profile depth
CA E6d
CA H7b
CB H7a
CB F7b
CC H7b
CC F7b
CCC H6d
CCC G7b
CD H7a
CD F6d
CDB H6d
CDB G6c
CFA H6d
CFA F6d
CFB/CFC H6c
CFB/CFC F6d
CFD F6d
CFD G7a
CGAA F6d
CGAA H6d
CGAB H6C
CGAB F6D
CGAB (h1) F6D
CGAB(h1) H7A
CGAC H6C
CGAC F6D
CH G7b
CH H6C
CH/Cl H6D
CIA H6D
CIA F6d
CIB H6C
CIB F6D
CIBh2 G6c
CIBh2 H6D
CJ G6C
CJ(A) H6D
CJ (B) H6D
CK/CL F6D
CK/CL H6C
CM F6D
CM H6C
CN/CO F6D
CN/CO H6C
CP F6D
CP H6D
CP H6C


Cu concentration (mg kg -1)
0
100
200
300
400
500
CA E6d
CA H7b
CB H7a
CB F7b
CC H7b
CC F7b
CCC H6d
CCC G7b
CD H7a
CD F6d
CDB H6d
CDB G6c
CFA H6d
CFA F6d
CFB/CFC H6c
CFB/CFC F6d
CFD F6d
CFD G7a
CGAA F6d
CGAA H6d
CGAB H6C
CGAB F6D
CGAB (h1) F6D
CGAB(h1) H7A
CGAC H6C
CGAC F6D
CH G7b
CH H6C
CH/Cl H6D
CIA H6D
CIA F6d
CIB H6C
CIB F6D
CIBh2 G6c
CIBh2 H6D
CJ G6C
CJ(A) H6D
CJ (B) H6D
CK/CL F6D
CK/CL H6C
CM F6D
CM H6C
CN/CO F6D
CN/CO H6C
CP F6D
CP H6D
CP H6C


Na concentration (mg kg-1)
0
50
100
150
200
Profile depth
CA E6d
CA H7b
CB H7a
CB F7b
CC H7b
CC F7b
CCC H6d
CCC G7b
CD H7a
CD F6d
CDB H6d
CDB G6c
CFA H6d
CFA F6d
CFB/CFC H6c
CFB/CFC F6d
CFD F6d
CFD G7a
CGAA F6d
CGAA H6d
CGAB H6C
CGAB F6D
CGAB (h1) F6D
CGAB(h1) H7A
CGAC H6C
CGAC F6D
CH G7b
CH H6C
CH/Cl H6D
CIA H6D
CIA F6d
CIB H6C
CIB F6D
CIBh2 G6c
CIBh2 H6D
CJ G6C
CJ(A) H6D
CJ (B) H6D
CK/CL F6D
CK/CL H6C
CM F6D
CM H6C
CN/CO F6D
CN/CO H6C
CP F6D
CP H6D
CP H6C


V concentration (mg kg -1)
0
200
400
600
CA E6d
CA H7b
CB H7a
CB F7b
CC H7b
CC F7b
CCC H6d
CCC G7b
CD H7a
CD F6d
CDB H6d
CDB G6c
CFA H6d
CFA F6d
CFB/CFC H6c
CFB/CFC F6d
CFD F6d
CFD G7a
CGAA F6d
CGAA H6d
CGAB H6C
CGAB F6D
CGAB (h1) F6D
CGAB(h1) H7A
CGAC H6C
CGAC F6D
CH G7b
CH H6C
CH/Cl H6D
CIA H6D
CIA F6d
CIB H6C
CIB F6D
CIBh2 G6c
CIBh2 H6D
CJ G6C
CJ(A) H6D
CJ (B) H6D
CK/CL F6D
CK/CL H6C
CM F6D
CM H6C
CN/CO F6D
CN/CO H6C
CP F6D
CP H6D
CP H6C

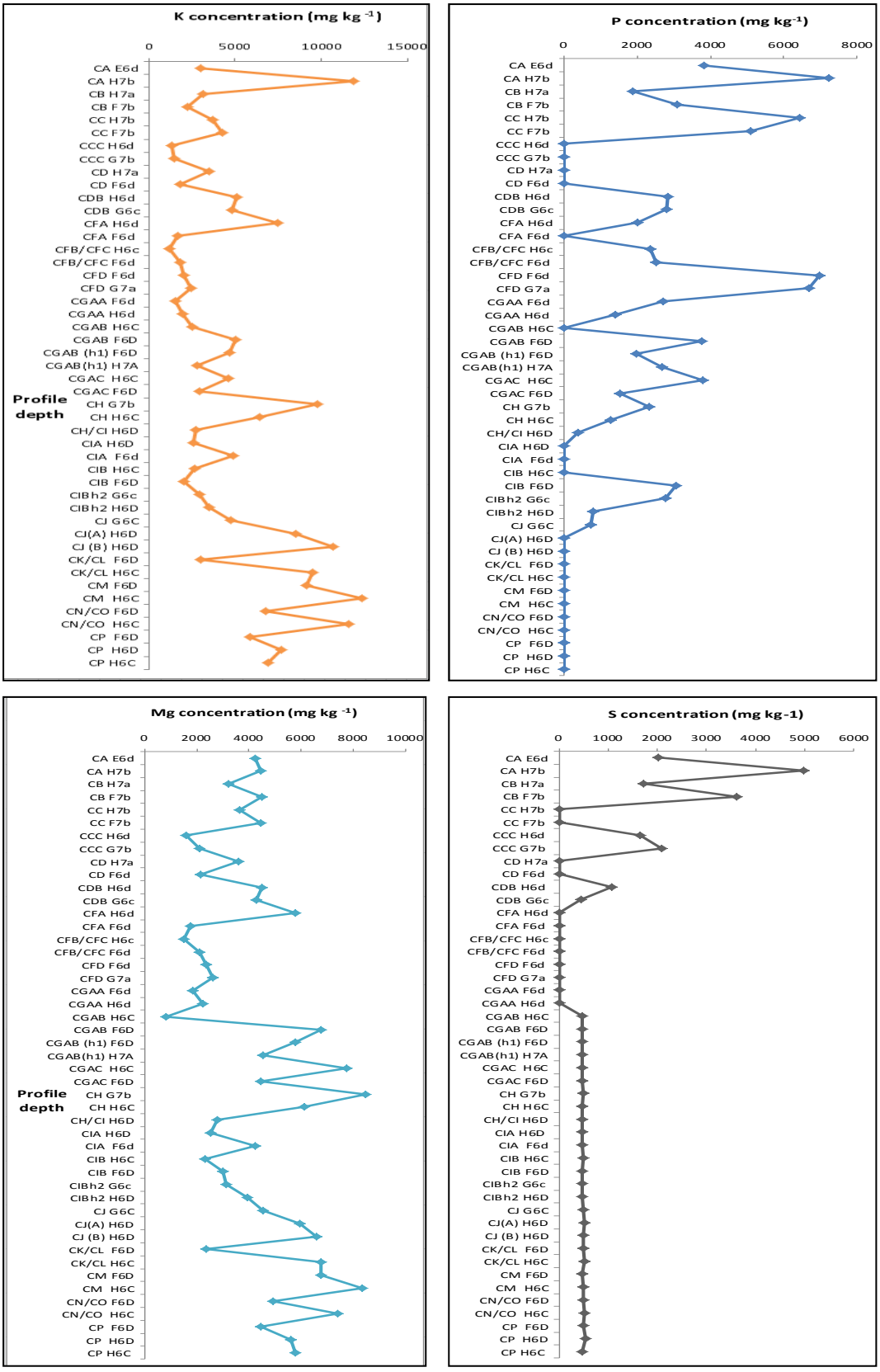


Figure 6.4 Variations in trace elemental content down the profile depth at Blombos Cave

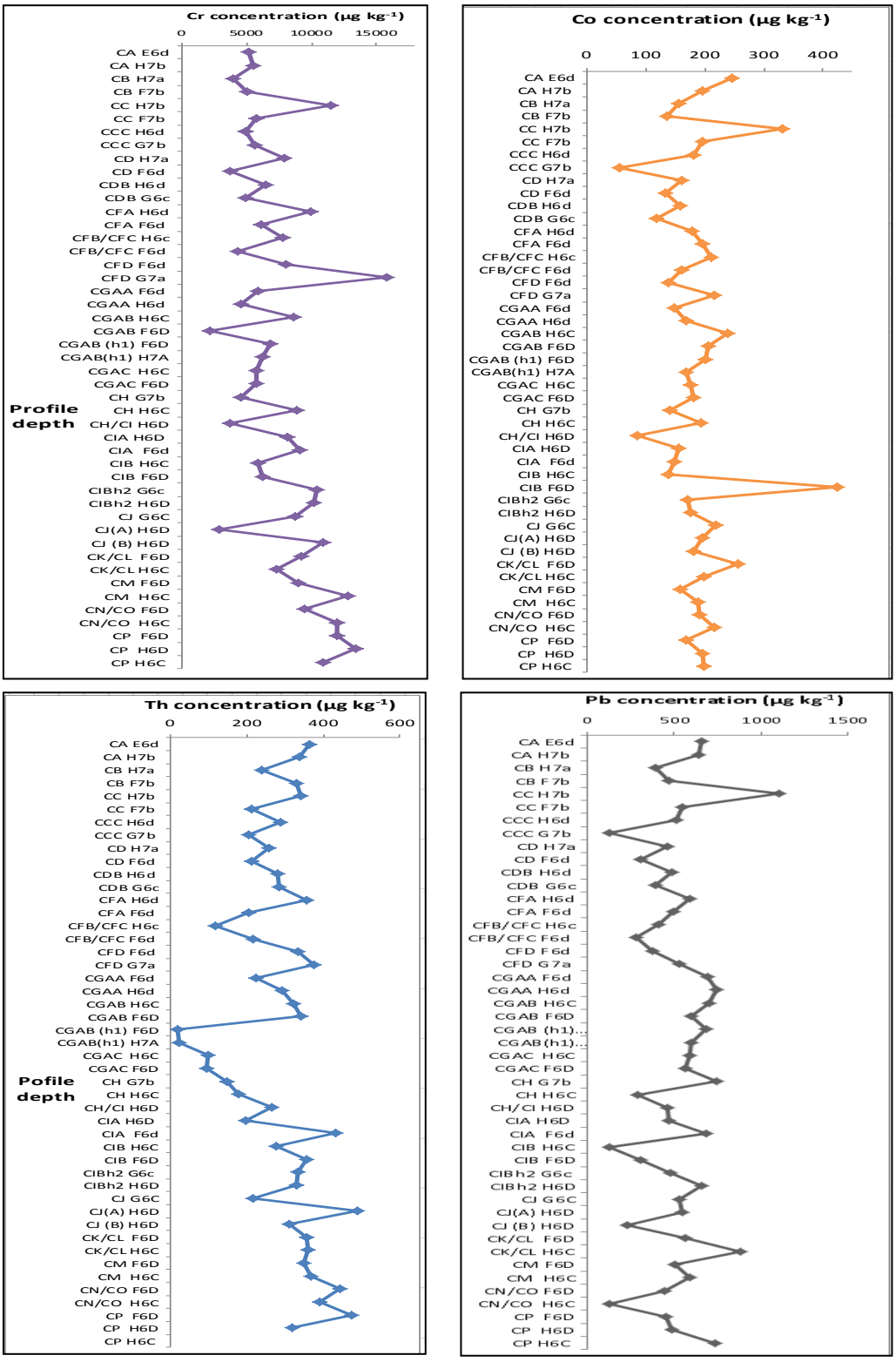


Figure 6.5 Variations in trace metal content down the profile depth at Blombos Cave

6.1.3.1 M1 phase (units CA-CDB)

In this phase, P, Al, Fe, Mg, S and K were observed to be present in high quantities. As mentioned in section 1.2, the M1 phase constituted of a large number of artifacts including the Still Bay type bifacial stone points, bone tools, marine shell beads, and engraved ochre. Further, the dark coloured layers confirm prolonged human activities during this period of occupation. The most common chemical elements affected by human activity are C, N, K, Na, P, and Ca, with lesser; amounts of Mg, S, Cu, Zn, and other metals (Cook and Heizer, 1965; Eidt, 1984). However, P is less susceptible to leaching when compared to most of these elements (Carr, 1982). Also, extended human occupation of an archaeological site, results in the accumulation of anthropogenic P becoming larger then natural P in the soil (Holliday and Gartner, 2007).

Elements like P, K, Mg and Ca are good indicators or markers of *in situ* burning or heating (Wilson, Davidson and Cresser, 2009). These elements become incorporated in the humus of the soil hence an anomalous increase of these elements in an archaeological site is indicative of the past use of the area (Carr, 1982). According to Schmidt *et al.* (2015), the heat treatment of silcrete, in order to produce stone tools, was conducted directly over an open fire using wood. The element K is a useful indicator for intense fire use because it can be integrated into the soil from wood ash (Middleton and Price, 1996). In this phase the amount of K remained high, confirming the notion put forth by Schmidt *et al.* (2015) that the heat treatment process involved the burning of wood. The burning of wood also increases Mg concentrations (Heidenreich and Navratil, 1973). Consequently increased levels of this element were observed in the M1 phase sediments.

The use of bone as a fuel source is known from historic and ethnographic case studies and has usually been suggested in relation to wood scarcity during the Palaeolithic (Théry-Parisot, 2002; Schiegl *et al*., 2003 and Niven, 2007).

Bone can be used in addition to wood as fuel because of its particular characteristics. Bone increases the combustion time of fires and also produces more light than wood during its burning process. In prehistoric (northern) environments, bone could have been used as a light source in dwellings

(Vaneeckhout *et al*., 2010). The evidence of a large amount of fragmented bone remains very well implies that bone was also burnt, thus contributing to the increase of P, K, Ca and Mg in the sediments.

Soil pH affects the availability of phosphorus (P), in acidic soils P combines with Fe and Al while in alkaline soils most of the P exists in the form of insoluble calcium compounds such as apatite ($Ca_5(PO_4)_3(F,Cl,OH)$) (Holliday and Gartner, 2007). This makes P immobile in soil (not leached). Cook and Heizer (1965) proposed that in basic soils Ca and P distinguish areas with high bone (high in P) from areas with high shell density (high Ca). As reported in section 6.1.1, the sediments at Blombos Cave are alkaline hence the elevated P levels (apart from the excessive use of heating techniques by the site occupants) can also be attributed to the insoluble calcium compounds formed in the sediments.

Table 6.2 illustrates the percentage distribution of ochre across the MSA phases at Blombos Cave.

Table 6.2 Percentage distribution of ochre raw material categories by frequency and mass across the MSA phases at Blombos Cave.

Phase	M1		M2		M3		Total *n*	Total g
	% *n*	% mass	% *n*	% mass	% *n*	% mass		
FGS	59.4	57.7	82.4	63.8	90.7	86.1	1306	4533.0
Sandstone	17.7	14.8	10.8	30.3	4.6	6.8	109	489.4
Haematite	18.1	16.8	6.8	5.9	3.6	6.1	95	429.9
Other	4.7	10.8	0.0	0.0	1.0	0.9	24	128.7
Total %	100.0	100.0	100.0	100.0	100.0	100.0		
Total *n*	254		74		1206		1534	
Total g		821.4		182.22		4577.39		5581.0

*(extracted from Henshilwood *et al.*, 2009)

Table 6.2 indicates that the M3 occupation phase contained the highest number of ferruginous siltstone (ochre) pieces followed by the M1 phase. According to Goodall (2007), iron-oxides happen to be the most readily available minerals, and to southern African cave/rock shelter sequences, the use of red ochre (mainly composed of clays and hematite) is effectively abundant (Watts, 1999; Henshilwood *et al.*, 2001a; Wadley, 2005b; Rigaud *et al.*, 2006). It can be

inferred that red ochre was the preferred iron-oxide pigment and was easily accessed by the site occupants; this is supported by the high hematite and ochre masses found in the phases (as indicated in Table 6.2).

In the soil matrix Al often co-occurs with Fe (Wilson, Davidson and Cresser, 2009), hence the constant association between the two elements. When compared to the distribution in the mass of ochre pieces (all kind of raw materials), it can be said that the concentrations of Fe and Al are connected to the presence of micro-particles in the sediments due to the processing of red ochre (whether by striating of knapping ochre pieces).

6.1.3.2 Upper and lower M2 phase (layers CFA-CGAC)

Moving from the M1 phase to the M2 phase, a drop in the Fe, Mg, S and K levels can be observed. As a result of the low Fe content, Al subsequently dropped. The drop in Fe can be attributed to the low amounts of hematite recovered from this phase (illustrated in Table 6.2). The upper section (CFA-CFD) was typified by layers of carbonised deposits, large hearths, bone and shellfish. It also constituted of a few Still Bay bifacials and bone tools. Contrary the lower section (CGAA-CGAC) was short lived, with only a few basin hearths, one large hearth in the CGAC layer and no artifacts associated with the Still Bay bifacials. The presence of hearths implies a domestic fire feature during occupation, hence the peaking P concentrations in these layers.

Additionally the layer CFD constituted of white ash which explains the very high P concentration for that layer. However, K and Mg (also good indicators for burning activities) had low concentrations; this is justified by the fact that these elements (unlike P which leaves a prolonged chemical signature) are readily leached from the soil (Holliday, 2004).

6.1.3.3 M3 phase (layers CH-CP)

The high Fe concentration range observed for the lower layers of the profile is due to the abundant pigment assemblages (including the pigment processing toolkits) recovered from them. Al is correlated well with the increased Fe levels. The M3 phase is dominated by shell, bone, stone middens, high densities of ochre, hearths

and ash deposits. The hearths (CIB layer) and ash deposits increased the P, K and Mg while the shell middens resulted in large Ca levels.

6.1.3.4 Conclusion

The calcite ($CaCO_3$)-rich cave rock greatly contributed to the high Ca content in the sediments. Further, Aston *et al.* (1998) lists five ways of enriching soil with trace metals and elements as a result of prehistoric human activity: establishment of settlements, breeding of animals in enclosed areas, use of fire, ancient metallurgy and handicrafts (pigment production).

A large number of the bone remains from the MSA layers were fragmented with bones of larger ugulates and seal being more heavily fragmented. Post-depositional fragmentation was more severe in the M1 and upper M2 phase than in the lower M2 phase. This was attributed to more intensive occupations at Blombos Cave. According to Thompson and Henshilwood (2011) majority of the fragmentation occurred while the bones were in a fresh state; implying marrow extraction activities by the site occupants. The exploitation of bone marrow is a simple procedure; one breaks into the medullary cavity of a long bone or mandible. This will generally occur whilst the bone is still relatively fresh (Outram, 2002). The extracted marrow and fat was then used as a binder during the pigment production. Some of the broken and marrow-extracted bones were heated and used as fuel during seasons when wood was scarce while the other bones were deliberately engraved for symbolic intent.

Davies *et al.* (1988) reported that the production and use of pigments causes an elevation in the Cu and Pb concentrations in the soil, hence the high levels of Pb observed throughout the profile. And generally, the concentrations of trace elements like V, Co and Cr reflect the soil mineral composition and are not necessarily due to human inputs (Linderholm and Lundberg, 1994).

6.1.4 Differentiating between calcite origins using FT-IR spectroscopic analysis

FT-IR spectroscopy is a common and useful tool for studying organic and inorganic materials. It is rapid, requires very little material and can be operated on-site (Weiner and Goldberg, 1990). The ability of FT-IR to provide information on the extent of atomic order of the mineral phase (Farmer, 1974), was exploited in this study.

FT-IR spectroscopy and grinding curves (discussed in section 2.6.2) were used to determine whether the sediments from Blombos Cave were composed of anthropogenic, biogenic or geogenic calcite.

The three major IR absorption peaks which classify calcite are 713 cm^{-1} (ν 4, in-plane CO_3 bend), 874 cm^{-1}(ν2, out-of-plane CO_3 bend), and 1420 cm^{-1} (ν3, asymmetric CO_3 stretch) (White, 1974). When a calcite sample is ground, during sample preparation, grinding dependent changes are shown in the infrared spectrum. Further grinding, narrows the v3 peak and the heights of the v2 and v4 peaks decrease, when both are normalized to the v3 height.

The calcite spectra for the sediments (Figure C1 in appendix C) were obtained by running a search on the Weiner and minerals library. A macro (Thermo Fisher Scientific Inc OMNIC macro/basic, 2012) was then run to calculate the v2/v4 height ratio, the heights of the normalized v2 vs v4 peaks were then plotted to form the distinctive grinding curves for the calcites (Figure C44). These curves were used to deduce the origin of the calcite. The grinding curves of geogenic calcites have the shallowest slopes and highest v4 values when compared to pyrogenic calcites (Regev *et al.*, 2010).

The results from the FT-IR analysis of the sediments are presented in Table 6.3. The classification of the sediments according to their calcite origins is included in the table. The sediments were classified into three calcite groups; biogenic, geogenic and pyrogenic calcite

Table 6.3 Classification of the sediments according to calcite origin and the distribution of major elements in the sediments

MSA phases	Layers	Quadrates									
		E6b	F6d	F7b	G6c	G7a	G7b	H6c	H6d	H7a	H7b
M1 phase	CA (top)	Ca									Fe,K, P, Mg (BF)
	CB										
	CC			K, Mg, P							P,K,Mg
	CCC						Ca		Ca		
	CD									Fe, K, Ca, Mg (BF)	
	CDB				Fe,P, K,Mg				Fe, K, P, Mg		
M2 phase	CFA								Fe,K,P,Mg		
	CFB/CFC										
	CFD		P			P					
	CGAA										
	CGAB		P,Fe,K,Mg, Ca								
	CGAB (h1)		P,Fe,K,Mg, Ca							P,K,Mg,Ca	
	CBAC						P,K,Mg,Ca (BB)		P,K,Mg,Ca (BB)		
M3 phase	CH						Fe,P ,Mg,Ca K	K, Mg, Fe			
	CH/CI										
	CIA		Fe,K,Ca,Mg						Ca		
	CIB		P					Ca			
	CIB (h2)				Ca, Fe				P,Fe, Ca		
	CJ				P,Mg,Fe,Ca						
	CJ(A)								Fe,K,Mg		
	CJ(B)								Fe,K,Mg		
	CK/CL							Fe,K,Mg, Ca			
	CM		Fe,K,Mg					Fe,K,Mg			
	CN/CO		Fe					Fe, K, Mg			
	CP (bottom)		Fe					Fe,Ca	Fe,Ca		

Geogenic calcite: ochre/ geological material

Pyrogenic calcite: burnt animal bones or wood

Biogenic calcite: aragonite/ biological material

BB: burnt bone, BF: bone fossil

6.1.5 Conclusion

A physico-chemical characterisation of the sediments profile at Blombos Cave was done with an aim to determine the degree to which past human activities leave detectable chemical residues in the sediments. The investigations carried out showed a correlation between the elemental content, pH, EC, calcite origin (using FT-IR) and the colour of the sediments. The duration and intensity of occupation, the type of artifact recovered (for example bone or pigment-coated stone tools) and the physical state of the stratigraphic unit (for example, hearth or midden) influence the elemental content, pH, EC and the colour of the sediment deposits. The calcite origin is influenced by whether pyrotechnology was employed during the unit occupation or not. Typically darker deposits implied heavy human activity including the use of fire. As a result the amount of K, P, Mg, Ca and C, pH and EC were escalated. The calcite origin for such deposits was confirmed to be pyrogenic (orange shading in Table 6.3). The shell and bone midden-containing layers (with no evidence of fire use) had high levels of P, high Ca and low EC. The calcite origin for these deposits was geogenic (red shading in Table 6.3). The layers containing pigment assemblages were found to be either pyrogenic or geogenic, this depended on whether fire was used or not. An example would be the CC layer. Biogenic (green shading in Table 6.3) calcite was only observed in the more recent CA and CC layers. In conclusion, analysis of Blombos Cave sediments provided information on the activities carried out by the site occupants and the availability of resources (ochre and fauna).

6.2 Physico-chemical characterisation of a 100 ka ochre processing toolkit

The aim of this study was to carry out a physico-chemical characterisation of the 100 ka ochre processing toolkit recovered from the CP occupation unit.

6.2.1 Geochemical characterisation, differentiation and provenance of ochre

The geochemical characterisation of ochre was achieved by mineralogical analysis and elemental fingerprinting.

6.2.1.1 Mineralogical analysis of ochre using FT-IR and PXRD

FT-IR was used in the identification of the mineral composition of the CP layer ochre as well as determining the general matrix of the ochre. PXRD was employed as a complementary technique to confirm the mineral composition and determine the mineral phases. Presented in Table 6.4 are the mineralogical composition and the mineral phases identified for the ochre. PXRD and FT-IR analyses were limited by the availability of the sample quantity. Complete sets of diffractograms and IR spectra are included in appendix D as Figures D1 and D2, respectively.

From the data presented in Table 6.4, it can be inferred that the CP layer ochre were similar in their mineralogy; with quartz and kaolinite as the principle minerals. The general matrix of the ochre comprises of two components: the main chromophore which consists of the iron-oxide (hematite (Fe_2O_3) or goethite (α-FeO (OH)) and the accessory minerals, these can be clay minerals such as kaolinite ($Al_2Si_2O_5(OH)_4$) and illite [$K(Al_4Si_2O_9(OH)_3)$], carbonates such as calcite ($CaCO_3$) and silicates such as quartz (SiO_2) (Deer, Howie and Zussman, 1992).

It is noteworthy to point out that the clay mineral, kaolinite, was predominant in the ochre from the CP layer (evident in Table 6.4). This supposes a particular preference by the prehistoric site occupants for the clay mineral. Judson (1959) suggested that white kaolinite, which was found in late Palaeolithic excavations, was predominantly used as an extender pigment in a mixture with hematite in order to mix with colours such as those derived from hematite. Kaolinite is still being used as an extending pigment in the paint manufacturing industry; therefore clay extenders retain their importance until the present time (Lawrence, 1960).

Table 6.4 FT-IR and PXRD mineralogical characterisation of the material associated with the ochre processing toolkit

Layer	Quadrate	Plot number	Artifact number	Sample number	Sample type	Mineral composition/ phases
CP	G6D	O1	476		Ochre	Quartz, calcium phosate, kaolinite , hematite
CP	H6C	L23	519			Calcite, quartz
CP	H6C				Ochre flake	Quartz, kaolinite, hematite
CP/CPA	H6C					Calcite
CP	H6C	L28	527			Loess(Aeolian sand)/quartz
CP	H6C		477			Quartz
CPA	H6C		470		Mixture	Loess (Aeolian sand) quartz
CP	H6C				Pigment drop 1	Calcite
CP	H6C				Pigment drop 2	Calcite
CP	H6C	O7	506		Ochre 3	Quartz, hematite
CPA 1	H6C					Calcite
CPA2	H6C					Calcite
CP	H6C	O1	442	S1	Mastic	Calcite, quartz
CP	H6C	L9	438	S1		Quartz. kaolinite
CP	H6C	L24	520			Quartz, vermiculite/chlorite
CP	H6C	L26	524			Quartz, smectite
CP	H6C				Ochre 2	Quartz, kaolinite
CP	H6C	L1	416		Ochre	Quartz, kaolinite, muscovite/illite
CP	H6C	O9		S10	Ochre 6	Quartz, kaolinite
CP	H6C		509		Ochre 8	Quartz, montmorillonite, kaolinite,
CP	H6C	L30	529			Quartz, kaolinite, hematite, muscovite/illite
CPA	F6D			S1		Quartz, hematite
CPA	G6D				Ochre fragments	Quartz, hematite, muscovite/illite, anatase, kaolinite
CP	H6C	L20	514			Quartz, hematite, muscovite/illite, anatase
CPA	H6C	O2	470			Quartz, kaolinite, goethite, illite , muscovite
CP	H6C				Ochre 7	Quartz, hematite
CP	H6C	L35	534			Quartz, walrakite, kaolinite, vermiculite, hematite
CP	G6D	L1	473	S1		Quartz, kaolinite and hematite
CP	H6C		510		Ochre 9	Quartz, hematite, kaolinite, muscovite
CP	H6C		497		Ochre 4	Quartz, hematite, kaolinite
CP	H6C	L16	453			Quartz, hematite, goethite, kaolinite

For a material to qualify as an extending pigment it should have a low opacity, and the index of refraction of kaolinite ranges from (1.560 to 1.570) thus allowing it to meet this requirement (Judson, 1959). It is therefore probable that the site occupants sourced the clay mineral to use during the manufacturing of the

pigment. The main objective for this part of the study was to perform a mineralogical characterisation of the ochre associated with the CP layer toolkit. Part of this characterisation involved the classification of the ochre into three subgroups highlighting the chromophores and accessory minerals (Table 6.5). The ochre samples were separated into those with kaolinite, illite/muscovite and quartz as the accessory minerals and those with only quartz as the accessory mineral. Hematite and goethite were the two iron-oxides identified in the CP layer ochre samples. The characteristic IR bands were also included in the classification table. An IR correlation chart for inorganic minerals (Table D1) was used for the interpretation of the absorption bands.

Most of the ochre samples were categorized under the second group where hematite was the chromophore while kaolinite and quartz formed part of the accessory minerals.

Table 6.5 Classification of ochre according to their chromophores and accessory minerals.

Group	Sample name	Chromophore	Accessory mineral/ matrix	Characteristic bands (cm^{-1})	Vibrational modes
1	CPA F6d S1 CP H6c ochre 7 CP H6c L20 514 CP H6c 506 ochre	Hematite	Quartz Muscovite/illite	3439 1630 1084 1033 798 779 695 539	*v* OH clay O-H bend, clay Si-O , quartz Si-O stretch, clay Si-O bend , clay *v*Si-O doublet ,quartz δSi-O, quartz Fe-O, Hematite
2	CP G6d L1 473 S1 CPA G6d ochre fragments CP H6c ochre flake CP G6D O1 476 CP H6c ochre 4 497 CP H6c ochre 9 510 CP H6c L30 529	Hematite	Quartz, Kaolinite Muscovite/illite	3737 3698, 3666, 3653, 3620 3425 1630 1438 1084 1033 1047, 1011 935, 914 798 779 695 536	*v* OH, Illite *v* OH, Kaolinite *v* OH, clay O-H bend, clay *v*$3CO_3$, calcite Si-O , quartz Si-O stretch, clay Si-O-Si, Si-O-Al, Al-O-H, Kaolinite Si-O bend, clay *v*Si-O doublet,quartz δSi-O, quartz Fe-O, Hematite
3	CP H6c L1 416 CPA H6c O2 470	Goethite	Quartz, Kaolinite, Muscovite/illite	3737 3698, 3666, 3653, 3620 3425 3134 1658 1630 1438 1084, 1033 1047, 1011 935, 914 913, 800 798 779 695 536	*v* OH, Illite *v* OH, Kaolinite *v* OH, clay *v* OH, Goethite O-H bend, Goethite O-H bend, clay *v*$3CO_3$, calcite Si-O , quartz Si-O stretch, clay Si-O-Si, Si-O-Al, Al-O-H, Kaolinite *v*(OH), Goethite Si-O bend, clay *v*Si-O doublet,quartz δSi-O bend , quartz Fe-O, Hematite

Figures 6.6-6.7 entail IR spectra which show hematite and goethite embedded in the accessory minerals, kaolinite and quartz.

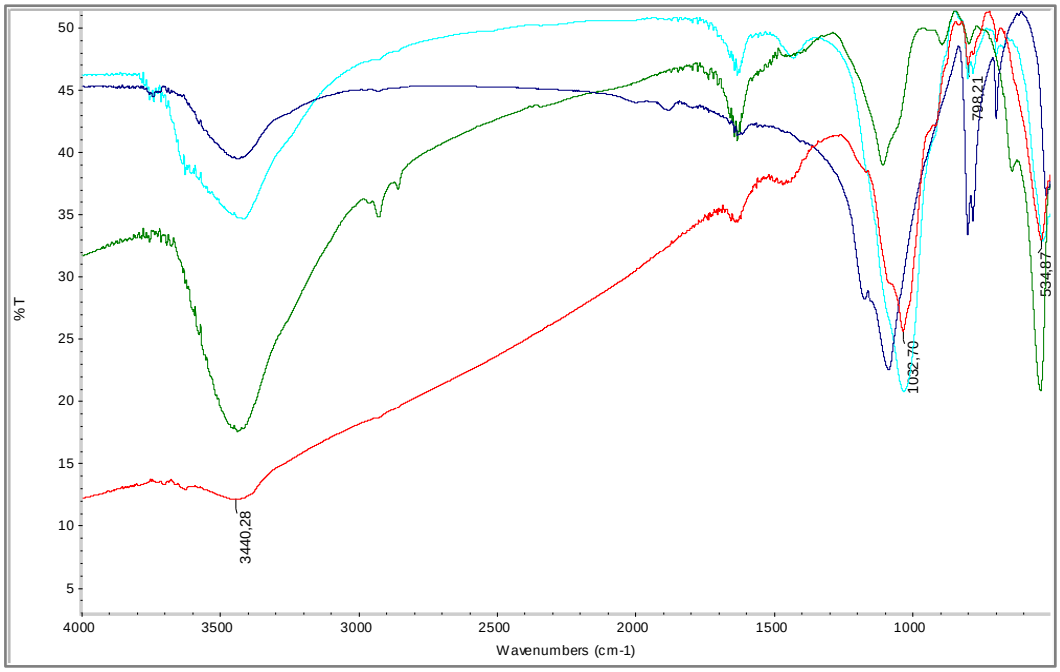


Figure 6.6 Transmission IR spectrum showing hematite (green) embedded in the accessory minerals, quartz (purple) and illite (blue). Representative sample is BBC CP H6c L20 514 (red)

This IR spectrum illustrates a representative ochre sample of the first group. This ochre is rich in quartz which is characterised by the following bands: a broad νOH stretch of adsorbed water (possibly in clay minerals) observed at 3440.28 cm^{-1}, a strong Si-O stretch for clay minerals appearing at 1032.70 cm^{-1} and the quartz doublet band at 798.21 cm^{-1}. For the chromophore, hematite, the characteristic bands can be observed between 560 cm^{-1} and 450 cm^{-1} these are due to the Fe-O bond (Helwig, 1998).

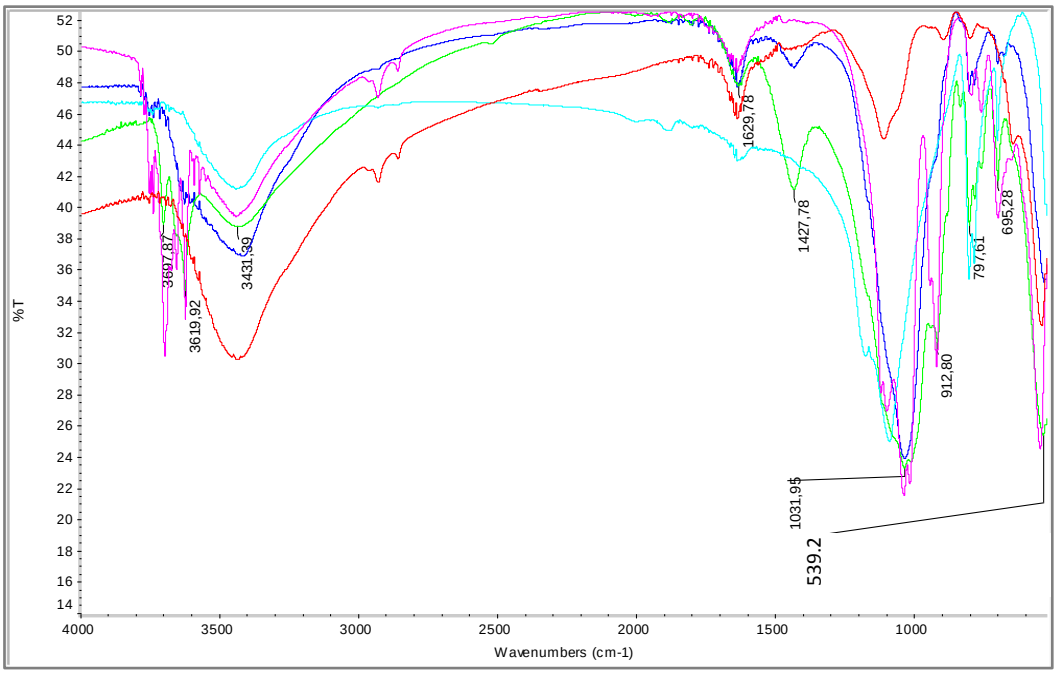


Figure 6.7 Transmission IR spectrum showing hematite (red) embedded in the accessory minerals, quartz (light blue), kaolinite (purple) and illite (dark blue). Representative sample is BBC CPA G6d ochre fragments (green)

The IR spectrum depicted by Figure 6.7 represents an ochre sample of the second group. This sample is rich in quartz, aluminosilicates kaolinite and illite/muscovite. The absorption bands for kaolinite occur at 1047 cm^{-1} *v* asymmetric (Si–O–Si), 1011 cm^{-1} (Si–O–Al), 935 cm^{-1} and 914 cm^{-1} (Al–O–H) (Derrick, Stulik and Landry, 1999). The absorption bands associated with kaolinite´s outer OH ions occur at 3698 cm^{-1}, 3666 cm^{-1}, 3653 cm^{-1}, and the corresponding absorption band for the inner OH ion appears at 3620 cm^{-1} (Bikiaris *et al*., 2000). Illite/muscovite are characterised by the following bands; an outer OH ion band at 3737 cm^{-1}, a broad *v*OH stretch at 3411 cm^{-1} due to the adsorption of water by the clay minerals, O-H bend for clay minerals at 1630 cm^{-1} ,*v*Si-O-Si stretch for clay minerals at 1033 cm^{-1} and *v*Si-O at 800 cm^{-1}. In this particular sample, the bands due to the outer OH ions for kaolinite appeared at 3697 and 3691 cm^{-1}. The broad *v*OH stretch at 3431 cm^{-1} is due to the adsorption of water by the clay minerals. The band at 1629 cm^{-1} is the O-H bend due to clay

minerals. The Si-O stretch for clay minerals came at 1033 cm^{-1}. The band at 912 cm^{-1} is due to the (Al–O–H) stretch from kaolinite. Quartz was detected as the predominant mineral in the matrix of the ochre sample BBC CPA G6d ochre fragments. The typical characteristic bands for quartz were observed at 798 cm^{-1} (νSi-O) doublet and 696 cm^{-1} (δSi–O). An additional band made an appearance at 1438 cm^{-1} this band is due to the ν3, asymmetric CO_3 stretch, of calcite. The Fe-O bond due to the iron oxide, hematite, came at 539 cm^{-1}.

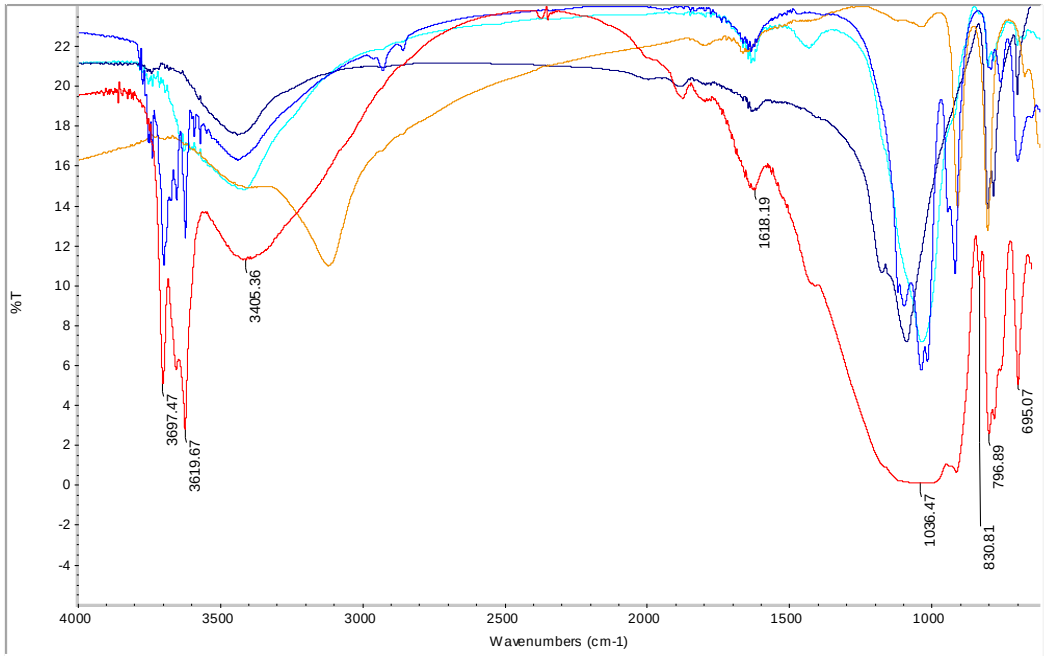


Figure 6.8 Transmission IR spectrum showing goethite (orange) embedded in the accessory minerals, quartz (black), kaolinite (dark blue), illite (light blue). Representative sample is BBC CP H6c L1 416 (red)

The spectrum depicts a sample from the third group, one which has a similar matrix to the second group (that is kaolinite, illite/muscovite and quartz rich). However in this group goethite was identified as the main chromophore. The bands due to the outer OH ions of kaolinite appear at 3667 and 3617 cm^{-1}, respectively. The broad band at 3405 cm^{-1} is due to νOH stretch of adsorbed water (possibly in clay minerals). The Si-O stretch for clay minerals came at 1033 cm^{-1} .The quartz characteristic bands are seen at 796 (doublet) and 695 cm^{-1}. Bands

typical for goethite are observed at approximately 800 and 897cm^{-1} (Ruan *et al*., 2002). This band could belong to illite or vermicullite (Hong *et al*. 2014). According to Shilito *et al.* (2009), the OH bend distinctive for clay minerals, can appear at energies as low as 1616 cm^{-1}, for this sample this bend is seen at 1618 cm^{-1} .

The PXRD diffraction patterns for the three representative samples from each ochre group are presented in Figures 6.9 to 6.10. The diffractograms give the mineral phases identified in each sample.

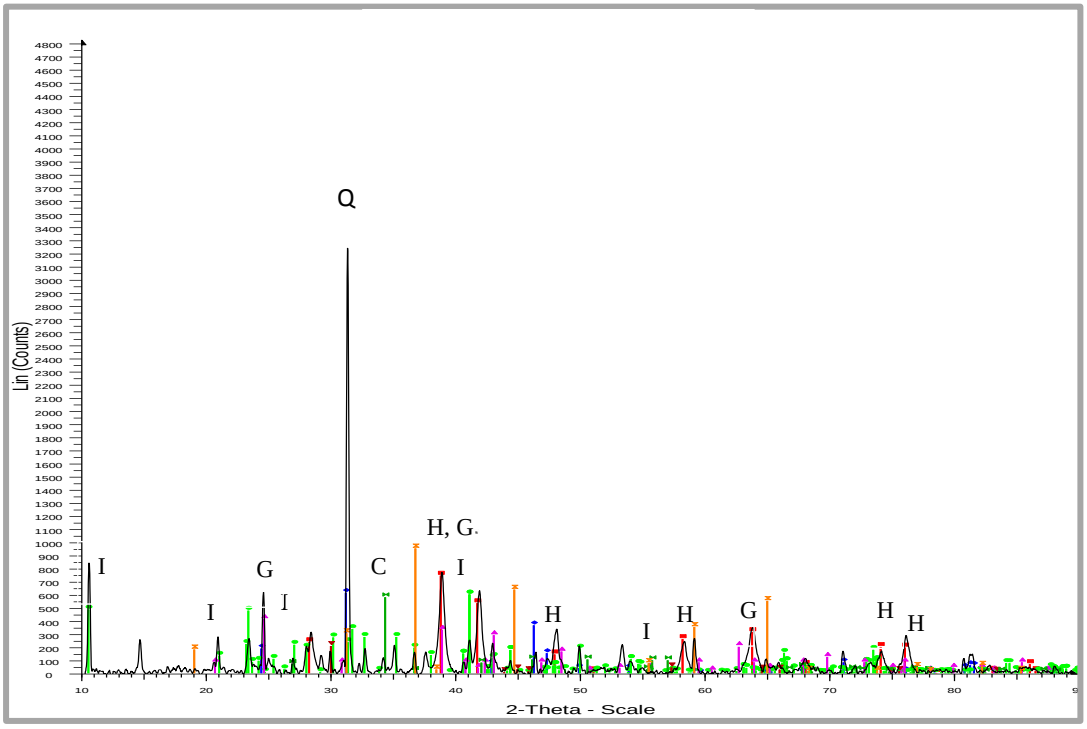


Figure 6.9 Diffraction pattern for the group one ochre sample CP H6c L20 514. (K: kaolinite; H: hematite; C: calcite; G: goethite; Q: quartz; I: illite)

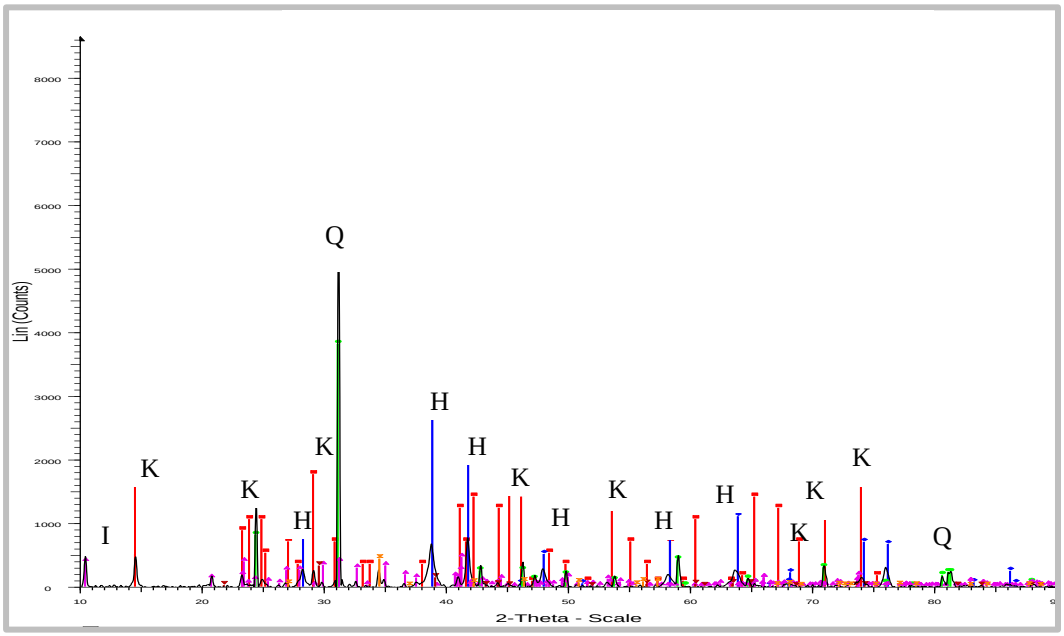


Figure 6.10 Diffraction pattern for the group two ochre sample CPA G6d ochre fragments. (K: kaolinite; Q: quartz; I: illite, H: hematite)

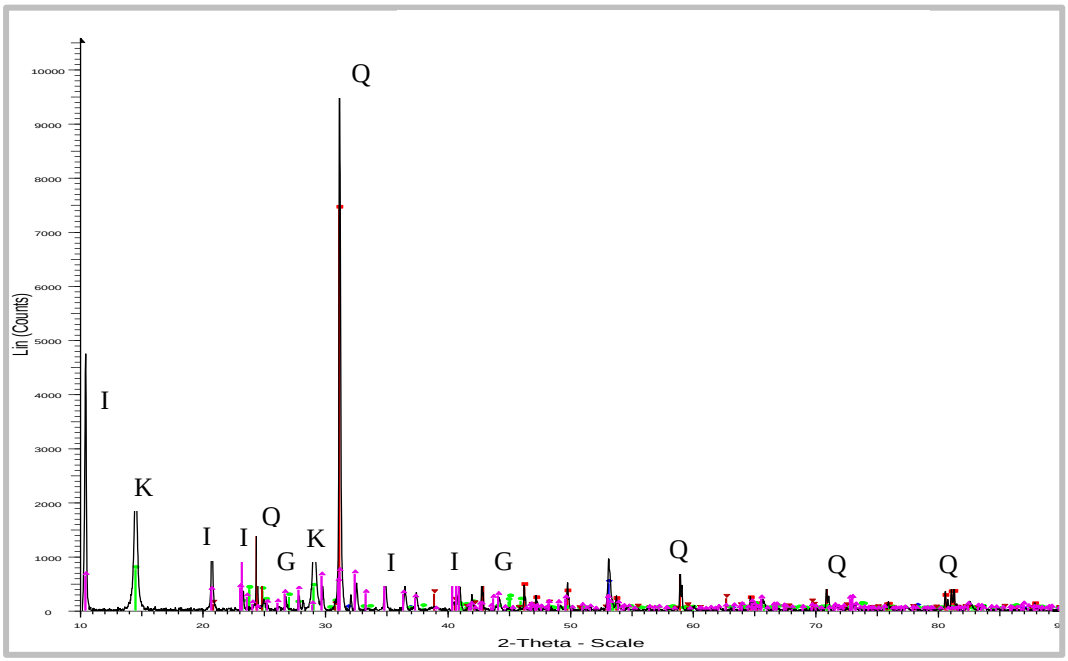


Figure 6.11 Diffraction pattern for the group three ochre sample BBC CP H6c L1 416. (K: kaolinite; Q: quartz; I: Illite; G: goethite)

The diffractogram on Figure 6.9 shows hematite (αFe_3O_2), as the predominant mineral phases (greatest intensity) in this sample. Phases of illite [$K(Al_4Si_2O_9(OH)_3)$] and quartz (αSiO_2), are also present in standard amounts. Calcite ($CaCO_3$), and anatase (TiO_2) had low peak intensities.

The CPA G6d ochre fragments diffractogram indicates that this sample comprises of the following minerals: kaolinite [$(Al)_2(Si_2O_5)(OH)_4$], hematite (αFe_3O_2), quartz (αSiO_2), illite [$K(Al_4Si_2O_9(OH)_3)$], anatase (TiO_2). In this sample, the quartz, hematite and kaolinite mineral phases have the greatest intensities implying they were largely present (principle minerals). However the illite and anatase phases had relatively low peak intensities when compared to those due to kaolinite, hematite and quartz. These ochre fragments had a white, soft- clayey texture which can be attributed to the kaolinite.

The ochre sample, BBC CP H6c L1 416, was composed of quartz (αSiO_2), kaolinite [$(Al)_2(Si_2O_5)(OH)_4$], goethite, FeO(OH) and illite [$K(Al_4Si_2O_9(OH)_3)$]. The peak intensities for the quartz mineral are very high, which makes it the principle component in this sample. The illite mineral phase (very common in ochre) displayed more average peak intensities, while the remaining minerals (goethite and kaolinite) had low peak intensities.

The PXRD investigation was useful in that it identified the mineral phases present and the peak intensities aided in recognising the principle minerals in the ochre samples. From the PXRD analysis, the following elements were identified: Fe, Si, Al, K, Ti and Ca. The presence of these was confirmed by elemental analysis using ED-XRF and ICP-OES (discussed in section 6.2.1.2). Furthermore, it can be deduced that in an ochre sample, iron oxide or oxy-hydroxide (chromophore) and accessory minerals are present in varying quantities. The principle mineral can either be the chromophore or the accessory mineral, this however does not impact on the red, brown or yellow hue portrayed by the ochre. The strong tinting power of iron oxides is not determined by whether or not they are principle minerals (that is whether they are present in low or high quantities) (Helwig 1998). It is noted that only very small amounts of iron oxide are needed to colour a rock; six percent or less iron is contained in the rock, yet it produces an intense colour

(Judson *et al.*, 1987). High cumulative X-ray peak intensities and low cumulative peak widths were observed for the samples, this implies that the ochre pieces were of good crystallinity as the peaks were well-defined. Therefore PXRD is the most reliable way of achieving reasonable data from an array of crystallites and has been exploited in several ochre analysis studies (Rendle, 2003).

6.2.1.2 Elemental fingerprinting of the ochre using ICP-OES and ED-XRF

Elemental composition analysis was done to acquire a fundamental understanding of the geochemical composition of the ochre as well as the relationship between the ochre sources. Elemental fingerprinting is particularly important if the ochre samples exhibit similar mineralogical composition. Under such circumstances elemental fingerprinting can be employed to differentiate the ochre. The heterogeneous nature of ochre inferred the need to apply multivariate and discriminant statistics on the elemental data (Popelka-Filcoff, 2006). Statistical analysis and data interpretation were then used in understanding the procurement and exchange of ochre by the prehistoric humans. ICP-OES and ED-XRF were employed in the identification and quantification of the bulk chemical compositions (both the major elements and trace elements) of the ochre. ICP-OES has a lower detection limit and gives a large amount of data when compared to ED-XRF; hence it was used to determine the trace elemental composition of the ochre samples. ED-XRF identified and quantified the major elemental composition. The two techniques were employed because they complement each other in the elements that can be quantified in ochre samples (Popelka-Filcoff, 2006). Also, the less sensitive ED-XRF method was used as a substitute for ICP-OES when sample quantities were limited and when the samples were archaeologically valuable and could not be destroyed.

The list of samples analysed by ICP-OES, the elements detected as well as their concentrations are presented in Table 6.6.

Table 6.6 ICP-OES elemental data for the ochre samples from the CP layer (presented as mean ± SD $x10^3$ mg kg^{-1}) (n=3)

Sample name	V	Cr	Zn	Cu	Mn	Zr	Cd	As	Sc
BBC CP H6c 506	0.17±0.02	0.048±0.002	0.03±0.03	0.012±0.001	0.29±0.02	0.082±0.008	0.017±0.001	0.023±0.001	0.0014±0.0001
BBC CP G6d O1 476	0.036±0.002	0.11±0.01	0.016±0.001	0.021±0.001	0.028±0.001	0.056±0.003	0.0018±0.0007	0.066±0.003	0.0012±0.0001
BBC CP ochre flake	0.19±0.02	0.073±0.006	0.11±0.01	0.028±0.001	0.055±0.003	0.026±0.001	0.0008±0.0007	0.034±0.001	0.016±0.001
BBC CP H6c L1 416	0.027±0.001	0.14±0.01	0.024±0.002	nd	0.16±0.02	0.038±0.001	0.0018±0.0001	0.26±0.01	nd
BBC CP H6c L30 529	0.12±0.01	0.043±0.002	0.17±0.01	0.12±0.01	0.41±0.04	0.032±0.001	0.022±0.001	0.28±0.01	0.0014±0.0001
BBC CP H6c L35 534	0.17±0.02	0.17±0.02	0.038±0.03	0.0038±0.0002	0.17±0.01	0.040±0.002	0.0090±0.0008	0.044±0.002	0.0094±0.0009
BBC CP H6c L16 453	0.14±0.01	0.10±0.01	0.022±0.002	0.15±0.02	0.46±0.04	0.040±0.002	0.016±0.001	nd	0.006±0.004

Sr	Ba	Co	Ca	K	Al	Ti	Si	Fe	Mg	Y
0.072±0.008	0.040±0.003	0.02±0.02	1.53±0.07	37.0±2.1	153.1±5.3	15.2±1.6	441.3±5.0	281.4±19.6	0.13±0.01	0.049±0.003
0.024±0.001	0.028±0.001	0.012±0.001	1.68±0.08	48.6±3.7	122.2±1.8	11.2±1.1	218.7±6.4	139.4±14.7	0.025±0.002	0.018±0.001
0.084±0.009	nd	0.0094±0.0009	3.66±0.3	53.6±4.2	235.4±8.7	8.4±0.6	472.5±7.2	247.3±5.1	0.10±0.01	0.058±0.004
0.079±0.008	nd	nd	0.96±0.04	22.8±1.3	130.4±2.6	14.3±1.5	448.1±4.6	171.8±6.9	0.16±0.01	0.020±0.001
0.36±0.02	nd	0.0092±0.0009	3.28±0.27	59.6±5.0	222.6±1.6	10.4±0.8	540.4±5.5	387.6±21.6	0.028±0.002	0.022±0.001
0.081±0.007	0.042±0.03	nd	2.1±0.1	60.0±5.2	139.1±5.7	11.9±1.1	336.0±20.1	276.8±18.4	0.033±0.003	0.048±0.003
0.077±0.007	0.032±0.002	0.021±0.002	2.8±0.2	37.3±20.8	145.3±4.5	7.2±0.6	512.8±34.8	318.4±19.8	0.014±0.001	0.038±0.002

*ND refers to the concentrations which were below the detection limit

Relative standard deviations (RSD's) for values across Table 6.6 were below 10% demonstrating good precision of the technique. The identified elements can be arranged into the following descending order of magnitude: Si> Fe > Al>K>Ti>Ca> Mn> V >Cr> Mg>Zn>Sr> As > Zr >Ba> Co>Cu> Y> Cd >Sc. This trend suggests that in most of the ochre samples from the CP layer, quartz (SiO_2) and aluminosilicates; such as kaolinite [$(Al)_2(Si_2O_5)(OH)_4$], illite [$K(Al_4Si_2O_9(OH)_3)$] or muscovite [$(KF)_2(Al_2O_3)_3(SiO_2)_6(H_2O)$] are the principle minerals in the general ochre matrix (a similar conclusion was made for the PXRD analysis).

The major elements identified by ED-XRF are shown in Table 6.7. Only the elements with an atomic number greater than Na were identified.

Table 6.7 Major elements identified using ED-XRF

Ochre	**Principle mineral**	**Identified major and (trace) elements**								
		Al	Si	K	Ca	Ti	Fe	(V	Cr	Mn)
CP H6C 506 ochre 3	I/M/K+Q	√	√	√	√	√	√	√		√
CP G6D O1 476	I/M/K+Q	√	√	√	√	√	√		√	
CP H6C ochre flake	I/M/K+Q	√	√	√	√	√	√	√	√	
CP H6C L1 416	I/M/K+Q	√	√	√	√	√	√		√	√
[a]CP [b]H6C [c]L30 [d]529	I/M/K+Q	√	√	√	√	√	√	√		√
CP H6C L35 534	I/M/K+Q	√	√	√	√	√	√	√	√	√
CP H6C L16 453	I/M/K+Q	√	√	√	√	√	√	√	√	√

K=kaolinite, I= illite, M= muscovite, Q=quartz

a=layer, b=quadrate, c=plot number, d=artifact number (Moyo *et al*., 2015)

In all the samples the following major elements were found to be common: Al, Si, K, Ca, Ti and Fe. ED-XRF detected the following as discriminating trace elements Mn, V and Cr. It can be seen that although some of ochre had similar mineral composition (quartz and kaolinite or illite/muscovite) differences were observed in the elemental profiles for these ochre residues. For the CP layer ochre five groups emerged (based on the ED-XRF trace element profiles). These groups were as follows:

- Samples with Mn and V

- Sample with Cr only
- Sample with Cr and V
- Sample with Cr and Mn
- Samples with Cr, V and Mn

The identified elements confirm the notion that ochre is a heterogeneous material comprising of different minerals (Popelka-Filcoff, 2006). The elements identified by the ICP-OES and ED-XRF analyses are in agreement with those found in the mineral phases identified by PXRD.

The element concentrations (detected by ED-XRF) were obtained using the mudrock and stone calibration files element analysis from Bruker. The calibration included a procedure for standardising raw spectral data using the inelastic scattering or Compton peak from rhodium backscatter. This procedure compensated for errors arising from the uneven surfaces of the measured ochre pieces.

The concentrations of the identified elements for the CP ochre are presented in Table 6.8. To make further analysis simpler, the sample names were replaced by alphabetical symbols (as indicated in Table 6.8).

Table 6.8 Concentrations of the major and trace elements detected by ED-XRF in ochre from the CP layer (values in mg kg^{-1})

	Ochre	Al	Fe	K	Ti	V	Ca	Cr	Mn	Si
A	CP H6c 506	169085	296382	30863	15305	181	131	63	162	415618
B	CP G6d O1 476	105493	192599	39636	11110	46	194	131	39	321875
C	CP H6c ochre flake	179783	257928	50171	8081	195	348	91	63	496445
D	CP H6c L1 416	127937	235387	20395	14090	34	93	140	147	446197
E	CP H6c L30 529	173024	345409	53341	10230	170	326	29	179	594191
F	CP H6c L35 534	143591	320622	64227	11321	145	236	156	112	381069
G	CP H6c L16 453	157344	318596	34719	7004	133	253	128	200	551753

The Fe content across the elemental data for the ochre was high this implies that Fe contributed the most to the total weight percent for each sample. Since the Fe concentrations were large for the ochre samples any resulting variations had to be accounted for. So the elemental concentrations were normalised with Fe.

6.2.1.3 Statistical analysis of elemental data

In this study one of Glascock and Neff's approaches to provenance studies was employed in order to explore the pattern within the elemental concentration data. In their approach the artifacts are analysed as a group then statistics and pattern recognitions are used to cluster the samples into meaningful groups. These statistics help to identify the patterns within the data set. Finally, archaeological conclusions are drawn from the attributions of the artifacts to a particular geological origin (Glascock and Neff, 2003).

It is difficult to make comparisons between variables containing large values with variables containing very small values without the possibility of favouring the larger values. Hence the $\log_{10}$ transformation was used, this means that any possible "weighting effect" of a particular element due to high concentration (Fe in this case) is moderated, and all values are essentially on the same order of magnitude (Popelka-Filcoff, 2006). In addition, $\log_{10}$ transform reduces the effects due to possible non- normal distribution of the elements (Glascock, 1992). After the transformation, the data are assumed to be log-normalized (Baxter, 1994) and can be used in statistical analyses. The Fe-normalized and the $\log_{10}$ transformed values are added as Tables E1 and E2 (ICP-OES and ED-XRF, respectively).

The following statistical methods were applied to both the raw and transformed elemental data:

i. Cluster analysis and hierarchical dendrograms
ii. Pearson's correlation test
iii. Principal component analysis (PCA), using biplots, and
iv. ANOVA (one-way)

All statistical assessments in this study were made using the statistics packages Minitab ® 16, © 2010 Minitab Inc. software and XLSTAT software 2015.

i) Cluster analysis and hierarchical dendrograms

Cluster analysis is frequently employed as an initial method to discern possible patterning or clustering in the elemental data (Popelka-Filcoff *et al.*, 2008). In this study Hierarchical Cluster Analysis (HCA) using the agglomerative method was applied to the (ED-XRF) elemental data in order to observe the formation of clusters between related ochre samples. The method was set on a single linkage cluster algorithm, which assesses the two most similar samples in the data matrix based on the Euclidian distance between data points. The relationships between the samples are represented by a dendogram (Figure 6.12).

The dendogram in Figure 6.12 formed a "tree-like" structure which illustrated how the ochre samples were related to each other. Closely related ochre samples were clustered together these were further linked to other samples by similarity. The horizontal axis showed the dissimilarities between the clusters. The discriminating trace elements (Mn, Cr and V) afforded the clustering of similar ochre into groups. Two groups were observed: group one was composed of samples F, G, B and C, while group two consisted of samples A, E and D.

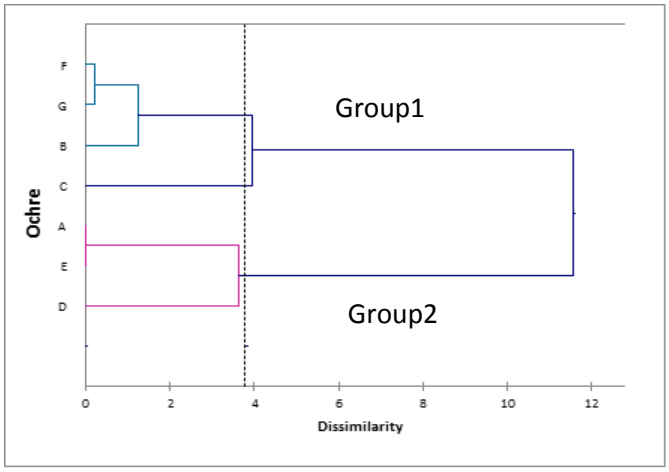


Figure 6.12 Dendogram showing the clustering of related ochre samples from the CP layer.

Although the ochre samples formed clusters, the dissimilarities between the individual samples suggested that the ochre samples might have different geological origins.

Cluster analysis merely outlines the grouping patterns within a data set and is not regarded as a final method for artifact grouping. This is because this analysis does not consider the correlation and co-variance of elements. Correlations between elements are often observed among the rare earth elements (REE) and other element groups in geological samples (Popelka-Filcoff, 2006). Therefore cluster was only a starting point in this data analysis.

The aim of the ochre study was to understand the trace elemental fingerprints associated with the individual ochre, to observe any similarities between the individual ochre and to deduce sourcing. As ochre are complex multiphase mixtures of minerals, the elemental signature must be associated with the original Fe concentration. In order to extract this association between the elements and the Fe concentration, a Pearson's correlation test (described in section 5.6.2) was used.

ii) Pearson's correlation test

The results from the Pearson's correlation test are summarized in Table 6.9. The coefficients highlighted in red are indicative of a good linear correlation between the elements.

Table 6.9 revealed a number of correlation trends between the elements, however the most important one is the correlation of Sc, Cd, Sr, Co,Y, Mg, Mn and Ti with Fe. In their study, Popelka-Filcoff *et al.* (2007) proposed that the elements associated with Fe are related to the Fe- oxide signature and to the sample origin. This implies that Sc, Cd, Sr, Co, Ti, Y, Mg and Mn are associated with the Fe- oxide signature and the ochre source. Natural iron-oxides/oxy-hydroxides (hematite and goethite) have the tendency to exhibit isomorphous octahedral substitution of the Fe-oxide by other cations hence they are often referred to as "sinks" for trace and heavy metals (Wells, Fitzpatrick *et al.*, 2006).

Table 6.9 Pearson's correlation matrix showing the coefficient values (r) for the major and trace elements

	As	Ba	Cu	Cd	Cr	Fe	Sc	Sr	V	Y	Zn	Zr	Al	Ca	K	Mg	Mn	Co	Si	Ti
As	**1**																			
Ba	0.122	**1**																		
Cu	**0.572**	0.494	**1**																	
Cd	0.495	**0.605**	**0.978**	**1**																
Cr	0.460	**0.576**	**0.935**	**0.918**	**1**															
Fe	0.264	0.211	0.423	**0.523**	0.315	**1**														
Sc	0.476	**0.616**	**0.963**	**0.990**	**0.907**	**0.546**	**1**													
Sr	**0.573**	**0.623**	**0.976**	**0.985**	**0.939**	**0.515**	**0.974**	**1**												
V	**0.529**	**0.540**	**0.975**	**0.975**	**0.967**	0.452	**0.958**	**0.974**	**1**											
Y	0.480	**0.587**	**0.970**	**0.994**	**0.894**	**0.522**	**0.969**	**0.974**	**0.965**	**1**										
Zn	0.115	-0.496	0.324	0.266	0.070	0.313	0.267	0.170	0.219	0.288	**1**									
Zr	**0.548**	-0.130	**0.638**	**0.562**	**0.553**	0.416	**0.618**	**0.557**	**0.599**	**0.508**	**0.618**	**1**								
Al	0.384	0.377	0.373	0.427	0.469	0.305	0.498	0.424	0.486	0.352	-0.118	**0.533**	**1**							
Ca	-0.268	-0.004	0.091	0.168	-0.152	0.303	0.111	0.055	0.021	0.252	**0.506**	-0.226	-0.488	**1**						
K	0.102	0.071	0.109	0.176	0.157	0.247	0.255	0.113	0.221	0.115	0.111	0.472	**0.888**	-0.283	**1**					
Mg	0.338	0.268	0.102	0.142	0.037	**0.593**	0.199	0.238	0.044	0.107	-0.154	0.155	0.069	-0.118	-0.160	**1**				
Mn	**0.599**	**0.632**	**0.952**	**0.961**	**0.914**	**0.551**	**0.955**	**0.992**	**0.941**	**0.946**	0.128	**0.545**	0.398	0.024	0.060	0.354	**1**			
Co	0.305	0.125	**0.553**	**0.617**	0.291	**0.818**	**0.626**	**0.549**	0.491	**0.637**	**0.677**	0.499	0.142	**0.623**	0.179	0.350	**0.548**	**1**		
Si	**0.602**	-0.110	**0.534**	**0.508**	0.386	0.418	**0.562**	**0.518**	0.493	0.467	**0.583**	**0.891**	0.466	-0.066	0.402	0.482	**0.543**	**0.707**	**1**	
Ti	0.113	0.263	0.029	0.157	0.130	**0.738**	0.194	0.133	0.205	0.125	-0.224	0.139	**0.807**	-0.214	**0.826**	0.022	0.107	0.151	0.245	**1**

*Good linear correlation, r > 0.5 (highlighted in red).

*Significant values were evaluated in the 95% confidence interval (α = 0.5)

These trace and heavy metals replace Fe^{3+} in the Fe-oxide octahedral lattice causing a variation in the pigment shade. Increasing amounts of Co and Ni tend to cause a red shift, while V and Mn result in a green shift (Deer, Howie and Zussman, 1992).

Further this cation substitution alters the unit cell parameter of the iron-oxide. For example the substitution of Ti for Fe increases the unit cell parameters while the substitution of the other elements serves to reduce the cell size (Jercher *et al.*, 1998). Transition metals and trace elements normally associated with the substitution of Fe in natural and synthetic goethite include Co, Cr, Ga, V, Sc, Y, Ge, Cu, Zn and Pb (Wells, Fitzpatrick *et al.*, 2006). On the other hand Cr, Rh, Ga, In, Nd, Cu, Ge, Y, Sn, Si and Ti are noted as substitution metal ions in hematite (Cornell and Schwertmann, 2003).

iii) Principal component analysis (PCA), using biplots

As part of the multivariate statistical analysis, PCA (described in section 5.6.3) was conducted. PCA was performed as part of a preliminary test to determine the elements that are responsible for variance in the elemental data set (detected by ICP-OES).

Figure 6.13 shows the cumulative variance % in the elemental data set.

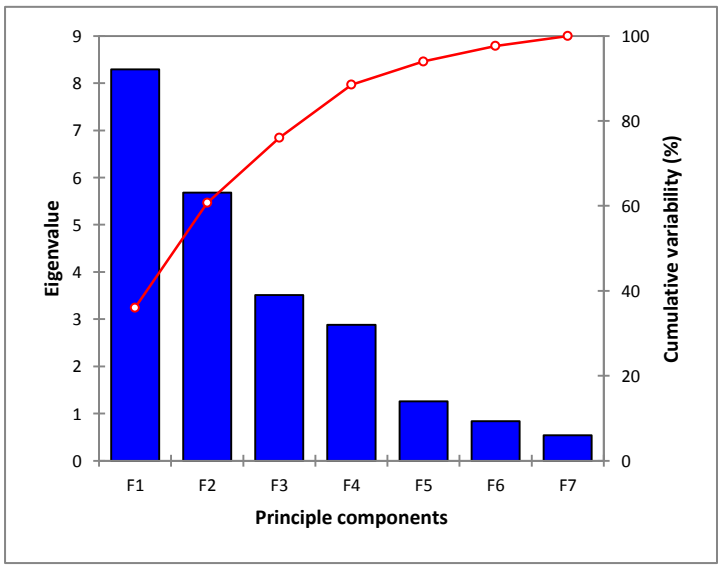


Figure 6.13 Scree plot of the cumulative variance % for the elemental data

Despite the Fe-normalization, the first principle component (termed as F1) tends to be driven most strongly by Fe concentration (Popelka-Filcoff, 2006; Dayet *et al*., 2015). This implies that other principal components demonstrate elements that drive the variance in the sample set more clearly than the first component, so these were used instead. Figure 6.14 displays the PC bi-plot for principal component 2 and 3 as a representative example of other PC bi-plots. This bi-plot shows variance in the elemental data set. The elements are represented by vectors which indicate magnitude and direction.

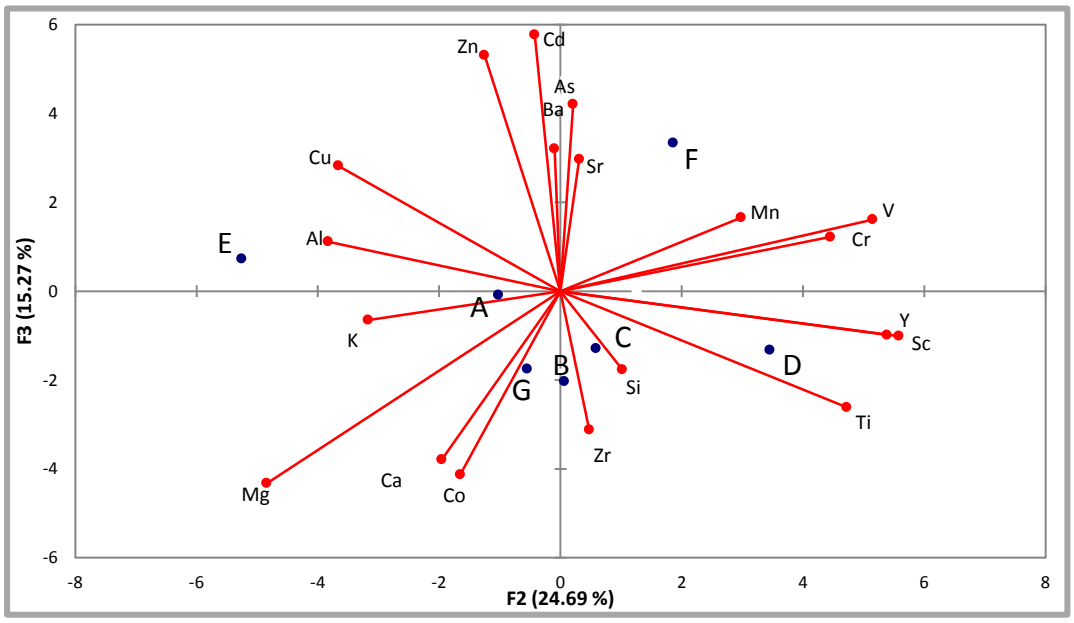


Figure 6.14 PC bi-plot showing principle component 2 vs principle component 3 for the elemental data set

*This bi-plot illustrates a 39.96% variance in the elemental data set

Elements with the longest vectors in the PC space imply the greatest variance in a data set (Popelka-Filcoff, 2006). In the PC biplot (Figures 6.14) the elements with the longest vectors (responsible for driving the variance) were Cr, Ti, Al, Mg, Mn, Cu, Y, Co, V, Zn and Sc (these are mostly the transition metals and REE). As illustrated by the Pearson correlation matrix (Table 6.9), some of these elements were correlated with Fe, and as suggested by Cornell and Schewertmann (2003) these elements contain signatures in the ochre that are characteristic of the

geological source despite weathering and other environmental changes (Popelka-Filcoff *et al.*, 2008).

According to Henderson (1984), elemental vectors with similar groups and properties in the periodic table tend to group together in the PC space. REE have similar electronic structures; hence they tend to group together in minerals and are never found alone. As anticipated the Y and Sc vectors occurred in the same quadrant and went in the same direction with similar magnitude as shown in the PC biplot (Figure 6.14).

iv) ANOVA- Analysis of variance

The trace elemental data (from ICP-OES) for the ochre was subjected to one-way ANOVA test. This statistical analysis was done in order to determine if there were significant differences between the mean square values of the elemental data and hence differences in the ochre samples. In order to determine the elemental data statistically, the following null hypothesis (H_0) was assumed; there is no statistical difference between and within the ochre samples. The F ratio was determined as follows:

$$\text{F ratio} = \frac{\text{mean square within the ochre samples}}{\text{mean square between the ochre samples}} \qquad (6.1)$$

For F-ratio greater than F-critical and a significant level at $P < 0.05$, the H_0 is not valid and there is statistical difference between and within the ochre samples.

The results from the ANOVA test on the elemental data for the ochre samples are presented in Table 6.10.

Table 6.10 ANOVA results for trace elemental data for the CP layer ochre

Source of Variation	SS	MS	F ratio	P-value	F critical
Between ochre samples	1.58E+12	9.88E+10	7.044791	1.22E-10	1.743622
Within ochre samples	1.43E+12	1.4E+10			
Total	3.01E+12				

Results from ANOVA indicated that F-ratio (7.044) was greater than F-critical (1.744) also the P-value was less than 0.05; therefore the H_0 was rejected since the means of the elemental data were not equal. It can be deduced that, even though the ochre samples exhibited a clustering pattern (Figure 6.12) due to similar mineralogy, there exists a statistically significant difference between the ochre samples in terms of trace elemental profiling. The variance suggests different geological origins.

6.2.1.4 Conclusion

After analysing the ochre from Blombos Cave, several trends became apparent. Firstly, most of the major elements formed part of the accessory minerals of the ochre (such as quartz, calcite and clays). Secondly, the elements found to be associated with Fe, as well as important for distinguishing sources, were a few members of the transition metals and REE. The Pearson correlation easily identified these elements (Table 6.9).

In ochre, Fe^{3+} is predominant; furthermore Fe^{3+} tends to act like a hard acid hence the substitution of small radii and highly charged atoms (hard acids) such as Co^{3+}, is more likely to occur. Additionally, similar oxidation states and electronic configurations (depending on the ion), can favour this substitution (Popelka-Filcoff, 2006).

The use of multivariate statistics and Fe ratios made it possible to identify elements important for differentiating ochre. PCA showed that the elements which drive the variance in the data set were largely the transition metals and two of the REE, a similar result was reported by Kiehn *et al*. in their 2007 study. This result was in agreement with the result illustrated by the Pearson correlation test (Table 6.9).

A study of the mineral phase and chemical composition of the ochre samples made it possible to deduce the following; the intrinsic properties of ochre are somehow influenced by the mineralogical composition. The prehistoric site occupants specifically obtained ochre, from different sources within the vicinity of the cave, to use during the pigment processing workshop. Majority of the ochre samples from the CP layer had hematite as the chromophore with kaolinite,

illite/muscovite and quartz as the accessory minerals. Clearly this specific type of ochre played a crucial role in the production of the pigment. The hematite contributed the red hue (generally associated with blood) and the clay minerals were good extenders of the pigment. The other components of the pigment mixture are the organic compounds which are discussed in section 6.3.2. These organic compounds may have been used as adhesives or binders in the pigment.

6.3 Organic residue analysis

The aim of this study was to analyse for amorphous ("invisible") organic residues. The preliminary step was to use FT-IR to screen samples which were suitable for organic residue analysis. The FT-IR spectra would reveal fragments (functional groups) of the organic compounds. By applying an appropriate separation (chromatographic) and identification (mass spectrometric) technique (GC-MS), the preserved and altered residues can be identified. Upon identifying the organic compounds, the next step in this investigation would be to understand where these residues came from (their origin). The best approach in understanding the origin of these organic residues was to use the concept of bio-molecular markers. The concept is based on the following principle: the bio-molecular markers associated with human activity survive in a wide variety of locations and deposits at archaeological sites. Also the archaeological information contained in organic residues is represented by the bio-molecular markers of the natural products that contribute to the formation of that given residue. For example cholesterol is a bio-molecular marker for animal derived material such as animal fat (Evershed, 2008).

6.3.1 FT-IR as a screening technique for organic residue identification

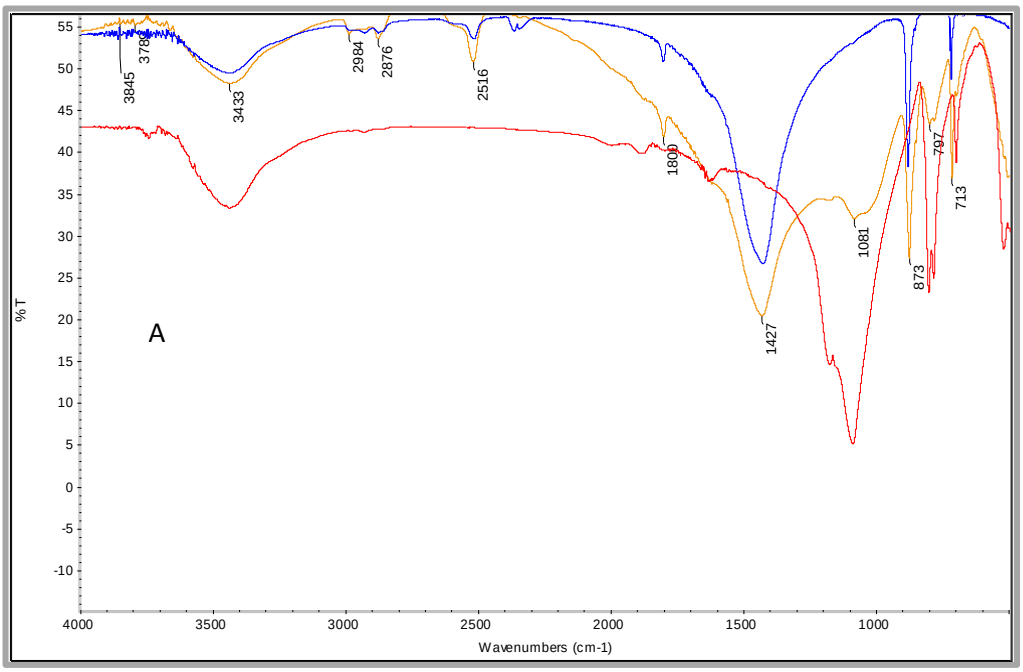
FT-IR is said to be a quick and cheap method of screening archaeological samples before subjecting them to the more expensive and time-consuming methods such as GC–MS (Shillito *et al.*, 2009). In this study, FT-IR was used as a screening technique for organic residues in the artifacts associated with the CP layer toolkit. A variety of archaeological materials may contain trace organic compounds

including stone tools, grinding stones, soil, sediments and mastics (Price and Burton, 2012). FT-IR screening was useful in eliminating inorganic samples such as clay minerals and ochre from GC–MS analysis, allowing only the screening of those samples which could potentially have a high concentration of preserved organic residues. Table 6.11 lists the samples screened by FT-IR for organic residue analysis. These samples showed features which suggested they were made by humans (for example mastic lumps). The typical organic residues preserved in human made archaeological samples are also presented in the table.

Table 6.11 Samples selected by FT-IR for organic residue analysis and the commonly preserved organic residues

Sample name	Organic residues	Reference
CP H6c Mastic O1 442 S1, CP H6c L24 520	Terpenes, fatty acids and sterols	Price and Burton, 2012

Figure 6.15 illustrates the transmission IR spectra for the selected samples.



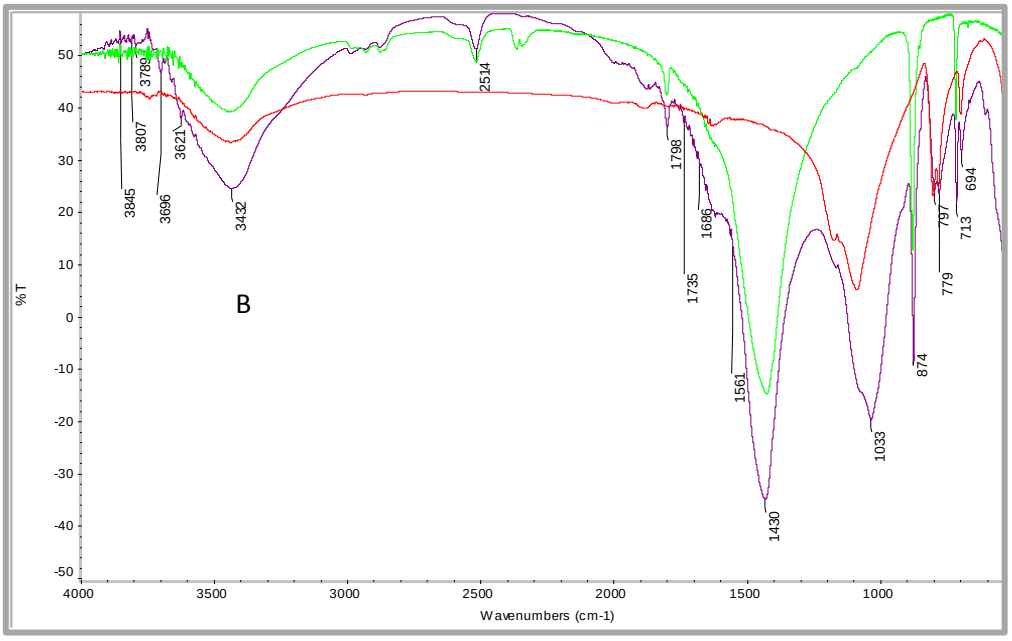


Figure 6.15 Transmission IR spectra show a) minerals; calcite (blue) and quartz (red) with representative sample CP H6c Mastic O1 442 S1 (yellow)**,** b) minerals; calcite (green) and quartz (red) with representative sample CP H6c L24 520 (purple)

Figure 6.15 indicates the presence of calcite, quartz and organic residues in the screened samples. Calcite and quartz are the principal minerals for these samples as confirmed by the characteristic IR bands for quartz (3434, 1164, 1117, 1084, 1032.70, 798, 779, 695 and 517 cm^{-1}) and for calcite (3854, 3736, 3435, 2512, 2360, 1798, 1421, 875 and 712 cm^{-1}). A broad OH peak, characteristic for minerals, was present in all spectra around 3430 cm^{-1}. IR spectrum A contains two distinctive stretching vibrations at 2984 and 2876 cm^{-1} due to CH_2 and CH_3 groups (alkanes) of the hydrocarbon skeleton of the resin (mastic) (Izzo *et al.*, 2012).

Spectrum B seems to be the only one showing a peak corresponding to the C=O stretching at 1735 and 1686 cm^{-1} this absorption frequency suggests a ketone, aldehyde, ester or carboxylic acid group. The frequency of the carbonyl is determined to a large extent by its immediate environment rather than the structure of the whole molecule (Bellamy, 1957).

A close inspection of the FT-IR spectra in Figure 6.15 reveals that it is probable that the samples have different organic components. This IR screening process allowed samples to be pre-selected for GC-MS analysis, in that samples showing organic residues were considered for further investigation. The physical appearance of the two samples was, however, identical. This indicates that the physical appearance does not necessarily relate to the chemical composition.

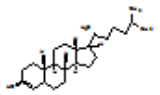
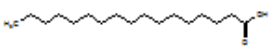
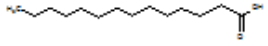
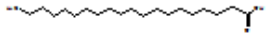
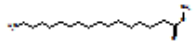
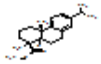
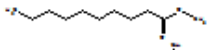
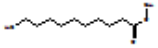
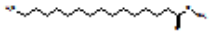
6.3.2 GC-MS in organic residue analysis

The analysis of organic residues, which have been absorbed into the structural matrix of archaeological materials, can provide information about past artifact function and diet. Common organic residues in archaeology include lipids (fatty acids and sterols), amino acids, nuclei acids, simple sugars, terpenes and hydrocarbons (Price and Burton, 2012). GC-MS (discussed in section 5.3.9) was employed for the identification of the organic residues present in the screened samples. Table 6.12 reports on the organic compounds detected from the following samples: CP H6c mastic O1 442 S1 and L24 520.

The organic residues were classified according to their functional groups. The corresponding total ion current (TIC) chromatograms and complete data set are included in appendix F as Figures F1 and F2 in Table F1.

It is evident from Table 6.12 that a number of organic residues were identified by GC-MS. Certain bio-molecular markers were preserved in these residues. Majority of the organic residues were lipids: heterogeneous molecules that include fats and oils. This class of organic compounds tends to survive better in archaeological contexts because of their hydrophobic nature (insolubility in water) and non-susceptibly to hydrolysis (Price and Burton, 2012). As a result lipids are amenable to sensitive techniques such as GC-MS. This technique has been successfully applied in the identification of ancient organic residues, contributing to the study of artifact use and food consumption by prehistoric humans (Heron and Evershed, 1993). There are various forms of lipids but the most pertinent in archaeological studies are the fatty acids and sterols. Their identification in archaeological contexts provides information on past activity areas and diet (Price and Burton, 2012).

Table 6.12 Classification of organic residues identified by GC-MS

Sample name	Class/Organic residues	Common name	Major/Minor Source	Structural Formula	Unique mass	Retention time (s)
	Lipids					
	Sterols					
CPH6c L24520 H6c CP mastic O1441 S1	Cholesterol		Animals		386	867
	Fatty acids					
H6c CP mastic O1441 S1	Octadecanoic acid	Stearic Acid (C 18:0)	Animal fat		171	845
CPH6c L24520	Tetradecanoic acid	Myristic Acid (C 14:0)	Animal fat		185	684
H6c CP mastic O1441 S1	Eicosanoic acid	Arachidic Acid (C 20:0)	Fish oil		116	892
	Esters					
H6c CP mastic O1441 S1	Methyl stearate		Animal fat		74	880
	Methyl dehydroabietate		Degradation of pine resin		239	914
CPH6c L24520	Dodecanoic acid, methyl ester		Animal fat		74	573
H6c CP mastic O1441 S1	Decanoic acid, methyl ester		Animal fat		186	667
CPH6c L24520	Hexadecanoic acid, methyl ester		Palm oil/ animal fat		74	753
	Terpenes					
	d-Limonene		Citrus oil		93	296
H6c CP mastic O1441 S1	Pinene		Essential oils in plants		93	236
	Ocimene		Essential oils in plants		93	283

i. Cholesterol, the only sterol identified by GC-MS, is a type of steroid lipid characterised by a carbon skeleton, four fused rings and a hydroxyl (OH) group in the third position of the A-ring. Cholesterol is a bio-molecular marker for animal derived fat; this implies the use of animal fat by the site occupants during the ochre-processing workshop. Animal fat is usually used as binder in pigment production (Regert, 2004).

ii. Fatty acids are characterised by the carboxylic acid (COOH) functional group and a long saturated or unsaturated aliphatic tail (long carbon chain). The fatty acids found in animals are mostly saturated while those found in vegetable oils are unsaturated (Pollard *et al.*, 2007). The fatty acids (stearic, myristic and arachidic acid) identified in this study were all saturated and instead of being mainly found in vegetable oil, these are major components of animal fat and other oils, for example arachidic acid is also presently found as a major constituent of peanut oil (Beare-Rogers, Dieffenbacher and Holm, 2001). These oils have been used as binders during pigment production (Colombini and Modugno, 2009).

iii. Methyl esters of dehydroabietic, stearic, palmitic, lauric and capric acid were detected. The methyl ester of dehydroabietic acid is said to be a biomarker for Pinaceae resin. This is because this ester is a typical oxidation product of a resin from the Pinaceae family (Izzo *et al.*, 2013).

iv. The GC-MS analysis also identified terpenes. These occur in all parts of plants but are often extruded as the major components of resins. In the past terpenes have been employed by humans for various reasons including; perfumes, medicines, adhesives, flavours and waterproofing agents (Langenheim, 1990; Pollard and Heron, 1996 and Lampert *et al.*, 2002). This class of organic compounds also exhibits good preservation (Eglinton and Logan, 1991). In this study three monoterpenes (C_{10} compounds) were detected and they are: d-limonene, pinene and ocimene. These are largely found in the volatile fraction (oil of turpentine) obtained upon the

distillation of pine resin. Hence monoterpenes are constituents of essential oils. Generally lower molecular weight terpenes (monoterpenes and sesquiterpenes) are rarely found in archaeological contexts due to their vulnerability to loss through evaporation. However in fossil resins, such as amber, GC-MS has been used to demonstrate the preservation of monoterpenes, within the natural polymer (Mills *et al.*, 1984). The detection of monoterpenes in resin lumps infers that the sediments at Blombos Cave provide favourable preservation conditions.

Due to their intrinsic properties, resins were used as adhesives in ancient times (Colombini and Modungo, 2012). The adhesives are then mixed with plasticisers such as beeswax or extenders such as clay or bone (Geneste and Plisson, 1986). Therefore it can be deduced that the resinous lumps were used as adhesives which were mixed with ochre and other components (such as charcoal, animal fat and marrow as well as water) to produce the pigment.

6.3.2.1 Conclusion

Under favourable circumstances, organic compounds are able to survive in archaeological sediments (Bull *et al.*, 1999b). An organic residue analysis on the components of the toolkit was done. The first step involved using FT-IR to screen for samples that would be suitable for the analysis and the second step was to separate and identify the amorphous organic residues preserved in the samples using GC-MS. The screened samples displayed carbonyl, alkane and hydroxyl peaks in their FT-IR spectra. Also, these samples contained high concentrations of organic residues which were detected by GC-MS. Therefore, FT-IR is a useful technique for screening organic residue-containing samples prior to further analysis by GC–MS.

Among the identified organic residues were bio-molecular markers which were exploited to provide insight into the origin of the residues. In context to Blombos Cave, particularly the CP layer (where the pigment processing toolkit was recovered) the use of bio-molecular markers for organic residue analysis was imperative in order to trace the origin of the organic residues. Knowing the origin

of the organic residue provided insight into the natural products such as resins, fats and oils, exploited by prehistoric site occupants, during the pigment-processing workshop.

From the organic residue analysis, the following remark can be made; the presence of cholesterol, fatty acids and terpenes supposes the use of resins, fats and oils by the site occupants. The exact use of these may not be clear; however they could have been used as binders and adhesives for the pigment.

Although the analysis of organic residues has a great potential in archaeological research, a number of problems remain and are worth mentioning. These problems arise as a result of post-depositional changes in the molecules either through contamination or the breaking down of the original molecules into small, unidentifiable components (Price and Burton, 2012). Contamination is a controllable measure and should be avoided in the manipulation of samples. Generally, sterols are seldom detected in archaeological residues because of their low concentration and tendency to undergo chemical degradation (Colombini and Modungo, 2009). According to Evershed (1993), cholesterol is among the lipid components of human skin and its occurrence in archaeological samples may simply suggest contamination. Therefore it is likely that cholesterol was accidentally introduced by the handling of artifacts after their recovery.

CHAPTER SEVEN

Overall conclusion and future research

This chapter summarizes the conclusions from this study and the recommendations identified for future studies.

7.1 Overall conclusion

The sediment deposits as well as the 100 ka ochre processing toolkit from Blombos Cave were successfully characterised.

The following conclusions can be made from the studying the sediment deposits:

- there was a non-contiunous anthropogenic occupation of Blombos Cave, as shown by the fluctuations in the bio-essential elements upon proceeding down the sediments profile,
- fire use and pigment processing, by the occupants, were the main activites which led to the elemental enrichment of the sediments.

Characterising the 100 ka ochre processing toolkit has led to the following hypothesis:

A group of prehistoric humans came to the cave some 100,000 years ago, with an intention of creating a mineral based pigment mixture they would use (probably for symbolic intent. They brought pieces of clayey iron-oxide material (ochre) which were specifically sourced to be used in the paint production. Red was the colour preferred by these humans (hue given by natural hematite or heated goethite) because of its significant role in cultures as a ritual representation of blood. Even though the prehistoric humans were not chemists, they developed a technique of heating substances to produce new substances and hence used it as a craft tool. Upon heating the ochre a chemical reaction in which the yellow/brown ochre (goethite) produces a new red substance, was taking place. The prehistoric humans were not aware they were changing the hydrated iron (III) oxide to anhydrous iron (III) oxide. Mineral based pigments have the advantage of being chemically stable and require little processing. Hence it can be said that these people were technologically advanced.

Part of their workshop involved grinding (using quartzite slabs) the iron-rich (red) material into fine powder. Both marine and terrestrial animal bones were heated and crushed in order to extract the marrow and fat. The extracted animal fat, charcoal, essential plant oils and some resinous substance were probably used as

binders to help the paint stick onto a surface while the crushed bones were used as extenders to help the paint cover a larger surface area. The pigment compound was stored in a few abalone shells then longer and thinner animal bones were dipped into the mixture to transfer or apply the pigment. These animal bones were found with pigment stains close to the abalone shell.

It seems as though the CP layer was primarily used as a workstation to produce the pigment.

Physico-chemical characterisation of ochre has shown to provide useful insights concerning selection criteria in MSA contexts.

7.2 Future research

As part of future research, sediment samples from other quadrates within the occupation units would have to be analysed in order to acquire an even better understanding of past human activities through the chemical signatures preserved in the sediments.

It is evident from the characterisation investigations carried out in this study that prehistoric populations at Blombos Cave widely utilized hematite and aluminosilicate- containing ochre pigments. According to the statistical analysis different sources for these ochre pigments are probable. Consequently it will be beneficial to sample and characterise the ochre from potential sources within the geographic proximity of Blombos Cave this is critical in order to establish the geographical extent of ochre procurement. This investigation would contribute to a further understanding of how far the cave inhabitants may have travelled to get ochre, and potentially the range of their resource catchments.

In addition, sampling of ochre pieces from other MSA sites in the Western Cape (for example Diepkloof Rock shelter) would help to further verify the extent of the movement of ochre materials, specifically between prehistoric sites.

List of conferences, seminar presentations and publications

Mphuthi, D., Cukrowska, E. and Rifkin, R. *Assessing the bioavailability of toxic trace elements in archaeological ochre using synthetic leachates*, ANALITIKA 2014, milestones in measurements, 7 to 11 September 2014, Khaya Ibhubesi conference centre, Free State. Oral presentation.

Mphuthi, D., Cukrowska, E. and Rifkin, R. *Assessing the bioavailability of toxic trace elements in archaeological ochre using synthetic leachates*, 6th Cross-Faculty Graduate Symposium, 28 to 29 October 2014, University of the Witwatersrand Johannesburg. Poster presentation.

Moyo, S., Mphuthi, D., Cukrowska, E., Henshilwood, C.S., van Niekerk, K. and Chimuka, L. (2015) Blombos Cave: Middle Stone Age ochre differentiation through FT-IR, ICP OES, ED XRF and XRD, *Quartenary International* (in press) http://dx.doi.org/10.1016/j.quaint.2015.09.041.

REFERENCES

Abdeljalil, B., Barton, N., Vanhaeren, M., d'Errico, F., Collcutt, S., Higham, T. and Edward Hodge (2007) 82,000-year-old shell beads from North Africa and implications for the origins of modern human behaviour. *Proceedings of the National Academy of Sciences of the USA*, vol. 104, no.24, pp. 9964–9969.

Aldenderfer, M. S. and Blashfield, R. K., (1992) Cluster Analysis. Sage Publications, Inc.: Newbury Park, 1984; vol. 44.Glascock, pp 11-26.

Allain, J. and Rigaud, A (1986) Décor et function: quelques exemles tirés du Magdalénien, *L'Anthropologie,* vol. 90, pp. 713–738.

Arcinus, A. (2000), Overview of inductively coupled plasma optical emission spectroscopy (ICP-OES) for use in barium concentration determination.

Arrhenius, G. (1963) Pelagic sediments. In the sea,3 (M.N. Hill ed), pp. 655-727.

Armbruster D. A. and Pry T., (2008) Limit of Blank, Limit of Detection and Limit of Quantitation, the Clinical Biochemist Reviews. Available online at: http://www.ncbi.nlm.nih.gov/pmc/articles/PMC2556583/

Aston, M.A., Martin, M.H., and Jackson, A.W. (1998) The potential for heavy metal soil analysis on low status archaeological sites at Shapwick, Somerset. *Antiquity*, vol.72, pp. 836–847.

Balakhnina, I. A., Brandt, N. N., Kimberg, Y. S., Rebrikova, N. L. and Chikishev, A. Y. (2011) Variations in the IR spectra of yellow ochre due to mixing with binding medium and drying. *Journal of Applied Spectroscopy* vol. *78*, no. 2, pp. 183-188.

Barham, L. (2001) Central Africa and the emergence of regional identity in the Middle Pleistocene, *In Human roots: Africa and Asia in the Middle Pleistocene*. (ed.s Barham, L.S. and Robson-Brown, K.) pp. 65–80. Bristol: Western Academic & Specialist.

Baxter, M. J. (1994) Exploratory multivariate analysis in archaeology. Edinburgh University Press: Edinburgh, pp. 12.

Baxter, M. J. (1995) Standardization and transformation in principal components analysis, with applications to archaeometry, *Applied Statistics*, vol. 44, no. 4, pp. 513-527.

Beare-Rogers, A. Dieffenbacher and J. V. Holm (2001) Lexicon of lipid nutrition (IUPAC Technical Report), vol. 73,no. 4, pp. 685-744

Bellamy L.J. (1958) The Infrared Spectra of Complex Molecules. Methuen, London.

Berna, F., and Goldberg, P. (2008) Assessing Paleolithic pyrotechnology and associated hominin behaviour in Israel, *Israel Journal of Earth Science*, vol. 56 , pp. 107-121.

Berna, F., Behar, A., Shahack-Gross, R., Berg, J., Boaretto, E., Gilboa, A. (2007), Sediments exposed to high temperatures: Reconstructing pyrotechnological processes in Late Bronze and Iron Age Strataat Tel Dor (Israel), *Journal of Archaeological Science,* vol.34, no. 3, pp. 358-373.

Bernatchez, J. A. (2008). Geochemical characterisation of archaeological ochre at Nelson Bay Cave (Western Cape Province), South Africa. *The South African Archaeological Bulletin*, 3-11.

Bethell, P.H. and Mate, I. (1989) The use of soil phosphate analysis in archaeology: A critique. *In J. Scientific analysis in archaeology and its interpretation* (pp. 1–29), (ed.s Henderson), Oxford University Commission for Archaeology Monograph 19. Oxford: Oxford University Press.

Bikiaris, D., Daniilia, S., Sotiropoulou, S., Katsimbiri, O., Pavlidou, E., Moutsatsou, A.P. and Chryssoulakis, Y. (1999). Ochre-differentiation through micro-Raman and micro-FT-IR spectroscopies, application on wall paintings at Meteora and Mount Athos, Greece. *Spectrochimica Acta* Part A, vol. 56, pp. 3–18.

Birkeland, P.W. (1999) *Soils and geomorphology*, Oxford university press, pp. 18-19.

Bishop, R. L.,Neff, H., (1989) Compositional Data Analysis in Archaeology. In *Archaeological chemistry IV* : developed from a symposium sponsored by the Division of History of Chemistry at the 193rd meeting of the American Chemical Society, Denver, Colorado, April 5-10 (1987) Allen, R. O., Ed. American Chemical Society: Washington, DC, pp 13.

Bleek, W.H.I., Lloyd, L. (1911) Specimens of Bushman Folklore. George Allen, London.

Blome, M. W., Cohen, A.S., Tryon, C.A., Brooks, A.S. and Russell, J. (2012) The environmental context for the origins of modern human diversity: A synthesis of regional variability in African climate 150,000–30,000 years ago, *Journal of Human Evolution*, vol. 62, no. 5, pp. 563-592.

Bohn, H.L, McNeal, B.L. and O Connor, G.A. (1985) *Soil Chemistry*. 2nd edition. Wiley, New York.

Bonneau, A., Pearce, D.G. and Pollard, A.M. (2012) A multi-technique characterisation and provenance study of the pigments used in San rock art, South Africa. *Journal of Archaeological Science*, vol. 39, no. 2, pp. 287–294.

Braadbaart, F., Poole, I. and van Brussel, AA. (2009)Preservation potential of charcoal in alkaline environments: an experimental approach and implications for the archaeological record, Journal of Archaeological Science, vol.36, pp. 1672–1679.

Brandt, S.A., Weedman, K. (2002a) The ethnoarchaeology of hide working and stone tool use in Konso, southern Ethiopia: an introduction. *Le Travail du cuir le préhistoire à nos jours, vol.* 22, pp. 113–129.

Brandt, S.A., Weedman, K. (2002b) Woman the toolmaker: a day in the life of an Ethiopian woman who scrapes hides the old-fashioned way, *Archaeology*, Sep/Oct: pp. 50–53.

Brown, K., Marean, C., Roberts, D., Herries, A., Braun, D., Tribolo, C., Jacobs, Z. (2008) First documentation of heat treatment of silcrete in the Howiesons Poort and Still Bay Middle Stone Age industries, Southern Cape, South Africa. Paper Pre- sented to the Paleoanthropology Society Meeting in Vancouver, Canada.

Bu, K., Cizdziel, J. V., and Russ, J. (2013) The source of iron-oxide pigments used in Pecos River style rock paints, *Archaeometry*, vol. 55, pp. 1088–100.

Bull, I. D., Simpson, I. A., van Bergen, P. F., and Evershed, R. P. (1999b) Muck 'n' molecules: organic geochemical methods for detecting ancient manuring, *Antiquity*, vol. 73, pp. 86–96.

Burkitt, M.C. (1928) South Africa's past in stone and paint. London: Cambridge University Press.

Canti M.G, (1998) Origin of calcium carbonate granules found in buried soils and quaternary deposits, Boreas, vol. 27, pp. 275-288.

Canti, M.G., (2007) Deposition and taphonomy of earthworm granules in relation to their interpretive potential in Quaternary stratigraphy, *Journal of Quaternary Science*, vol. 22, no. 2, pp. 108-111.

Carr, C. (1982) Handbook on soil resistivity surveying, chapter 5, Center for American archaeology, Evanston, Illinois, pp. 112, 127-131.

Charrié-Duhaut, A., Connan, J., Darnell, M., Spangenberg, J., Szymczyk, E., Bissada, A. and Albrecht P. (2009b), Molecular and isotopic characterisation of organic samples from the wreck of the Saint-Etienne merchant ship (18^{th} century): Identification of pitch, fat, hair and sulfur, *Organic Geochemistry*, vol.40, pp. 647- 665.

Chase, B. M. (2010) South African palaeoenvironments during marine oxygen isotope stage 4: a context for the Howiesons Poort and Still Bay industries, *Journal of Archaeological Science* vol. 37, no. 6, pp. 1359-1366.

Colombini, M.P. and Bonaduce,I. (2004) Characterisation of beeswax in works of art by gas chromatography-mass spectrometry and pyrolysis-gas chromatography-mass spectrometry procedures, *Journal of Chromatography*, vol 1028, pp. 297-306.

Colombini, M.P. and Modugno, F. (2004) Characterisation of proteinaceous binders in artistic paintings by chromatographic techniques, Journal of Separation Science, vol. 27, no. 3, pp 147–160.

Colombini, M.P. and Modugno, F. (2009), Chapter 1: *Organic Materials in Art and Archaeology*, John Wiley & Sons, Ltd, pp 4.

Compton, J. S. (2011) Pleistocene sea-level fluctuations and human evolution on the southern coastal plain of South Africa, *Quaternary Science Reviews*, vol. 30, no. 5-6, pp. 506-527.

Cook, S. F., and Heizer, R. F. (1962) Chemical analysis of the Hotchkiss Site, *Reports of the University of California Archaeological Survey no. 57, part 1*, University of California, Berkeley.

Cook, S. F., and Heizer, R. F. (1965) *Studies on the chemical analysis of archaeological sites*, University of California Publications in Anthropology No. 2. University of California, Berkeley.

Cornell, R. M. and U. Schwertmann (2003). The iron-oxides: structure, properties, reactions, occurrences, and uses. Weinheim, Wiley-VCH.

Courty, M.-A. (2001) Microfacies analysis assisting archaeological stratigraphy. *Earth Sciences and Archaeology*. (ed.s P. Goldberg, V. T. Holliday and C. R. Ferring), London, Kluwer, pp. 205-239.

Datnoff , L. E., Rodrigues, F. A. and Seebold, K.W. (2007) Silicon and plant disease. In: *Mineral Nutrition and Plant Disease*. (eds. Datnoff, L.E. , Elmer, W.H., Huber, D.M.), St. Paul MN, EUA. APS Press. pp. 233-246.

Davies, B.E., Bintliff, J.L., Gaffney, C.F., and Water, A.T. (1988) Trace metal residues in soil as markers of ancient site occupation in Greece. In *proceedings of the 22nd Trace Substances in Environmental Health Symposium*, pp. 391–398, (eds Hemphill, D.D.) ,St. Louis, MO: University of Missouri.

Dayet, L., Texier, P-J., Daniel, F. and Porraz, G. (2013). Ochre resources from the Middle Stone Age sequence of Diepkloof Rock Shelter, Western Cape, South Africa. *Journal of Archaeological Science, vol.* 40, no. 9, pp. 3492–3505.

Dayet, L., Le Bourdonnce, F-X., Daniel, F., G. Porraz., F.G. and Texier, P.J. (2015) Ochre Provenance and Procurement Strategies During The Middle Stone Age at Diepkloof Rock Shelter, South Africa. Archaeometry (doi: 10.1111/arcm.12202)

Deer, W.A., Howie, R.A. and Zussman, J. (1992). 2nd ed. *An Introduction to the Rock-forming Minerals*. Essex: Longman Scientific and Technical; New York: Wiley. pp. 696.

Delhez, R., de Keijser, Th.H., Langford, J.I., Louër, D., Mittemeijer, E.J., Sonneveld, E.J. (1993) Crystal imperfection broadening and peak shape in the Rietveld method In: The Rietveld Method, (eds. Young, R.A.) *International Union of Crystallography*. Oxford Science Publications, pp. 132-166, invited paper.

Derrick, M.R., Stulik, D. and Landry, J.M. (1999) Infrared Spectroscopy in Conservation Science, Scientific Tools for Conservation, The Gety Conservation Institute Los Angeles.

d'Errico, F., Henshilwood,C.S. and Nilssen, P. (2001) An Engraved Bone Fragment From c. 70,000- Year-Old Middle Stone Age Levels at Blombos Cave, South Africa: Implications for the Origin of Symbolism and Language, *Antiquity*, vol. 75, no. 288, pp. 309-318.

d'Errico, F., Henshilwood, C.S., Vanhaeren, M. and van Niekerk, K.L. (2005) Nassarius kraussianus shell beads from Blombos Cave: evidence for symbolic behaviour in the Middle Stone Age, *Journal of Human Evolution*, vol. 48, no. 1, pp. 3-24.

d'Errico, F., and Henshilwood, C.S. (2007) Additional evidence for bone technology in the southern African Middle Stone Age, *Journal of Human Evolution*, vol. 52, no. 2, pp. 142-163.

d'Errico, F., Moreno, G.R. and Rifkin, R.F. (2012) Technological, elemental and colorimetric analysis of an engraved ochre fragment from the Middle Stone Age levels of Klasies River Cave 1, South Africa, *Journal of Archaeological Science*, vol. 39, no. 4, pp. 942-952.

Dibble, H., Berna, F., Goldberg, P., McPherron, S. J. P., Mentzer, S., Niven, L., (2009) A preliminary report on Pech de l, Azé IV, Layer 8 (Middle Paleolithic, France). PaleoAnthropology, pp. 182-219.

Downer, N.R (2008) *Method development for the digestion and analysis of four common sedimentary lithologies using ICP-OES and ICP-MS*, Master's dissertation, Univesity of Johannesburg.

Dunteman, G. H. (1989) Principal Components Analysis. Sage Publications, Inc.: Thousand Oaks, CA, vol. 69.

Eglinton. G. and Logan, G.A. (1991) Molecular preservation, Philosophical Transactions of the Royal Society of London Series B vol. 333, 315–328.

Eidt, R.C. (1984) *Advances in abondened settlement analysis: Applications to prehistoric anthols in Colombia, S.A.*, Centre for Latin American studies, university of Wisconsin, MilwaukeePress, pp. 25–27.

Elias, M., Chartier, C., Prévot, G., Garay, H. and Vignaud, C. (2006). The colour of ochres explained by their composition. *Materials Science and Engineering B*, vol. 127, pp. 70–80.

Evans, U. (1994) Hollow Rock Shelter, a Middle Stone Age site in the Cederberg, *Southern African Field Archaeology*, vol. 3, no. 2, pp. 63–73.

Evershed, R.P. (1993) Biomolecular Archaeology and Lipids, *World Archaeology*, vol. 25, pp. 74-93.

Evershed, R.P. (2008) Organic residue analysis in archaeology: the archaeological biomarker revolution, *Archaeometry*, vol. 50, no. 6, pp. 895-924.

Farmer, V. C. (1974) The Infrared Spectra of Minerals. *Mineralogical Society*, London

Filippakis, S.E., Perdikatsis, B. and Assimenos, K. (1979) X-ray analysis of pigments from Vergina, Greece (second tomb). *Studies in Conservation*, vol. 24, pp. 54-58.

Freestone, I.C. and Middleton,A.P. (1987) Mineralogical applications of the analytical SEM in archaeology, *British Museum Research Laboratory*, London WC1B 3DG.

Friedel, J. and U. Schwertmann (1996). Aluminium influence on iron-oxides: 18, The effect of Al substitution and crystal size on magnetic hyperfine fields of natural goethites, *Clay Minerals*, vol.31, pp. 455-464.

Gebauer D., Volkel, A and Coelfen, H. (2008) Stable production of prenucleation of calcium carbonate clusters, *Science*, pp.1819-1822.

Genestar, C. and Pons, C. (2005) Earth pigments in painting: characterisation and differentiation by means of FT-IR spectroscopy and SEM-EDS microanalysis, *Analytical and bioanalytical chemistry, vol. 382, no.* 2, pp. 269-274.

Geneste, .M. and Plisson, H. (1986) Le Solutréen de la Grotte de combe sauniére 1 (Dordogne) premiére approche palenthnologique, Gallia Préhistoire, vol. 29, no. 1, pp. 9-27, *Geoarchaeology*, vol. 22, no. 7, pp. 775 – 796.

Gil, M., Carvalho, M. L., Seruya, A., Candeias, A. E., Mirão, J. and Queralt, I. (2007). Yellow and red ochre pigments from southern Portugal, elemental composition and characterisation by WDXRF and XRD. *Nuclear Instruments and Methods in Physics Research A* 580, pp. 728–731.

Glascock, M. D. (1992) Characterisation of Archaeological Ceramics at MURR by Neutron Activation Analysis and Multivariate Statistics. In, *Chemical Characterisation of Ceramic Pastes in Archaeology*, (eds. Neff, H.), Madison Wisconsin: Prehistory Press. pp.11-29.

Glascock, M. D.,Braswell, G. E. and Cobean, R. H., (1998) A systematic approach to obsidian source characterisation. In *Archaeological Obsidian Studies*: *Method and Theory*, (eds. Shackley, M. S.) Plenum Press: New York and London, pp 15-65.

Glascock, M. D. and Neff, H. (2003) Neutron Activation Analysis and Provenance Research in Archaeology, *Measurement Science and Technology*, vol. 14, pp. 1516-1526.

Goldberg, P., Weiner, S., Bar-Yosef, O., Xu, Q., and Liu, J. (2001), Site formation processes at Zhoukoudian, China. *Journal of Human Evolution*, vol. 4, no. 5, pp. 483-530.

Goldberg, P., and Macphail, R. (2006) Practical and Theoretical Geoarchaeology. Oxford: Blackwell, Ch 8, 10 and 11.

Goldberg, P., Miller, C., Schiegl, S., Ligouis, B., Berna, F., Conard, N. (2009) Bedding, hearths, and site maintenance in the Middle Stone Age of Sibudu Cave, KwaZulu-Natal, South Africa, *Archaeological and Anthropological Sciences*, vol. 1, no. 2, pp.95 – 122.

Goldberg, P., Dibble, H., Berna, F., Sandgathe, D., McPherron, S. J. P., and Turq, A. (2012) New evidence on Neandertal use of fire: Examples from Roc de Marsal and Pech de l Azé IV, *Quaternary International*, vol.247 ,pp. 325-340.

Goldstein, J., Newbury, D.E., Joy, D.C., Lyman, C.E., Echlin, P., Lifshin, E., Sawyer, L. and Michael, J.R. (2003) Scanning Electron Microscopy and X-ray Microanalysis Third edition.

Goodall, R.; David, B.; Bartley, J. (1996) Non-destructive Techniques for the Analysis and Characterisation of Pigments from Archaeological Sites: The Case of Fern Cave. In 283 Australian Archaeology '95: Proceedings of the 1995 Australian Archaeological Association Annual Conference, Ulm, S.; Lilley, I.; Ross, A., Eds. The University of Queensland: St Lucia, Queensland, vol. 6, pp 183-187.

Goodall, R. A, Hall, J, Edwards, H. G. M, Sharer, R. J, Viel, R, and Fredericks, P. M. 2007. Raman microprobe analysis of stucco samples from the buildings of Maya Classic Copan. Journal of Archaeological Science 34(4), p. 666-673.

Goodall, R.A., Hall, J., Viel, R. and Fredericks, P.M. (2009) A spectroscopic investigation of pigment and ceramic samples from Copán, Hondurar, Archaeometry, vol. 51, pp. 95-109.

Goodwin, A. J. H., and Van Riet Lowe, C. (1929) The Stone Age cultures of South Africa. New York: AMS Press.

Grine, F. E., and Henshilwood, C.S. (2002) Additional human remains from Blombos Cave, South Africa: (1999-2000 excavations), *Journal of Human Evolution*, vol. 42, no. 3, pp. 293-302.

Groenman van Waateringe, W. and Robinson,M. (1988) Man made soils. British archaeological reports IS 410, Oxford.

Haaland, M.M. (2012) *Intra-site spatial analysis of the Still Bay units in Blombos Cave, South Africa,* Master's thesis, University of Bergen.

Heidenreich, C.E., and Navratil, S. (1973) Soil analysis at the Robitaille site. Part 1: Determining the perimeter of the village. *Ontario Archaeology*, vol. 20, pp. 25–32.

Helwig, K. (1998) Mars colours: preparation methods and chemical composition, *Painting Techniques History, Materials and Studio Practice*, Summaries of Posters at the IIC Dublin Congress, 7-11 September, London.

Helwig, K. (2007) Iron-oxide pigments: Natural and synthetic. Artists' Pigments: A Handbook of Their History and Characteristics. B. H. Berrie. Oxford, Archetype Publications, vol. 4, pp. 39 – 109.

Henderson, P. (1984) *Rare earth element geochemistry*, Elsevier: Amsterdam; New York, pp 18.

Henshilwood, C. S., and Sealy, J. (1997) Bone Artifacts from the Middle Stone Age at Blombos Cave, Southern Cape, South Africa, *Current Anthropology*, vol. 38, no. 5, pp. 890-895.

Henshilwood, C. S., d'Errico, F., Marean, C.W., Milo, R.G. and Yates, R. (2001a) An early bone tool industry from the Middle Stone Age at Blombos Cave, South Africa: implications for the origins of modern human behaviour, symbolism and language, *Journal of Human Evolution*, vol. 41, no. 60, pp. 631-678.

Henshilwood, C. S., Sealy, J.C., Yates, R., Cruz-Uribe, K., Goldberg, P., Grine, F.E., Klein, R.G., Poggenpoel, C., van Niekerk, K.L. and Watts. I (2001b) Blombos Cave, Southern Cape, South Africa: Preliminary Report on the 1992–1999 Excavations of the Middle Stone Age Levels, *Journal of Archaeological Science*, vol. 28, no. 40, pp. 421-448.

Henshilwood, C. S., d'Errico, F., Yates, R., Jacobs, Z., Tribolo, C., Duller, D.A.T., Mercier, N., Sealy, J.C., Valladas, H., Watts, I. and Wintle, A.G. (2002) Emergence of Modern Human Behaviour: Middle Stone Age Engravings from South Africa, *Science,* vol. 295, no. 5558, pp. 1278-1280.

Henshilwood, C. S., Marean, C. W., Clark, G., Errico, F., Kaufman, D., Shea, J., and Niekerk, K. Van. (2003) The origin of modern human behavior, *Current Anthropology*, vol. *44, no.* 5, pp. 627–651.

Henshilwood, C. S., d'Errico, F., Vanhaeren, M., van Niekerk, K.L. and Jacobs, Z. (2004) Middle Stone Age shell beads from South Africa, *Science*, vol. 304, no. 5669, pp. 404.

Henshilwood, C. S. (2006) Stratigraphic Integrity of the Middle Stone Age Levels at Blombos Cave. In *From tools to symbols: from early hominids to modern humans*; in honour of Professor Phillip V. Tobias, (ed.s d'Errico, F. and Backwell, L.), Johannesburg: Witwatersrand University Press, pp. 441-448.

Henshilwood, C. S., d'Errico, F. and Watts, I. (2009) Engraved ochres from the Middle Stone Age levels at Blombos Cave, South Africa. *Journal of Human Evolution*, vol. 57, no. 1, pp. 27-47.

Henshilwood, C. S., and Dubreuil, B. (2009) Reading the artifacts: gleaning language skills from the Middle Stone Age in southern Africa. *In the cradle of language*, (ed.s Botha, R.P. and Knight, C.), Oxford ; New York: Oxford University Press vol. 18, pp. 386.

Henshilwood, C. S., d'Errico, F, van Niekerk, K.L., Coquinot, Y., Jacobs, Z., Lauritzen, S.E., Menu, M. and García-Moreno, R. (2011) A 100,000-Year-Old Ochre-Processing Workshop at Blombos Cave, South Africa, *Science*, vol. 334, no. 6053, pp. 219-222.

Henshilwood, C. S., and Dubreuil, B. (2011) The Still Bay and Howiesons Poort, 77–59 ka: Symbolic Material Culture and the Evolution of the Mind during the African Middle Stone Age, *Current Anthropology*, vol. 52, no. 3, pp. 361-400.

Henshilwood, C. S. (2012) The Still Bay and Howiesons Poort: 'Palaeolithic' techno-traditions in southern Africa. *Journal of World Prehistory*, vol. 25, pp. 205-237.

Henshilwood, C.S. and van Niekerk, K.L. (2013) Blombos Cave: The Middle Stone Age Levels, *Encyclopaedia of Global Archaeology*, vol. 240.

Heron, C. and Evershed, R.P. (1993) The analysis of organic residues and the study of pottery use. In *Archaeological Method and Theory* 5 (ed.s. Schiffer, M.) University of Arizona Press, Arizona, pp. 247-284.

Hodgskiss, T. (2013). Ochre use in the Middle Stone Age at Sibudu, grinding, rubbing,
scoring and engraving. *Journal of African Archaeology, vol.* 11, no. 1, pp. 75–95.

Högberg, A., and Larsson, L. (2011) Lithic technology and behavioural modernity: New results from the Still Bay site, Hollow Rock Shelter, Western Cape Province, South Africa, *Journal of Human Evolution*, vol. 61, no. 2, pp. 133-155.

Holliday, V.T. (2004). *Soils and Archaeological Research.* Oxford University Press.

Holliday, V.T. and Gartner, W.G. (2007) Methods of soil P analysis in archaeology, *Journal of archaeological science,* vol. 34, pp.301-333.

Hong, H.,Cheng, F., Yin, K., Churchman, G.J., Wang, C. (2014) Three-component mixed-layer illite/smectite/kaolinite (I/S/K) minerals in hydromorphic soils, south China, *American Mineralogist*, vol. 100, no. 8-9, pp 1883–1891.

Hradil, D., Grygar, T., Hradilová, J. and Bezdièka, P. (2003). Clay and iron-oxide pigments in the history of painting. *Applied Clay Science*, vol. 22, pp. 223–236.

Hutter J. W., (2011) Performance characteristics of analytical tests, AL control laboratories, Intersol, pp. 6-9.

Iriarte, E., Foyo, A., Sánchez, M. A., Tomillo, C. & Setién, J. (2009). The origin and geochemical characterisation of red ochres from the Tito Bustillo and Monte Castillo caves (northern Spain)., *Archaeometry , vol. 5, no.* 2, pp. 231–51.

Izzo, F.C., Ferriani, B., Van den Berg, K.J., Van Keulen, H. and Zendri, E. (2013) 20th century artists, oil paints the case of the Olii by Lucio Fontana, J Cult Herit.

Jacobs, Z., Duller, G.A., Wintle, A.G. and Henshilwood, C.S. (2006) Extending the chronology of deposits at Blombos Cave, South Africa, back to 140 ka using optical dating of single and multiple grains of quartz, *Journal of Human Evolution*, vol. 51, no. 3, pp. 255-273.

Jacobs, Z., Roberts, R. G., Galbraith, R. F., Deacon, H. J., Grün, R., Mackay, A., Wadley, L. (2008) Ages for the Middle Stone Age of southern Africa: implications for human behavior and dispersal. *Science*, vol. 322, pp. 733–735.

Jercher, M., Pring, A., Jones, P. G. and Raven, M. D. (1998) Rietveld X-Ray Diffraction and X-Ray Flourescence analysis of Australian Aboriginal ochres. *Archaeometry, vol.* 40, no. 2, pp. 383–401.

Jones, R. and Hanson, H.C. (1985). Mineral licks, geophagy, and biogeochemistry of North American ungulates. Ames: Iowa State Press, *Journal of Archaeological Science* , vol. 37, pp. 3022.

Judson, S. (1959) Paleolithic paint, *Science*, vol. 130, pp 708.

Karkanas, P. (2007) Identification of lime plaster in prehistory using petrographic methods: A review and reconsideration of the data on the basis of experimental and case studies.

Kedrowski, B.,Crass, B.A., Behm, J.A., Luetke, J.C., Nichols,A.L. and Moreck, A.M. (2009) GC/MS analysis of fatty acids from ancient hearth residues at the swan point archaeological site, *Archaeometry*, vol.5, no. 10, pp. 110-112.

Kiehn, A.V., Brook, G.A., Glascock, M.D., Dake, J.Z., Robbins, L.H., Campbell, A.C. and Murphy, M.L. (2007) Fingerprinting specular hematitefrom mines in Botswana, Southern Africa. In *Archaeological chemistry: analytical techniques and archaeological interpretation*, ACS Symposium Series No. 968, Oxford University Press, (ed.s Glascock, M.D., Speakman, R.J. and Popelka-Filcoff, R.S.) pp.460-479.

Knezevich, M. (1998) Geophagy as therapeutic mediator of endoparasitism in a free-ranging group of rhesus macaques (*Macaca mulatta*), *American Journal of Primatology, vol.* 44, pp. 71-82.

Knudson, K.J., Frink, L., Hoffman, B.N. and Price, T.D. (2004) Chemical characterisation of Arctic soils: activity area analysis in contemporary Yupík fish camps using ICP-AES, *Journal of archaeological science*, vol. 31, pp. 443-456.

Kotronarou, A., Mills, G., and Hoffmann, M. R. (1992). Decomposition of parathion in aqueous solution by ultrasonic irradiation, *Envir. Sci. and Technol*.,vol 26, no. 10, pp. 1460–1462.

Krekel C., Polborn, K. (2003) Lime Blue: A Mediaeval Pigment for Wall Paintings*? Studies in Conservation*, vol. 48, pp. 171-182.

Kreulen, D. A.(1985). Lick use by large herbivores, A review of benefits and banes of soil consumption. *Mammal Review* , vol. 15, pp.107-123.

Langenheim, J.H. (1981) Terpenoids in the leguminosae in Advances in legume systematics, Royal Botanic gardens, Kew, pp. 627-655.

Lawrence, W. (1960) Review of extender pigments. *Paint industry magazine*, vol 75, pp.16-61.

Leonardi, G., Miglavacca, M., and Naradi, S. (1999) Soil phosphorus analysis as an integrative tool for recognizing buried ancient plough soils, *Journal of Archaeological Science*, vol. 26, pp. 343–52.

Linderholm, J., and Lundberg, E. (1994). Chemical characterisation of various archaeological soil samples using main and trace elements determined by inductively coupled plasma atomic emission spectrometry. *Journal of Archaeological Science*, vol. 21, pp. 303–314.

Littlewood, A.B. (1970) Gas chromatography principles, techniques and applications, 2nd ed, Academic press, New York, 6.

Lombard, M. (2006a) First impressions of the functions and hafting technology of Still Bay pointed artifacts from Sibudu Cave, *Southern African Humanities*, vol. 18, no. 1, pp. 27-41.

Lombard, M. (2007) The gripping nature of ochre: The association of ochre with Howiesons Poort adhesives and Later Stone Age mastics from South Africa. *Journal of Human Evolution*, vol. 53, no. 4, pp. 406-419.

Lombard, M. and Phillipson, L. (2010) Indications of bow and stone-tipped arrow use 64,000 years ago in KwaZulu-Natal, South Africa, *Antiquity*, vol. 84, no. 325, pp.635–648.

Lombard, M. (2011) Quartz-tipped arrows older than 60 ka: further use-trace evidence from Sibudu, KwaZulu-Natal, South Africa, *Journal of Archaeological Science*, vol. 38, no. 8, pp. 1918-1930.

Lombard, M. (2012) Thinking through the Middle Stone Age of sub-Saharan Africa, *Quaternary International*, vol. 270, pp. 140-155.

Lozano, G. (1998) Parasitic stress and self-medication in wild animal, *Advances in the Study of Behaviour* , vol.27, pp. 291-317.

MacDonald, B. L., Hancock R. G. V. Cannon, A. and Pidruczny, A. (2011) Geochemical characterisation of ochre from central coastal British Columbia, Canada, *Journal of Archaeological Science*, vol. 38, pp.3620-3630.

Mackay, A., and Welz, A. (2008) Engraved ochre from a Middle Stone Age context at Klein Kliphuis in the Western Cape of South Africa, *Journal of Archaeological Science*, vol. 35, no. 6, pp. 1521-1532.

Makiese, J.G., (2012) Characterisation and modelling of mercury speciation in industrially polluted areas due to energy production and mineral processing in South Africa, PhD thesis, University of the Witwatersrand Johannesburg.

Mallol, C., Marlowe, F. W., Wood, B. M., and Porter, C. C. (2007) Earth, wind, and fire: Ethnoarchaeo-logical signals of Hadza fires, *Journal of Archaeological Science, vol.34*, no. 12, pp. 2035-2052.

Marean, C.W., Bar-Matthews,M., Bernatchez, J., Fisher, E., Goldberg, P., Herries, A.I.R., Jacobs, Z. (2007) Early human use of marine resources and pigment in South Africa during the Middle Pleistocene. *Nature*, vol. 449, no. 7164, pp.905–908.

Marshall, L., (1976) The Kung of Nyae Nyae. Harvard University Press, Cambridge.

Mayerhöfer T. G., (2004) Modelling IR-spectra of single-phase polycrystalline materials with random orientation –A unified Approach. *Vibration Spectroscopy*, vol. 35, pp. 67-76.

McBrearty, S. and Brooks, A.S. (2000) The revolution that wasn't: a new interpretation of the origin of modern human behaviour. *Journal of Human Evolution*, vol. 39, no. 5, pp. 453-563.

Middleton, W.D., and Price, T.D. (1996). Identification of activity areas by multi-element characterisation of sediments from modern and archaeological house floors using inductively coupled plasma atomic emission spectroscopy, *Journal of Archaeological Science*, vol. 23, pp. 673–687.

Middleton,W.D. (2004) Identifying chemical activity residues on prehistoric house floors: a methodology and rationale for multi-elemental characterisation of a mild acid extract of anthropogenic sediments *Archaeometry*, vol.46,no. 1, pp. 47–65.

Mills, J.A., Lavers, R.B. and Lee, W.G. (1984) The takahe- a relic of the Pleistocene grassland avifauna in New Zealand, *Journal of ecology*, vol.7, pp. 55-70.

Minichillo, T. (2005) *Middle Stone Age lithic study, South Africa: An examination of modern human origins*. PhD dissertation. Seattle: University of Washington.

Mitra, S. (2003) Sample Preparation Techniques in Analytical Chemistry, A series of monographs on analytical chemistry and its applications, (John wiley & sons, inc., publication, 162). pp 140, 145, 163-172, 230.

Montagner, C., Sanches, D., Pedroso, J., Melo, M.J. and Vilarigues, M., (2013) Ochres and earths: Matrix and chromophores characterisation of 19th and 20th century artist materials. Spectrochimica Acta Part A: Molecular and Biomolecular Spectroscopy, vol. 103, pp. 409–416.

Mortimore, J. L., Marshall, L.J. R., Hollins, M. P. and Matthews, W. (2004). Analysis of red and yellow ochre samples from Clearwell Caves and Çatalhöyük by vibrational spectroscopy and other techniques, *Spectrochimica Acta Part A* vol. 60, pp. 1179–88.

Mourre, V., Villa, P. and Henshilwood, C.S. (2010) Early Use of Pressure Flaking on Lithic Artifacts at Blombos Cave, South Africa, *Science*, vol. 330, no. 6004, pp.659-662.

Neff, H. and Glascock, M. D. (1995) The state of nuclear archaeology in North America, *Journal of Radioanalytical and Nuclear Chemistry*, Articles, vol. 196, no. 2, pp. 275-286.

Niven, L. (2007) From carcass to cave: Large mammal exploitation during the Aurignacian at Vogelherd, Germany, *Journal of Human Evolution*, *vol.* 53, pp. 362–382.

Nunez, M., and Vinberg, A. (1990) Determination of anthropic soil phosphate on Åland, *Norwegian Archaeological Review*, vol. 23, no.1–2, pp. 93–104.

Outcalt, K.W. and Kennard, D.K. (2006) Managing composition of piedmont forests with prescribed fire. Gen. Tech. Rep. SRS-92. Asheville, NC: U.S. Department of Agriculture, Forest Service, Southern Research Station. pp. 531.

Outram, A.K. (2002) Distinguishing bone fat exploitation from other taphonomic what the high level of bone fragmentation at the Middle Neolithic site of Ajvide, Gotland, 9th

ICAZ Conference, Durham 2002 The Zooarchcteology of Milk cLnd Fats (eds. Mulville, J. and Outram, A.) pp. 32-43

Parker, S. P. (1993) *McGraw-Hill encyclopedia of chemistry*, McGraw-Hill, New York.

Parnell, J.J., Terry, R.E. and Nelson, Z. (2002) Soil chemical analysis applied as an integrative tool for ancient human activities in Piedras Negras, Guatemala. *Journal of Archaeological Science*, vol. 29, pp. 379–404.

Pavia, D., Lampman, G.M., Kriz, G.S. and Vyvyan, J.R. (2008) Introduction to spectroscopy 4th ed. (BROOKS/COLE cenage learning) pp. 24.

Poduska , K.M., Regev , L., Boaretto , E., Addadi , L., Weiner , S., Kronik , L., and Curtarolo , S. (2011) Decoupling Local Disorder and Optical Effects in Infrared Spectra: Differentiating Between Calcites with Different Origins, *advanced materials*, vol. 23, pp. 550–554.

Pollard, M.A.and Heron, C. (1996) *Archaeological chemistry*. Royal Society of chemistry, Cambridge, pp. 239-270.

Pollard, M., Batt, C., Stern, B. and Young, M.M. (2007) Analytical chemistry in archaeology Cambridge manuals in archaeology (Cambridge university press) pp. 77-78.

Popelka, R.S., Glascock, M.D., Robertshaw, P. and Wood, M. (2005) Laser Ablation ICP-MS of African Glass Trade Beads, *In Laser Ablation ICP-MS in Archaeological Research*, edited by R. J. Speakman and H. Neff, pp. 84–93. University of New Mexico Press, Albuquerque.

Popelka-Filcoff, R.S. (2006) *Applications of Elemental Analysis for Archaeometric Studies: Analytical and Statistical Methods for Understanding Geochemical Trends in Ceramics, Ochre and Obsidian*, PhD. Dissertation.

Popelka-Filcoff, R.S., Robertson, J.D., Glascock, M.D. and Descantes, C. (2007) Trace element characterisation of ochre from geological sources. *Journal of Radioanalytical and Nuclear Chemistry*, vol. 272, no. 1, pp. 17–27.

Popelka-Filcoff, R.S., Miksa, E.J., Robertson, J.D., Glascock, M.D. and Wallace, H (2008) Elemental analysis and characterisation of ochre sources from southern Arizona, *Journal of Archaeological Science*, vol. 35, pp. 752–62.

Price, T.D. and Burton, J.H. (2012) *An introduction to archaeological chemistry*, Springer, pp. 102-116.

Prinsloo, LC, Wadley, L and Lombard, M (2014), Infrared reflectance spectroscopy as an analytical technique for the study of residues on stone tools: potential and challenges, *Journal of Archaeological Science*, vol. 41, pp. 732-739.

Quine, T. A. (1995) Soil analysis and archaeological site formation studies, in *Archaeological sediments and soils: analysis, interpretation and management* (eds. Barham, A.J. and Macphail, R.I.), pp. 77–98, The Institute of Archaeology, University College London.

Regert, M., (2004) Investigation of prehistoric glues by gas chromatography—mass spectrometry, *Journal of Separation Science*, vol. 27, pp. 244–254.

Regev , L, Poduska , K.M., Addadi , L., Weiner , S. and Boaretto , E. (2010) Distinguishing between calcites formed by different mechanisms using infrared spectrometry: archaeological applications, *Journal of Archaeological Science*, vol. 37, no. 12, pp. 3022-3029

Rendle, D. F. (2003). X-Ray Diffraction in Forensic Science. *The Rigaku Journal*, vol. 19, no. 20, pp. 11-22.

Repacholi, M. H. (Ed.). (2012) Clay mineralogy: spectroscopic and chemical determinative methods. Springer Science and Business Media.

Retallack, G.J. and Wright, V.P. (1990) Micromorphology of lithified paleosols. In, Douglas, L.A. (editor), Soil micromorphology: a basic and applied science. Elsevier, Amsterdam, 641-652.

Retallack, G.J. (2000) Depth to pedogenic carbonate horizon as a paleoprecipitation indicator. *Geology*, vol. 28, pp. 572-573.

Reynolds, A. J., Plumptre, J. and Greenham, J. (1998) Condensed tannins and sugars in the diet of chimpanzees (*Pan troglodytes schweinfurthii*) in the Budongo Forest, Uganda. *Oecologia*, vol.115, no. 93, pp. 331-336.

Rifkin, R. F. (2011) Assessing the efficacy of red ochre as a prehistoric hide tanning ingredient, *Journal of African Archaeology,* vol. 9, no. 2, pp. 131–158.

Rifkin, R. F (2012) *The symbolic and functional exploitation of ochre during the South African Middle Stone Age*, PhD Dissertation, Institute for Human Evolution (IHE), University of the Witwatersrand.

Rigaud, J-P., Texier, P-J, Parkington, J. and Poggenpoel, C. (2006) Le mobilier Stillbay et Howiesons Poort del'abri Diepkloof: la chronologie du Middle Stone Age sud-africain et ses implications. *Comptes Rendus Pale´*vol 5, no.6, pp. 839–849.

Roberts, D.L. (2003) Age, Genesis and Significance of South African Coastal Belt Silcretes. Council for Geoscience, South Africa. Memoir 95.

Rogério B. R., Munita,C.S., Oliveira, P.M.S., Neves, E.G. and Tamahara, E.K. (2011) A preliminary study of archaeological ceramics from the São Paulo ii archaeological site by INAA, *International Nuclear Atlantic Conference* .

Rots, V. (2002) *Hafting Traces on Flint Tools: Possibilities and Limitations of Macro and Microscopic Approaches*, PhD Thesis, Katholieke Universiteit, Leuven.

Rottländer, R.C.A (1983) Einfuhrung in die naturwissentschaftlichen methoden in die Archáologie. Archaeologica Venatoria 6. Tubingen.

Ruan , H.D., Frost, R.L, Kloprogge, J.T. Duong, L. (2002) Infrared spectroscopy of goethite dehydroxylation. II. Effect of aluminium substitution on the behaviour of hydroxyl units, *Spectrochimica Acta Part A* , vol 58, pp 479 – 491

Russ, J., Bu, K., Hamrick, J., and Cizdziel, J. V. (2012) Laser ablation-inductively coupled plasma-mass spectrometry analysis of Lower Pecos rock paints and possible pigment sources, in *Collaborative endeavors in the chemical analysis of art and cultural heritage materials* (eds. P. L. Lang and R. A. Armitage), pp. 91–121, American Chemical Society, Washington, DC.

Schiegl, S., Goldberg, P., Bar-Yosef, O., and Weiner, S. (1996) Ash deposits in Hayonim and Kebara Caves, Israel: Macroscopic, microscopic and mineralogical observations, and their archaeological implications, *Journal of Archaeological Science*, vol. 23, pp. 763-781.

Schiegl, S., Goldberg, P., Pfretzschner, H.N. and Conard, N. (2003) Paleolithic Burnt Bone Horizons from the Swabian Jura: Distinguishing between *In situ* Fireplaces and Dumping Areas, *Geoarchaeology: an international journal*, vol. 18, no.5, pp. 541–565.

Schirmer, G. R. (1975) An analysis of lithic material from Dale Rose Parlour, Trappies Kop, Kalk Bay, Cape Peninsula. Archaeology additional report, Cape Town: University of Cape Town.

Schmidt, P., Porraz, G. , Bellot-Gurlet, L., , February, E., Ligouis, B., Paris, C., Texier, P-J., Parkington , J.E., Miller, C.E., Nickel, K.G. and Conard, N.J. (2015)

A previously undescribed organic residue sheds light on heat treatment in the Middle Stone Age, *Journal of Human Evolution* , vol. 85, pp. 22-34.

Scott, D. A., Scheerer, S. and Reeves, D. J. (2002). Technical examination of some rock art pigments and encrustations from the Chumash Indian site of San Emigdio, California. *Studies in conservation*, vol. 47, no.3, pp. 184-194.

Settle, F. (1997) Handbook of instrumental techniques for analytical chemistry (Prentice Hall) pp. 125, 247, 339, 395, 459, 567 and 609.

Severson, R. C., and Shacklette, H. T. (1988) *Essential elements and soil amendments for plants: sources and use for agriculture*, USGS Circular 1017, US Geological Survey, Denver.

Shillito, L. M., Almond, M. J., Wicks, K., Marshall, L. J. R. and Matthews, W. (2009) The use of FT-IR as a screening technique for organic residue analysis of archaeological samples. *Spectrochimica Acta Part A, Molecular and Biomolecular Spectroscopy*, vol. 72, no.1, pp. 120-125.

Smith, M. A., Fankhauser, B. and Jercher, M. (1998) The changing provenance of red ochre at Puritjarra Rock Shelter, Central Australia, Late Pleistocene to Present, *Proceedings of the Prehistoric Society*, vol. 64, pp. 275-292.

Stafford, M. D., Frison, G.C., Stanford, D. and Ziemans, G. (2003) Digging for the Colour of Life: Palaeoindian Red Ochre Mining at the Powars II Site, Platte County, Wyoming, U.S.A. *Geoarchaeology*, vol.18, pp.71-90.

Sullivan, K.A. and Kealhofer, L. (2004) Identifying activity areas in archaeological soils from a colonial Virginia house lot using phytolith analysis and soil chemistry, *Journal of archaeological science*, vol.31, no.12, pp.1659-1673.

Tankersley, K.B., Tankersley,O.K., Shaffer,N.R., Hess, M.D., Benz,J.S., Turner, F.R., Stafford, M.D., Zeimans, G.M. and George C.F. (1995) They Have a Rock That Bleeds: Sunrise Red Ochre and its Early Palaeoindian Occurrence at the Hell Gap Site, Wyoming. *Plains Anthropologist*, vol.40, pp.185- 194.

Texier, P.-J.,Porraz, G., Parkington, J., Rigaud, J.P., Poggenpoel, C., Miller, C., Tribolo, C., Cartwright, C., Coudenneau,A., Klein, R., Steele, T. and Verna, C. (2010) A Howiesons Poort tradition of engraving ostrich eggshell containers dated to 60,000 years ago at Diepkloof Rock Shelter, South Africa, *Proceedings of the National Academy of Sciences*, vol. 107, no. 14, pp. 6180-6185.

Théry-Parisot, I. (2002) Fuel Management (Bone and Wood) During the Lower Aurignacian in the Pataud Rock Shelter (Lower Palaeolithic, Les Eyzies de Tayac, Dordogne, France*), Journal of Archaeological Science* vol. 29, pp. 1415–1421.

Thompson, J. and Henshilwood, C. S. (2011) Taphonomic analysis of the Middle Stone Age larger mammal faunal assemblage from Blombos Cave, southern Cape, South Africa, *Journal of Human Evolution*, vol. 60, pp. 746-767.

Thompson, J. C., and Henshilwood, C. S. (2014) Nutritional values of tortoises relative to ungulates from the Middle Stone Age levels at Blombos Cave, South Africa: Implications for foraging and social behaviour, *Journal of Human Evolution*, vol. *67*, pp. 33–47.

Tsolakidou, A., and Kilikoglou, V. (2002) Comparative analysis of ancient ceramics by INAA, ICPS and XRF, *Analytical and Bioanalytical Chemistry*, vol. 374, pp. 566–72.

van Niekerk, K. L. (2011) *Marine fish exploitation during the Middle and Later Stone Age of South Africa*, PhD dissertation, University of Cape Town.

Vaneeckhout, S., Junno, J-A, Puputti, A-K. and Äikäs,T. (2010) Prehistoric burned bone: use or refuse – results of a bone combustion experiment, *Faravid,* vol. 34.

Vanhaeren, M, d'Errico, F., Stringer, C., James, S.L.,Todd, J.A. and Mienis, H.A. (2006) Middle Paleolithic shell beads in Israel and Algeria. *Science,* vol. 312, no. 578, pp.1785–1788.

Vanhaeren, M., d'Errico, F., van Niekerk, K. L., Henshilwood, C. S., and Erasmus, R. M. (2013) Thinking strings: Additional evidence for personal ornament use in the Middle Stone Age at Blombos Cave, South Africa. *Journal of Human Evolution*.

Velo, J. (1984) Ochre as medicine: a suggestion for the interpretation of the archaeological record. *Current Anthropology* , vol. 25, no. 5, pp. 674.

Velo, J. (1986). The Problem of Ochre, *Mankind Quarterly, vol.* 26, no. 3-4, pp. 229-237.

Villa, P., Soressi, M., Henshilwood, C.S. and Mourre, V. (2009) The Still Bay points of Blombos Cave (South Africa), *Journal of Archaeological Science*, vol. 36, no. 2, pp. 441-460.

Wadley, L. (2001*a*) Preliminary report on excavations at Sibudu Cave, Kwazulu-Natal. *Southern African Humanities*, vol. 13, pp. 1–17.

Wadley, L. (2001) What is Cultural Modernity? A General View and a South African Perspective from Rose Cottage Cave, *Cambridge Archaeological Journal*, vol. 11, no. 2, pp. 201-221.

Wadley, L. (2007) Announcing a Still Bay industry at Sibudu Cave, South Africa, *Journal of Human Evolution*, vol. 52, no. 6, pp. 681-689.

Wadley, L., Hodgskiss, T. and Grant, G. (2009) Implications for complex cognition from the hafting of tools with compound adhesives in the Middle Stone Age, South Africa. *Proceedings of the National Academy of Sciences*.

Wadley, L., Williamson, B. and Lombard, M. (2004) Ochre in hafting in Middle Stone Age southern Africa: a practical role, *Antiquity*, vol. 78, no. 301, pp. 661–675.

Wadley, L.and Mohapi, M. (2008) A segment is not a monolith: evidence from the Howiesons Poort of Sibudu, South Africa, *Journal of Archaeological Science, vol.*35, no.9, pp. 2594–2605.

Wadley, Lyn (2005) Putting Ochre to the Test: Replication Studies of Adhesives that May Have Been Used for Hafting Tools in the Middle Stone Age. *Journal of Human Evolution*, vol. 49, pp. 587-601.

Wattez, J. (1988) Contribution a la connaissance des foyers prehistoriques par l'etude des cendres, Bulletin de la Societe Prehistorique Francaise, vol. 85, pp 353-366.

Wattez, J., Courty, M.A. and Macphail, R.I. (1990) Burnt organo-mineral deposits related to animal and human activities. In Douglas, LA (editor*), Soil micromorphology: A Basic and Applied Science* (Amsterdam Elsevier) pp. 431-440.

Watts, I. (1999) The origin of symbolic culture, *The evolution of culture*, pp. 113-146.

Watts, I. (2002) Ochre in the Middle Stone Age of southern Africa: ritualised display or hide preparation? *South African Archaeological Bulletin*, vol. 57, pp. 1–14.

Watts, I. (2009) Red ochre, body painting, and language: interpreting the Blombos ochre. In *the cradle of language*, (ed.s Botha, R.P. and Knight, C.) 18, 386. Oxford; New York: Oxford University.

Watts, I., (1999) The origin of symbolic culture. In *The Evolution of Culture,* : (eds. Dunbar, R., Knight, C., Power, C.), Edinburgh University Press, Edinburgh, pp.113–146.

Watts, I., (2010) The pigments from Pinnacle Point Cave 13B, Western Cape, South Africa, *Journal of Human Evolution*, vol. 59, pp. 392–411.

Weide, D.L. (1966) *Soil pH as a guide to archaeological investigations*, University of California (Los Angeles), Archaeological survey report no.8, pp.155-163.

Weiner, S., and Goldberg, P. (1990) On-site Fourier transform infrared spectrometry at an archeological excavation. *Spectroscopy,* vol. 5, pp. 46–50.

Weiner, S., Xu, Q., Goldberg, P., Liu, J., and Bar-Yosef, O. (1998) Evidence for the use of fire at Zhoukoudian, China. *Science,* vol. 281, no.5374, pp. 251-253.

Weiner, S. (2010) Microarchaeology: beyond the visible mircoarchaeological record, Cambridge university press.

Wells, A.M., Fitzpatrick, R.W. and Gilkes, R.J. (2006) Thermal and mineral properties of Al-, Cr-, Mn-, Ni- and Ti-substituted goethite, *Clays and Clay Minerals*, vol. 54, no. 2, pp.176-194.

White WB (1974) The carbonate minerals. In: Farmer VC (ed), Infrared spectra of minerals. *Mineral Soc Monogr*, vol. 4, pp. 227-284.

Wilson, C.A., Davidson, D.A., Cresser, M.S. (2007) Evaluating the use of multi-element soil analysis in archaeology: a study of a post-medieval croft (Olligarth) in Shetland. *Atti della Società Toscana di Scienze Naturali*, vol. 112, pp. 69–78.

Wilson, C.A., Davidson, D.A., Cresser, M.S. (2008) Multi-element soil analysis: an assessment of its potential as an aid to archaeological interpretation, *Journal of Archaeological Science*, vol. 35, pp. 412–424.

Wilson, C.A., Davidson, D.A., Cresser, M.S., (2009) An evaluation of the site specificity of soil elemental signatures for identifying and interpreting former functional areas, *Journal of Archaeological Science*, *vol.* 36, pp. 2327–2334.

Wreschner, E. E. (1980) Red Ochre and Human Evolution, A Case for Discussion, *Current Anthropology*, vol. 21, pp. 631-633.

Wrinn, P.J. and Rink, W.J. (2003) ESR Dating of Tooth Enamel From Aterian Levels at Mugharet el ‘Aliya (Tangier, Morocco), *Journal of Archaeological Science*, vol. 30, pp. 123–133.

Wurz, S. (2000) *The Middle Stone Age at Klasies River, South Africa*, PhD thesis, University of Stellenbosch.

Wurz, Sarah. (1999) The Howiesons Poort backed artifacts from Klasies River: an argument for symbolic behaviour, *South African Archaeological Bulletin*, vol. 54, no. 169, pp. 38–50.

Zipkin, A.M., Hanchar, J.M., Brooks, J.M., Grabowski, M.W, Thompson, J.C. and E. Gomani-Chindebvu (2015) Ochre fingerprints: distinguishing among Malawian mineral pigment sources with homogenized ochre chip LA–ICP-MS , *Archaeometry*, vol. 57, no. 2, pp. 297–317.

APPENDIX

Appendix A- Sample preparation

Microwave assisted digestion

Table A1 Actual weights of sediment samples

Sample name	Mass (mg)
CA E6D	250.2
CA H7B	250.8
CB F7B	250.4
CB H7A	250.2
CC F7B	250.2
CC H7B	250.1
CCC G7B	250.3
CCC H6D	250.2
CD H7A	250.9
CD F6D	249.2
CDB H6D	250.4
CDB F6D	250.9
CFA G6C	249.9
CFA G7A	249.0
CFC/CFB F6D	249.5
CFB/CFC	250.2
CFD F6D	250.3
CFD H6D	250.6
CGAA H6D	250.9
CGAAF6D	250.0
CGAB h1 H7A	250.7
CGAB h1 F6D	251.2
CGAB H6C	250.7
CGAB F6D	250.8
CGAC F6D	249.6
CGAC H6C	250.6
CH G7B	250.7
CH H6C	249.4
CH/CI H6D	250.3
CIA H6D	249.7
CIA F6D	249.9
CIB h2 G6C	250.6
CIB h2 H6D	249.3
CIB H6C	249.4
CIB F6D	250.8
CJ(A) H6D	250.8
CJ(B) H6D	249.7
	249.1
	250.1
	250.0
	250.2

CJ G6C	250.1
CK/CL H6C	250.7
CK/CL F6D	249.3
CM H6C	250.6
CM F6D	249.7
CN/CO H6C	250.4
CN/CO F6D	250.5
CP F6D	250.1
CP H6C	249.1
CP H6D	250.7

Table A2 Actual weights of ochre samples

Sample name	**Mass (mg)**
BBC H6c CP 506 TK3	250.9
BBC CP G6D TK3	250.4
BBC CP H6C L1 416 TK3	250.2
BBC CP H6C OCHRE FLAKE	249.4
BBC CP H6C L30 529	250.2
BBC CP H6C L35 534	249.4
BBC CP H6C L16 453	250.8

Table A3 Toolkit pieces, spatial references and descriptions (Compiled by Henshilwood *et al.*)

Quadrate	Layer	Plot number	Artifact number	Sample number	Description
G6d	CP	L1	473	S1	Sample of red residue from quartzite chunk
G6d	CPA	L1	473	S2	Sample of brown residue from quartzite chunk
H6C	CP	L23	519		Ball of red sand from the silcrete flake with bone
H6C	CP	L28	527		Ochre mass with bone embedded in sand, allocated on a silcrete
H6C	CP	O1	442		Mastic lumps
H6C	CP	L9	438	S1	Red ochre sampled from the surface of a stone
H6c	CP	L1	416		Chunk of finely laminated fissile shale (light pink)
H6c	CP	L16	453		Laminated cortical flake, smoothing areas on the cortex, with bright red residues
H6c	CP	L35	534		Cortical chunk indurated mudstone, with pitting and one striated convex facet
H6c	CP ochre3	O7	506		1. Bone visible on surface with some red sand 2. Ochre flake in sand and shell 3. Tooth at bottom of shell
G6d	CP	O1	476		S. Argenvillei shell with sand and ochre. In the apex there is bone and pink pigment adhering to the nacre. All the bone pieces lie on the apex with no sand beneath them.
H6c	CP	L30	529		Chunk of indurated shale
H6c	CP ochre 2				Laminated shale chunk (light pink)

H6c	CP ochre 7			Flakes of laminated dense concretion (Black, red)
H6c	CP	L20	514	Chunk of layered dense concretion (Black, red, white)
H6c	CP		489	Indurated shale with red spots
H6c	CP ochre 9		510	Chunks of laminated dense concretion (Black, red, yellow, white)
H6c	CP ochre 4		497	Chunk of laminated dense concretion (Black, red, white)
H6c	CP ochre			Sandstone chunks
H6c	CP ochre 5			Laminated shale flake (light pink)
H6c	CP ochre 8		509	Sandstone flakes
H6c	CP	O2	477	Flake has ochre on nacre with brown cemented soil and small fragments of ochre, spongy bone, burnt spongy bone and charcoal
H6c	CP	L24	520	Sediment, charcoal and resin sample
H6c	CP pigment drops 1and 2			
H6c	CPA		470	Ochre, bone and soil sample
H6c	CPA	O2	470	Red soil sample
H6c	CP conglomerate ashes			
G6d	CP charcoal 1 and 2			
H6c	CP ochre 6	O9	510	Triangular flake of pigment with small pits and an engraved line on one face
H6c	CP ochre	L26	524	Flaked cortical indurated shale or mudstone flake, bipolar impact scares
H6c	CPA ochre fragments			Ochre flakes/chunks
G6d	CP			Ochre flakes/chunks

Appendix B Analytical figures of merit for ICP-OES data

Equation B1 Converting elemental concentration from ppm to mg kg^{-1}

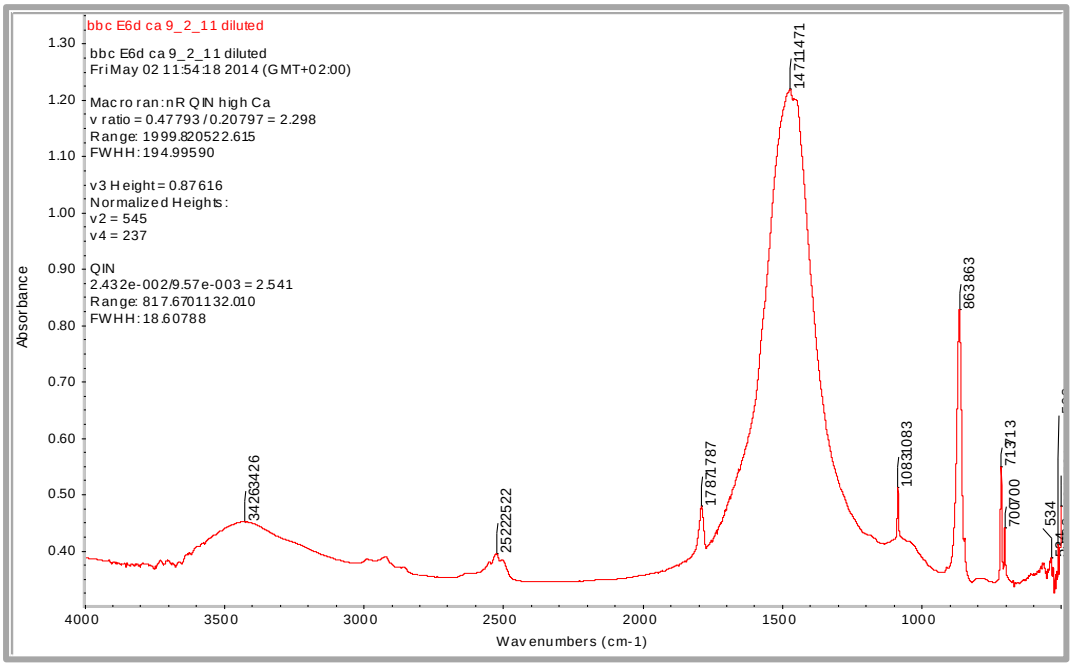
$$\frac{0{,}05L*\left[ipc-oes\frac{mg}{L}\right]*DF}{2{,}5x10^{-4}\ kg} = C_f\ (mg\ kg^{-1})$$

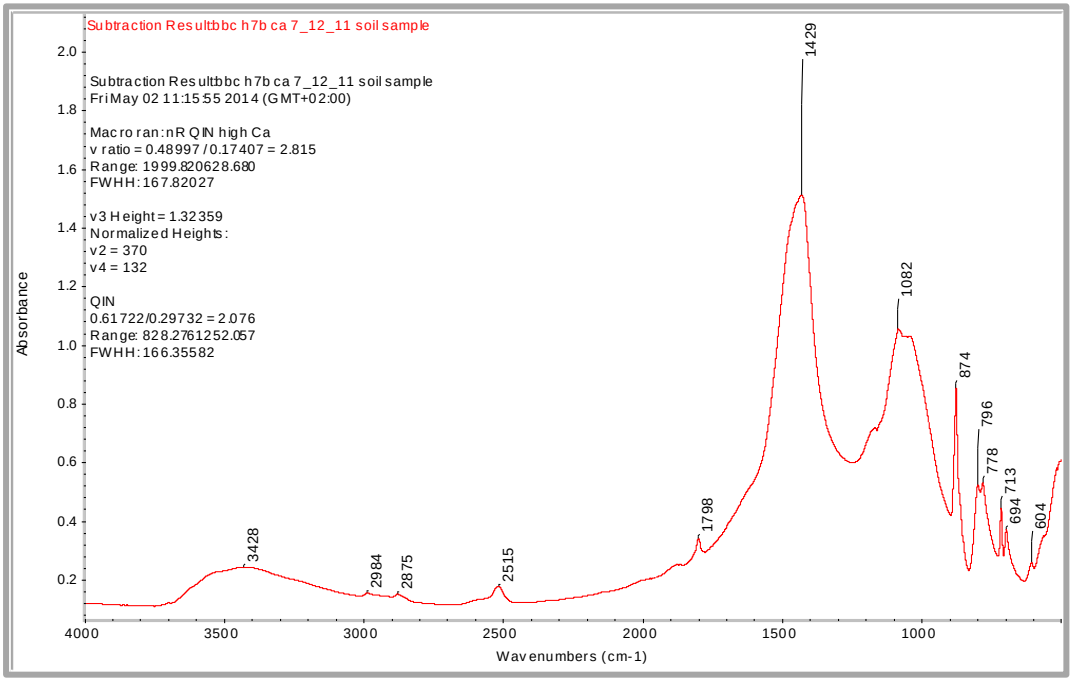
Table B1 Limit of detection values for ochre from CP layer

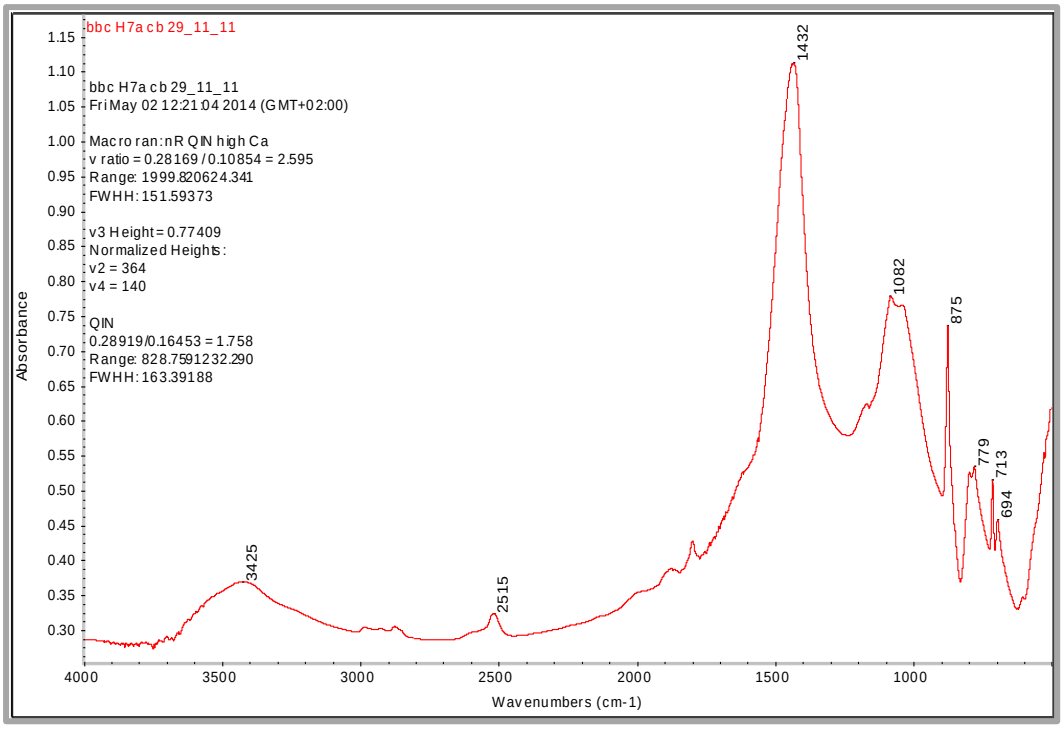
Element	Ti	V	Cr	Mn	Fe	Co	Ni	Cu	Zn	Zr	Cd	S	Se
Blank sd	0.001	0.001	0.007	0.001	0.001	0.001	0.002	0.001	0.001	0.001	0.004	0.005	0.005
LOD (mg kg^{-1})	0.6	0.6	4.2	0.6	0.6	0.6	1.2	0.6	0.6	0.6	2.4	3	3

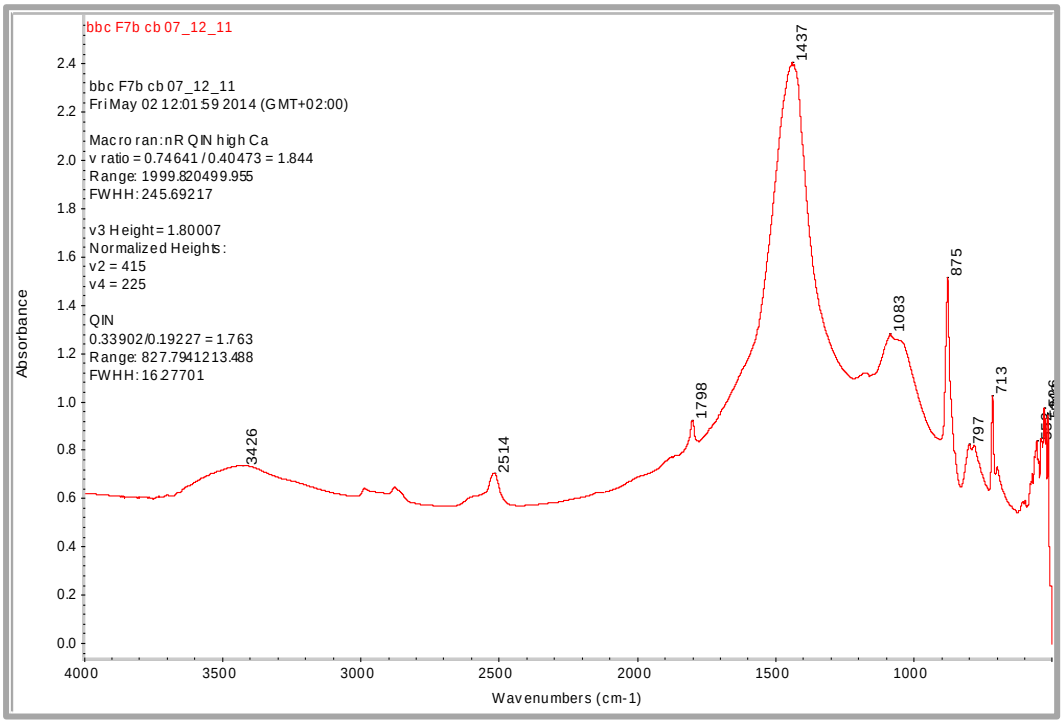
P	Al	Ca	K	Mg	Na	As	Si	Sc	Sr	Y	Ba
0.004	0.007	0.001	0.001	0.001	0.003	0.001	0.005	0.001	0.001	0.001	0.002
2.4	4.2	0.6	0.6	0.6	1.8	0.6	3	0.6	0.6	0.6	1.2

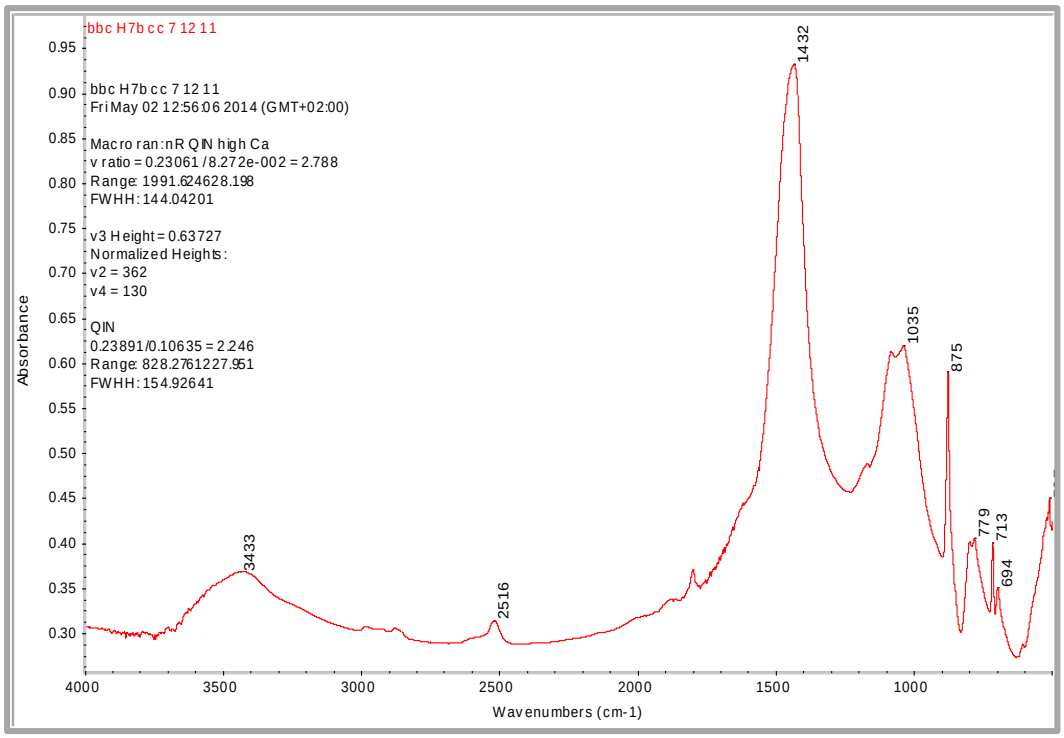
Appendix C 1 FT-IR analysis of sediments

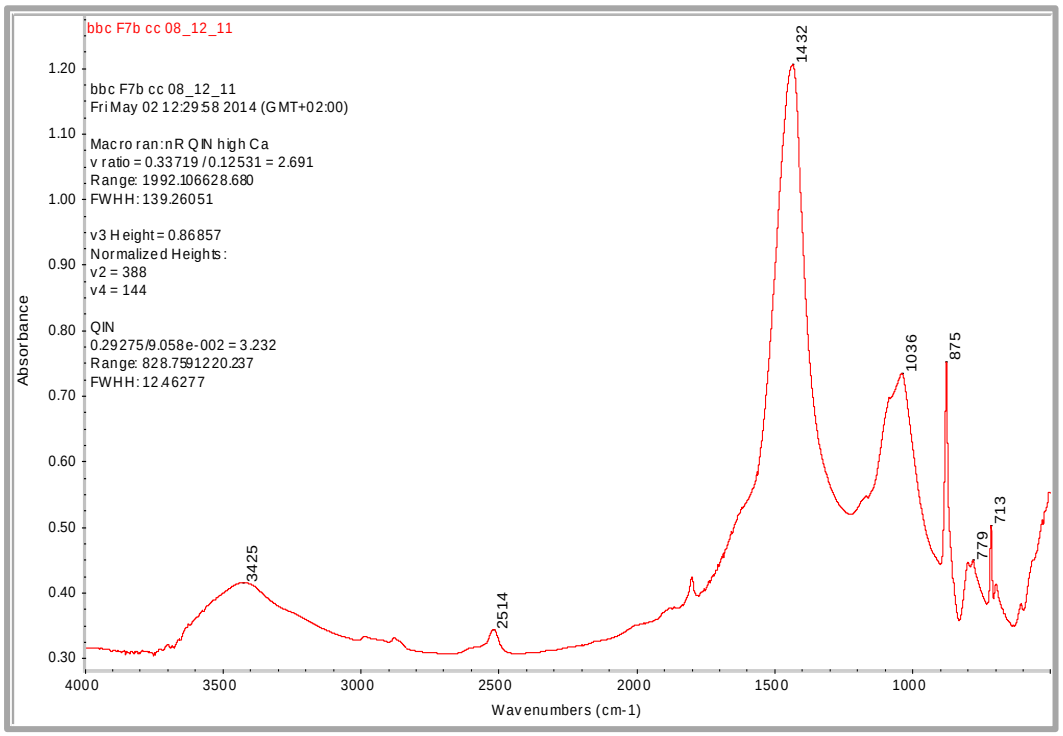


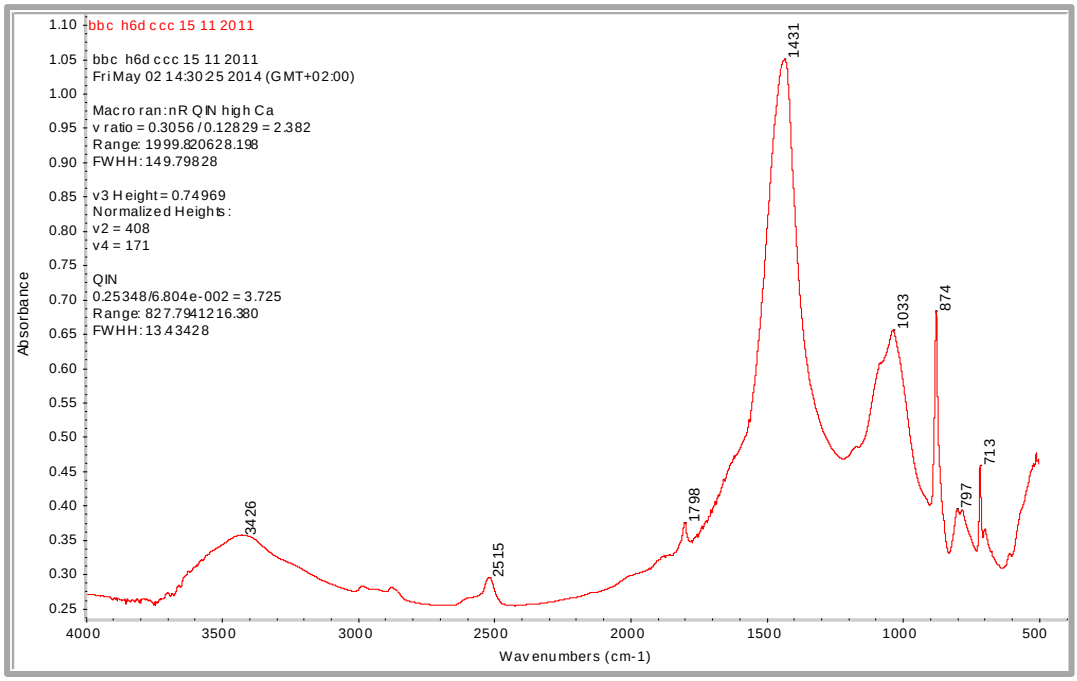


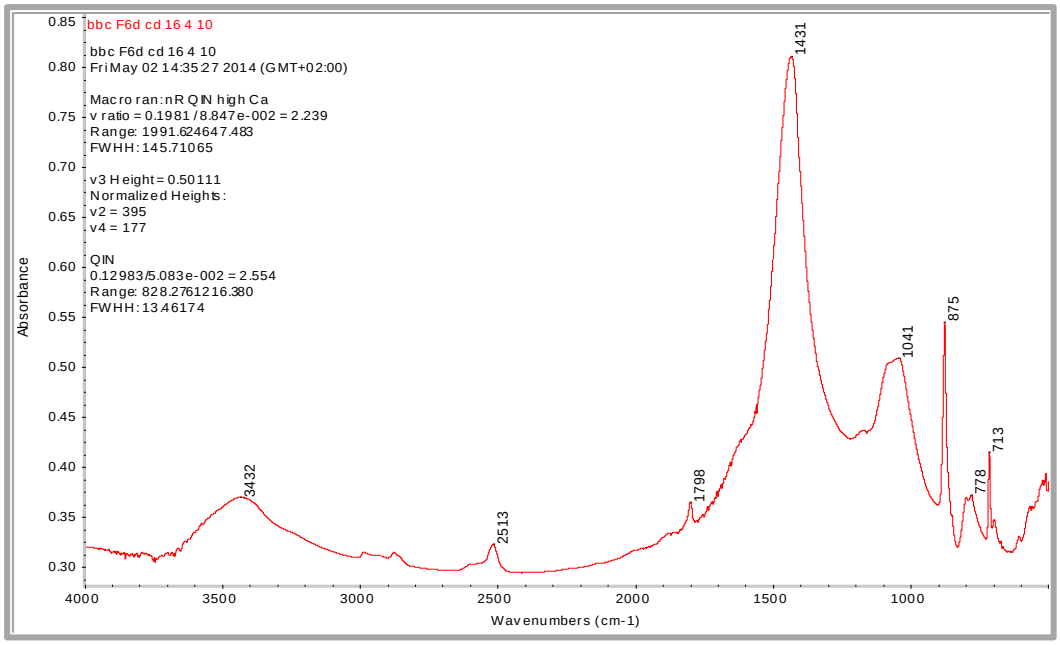

bbc H7a cb 29_11_11
bbc H7a cb 29_11_11
Fri May 02 12:21:04 2014 (GMT+02:00)
Macro ran:nR QIN high Ca
v ratio = 0.28169 / 0.10854 = 2.595
Range: 1999.820624.341
FWHH: 151.59373
v3 Height = 0.77409
Normalized Heights:
v2 = 364
v4 = 140
QIN
0.28919/0.16453 = 1.758
Range: 828.7591232.290
FWHH: 163.39188
Absorbance
Wavenumbers (cm-1)
3425
2515
1432
1082
875
779
713
694

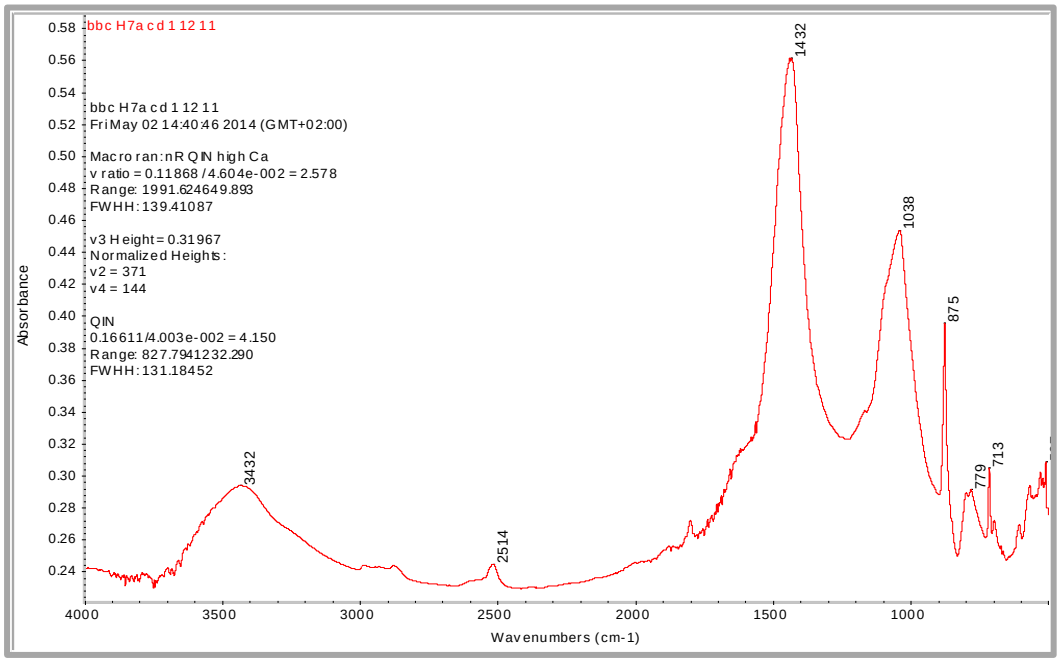

bbc F7b cb 07_12_11
bbc F7b cb 07_12_11
Fri May 02 12:01:59 2014 (GMT+02:00)
Macro ran:nR QIN high Ca
v ratio = 0.74641 / 0.40473 = 1.844
Range: 1999.820499.955
FWHH: 245.69217
v3 Height = 1.80007
Normalized Heights:
v2 = 415
v4 = 225
QIN
0.33902/0.19227 = 1.763
Range: 827.7941213.488
FWHH: 16.27701
Absorbance
Wavenumbers (cm-1)
3426
2514
1798
1437
1083
875
797
713

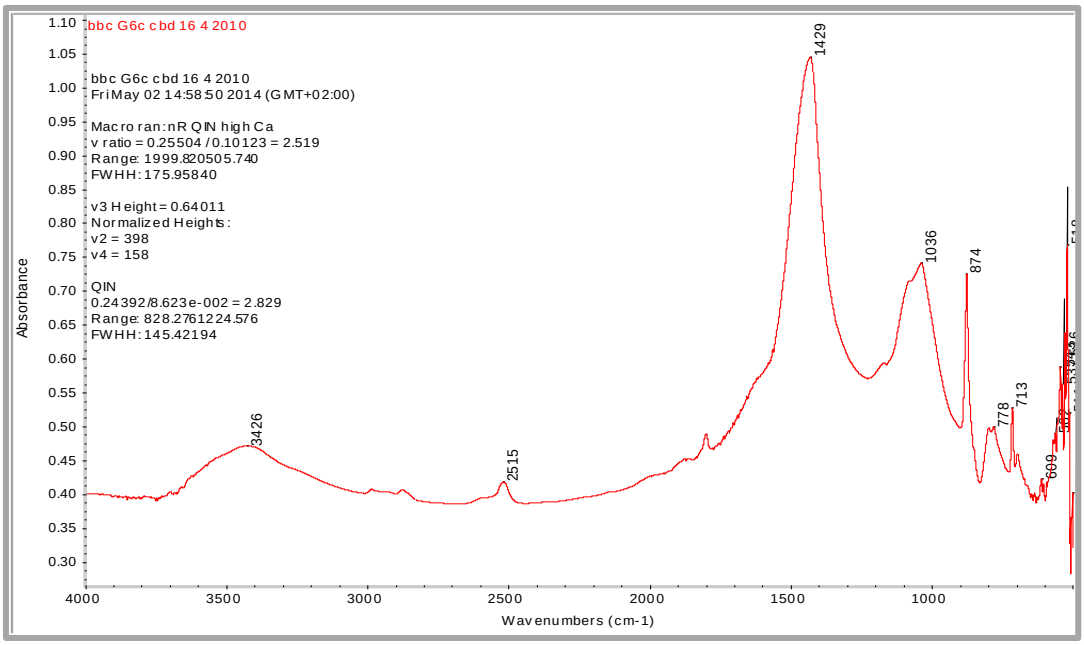

bbc H7b cc 7 12 11
bbc H7b cc 7 12 11
Fri May 02 12:56:06 2014 (GMT+02:00)
Macro ran:nR QIN high Ca
v ratio = 0.23061 / 8.272e-002 = 2.788
Range: 1991.624628.198
FWHH: 144.04201
v3 Height = 0.63727
Normalized Heights:
v2 = 362
v4 = 130
QIN
0.23891/0.10635 = 2.246
Range: 828.2761227.951
FWHH: 154.92641
Absorbance
Wavenumbers (cm-1)
3433
2516
1432
1035
875
779
713
694

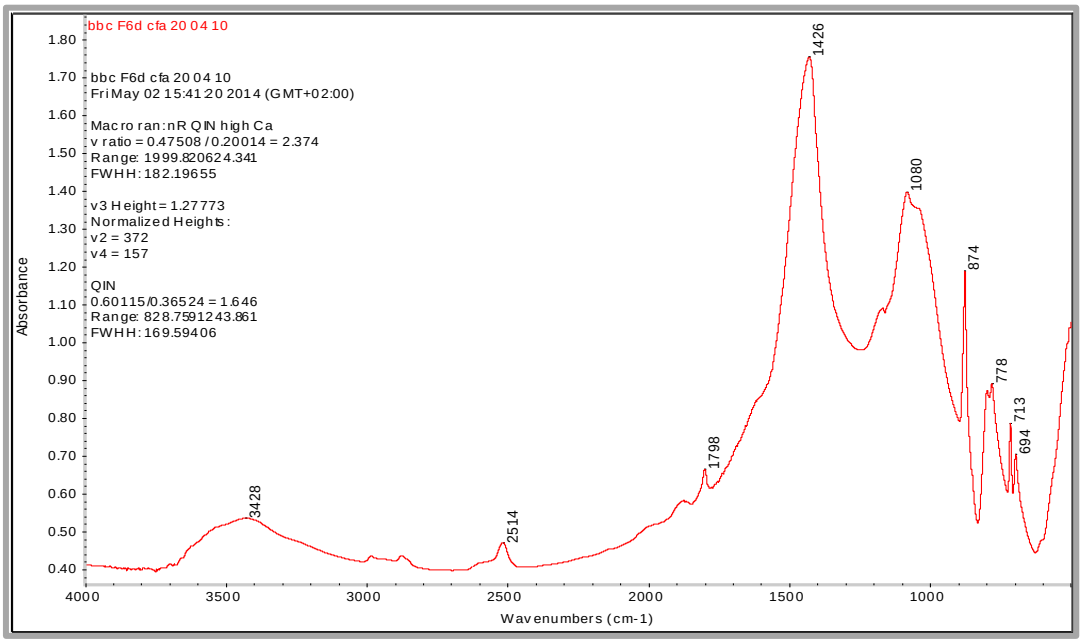

bbc F7b cc 08_12_11
bbc F7b cc 08_12_11
Fri May 02 12:29:58 2014 (GMT+02:00)
Macro ran:nR QIN high Ca
v ratio = 0.33719 / 0.12531 = 2.691
Range: 1992.106628.680
FWHH: 139.26051
v3 Height = 0.86857
Normalized Heights:
v2 = 388
v4 = 144
QIN
0.29275/9.058e-002 = 3.232
Range: 828.7591220.237
FWHH: 12.46277
Absorbance
Wavenumbers (cm-1)
3425
2514
1432
1036
875
779
713

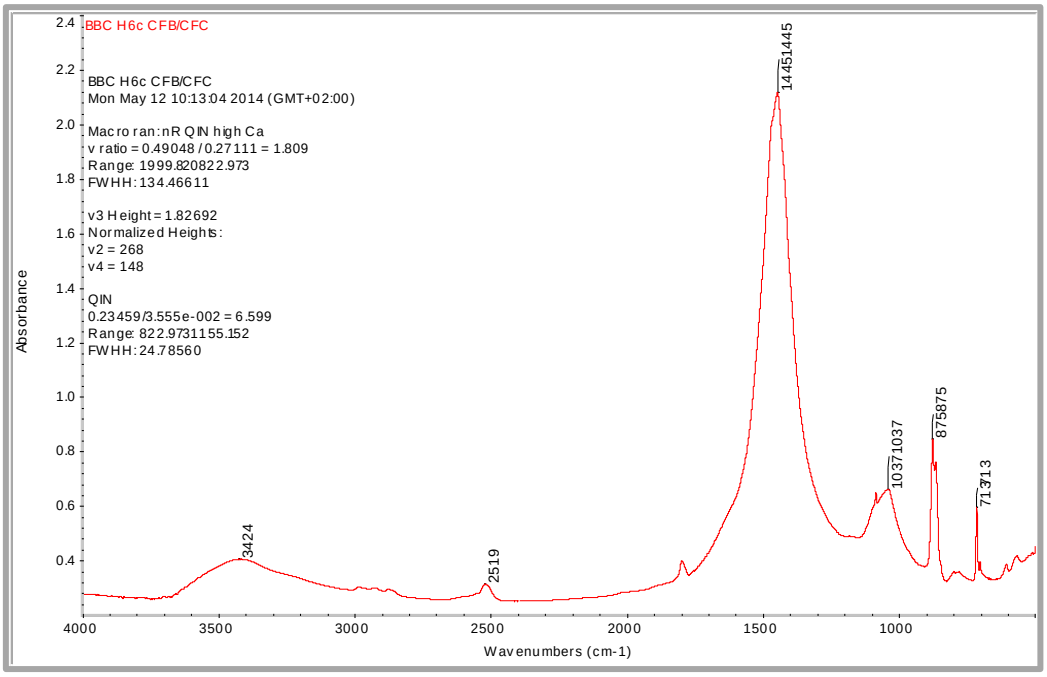

bbc h6d ccc 15 11 2011
bbc h6d ccc 15 11 2011
Fri May 02 14:30:25 2014 (GMT+02:00)
Macro ran:nR QIN high Ca
v ratio = 0.3056 / 0.12829 = 2.382
Range: 1999.82 0628.198
FWHH: 149.79828
v3 Height = 0.74969
Normalized Heights:
v2 = 408
v4 = 171
QIN
0.25348/6.804e-002 = 3.725
Range: 827.7941 2 16.380
FWHH: 13.43428
Absorbance
Wavenumbers (cm-1)
3426
2515
1798
1431
1033
874
797
713

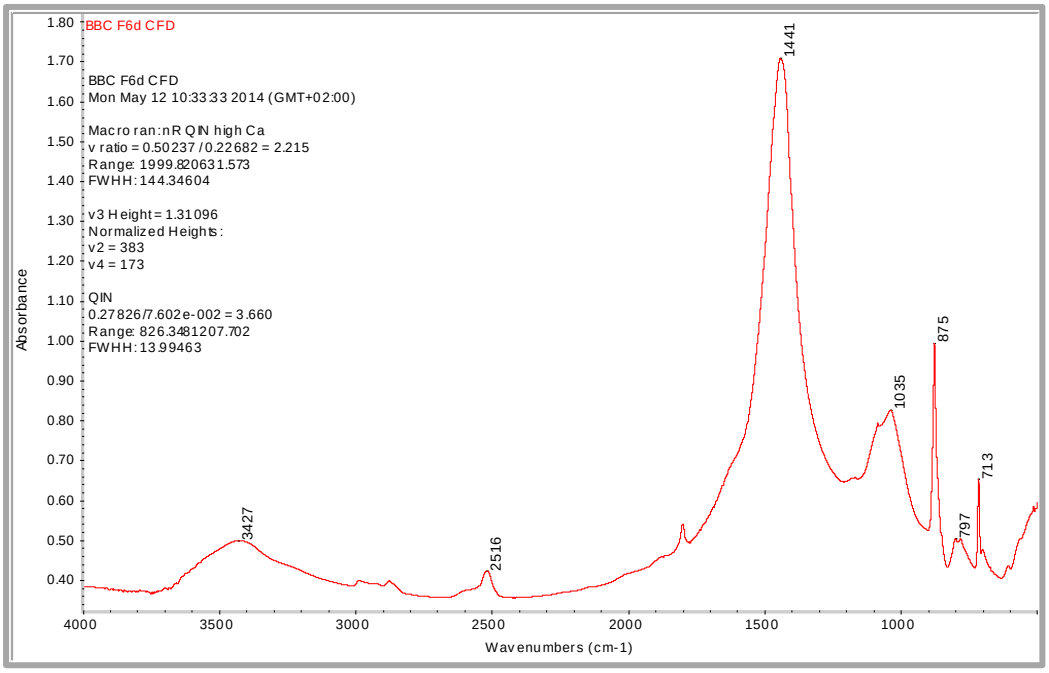

bbc F6d cd 16 4 10
bbc F6d cd 16 4 10
FriMay 02 14:35:27 2014 (GMT+02:00)
Macro ran:nR QIN high Ca
v ratio = 0.1981 / 8.847e-002 = 2.239
Range: 1991.62464 7.483
FWHH: 145.71065
v3 Height = 0.50111
Normalized Heights:
v2 = 395
v4 = 177
QIN
0.12983/5.083e-002 = 2.554
Range: 828.27612 16.380
FWHH: 13.46174
Absorbance
Wavenumbers (cm-1)
3432
2513
1798
1431
1041
875
778
713

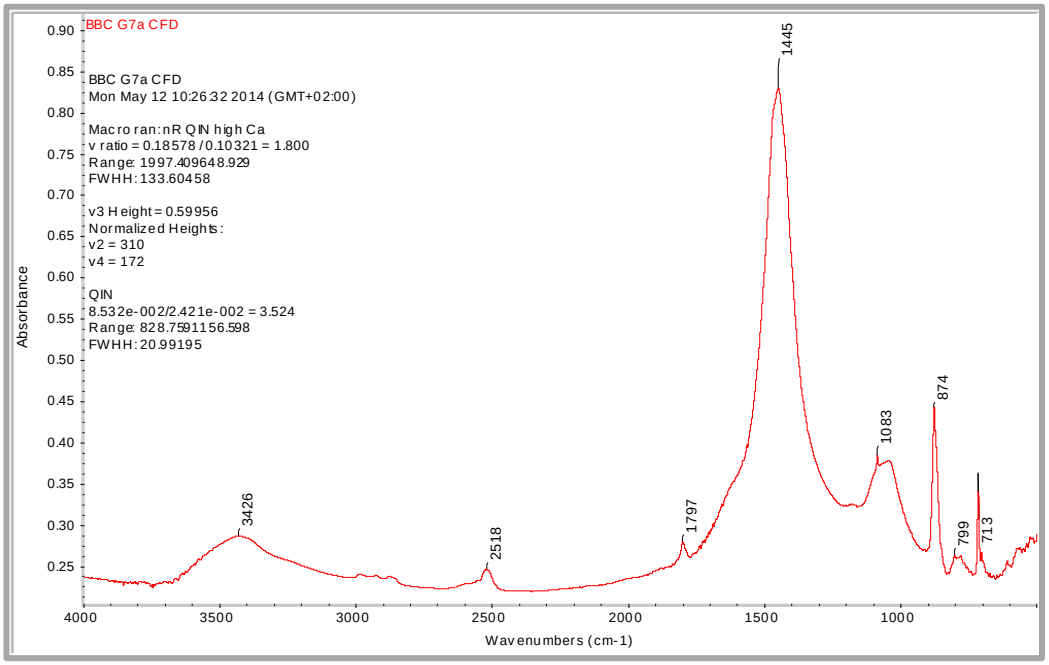

bbc H7a cd 1 12 11
bbc H7a cd 1 12 11
FriMay 02 14:40:46 2014 (GMT+02:00)
Macro ran:nR QIN high Ca
v ratio = 0.11868 / 4.604e-002 = 2.578
Range: 1991.62464 9.893
FWHH: 139.41087
v3 Height = 0.31967
Normalized Heights:
v2 = 371
v4 = 144
QIN
0.16611/4.003e-002 = 4.150
Range: 827.79412 32.290
FWHH: 131.18452
Absorbance
Wavenumbers (cm-1)
3432
2514
1432
1038
875
779
713

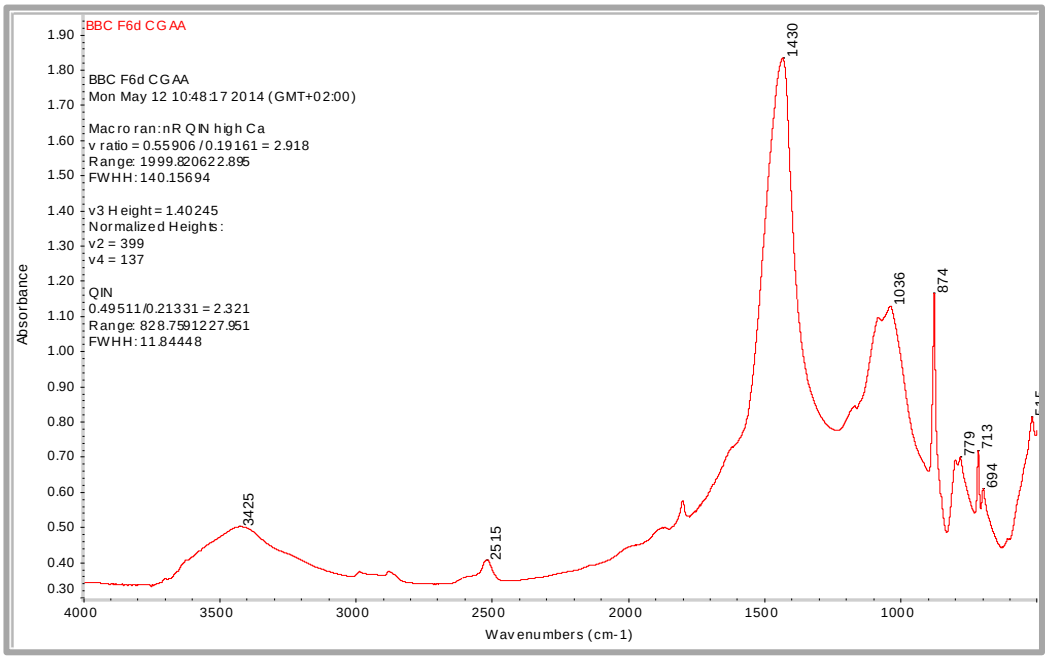

bbc G6c cbd 16 4 2010
bbc G6c cbd 16 4 2010
Fri May 02 14:58:50 2014 (GMT+02:00)
Macro ran:nR QIN high Ca
v ratio = 0.25504 / 0.10123 = 2.519
Range: 1999.820505.740
FWHH: 175.95840
v3 Height = 0.64011
Normalized Heights:
v2 = 398
v4 = 158
QIN
0.24392/8.623e-002 = 2.829
Range: 828.2761224.576
FWHH: 145.42194
Absorbance
Wavenumbers (cm-1)
3426
2515
1429
1036
874
778
713
669

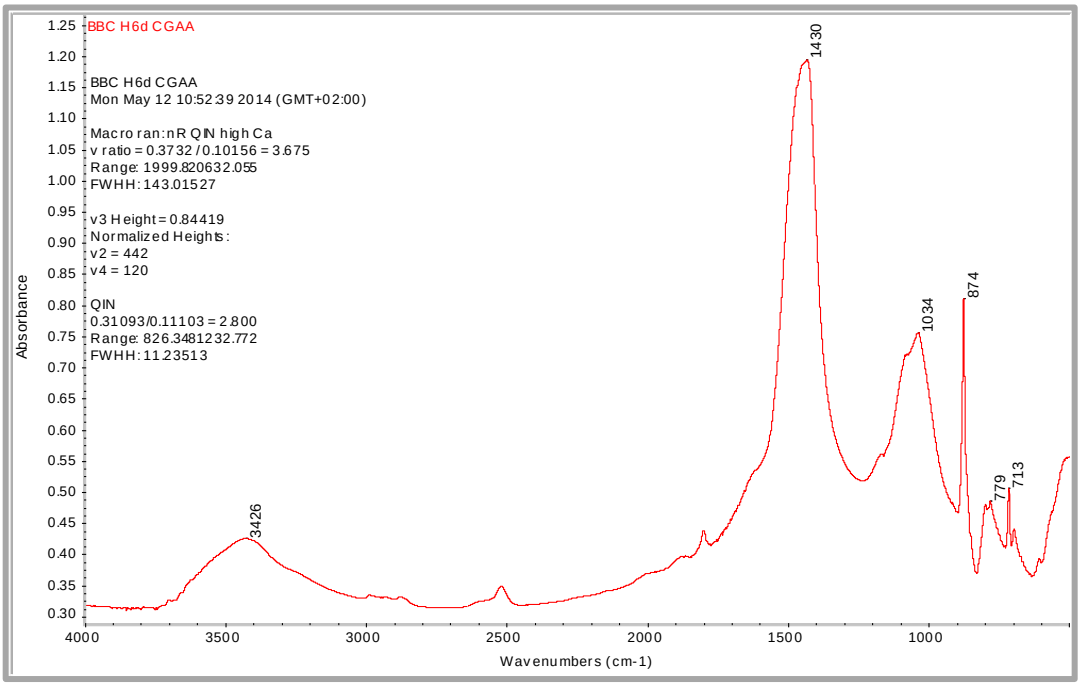

bbc F6d cfa 20 04 10
bbc F6d cfa 20 04 10
Fri May 02 15:41:20 2014 (GMT+02:00)
Macro ran:nR QIN high Ca
v ratio = 0.47508 / 0.20014 = 2.374
Range: 1999.820624.341
FWHH: 182.19655
v3 Height = 1.27773
Normalized Heights:
v2 = 372
v4 = 157
QIN
0.60115/0.36524 = 1.646
Range: 828.7591243.861
FWHH: 169.59406
Absorbance
Wavenumbers (cm-1)
3428
2514
1798
1426
1080
874
778
713
694

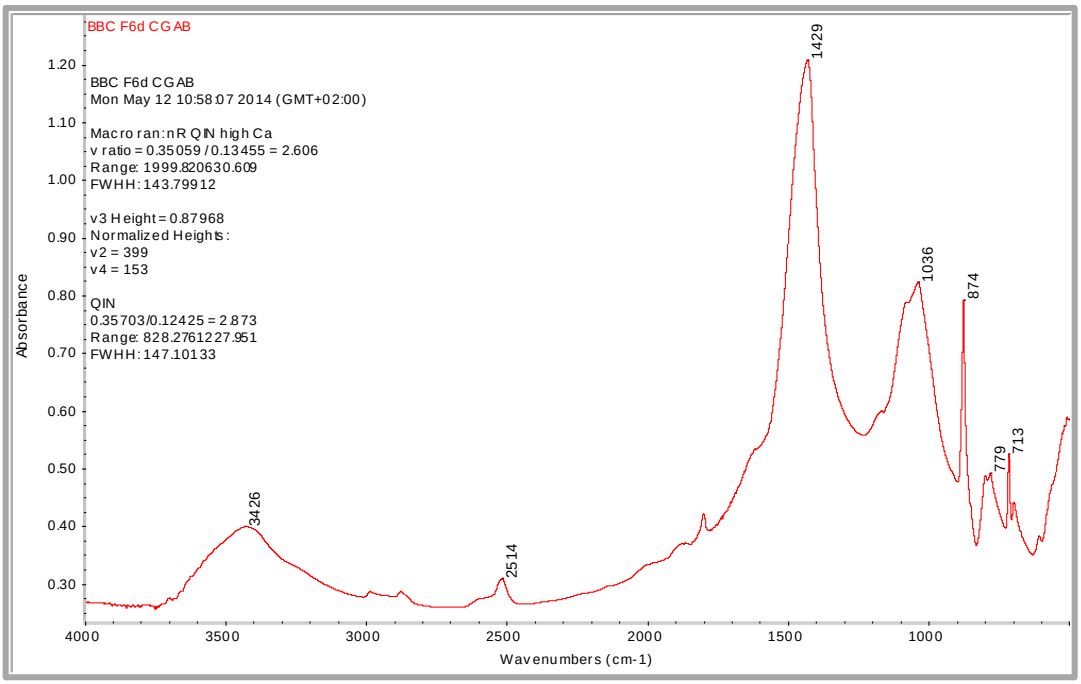

BBC H6c CFB/CFC
BBC H6c CFB/CFC
Mon May 12 10:13:04 2014 (GMT+02:00)
Macro ran:nR QIN high Ca
v ratio = 0.49048 / 0.27111 = 1.809
Range: 1999.820822.973
FWHH: 134.46611
v3 Height = 1.82692
Normalized Heights:
v2 = 268
v4 = 148
QIN
0.23459/3.555e-002 = 6.599
Range: 822.9731155.152
FWHH: 24.78560
Absorbance
Wavenumbers (cm-1)
3424
2519
1445
1037
875
713

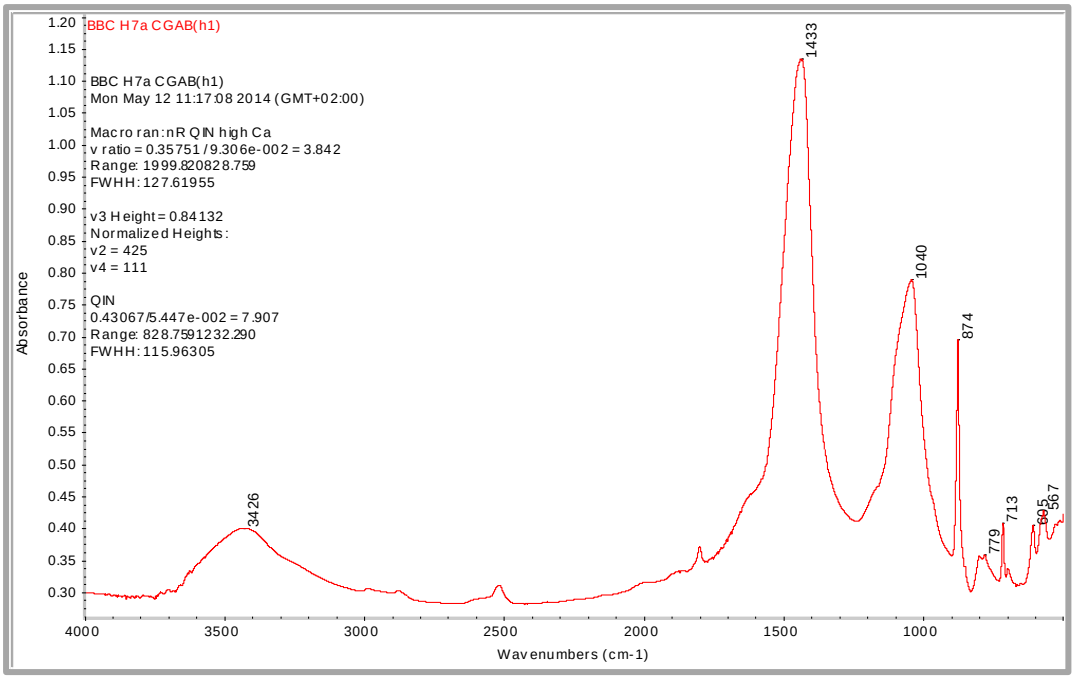

BBC F6d CFD
BBC F6d CFD
Mon May 12 10:33:33 2014 (GMT+02:00)
Macro ran:nR QIN high Ca
v ratio = 0.50237 / 0.22682 = 2.215
Range: 1999.820631.573
FWHH: 144.34604
v3 Height = 1.31096
Normalized Heights:
v2 = 383
v4 = 173
QIN
0.27826/7.602e-002 = 3.660
Range: 826.3481207.702
FWHH: 13.99463
Absorbance
Wavenumbers (cm-1)
3427
2516
1441
1035
875
797
713

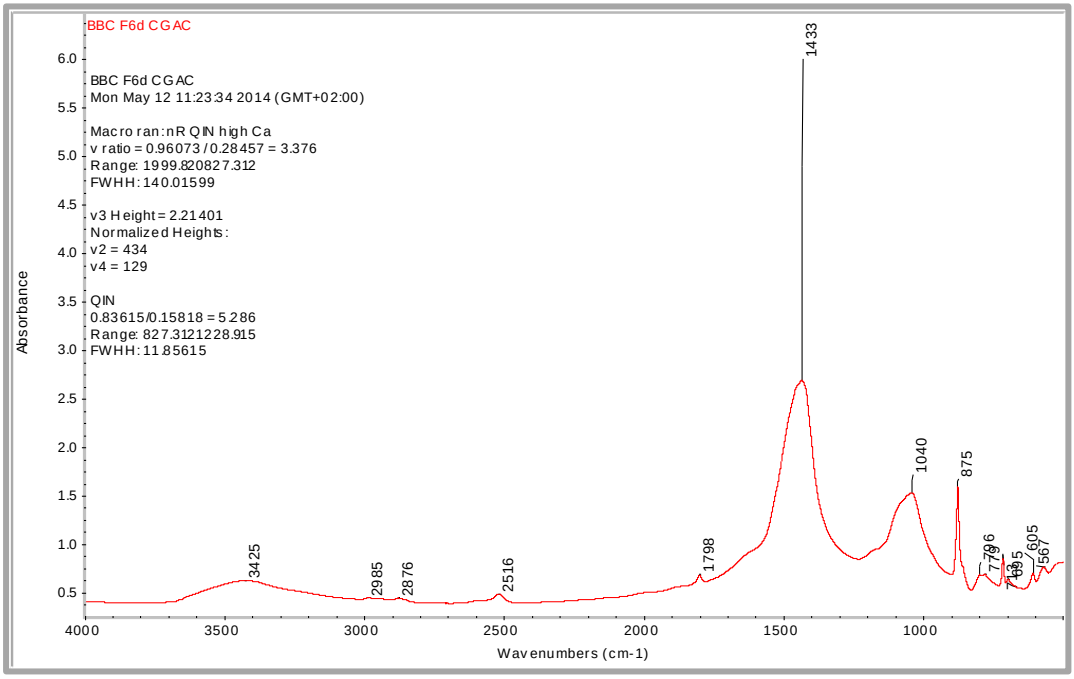

BBC G7a CFD
BBC G7a CFD
Mon May 12 10:26:32 2014 (GMT+02:00)
Macro ran:nR QIN high Ca
v ratio = 0.18578 / 0.10321 = 1.800
Range: 1997.40964 8.929
FWHH: 133.60458
v3 Height = 0.59956
Normalized Heights:
v2 = 310
v4 = 172
QIN
8.532e-002/2.421e-002 = 3.524
Range: 828.75911 56.598
FWHH: 20.99195
Absorbance
Wavenumbers (cm-1)
3426
2518
1797
1445
1083
874
799
713

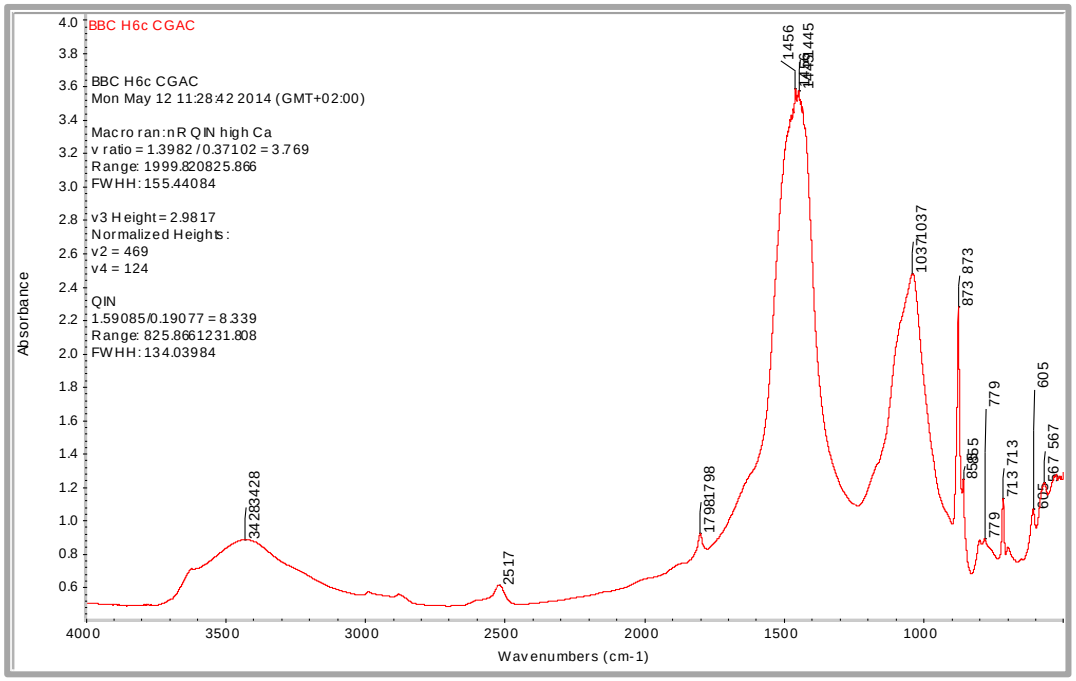

BBC F6d CG AA
BBC F6d CG AA
Mon May 12 10:48:17 2014 (GMT+02:00)
Macro ran:nR QIN high Ca
v ratio = 0.55906 / 0.19161 = 2.918
Range: 1999.82062 2.895
FWHH: 140.15694
v3 Height = 1.40245
Normalized Heights:
v2 = 399
v4 = 137
QIN
0.49511/0.21331 = 2.321
Range: 828.75912 27.951
FWHH: 11.84448
Absorbance
Wavenumbers (cm-1)
3425
2515
1430
1036
874
779
713
694

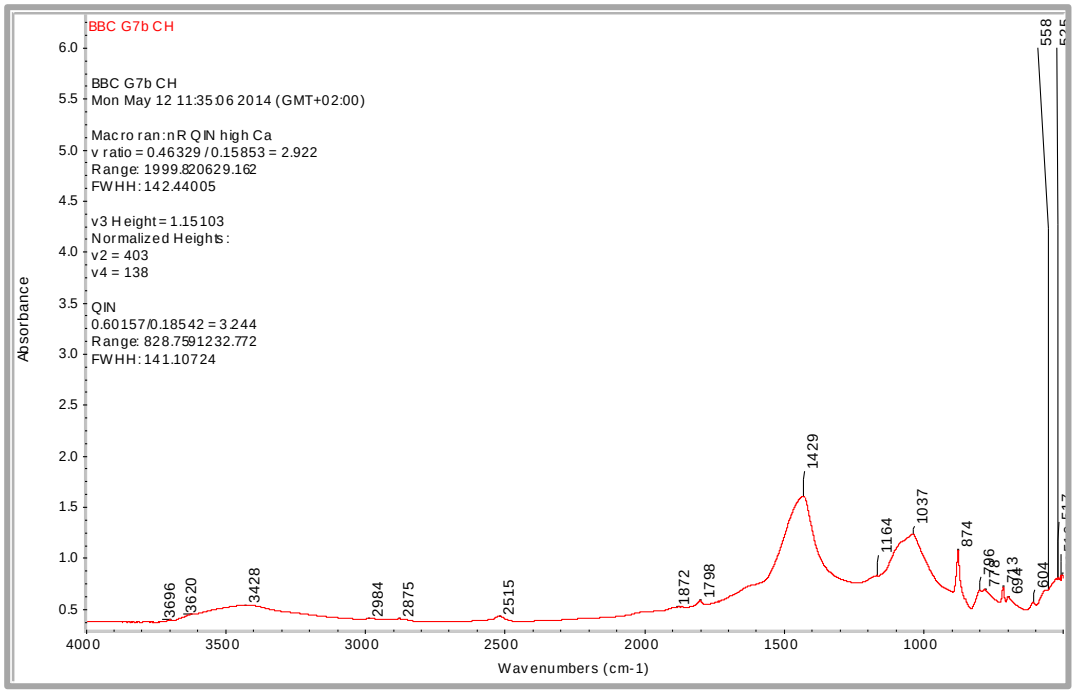

BBC H6d CGAA
BBC H6d CGAA
Mon May 12 10:52:39 2014 (GMT+02:00)
Macro ran:nR QIN high Ca
v ratio = 0.3732 / 0.10156 = 3.675
Range: 1999.820632.055
FWHH: 143.01527
v3 Height = 0.84419
Normalized Heights:
v2 = 442
v4 = 120
QIN
0.31093/0.11103 = 2.800
Range: 826.3481232.772
FWHH: 11.23513
Absorbance
Wavenumbers (cm-1)
3426
1430
1034
874
779
713

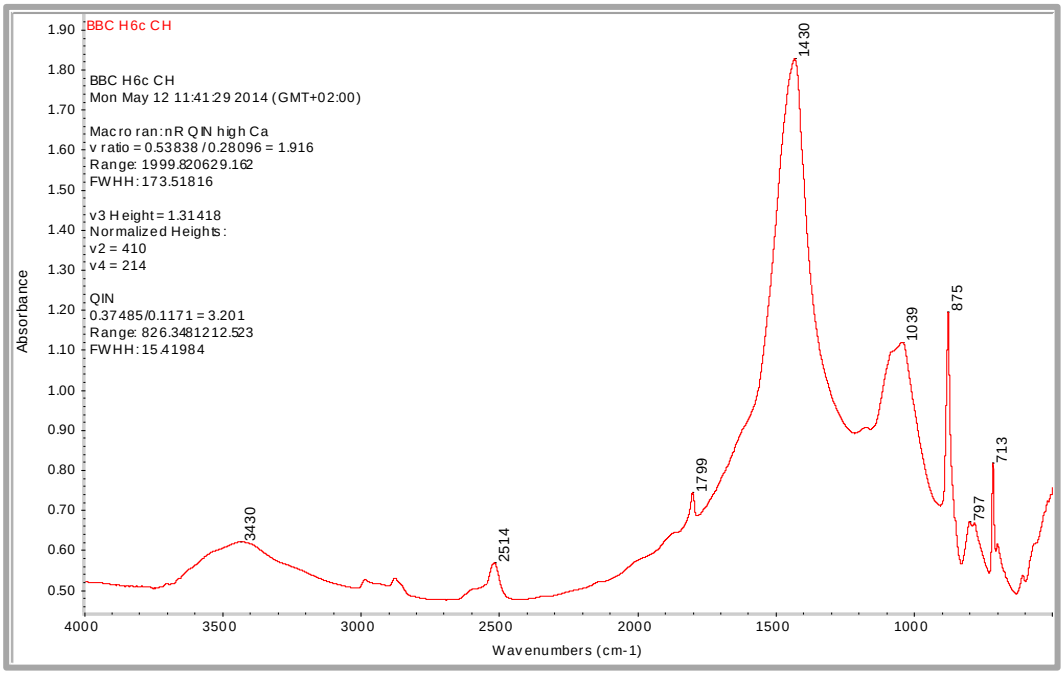

BBC F6d CGAB
BBC F6d CGAB
Mon May 12 10:58:07 2014 (GMT+02:00)
Macro ran:nR QIN high Ca
v ratio = 0.35059 / 0.13455 = 2.606
Range: 1999.820630.609
FWHH: 143.79912
v3 Height = 0.87968
Normalized Heights:
v2 = 399
v4 = 153
QIN
0.35703/0.12425 = 2.873
Range: 828.2761227.951
FWHH: 147.10133
Absorbance
Wavenumbers (cm-1)
3426
2514
1429
1036
874
779
713

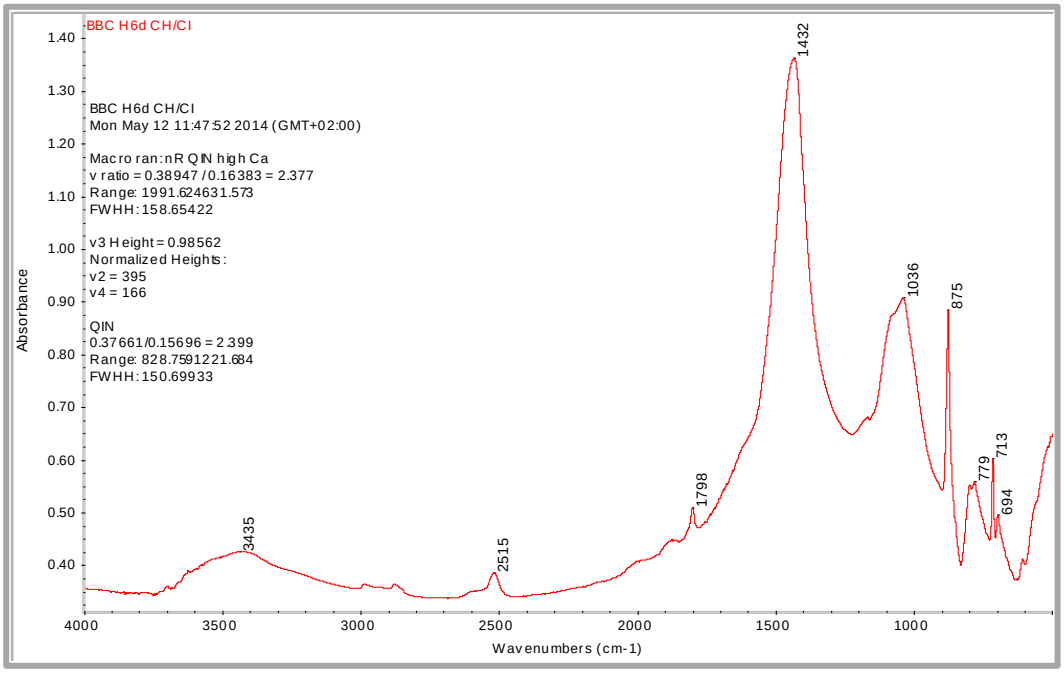

BBC H7a CGAB(h1)
BBC H7a CGAB(h1)
Mon May 12 11:17:08 2014 (GMT+02:00)
Macro ran:nR QIN high Ca
v ratio = 0.35751 / 9.306e-002 = 3.842
Range: 1999.82082 8.759
FWHH: 127.61955
v3 Height = 0.84132
Normalized Heights:
v2 = 425
v4 = 111
QIN
0.43067/5.447e-002 = 7.907
Range: 828.75912 32.290
FWHH: 115.96305
Absorbance
Wavenumbers (cm-1)
1433
1040
874
3426
779
713
695
567

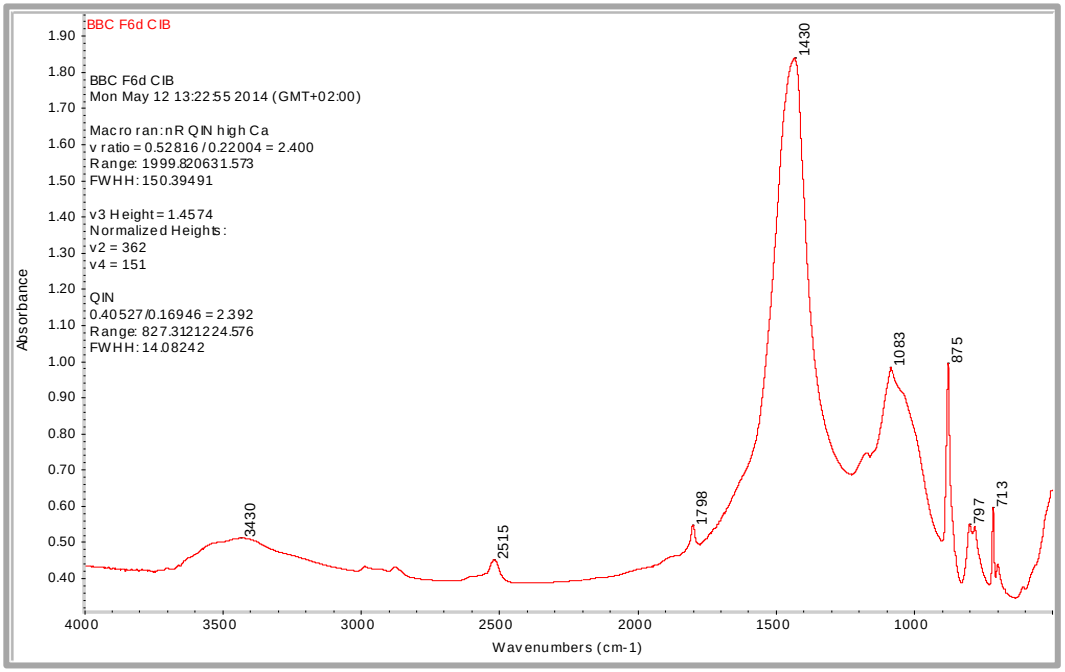

BBC F6d CGAC
BBC F6d CGAC
Mon May 12 11:23:34 2014 (GMT+02:00)
Macro ran:nR QIN high Ca
v ratio = 0.96073 / 0.28457 = 3.376
Range: 1999.82082 7.312
FWHH: 140.01599
v3 Height = 2.21401
Normalized Heights:
v2 = 434
v4 = 129
QIN
0.83615/0.15818 = 5.286
Range: 827.31212 28.915
FWHH: 11.85615
Absorbance
Wavenumbers (cm-1)
1433
1040
875
3425
2985
2876
2516
1798
779
695
605
567

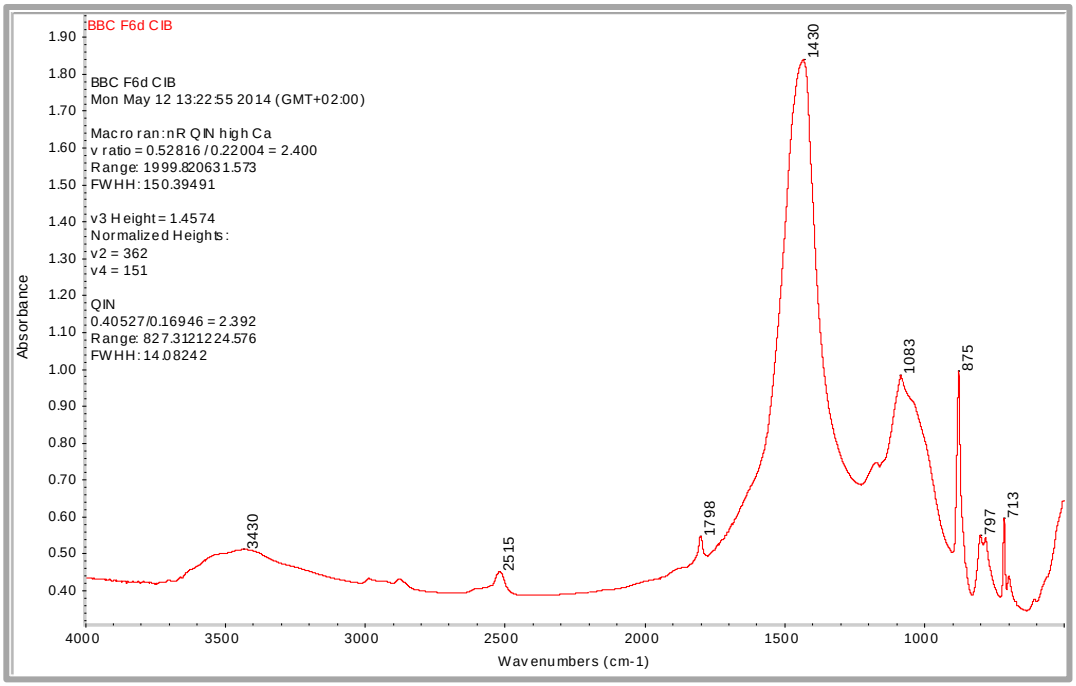

BBC H6c CGAC
BBC H6c CGAC
Mon May 12 11:28:42 2014 (GMT+02:00)
Macro ran:nR QIN high Ca
v ratio = 1.3982 / 0.37102 = 3.769
Range: 1999.820825.866
FWHH: 155.44084
v3 Height = 2.9817
Normalized Heights:
v2 = 469
v4 = 124
QIN
1.59085/0.19077 = 8.339
Range: 825.8661231.808
FWHH: 134.03984
Absorbance
Wavenumbers (cm-1)
3428
2517
1798
1456
1445
1037
873
779
713
605
567

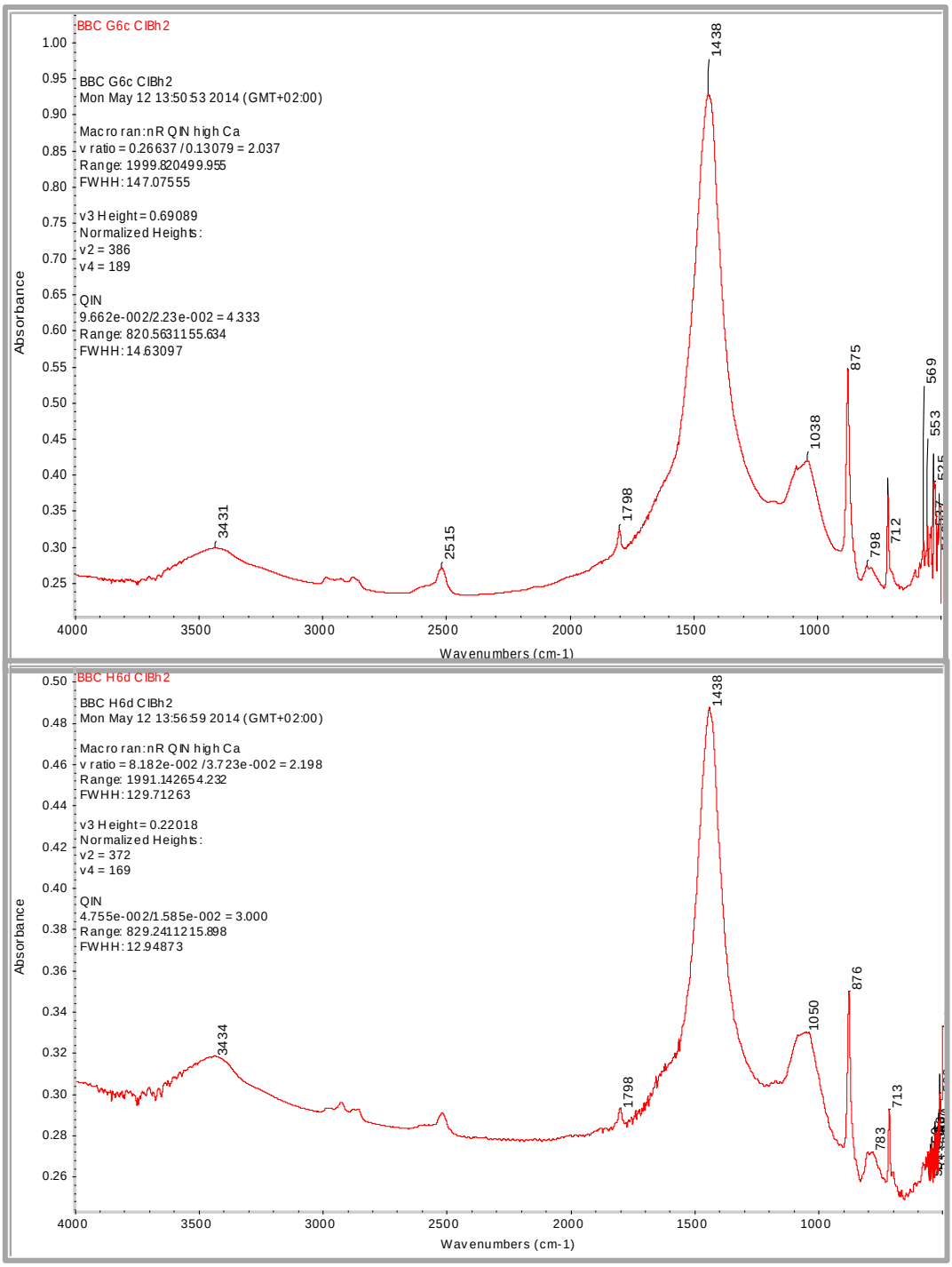

BBC G7b CH
BBC G7b CH
Mon May 12 11:35:06 2014 (GMT+02:00)
Macro ran:nR QIN high Ca
v ratio = 0.46329 / 0.15853 = 2.922
Range: 1999.820629.162
FWHH: 142.44005
v3 Height = 1.15103
Normalized Heights:
v2 = 403
v4 = 138
QIN
0.60157/0.18542 = 3.244
Range: 828.7591232.772
FWHH: 141.10724
Absorbance
Wavenumbers (cm-1)
3696
3620
3428
2984
2875
2515
1872
1798
1429
1164
1037
874
779
713
604
558

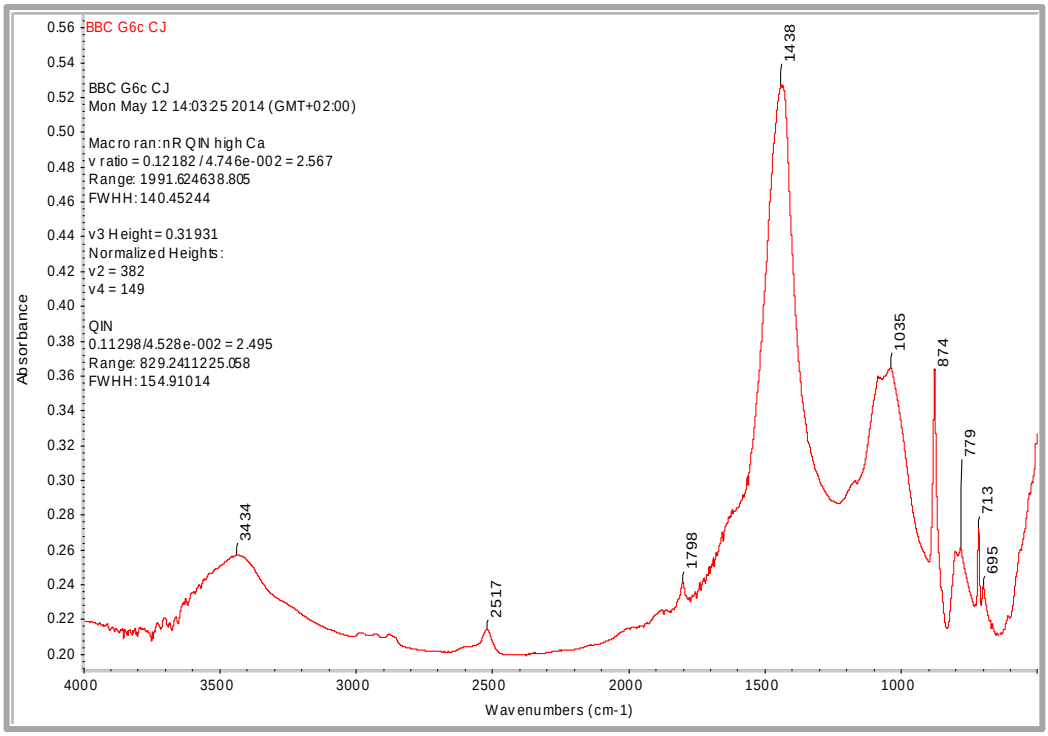

BBC H6c CH
BBC H6c CH
Mon May 12 11:41:29 2014 (GMT+02:00)
Macro ran:nR QIN high Ca
v ratio = 0.53838 / 0.28096 = 1.916
Range: 1999.82062 9.162
FWHH: 173.51816
v3 Height = 1.31418
Normalized Heights:
v2 = 410
v4 = 214
QIN
0.37485/0.1171 = 3.201
Range: 826.34812 12.523
FWHH: 15.41984
Absorbance
Wavenumbers (cm-1)
3430
2514
1799
1430
1039
875
797
713

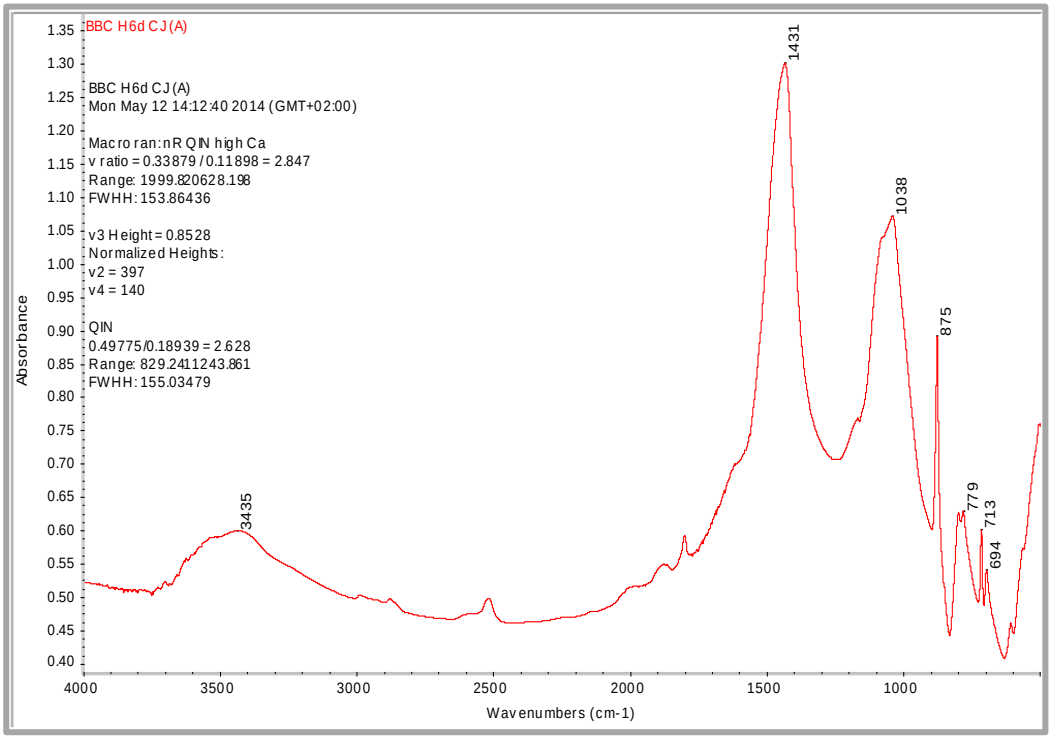

BBC H6d CH/Cl
BBC H6d CH/Cl
Mon May 12 11:47:52 2014 (GMT+02:00)
Macro ran:nR QIN high Ca
v ratio = 0.38947 / 0.16383 = 2.377
Range: 1991.62463 1.573
FWHH: 158.65422
v3 Height = 0.98562
Normalized Heights:
v2 = 395
v4 = 166
QIN
0.37661/0.15696 = 2.399
Range: 828.75912 21.684
FWHH: 150.69933
Absorbance
Wavenumbers (cm-1)
3435
2515
1798
1432
1036
875
779
713
694

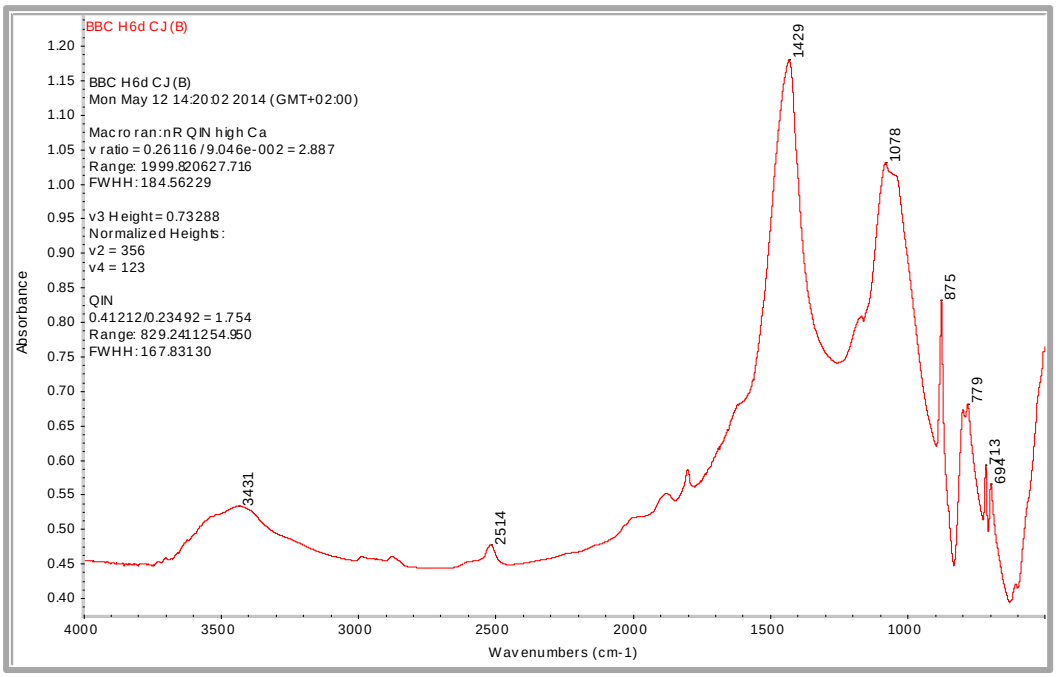

BBC F6d CIB
BBC F6d CIB
Mon May 12 13:22:55 2014 (GMT+02:00)
Macro ran:nR QIN high Ca
v ratio = 0.52816 / 0.22004 = 2.400
Range: 1999.820631.573
FWHH: 150.39491
v3 Height = 1.4574
Normalized Heights:
v2 = 362
v4 = 151
QIN
0.40527/0.16946 = 2.392
Range: 827.31212 24.576
FWHH: 14.08242
Absorbance
Wavenumbers (cm-1)
3430
2515
1798
1430
1083
875
797
713

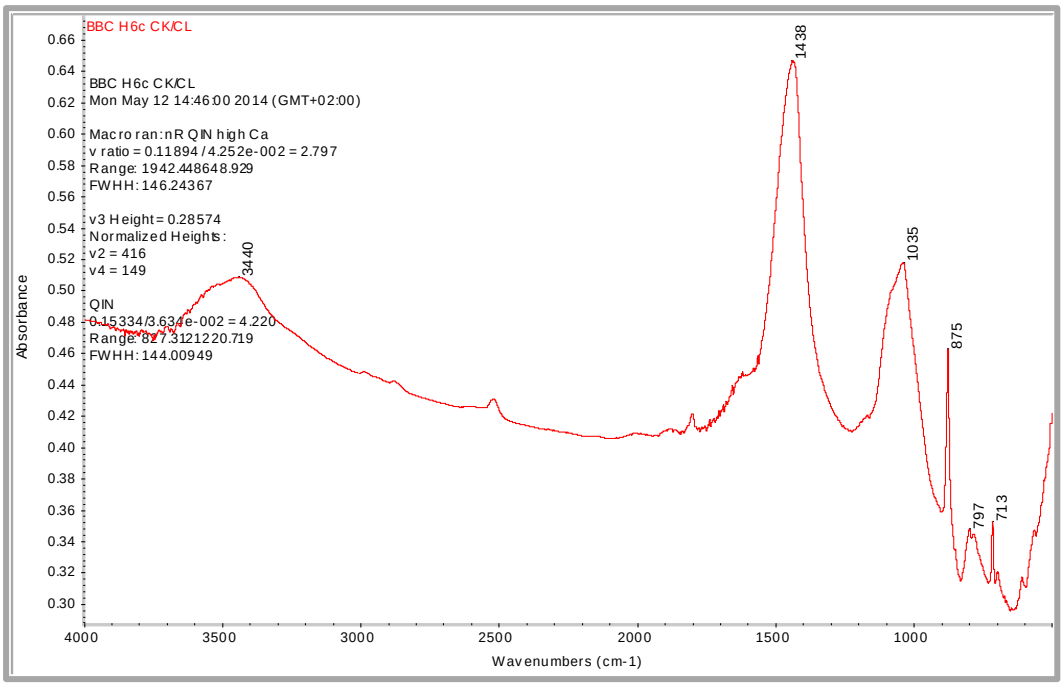

BBC F6d CIB
BBC F6d CIB
Mon May 12 13:22:55 2014 (GMT+02:00)
Macro ran:nR QIN high Ca
v ratio = 0.52816 / 0.22004 = 2.400
Range: 1999.820631.573
FWHH: 150.39491
v3 Height = 1.4574
Normalized Heights:
v2 = 362
v4 = 151
QIN
0.40527/0.16946 = 2.392
Range: 827.31212 24.576
FWHH: 14.08242
Absorbance
Wavenumbers (cm-1)
3430
2515
1798
1430
1083
875
797
713

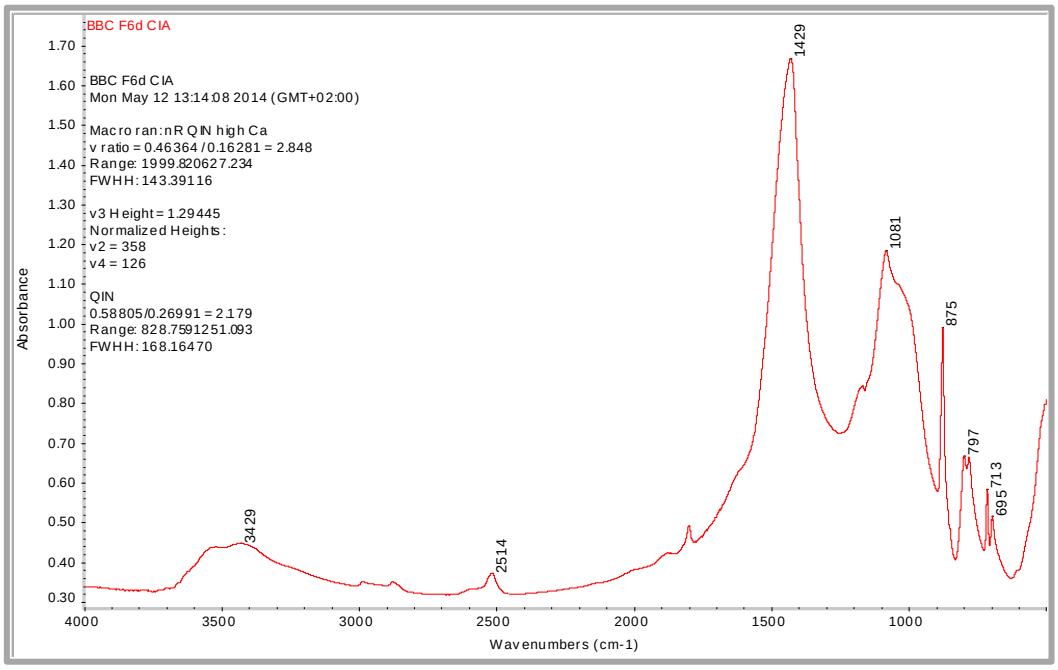

BBC G6c CIBh2
BBC G6c CIBh2
Mon May 12 13:50:53 2014 (GMT+02:00)
Macro ran:nR QIN high Ca
v ratio = 0.26637 / 0.13079 = 2.037
Range: 1999.820499.955
FWHH: 147.07555
v3 Height = 0.69089
Normalized Heights:
v2 = 386
v4 = 189
QIN
9.662e-002/2.23e-002 = 4.333
Range: 820.5631155.634
FWHH: 14.63097
Absorbance
Wavenumbers (cm-1)
3431
2515
1798
1438
1038
875
798
712
569
553
BBC H6d CIBh2
BBC H6d CIBh2
Mon May 12 13:56:59 2014 (GMT+02:00)
Macro ran:nR QIN high Ca
v ratio = 8.182e-002 / 3.723e-002 = 2.198
Range: 1991.142654.232
FWHH: 129.71263
v3 Height = 0.22018
Normalized Heights:
v2 = 372
v4 = 169
QIN
4.755e-002/1.585e-002 = 3.000
Range: 829.2411215.898
FWHH: 12.94873
Absorbance
Wavenumbers (cm-1)
3434
1798
1438
1050
876
783
713

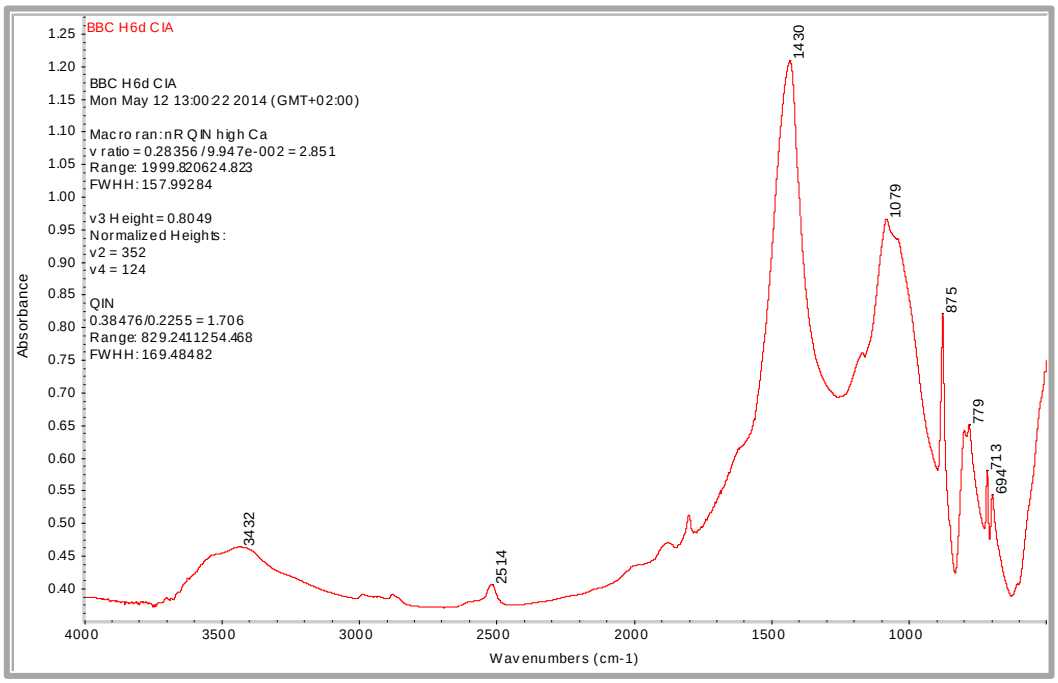

BBC G6c CJ
BBC G6c CJ
Mon May 12 14:03:25 2014 (GMT+02:00)
Macro ran:nR QIN high Ca
v ratio = 0.12182 / 4.746e-002 = 2.567
Range: 1991.624638.805
FWHH: 140.45244
v3 Height = 0.31931
Normalized Heights:
v2 = 382
v4 = 149
QIN
0.11298/4.528e-002 = 2.495
Range: 829.2411225.058
FWHH: 154.91014
Absorbance
Wavenumbers (cm-1)
3434
2517
1798
1438
1035
874
779
713
695

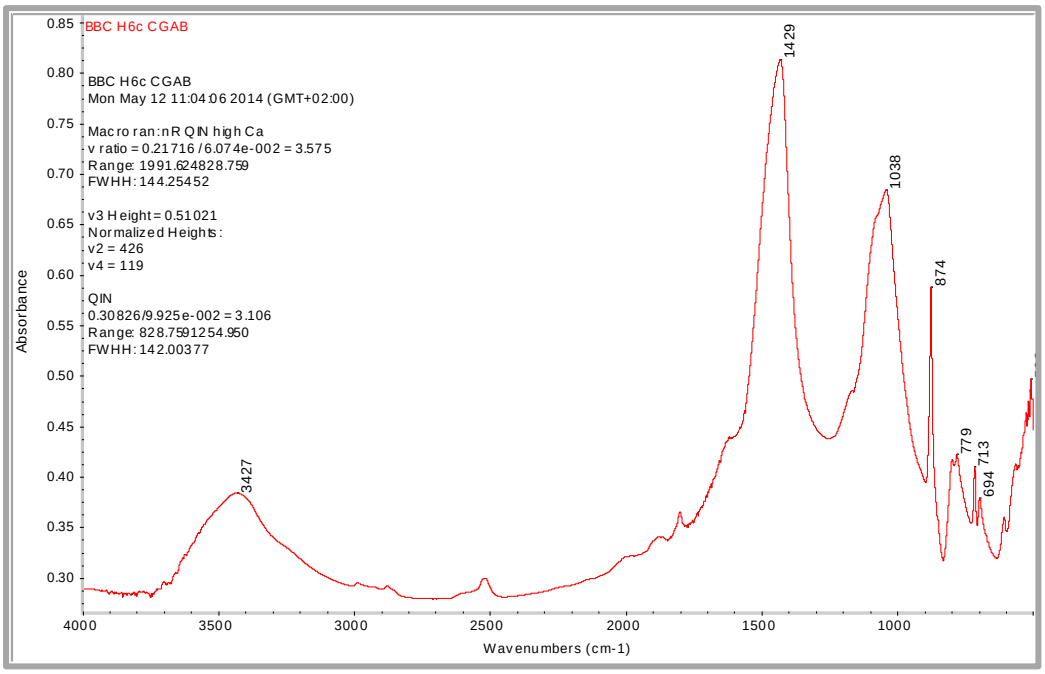

BBC H6d CJ (A)
BBC H6d CJ (A)
Mon May 12 14:12:40 2014 (GMT+02:00)
Macro ran:nR QIN high Ca
v ratio = 0.33879 / 0.11898 = 2.847
Range: 1999.820628.198
FWHH: 153.86436
v3 Height = 0.8528
Normalized Heights:
v2 = 397
v4 = 140
QIN
0.49775/0.18939 = 2.628
Range: 829.2411243.861
FWHH: 155.03479
Absorbance
Wavenumbers (cm-1)
3435
1431
1038
875
779
713
694

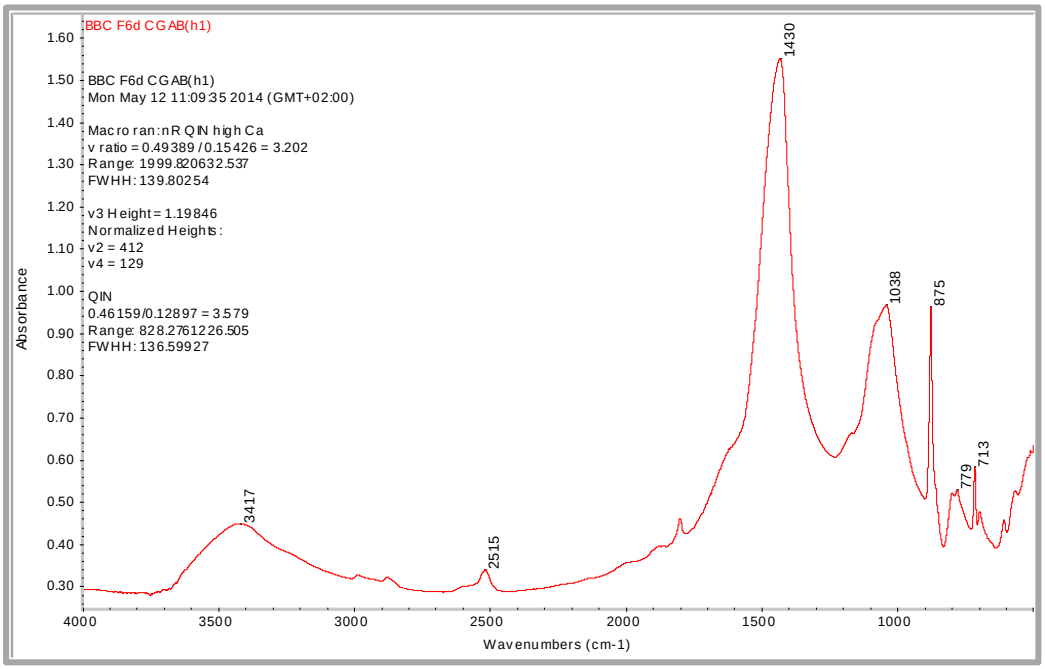

BBC H6d CJ (B)
BBC H6d CJ (B)
Mon May 12 14:20:02 2014 (GMT+02:00)
Macro ran:nR QIN high Ca
v ratio = 0.26116 / 9.046e-002 = 2.887
Range: 1999.820627.716
FWHH: 184.56229
v3 Height = 0.73288
Normalized Heights:
v2 = 356
v4 = 123
QIN
0.41212/0.23492 = 1.754
Range: 829.2411254.950
FWHH: 167.83130
Absorbance
Wavenumbers (cm-1)
3431
2514
1429
1078
875
779
713
694

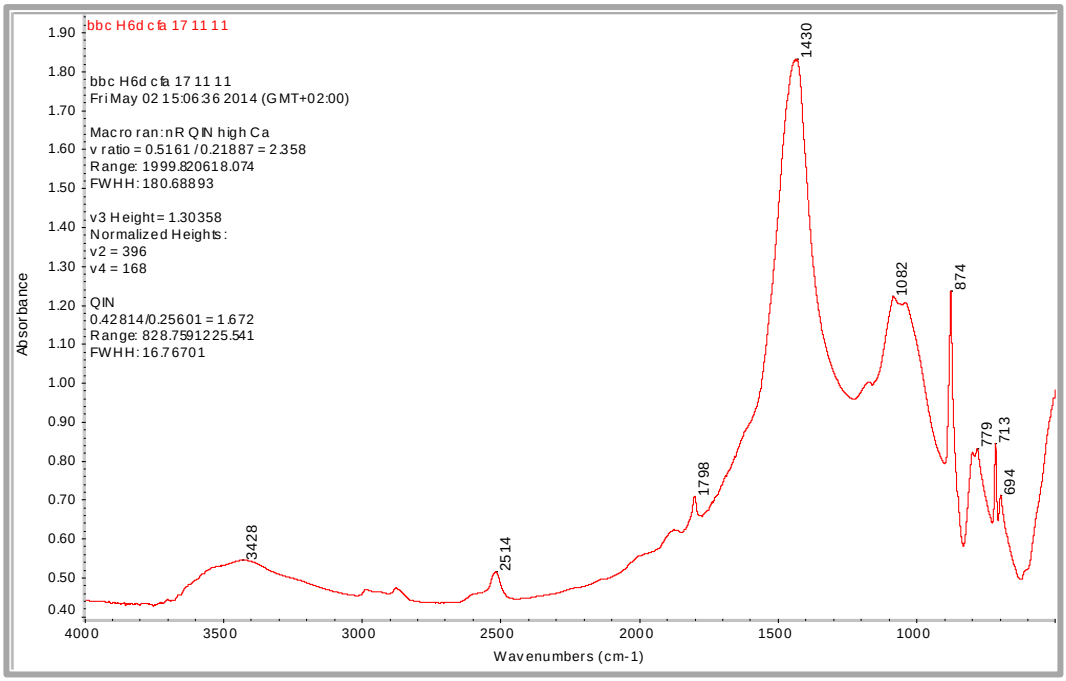

BBC H6c CK/CL
BBC H6c CK/CL
Mon May 12 14:46:00 2014 (GMT+02:00)
Macro ran:nR QIN high Ca
v ratio = 0.11894 / 4.252e-002 = 2.797
Range: 1942.448648.929
FWHH: 146.24367
v3 Height = 0.28574
Normalized Heights:
v2 = 416
v4 = 149
QIN
0.15334/3.634e-002 = 4.220
Range: 827.3121220.719
FWHH: 144.00949
Absorbance
Wavenumbers (cm-1)
3440
1438
1035
875
797
713

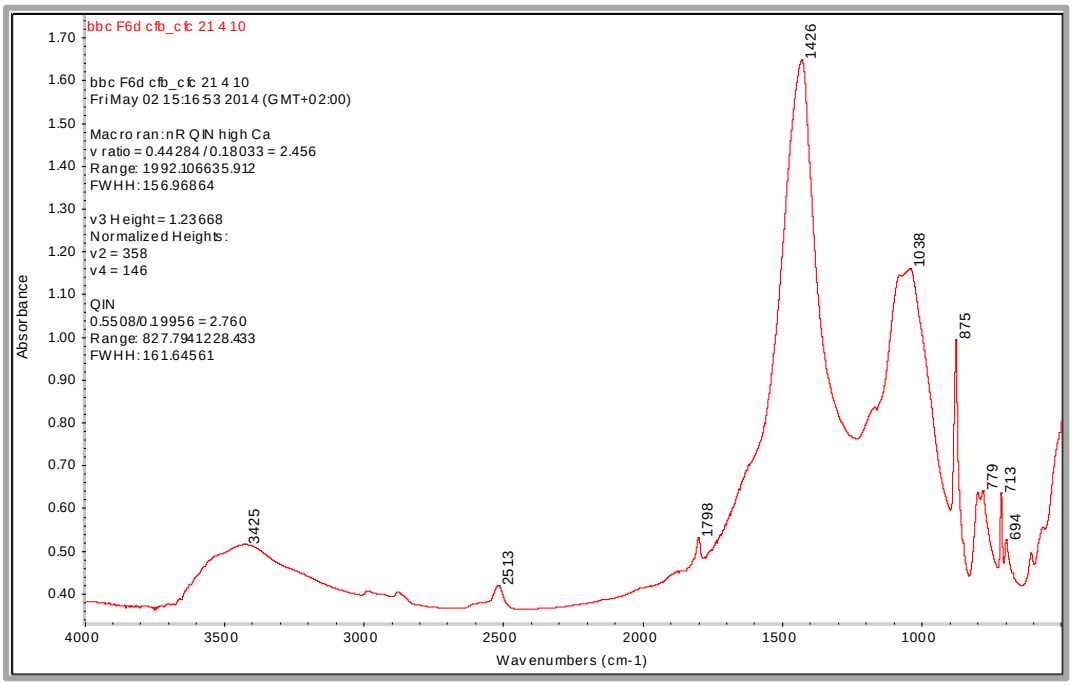

BBC F6d CIA
BBC F6d CIA
Mon May 12 13:14:08 2014 (GMT+02:00)
Macro ran: nR QIN high Ca
v ratio = 0.46364 / 0.16281 = 2.848
Range: 1999.82062 7.234
FWHH: 143.39116
v3 Height = 1.29445
Normalized Heights:
v2 = 358
v4 = 126
QIN
0.58805/0.26991 = 2.179
Range: 828.7591251.093
FWHH: 168.16470
Absorbance
Wavenumbers (cm-1)
1429
1081
875
797
713
695
3429
2514

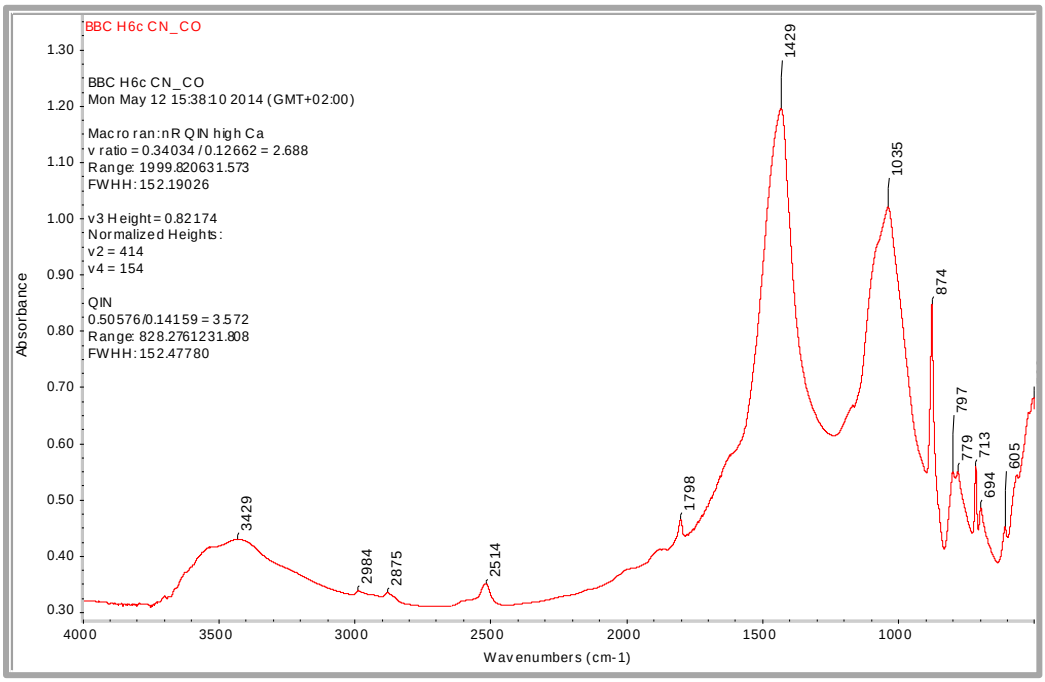

BBC H6d CIA
BBC H6d CIA
Mon May 12 13:00:22 2014 (GMT+02:00)
Macro ran: nR QIN high Ca
v ratio = 0.28356 / 9.947e-002 = 2.851
Range: 1999.82062 4.823
FWHH: 157.99284
v3 Height = 0.8049
Normalized Heights:
v2 = 352
v4 = 124
QIN
0.38476/0.2255 = 1.706
Range: 829.2411254.468
FWHH: 169.48482
Absorbance
Wavenumbers (cm-1)
1430
1079
875
779
713
694
3432
2514

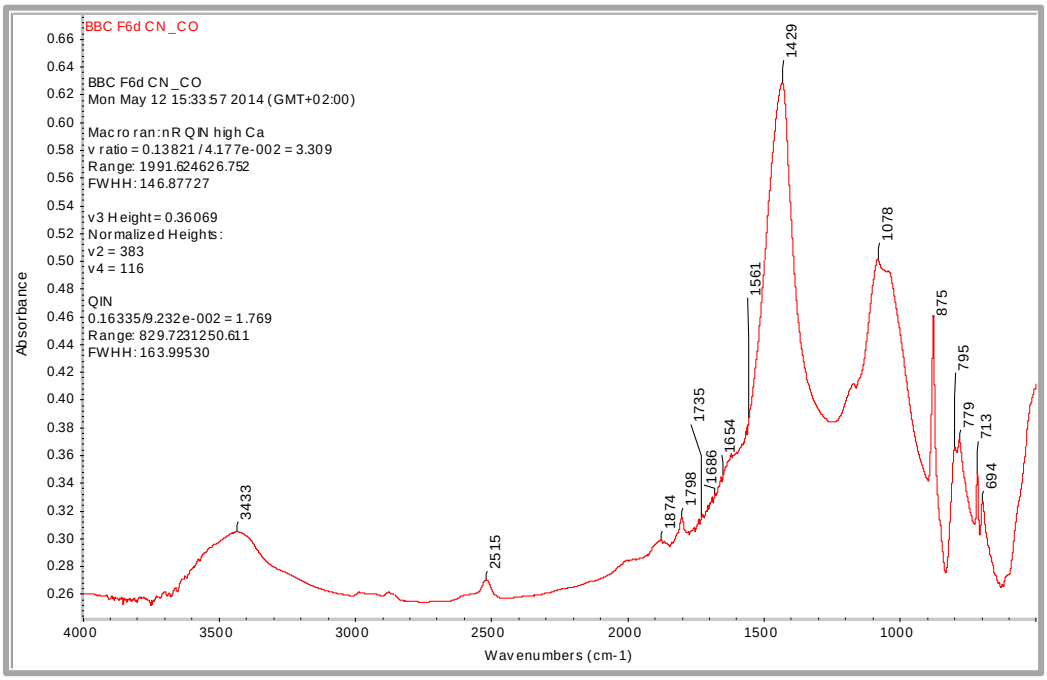

BBC H6c CGAB
BBC H6c CGAB
Mon May 12 11:04:06 2014 (GMT+02:00)
Macro ran:nR QIN high Ca
v ratio = 0.21716 / 6.074e-002 = 3.575
Range: 1991.624828.759
FWHH: 144.25452
v3 Height = 0.51021
Normalized Heights:
v2 = 426
v4 = 119
QIN
0.30826/9.925e-002 = 3.106
Range: 828.7591254.950
FWHH: 142.00377
Absorbance
Wavenumbers (cm-1)
1429
1038
874
779
713
694
3427

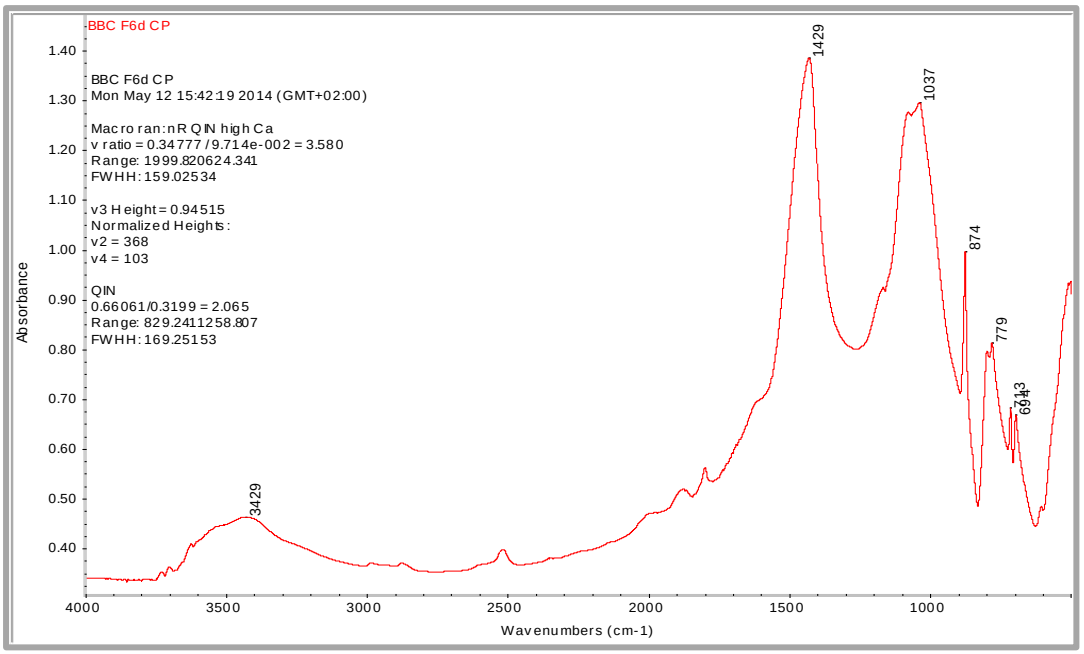

BBC F6d CGAB(h1)
BBC F6d CGAB(h1)
Mon May 12 11:09:35 2014 (GMT+02:00)
Macro ran:nR QIN high Ca
v ratio = 0.49389 / 0.15426 = 3.202
Range: 1999.820632.537
FWHH: 139.80254
v3 Height = 1.19846
Normalized Heights:
v2 = 412
v4 = 129
QIN
0.46159/0.12897 = 3.579
Range: 828.2761226.505
FWHH: 136.59927
Absorbance
Wavenumbers (cm-1)
1430
1038
875
779
713
3417
2515

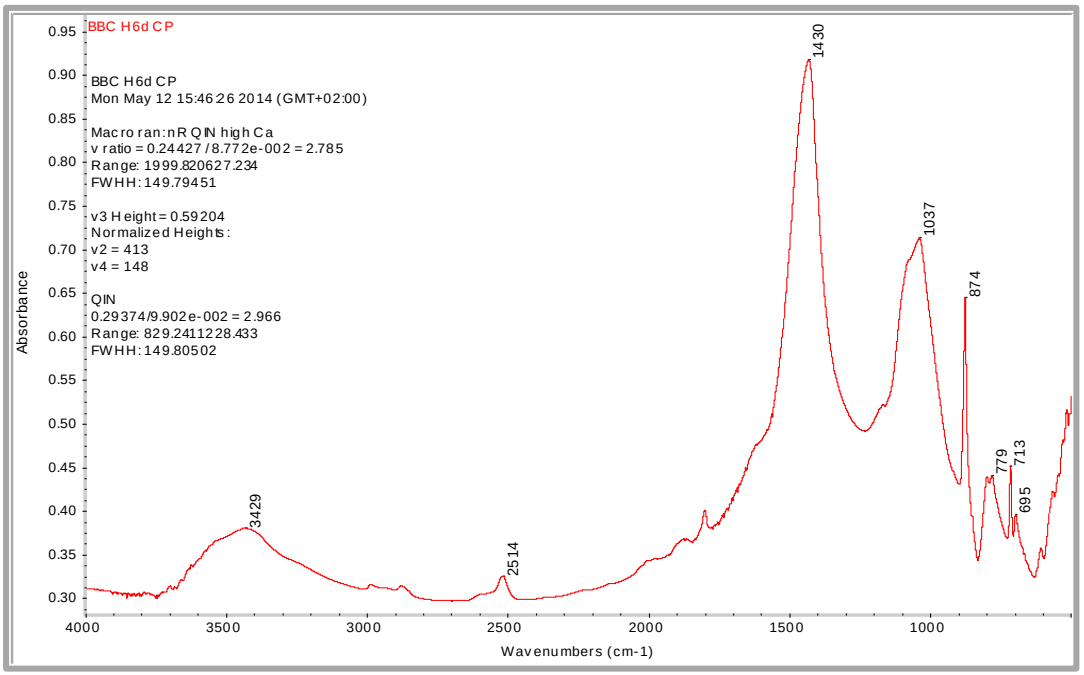

bbc H6d cfa 17 11 11
bbc H6d cfa 17 11 11
Fri May 02 15:06:36 2014 (GMT+02:00)
Macro ran: nR QIN high Ca
v ratio = 0.5161 / 0.21887 = 2.358
Range: 1999.820618.074
FWHH: 180.68893
v3 Height = 1.30358
Normalized Heights:
v2 = 396
v4 = 168
QIN
0.42814/0.25601 = 1.672
Range: 828.7591225.541
FWHH: 16.76701
Absorbance
Wavenumbers (cm-1)
3428
2514
1798
1430
1082
874
779
713
694

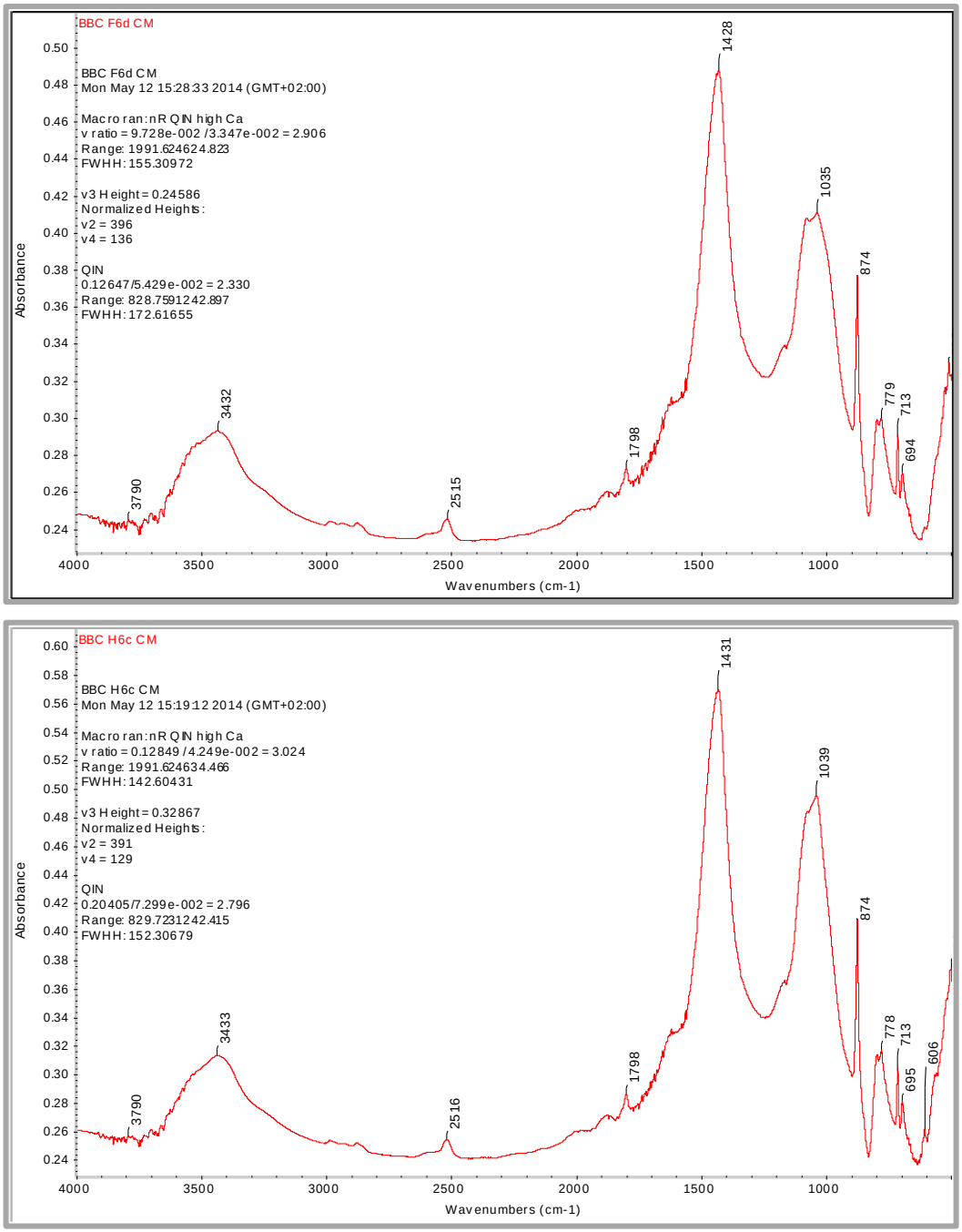

bbc F6d cfb_cfc 21 4 10
bbc F6d cfb_cfc 21 4 10
Fri May 02 15:16:53 2014 (GMT+02:00)
Macro ran: nR QIN high Ca
v ratio = 0.44284 / 0.18033 = 2.456
Range: 1992.106635.912
FWHH: 156.96864
v3 Height = 1.23668
Normalized Heights:
v2 = 358
v4 = 146
QIN
0.5508/0.19956 = 2.760
Range: 827.7941228.433
FWHH: 161.64561
Absorbance
Wavenumbers (cm-1)
3425
2513
1798
1426
1038
875
779
713
694


BBC H6c CN_CO
BBC H6c CN_CO
Mon May 12 15:38:10 2014 (GMT+02:00)
Macro ran:nR QIN high Ca
v ratio = 0.34034 / 0.12662 = 2.688
Range: 1999.82063 1.573
FWHH: 152.19026
v3 Height = 0.82174
Normalized Heights:
v2 = 414
v4 = 154
QIN
0.50576/0.14159 = 3.572
Range: 828.27612 31.808
FWHH: 152.47780
Absorbance
Wavenumbers (cm-1)
3429
2984
2875
2514
1798
1429
1035
874
797
779
713
694
605


BBC F6d CN_CO
BBC F6d CN_CO
Mon May 12 15:33:57 2014 (GMT+02:00)
Macro ran:nR QIN high Ca
v ratio = 0.13821 / 4.177e-002 = 3.309
Range: 1991.62462 6.752
FWHH: 146.87727
v3 Height = 0.36069
Normalized Heights:
v2 = 383
v4 = 116
QIN
0.16335/9.232e-002 = 1.769
Range: 829.72312 50.611
FWHH: 163.99530
Absorbance
Wavenumbers (cm-1)
3433
2515
1874
1798
1686
1654
1735
1561
1429
1078
875
795
779
713
694


BBC F6d CP
BBC F6d CP
Mon May 12 15:42:19 2014 (GMT+02:00)
Macro ran:nR QIN high Ca
v ratio = 0.34777 / 9.714e-002 = 3.580
Range: 1999.820624.341
FWHH: 159.02534
v3 Height = 0.94515
Normalized Heights:
v2 = 368
v4 = 103
QIN
0.66061/0.3199 = 2.065
Range: 829.2411258.807
FWHH: 169.25153
Absorbance
Wavenumbers (cm-1)
3429
1429
1037
874
779
713
694


BBC H6d CP
BBC H6d CP
Mon May 12 15:46:26 2014 (GMT+02:00)
Macro ran:nR QIN high Ca
v ratio = 0.24427 / 8.772e-002 = 2.785
Range: 1999.820627.234
FWHH: 149.79451
v3 Height = 0.59204
Normalized Heights:
v2 = 413
v4 = 148
QIN
0.29374/9.902e-002 = 2.966
Range: 829.2411228.433
FWHH: 149.80502
Absorbance
Wavenumbers (cm-1)
3429
2514
1430
1037
874
779
713
695



Figures C1-C43 FT-IR spectra for the sediments from Blombos Cave

Appendix C2 Grinding curve

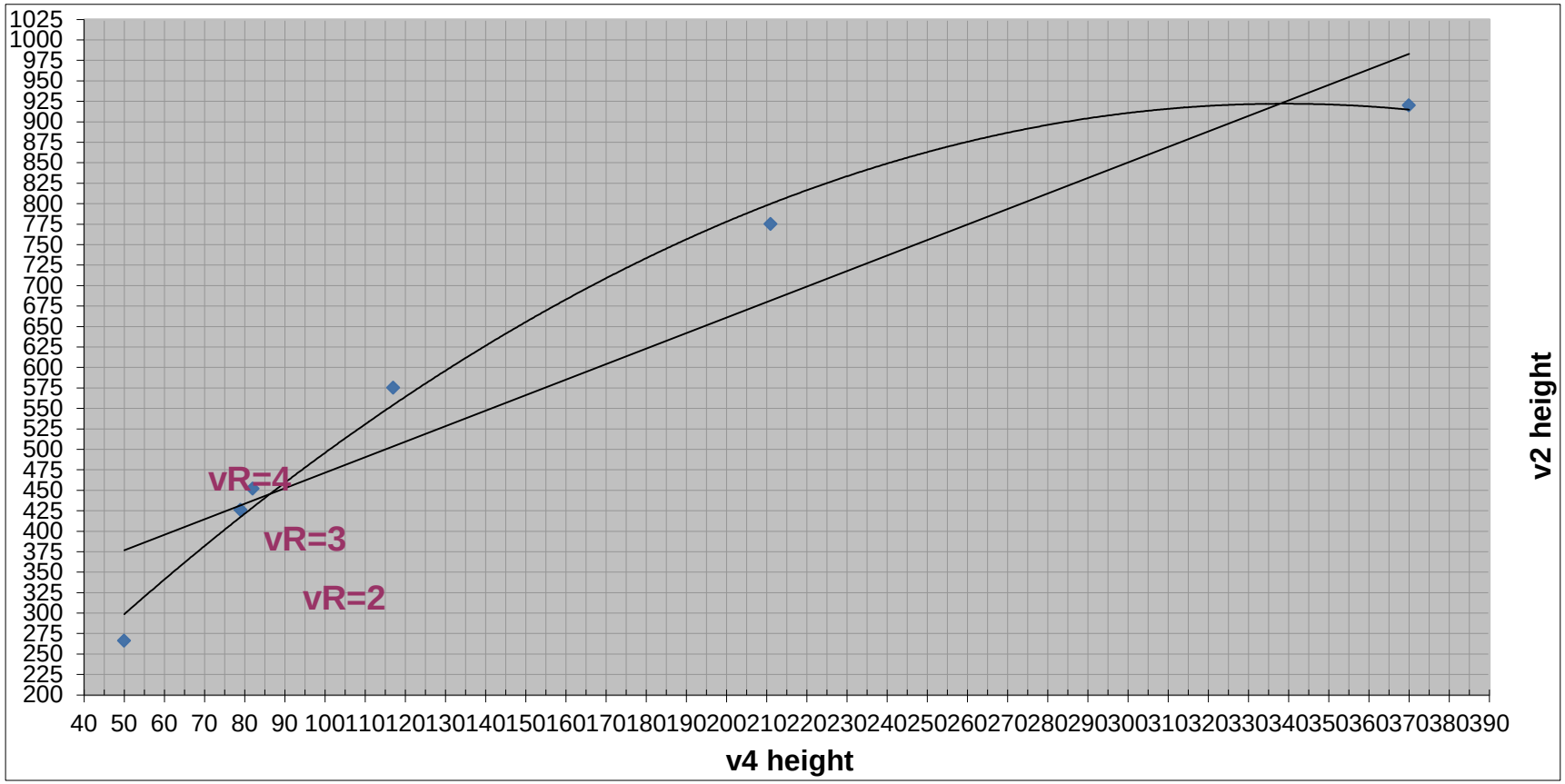
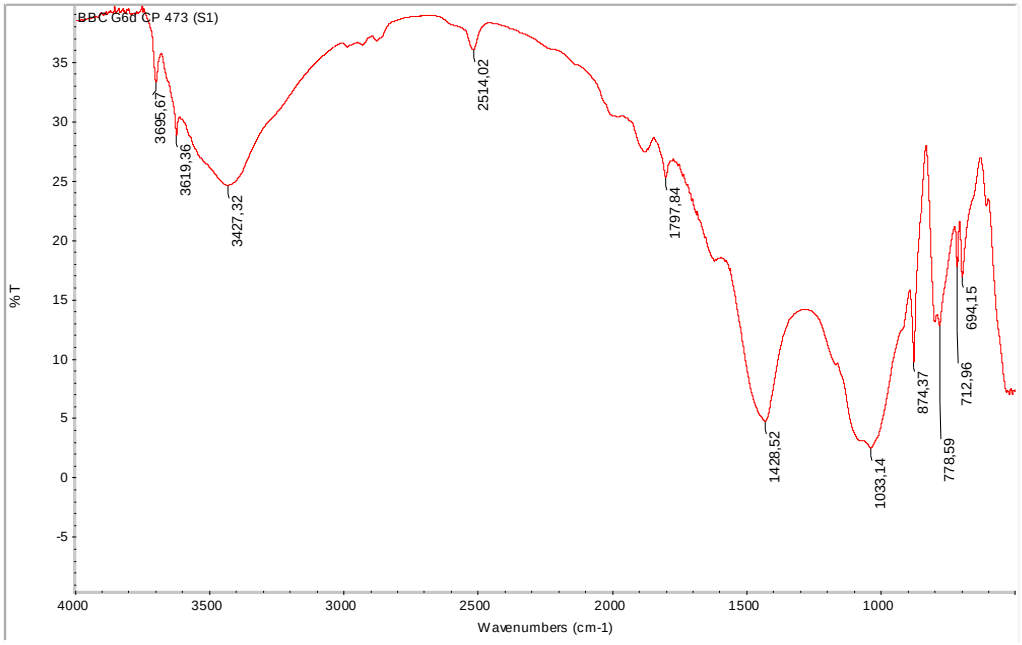
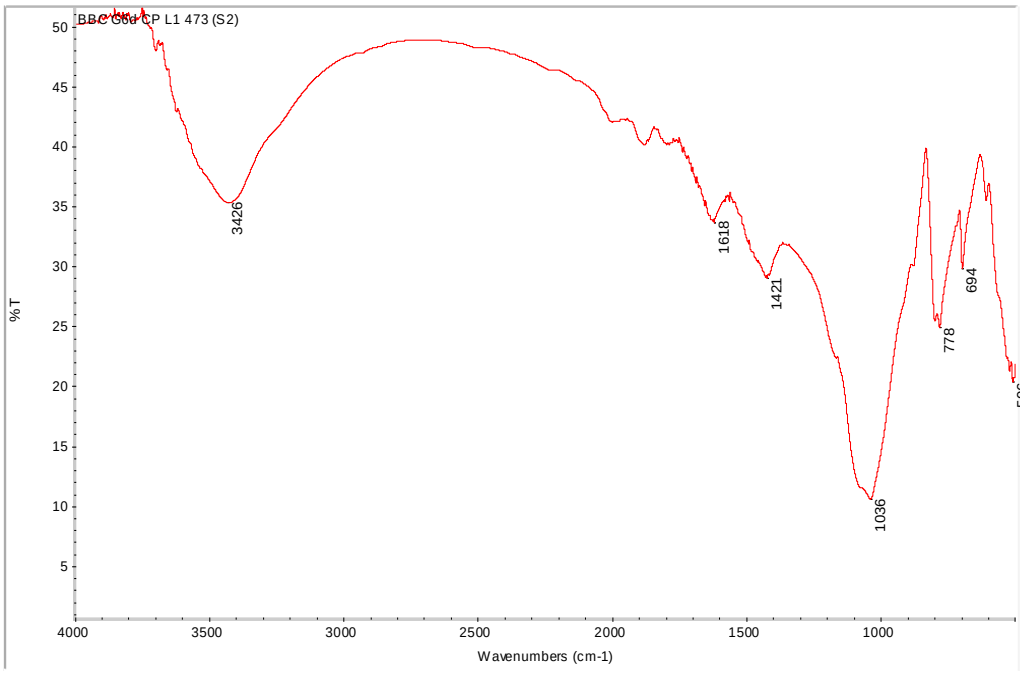


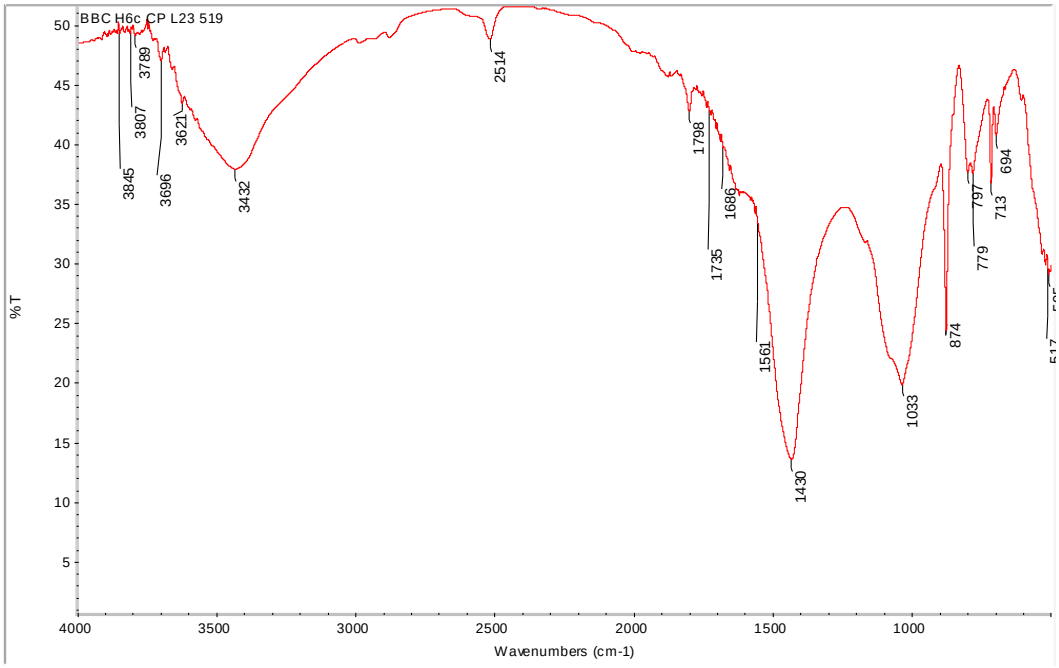
Figure C44 Grinding curve example of a calcite

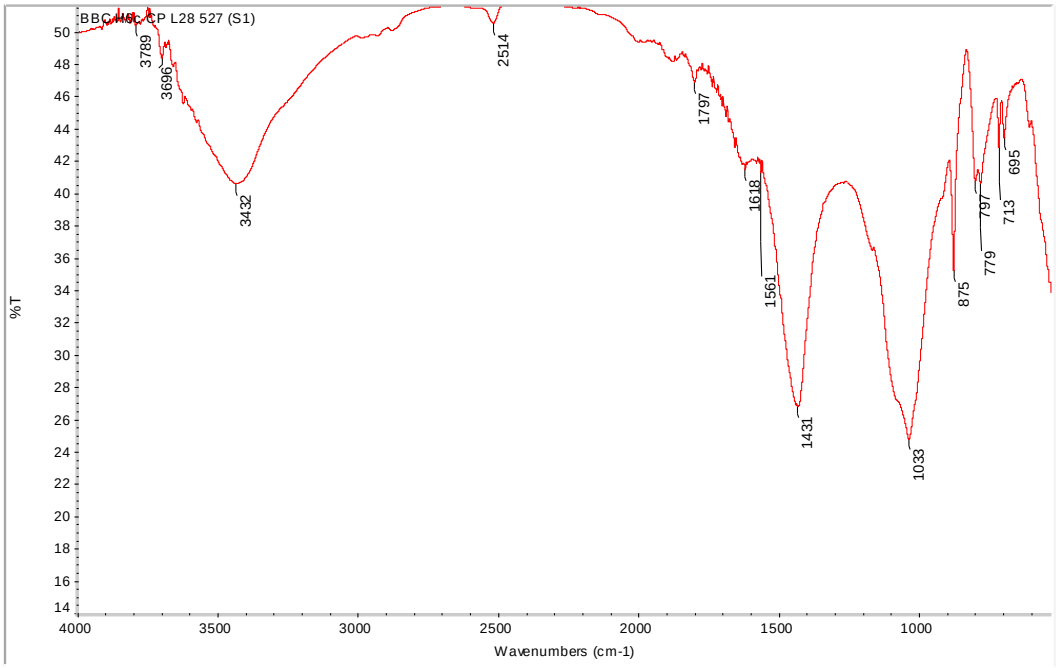
Appendix D FT-IR analysis of ochre

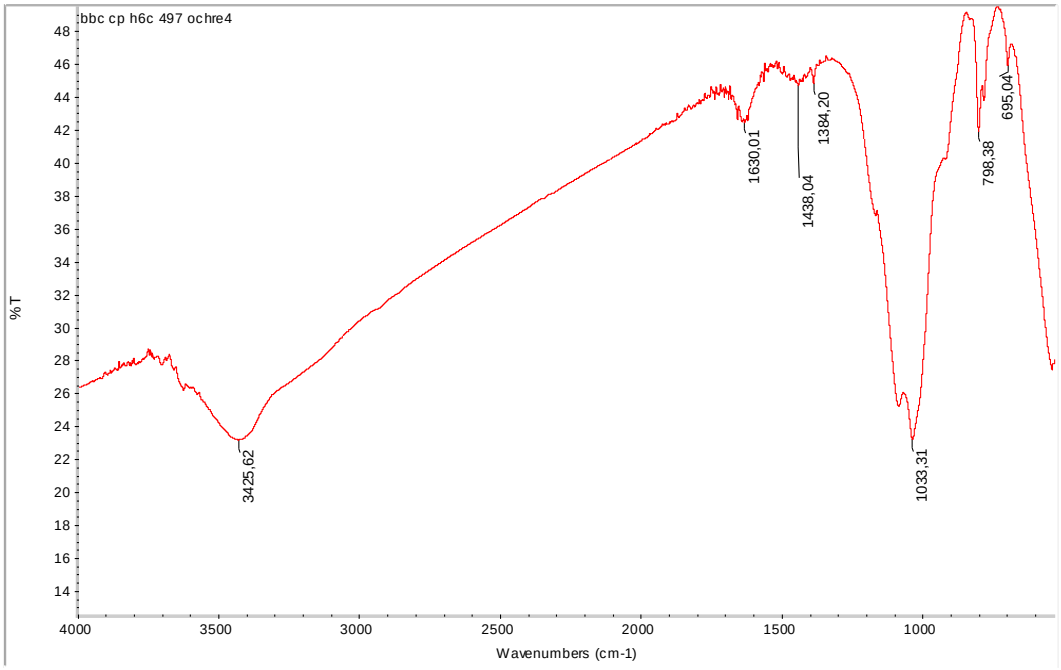
Appendix D1 FT-IR spectra of the CP layer ochre

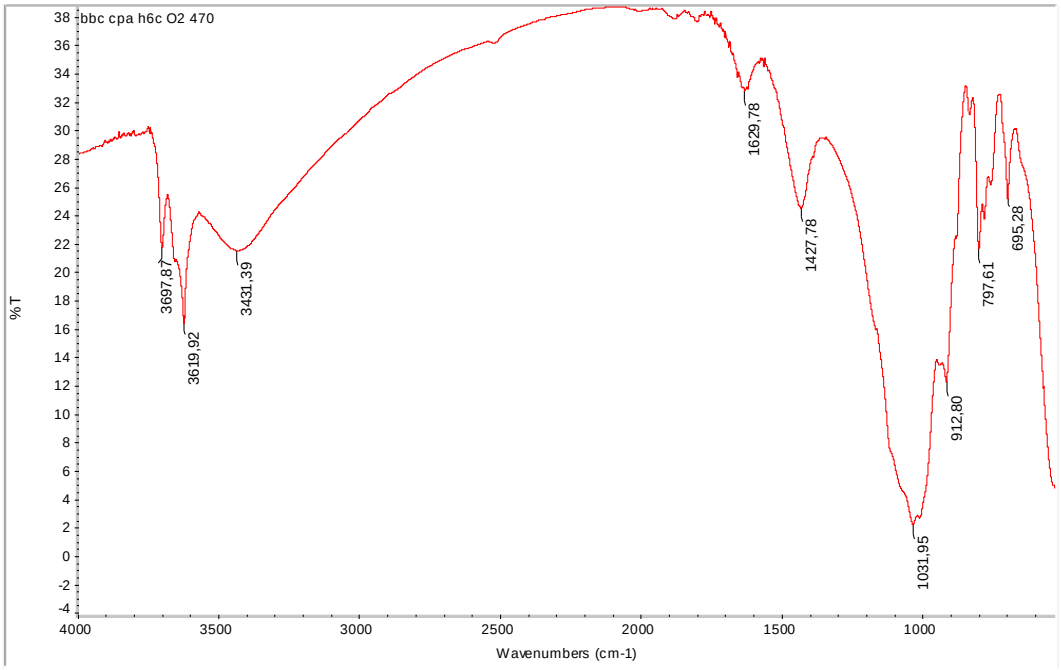


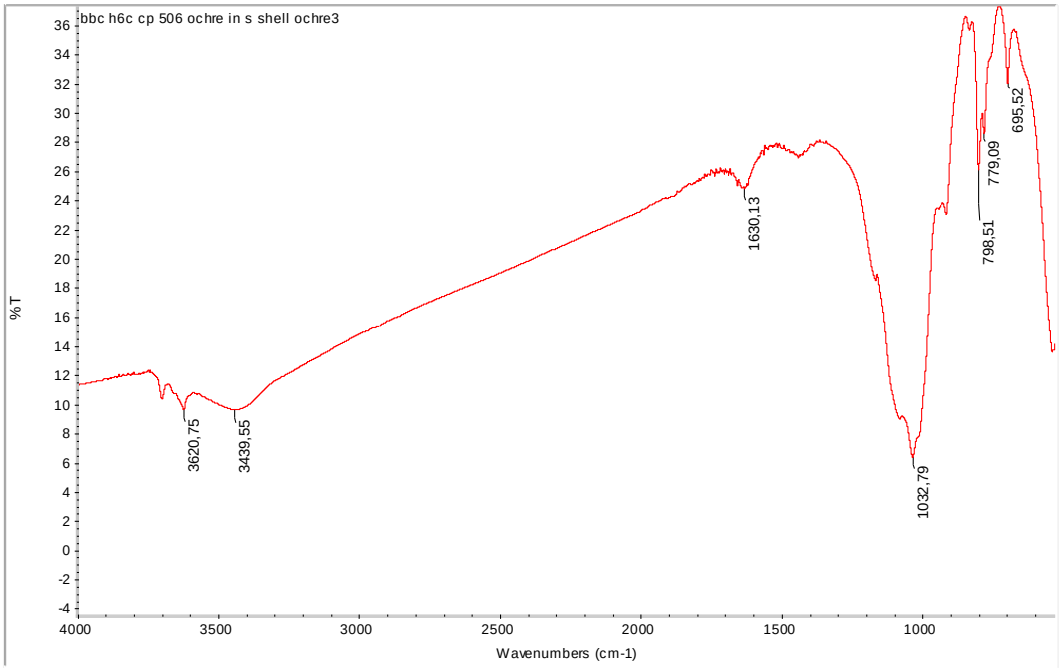


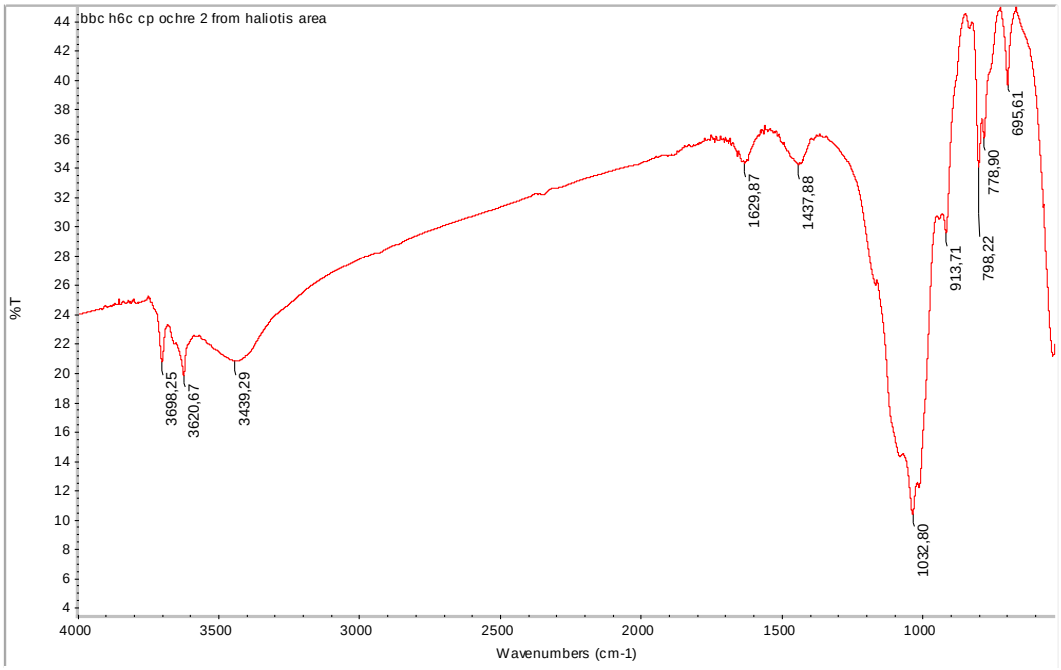

BBC H6c CP L23 519
%T
Wavenumbers (cm-1)
3845
3807
3789
3696
3621
3432
2514
1798
1735
1686
1561
1430
1033
874
797
779
713
694

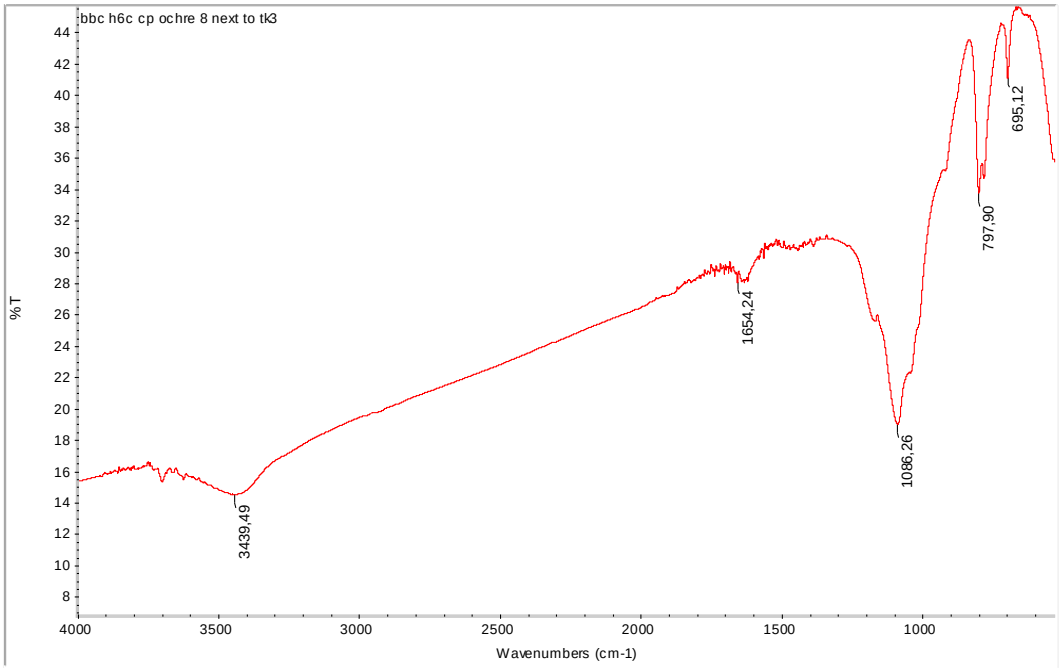

BBC H6c CP L28 527 (S1)
%T
Wavenumbers (cm-1)
3789
3696
3432
2514
1797
1618
1561
1431
1033
875
797
779
713
695

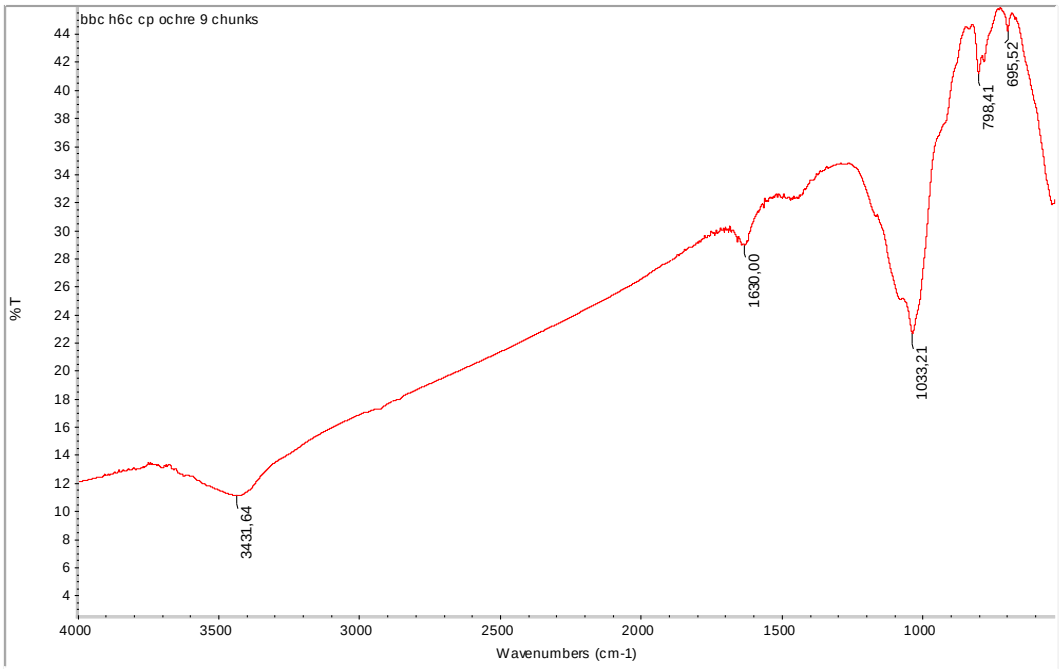

bbc cp h6c 497 ochre4
%T
Wavenumbers (cm-1)
3425,62
1630,01
1438,04
1384,20
1033,31
798,38
695,04

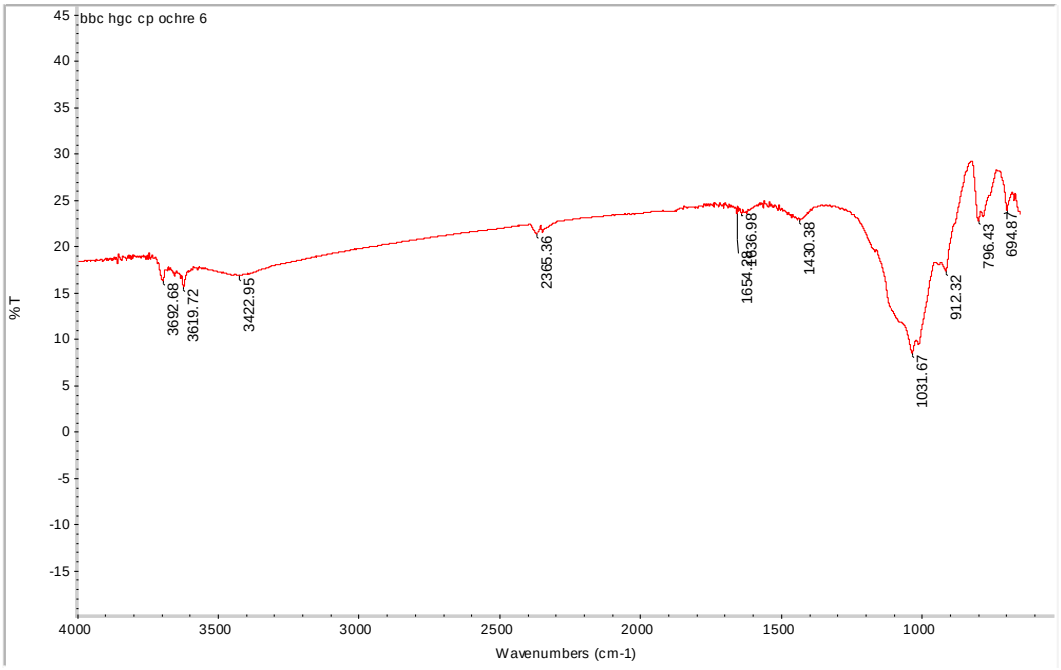

bbc cpa h6c O2 470
%T
Wavenumbers (cm-1)
3697,87
3619,92
3431,39
1629,78
1427,78
1031,95
912,80
797,61
695,28

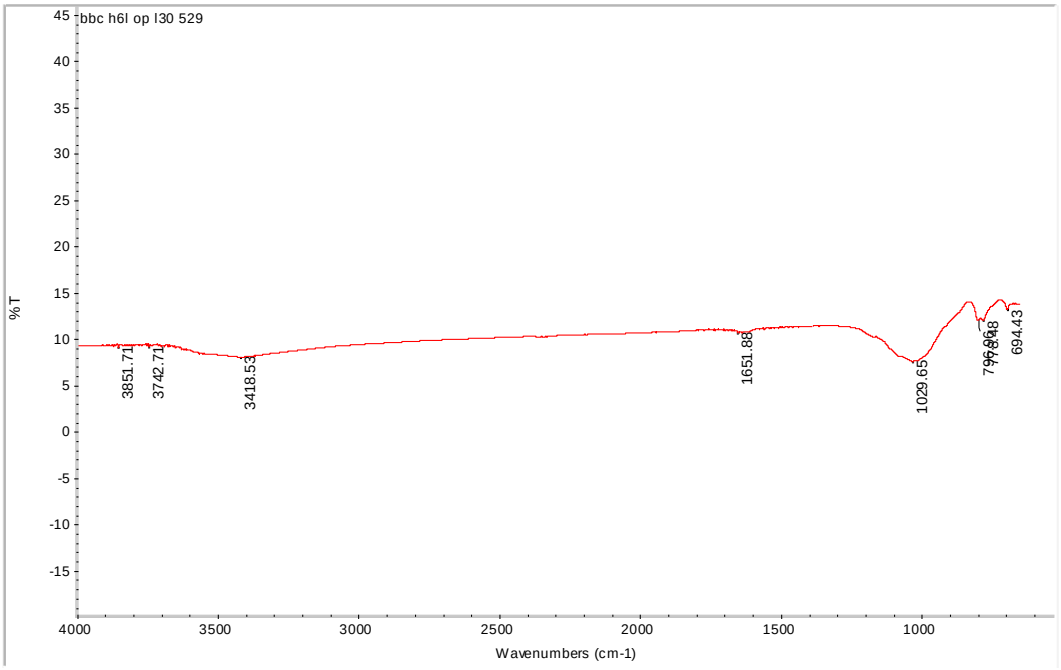

bbc h6c cp 506 ochre in s shell ochre3
%T
Wavenumbers (cm-1)
3620,75
3439,55
1630,13
1032,79
798,51
779,09
695,52


bbc h6c cp ochre 2 from haliotis area
%T
Wavenumbers (cm-1)
3698,25
3620,67
3439,29
1629,87
1437,88
1032,80
913,71
798,22
778,90
695,61


bbc h6c cp ochre 8 next to tk3
%T
Wavenumbers (cm-1)
3439,49
1654,24
1086,26
797,90
695,12


bbc h6c cp ochre 9 chunks
%T
Wavenumbers (cm-1)
3431,64
1630,00
1033,21
798,41
695,52





Figures D1-D13 FT-IR spectra for the ochre from the CP layer

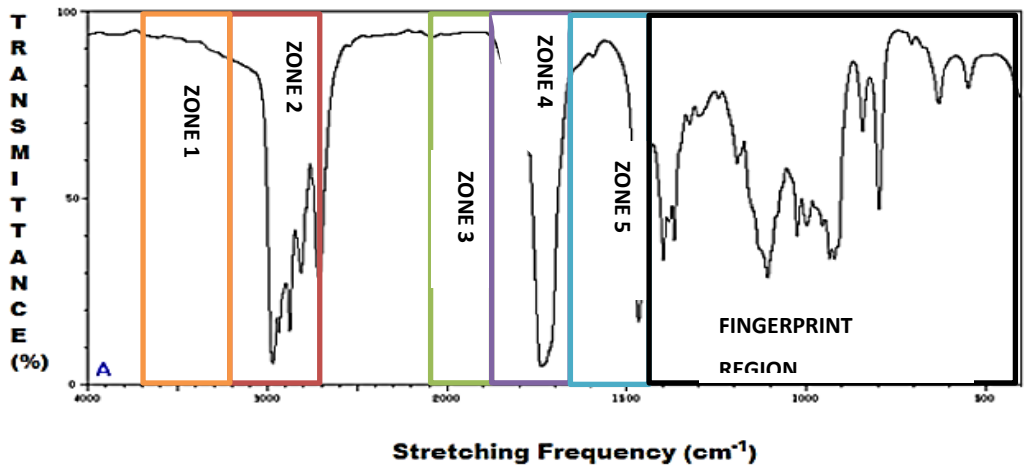


Figure D14 FT-IR frequency chart

Table D1 IR correlation chart for inorganic minerals

Zone 1: 3700-3200cm^{-1}

Mode of vibration	Stretching frequency (cm^{-1})	Intensity/shape	Functional group/mineral type
O-H stretch	3650-3200	Strong and broad	Alcohol/hydroxyl
	3695, 3666, 3645, 3621		Kaolinite
	3619, 3427		Montmorillonite
	3616		Al-rich Smectite
	3554		Fe-rich Smectite
	3735, 3623		Illite
	3500-3100		Hydroxyl in Fossil/burnt bone
N-H stretch	3500-3200	Medium and broad	Amine/amide

Zone 2: 3200-2700cm^{-1}

Mode of vibration	Stretching frequency (cm^{-1})	Intensity/shape	Functional group/mineral type
C-H stretch	~2900,~2700	Medium, two peaks	Aldehyde
C-H aliphatic	~2920	Medium	Bone mineral
O-H stretch	3000-2500	Strong and broad	Carboxylic acid
O-H stretch	3150	Strong	Iron-oxide hydroxide

*~2430, 2360, 2342 cm^{-1} due to CO_2

~2900 cm^{-1} due to organic matter

Zone 3: 2300-2000cm^{-1}

Mode of vibration	Stretching frequency (cm^{-1})	Intensity/shape	Functional group/mineral type
C≡C stretch	2260-2000	Variable, sharp	Alkyne
C≡N stretch	2260-2220	Variable, sharp	Nitrile

Zone 4: 1850-1650cm^{-1}

Mode of vibration	Stretching frequency (cm^{-1})	Intensity/shape	Functional group/mineral type

C=O stretch	1750-1705	Strong	Ketone
	1750-1735	Strong	Ester
	1740-1720	Strong	Aldehyde
	1725-1700	Strong	Carboxylic Acid
	1690-1650	Strong	Amide
	1650	Strong	Collagen/bone mineral

Zone 5: 1680-1450cm^{-1}

Mode of vibration	Stretching frequency (cm^{-1})	Intensity/shape	Functional group/mineral type
C=C stretch	~1600	Varies	Alkene
	~1500-1450	Varies	Benzene
C-O asymmetric stretch	~1470 (v_3)	Strong and broad	Carbonate/ Aragonite
	~1405	Weak	Carbonate/bone mineral

~1600cm^{-1} can also be due to H-O-H bending for clay minerals

Fingerprint region: below 1450cm^{-1}

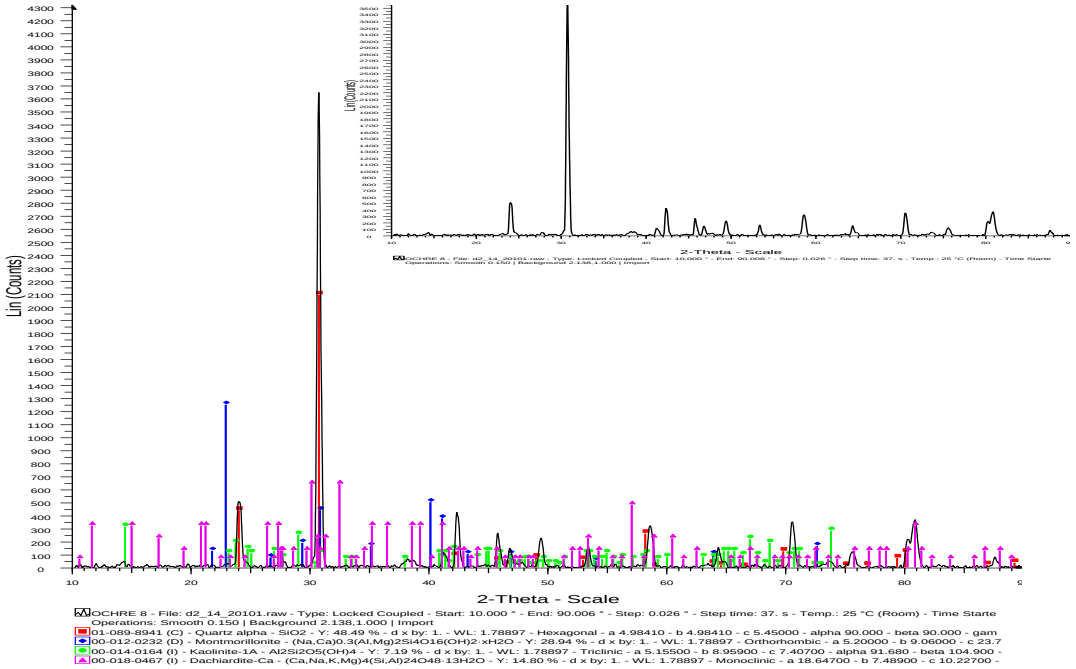
Mode of vibration	Stretching frequency (cm^{-1})	Intensity/shape	Functional group/mineral type
Si-O-Si	1167-1165, 1084-1082, doublet 798-779, 695, 517-515, 466	Strong	Quartz
	693	Medium	Kaolinite
	Doublet 798-778		
	517	Strong	Montmorillonite
	526	Strong	Illite

	Doublet 1032-1008		
Si-O-Al		Strong	Alumino silicates/kaolinite
	1030		
			Montmorillonite/Illite
		Strong	
	915-891shoulder		
			Montmorillonite
Al-O-H	1429 (*v*3), 874	Strong and broad	
	(v_2), 713 (v_4)		Carbonate/Calcite
C-O		Strong	
(asymmetric stretching *v*3, out of plane bending v_2, planar bending v_4)	863(v_2),712 (v_4)		Carbonate/Aragonite
		Strong	
Fe-O	640-615, 449-465		
			Iron-oxide
	560-525, 480-436	Strong	hydroxide/Goethite
	1116-540		Iron-oxide/Hematite
		Strong	
P-O stretch			
			Phosphates/ bone mineral
		Strong	

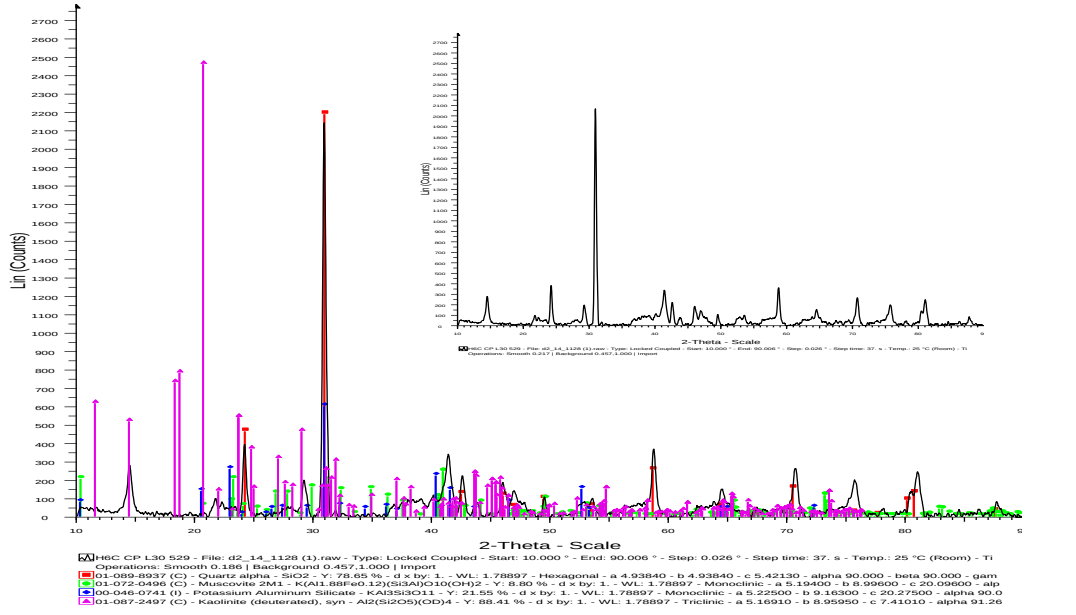
Useful for identifying unknown compounds

Appendix D2 PXRD diffractograms for the CP layer ochre

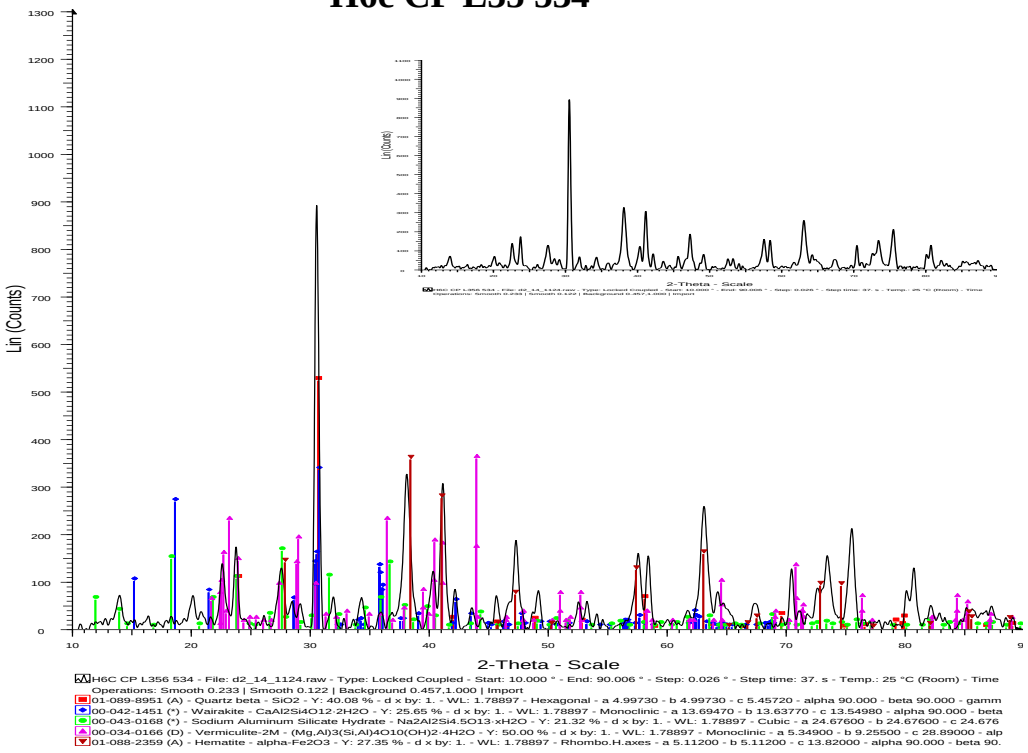
H6c CP Ochre 8 509



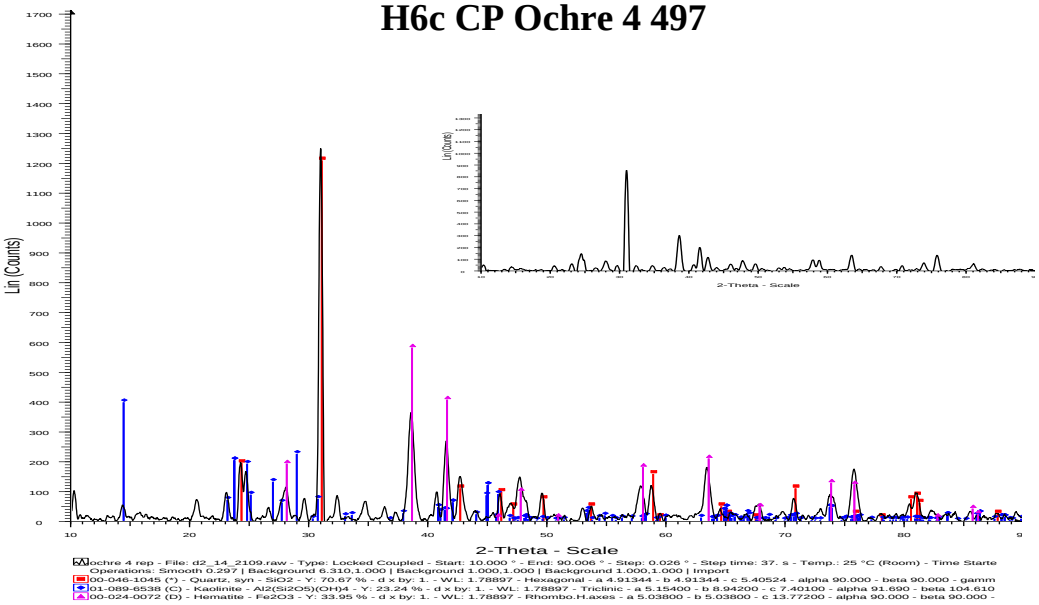
H6C CP L30 529



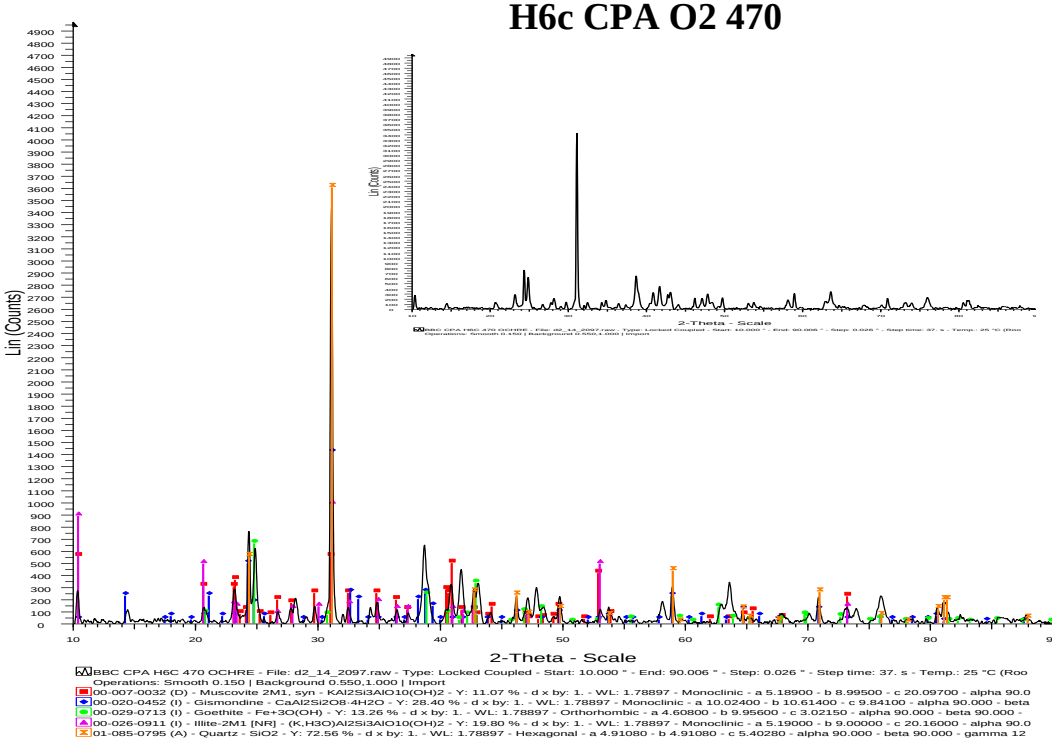
H6c CP L35 534

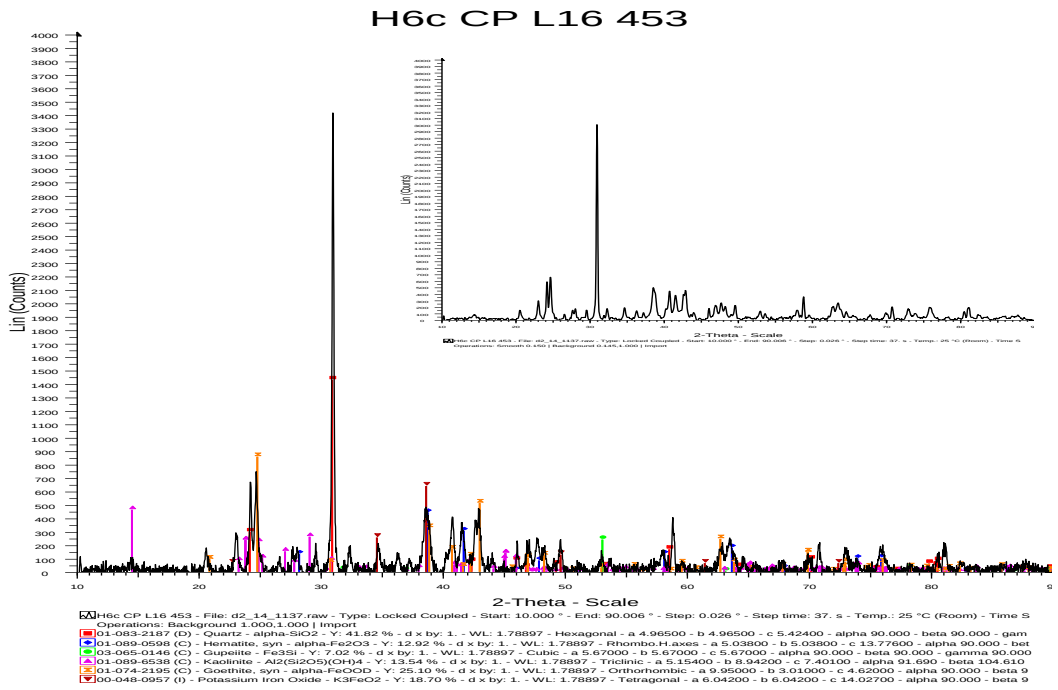


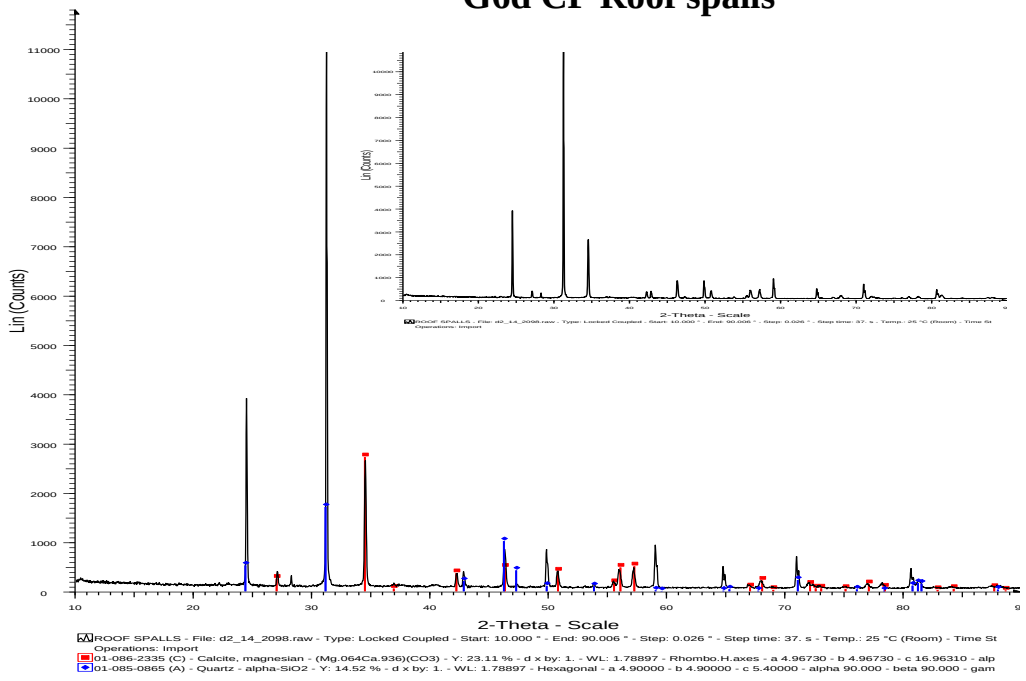
H6c CP Ochre 4 497

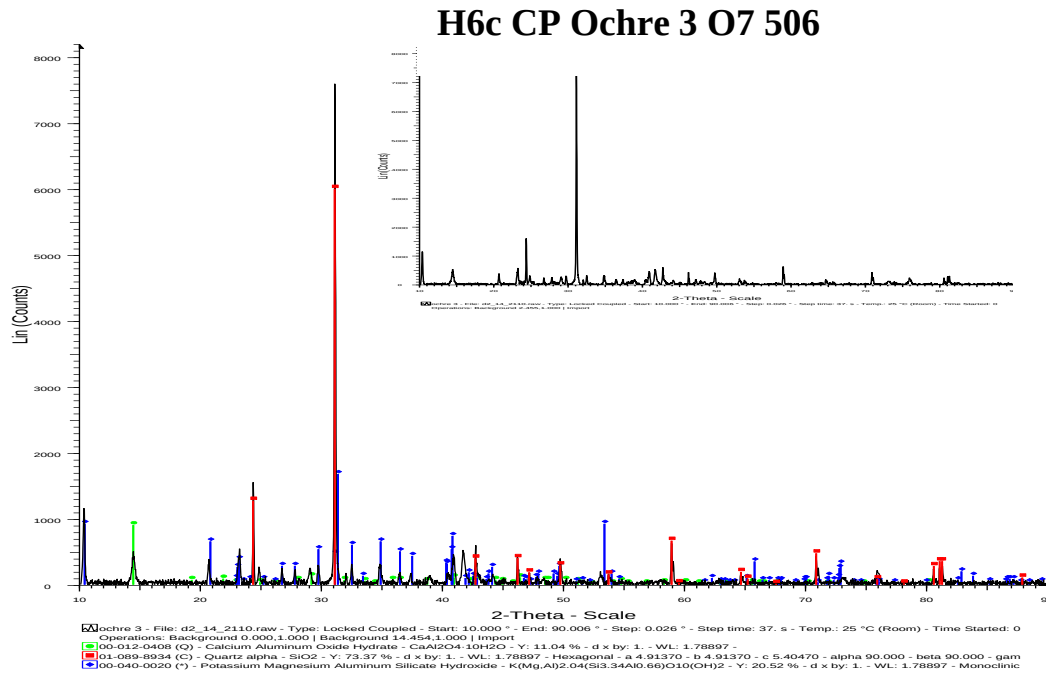


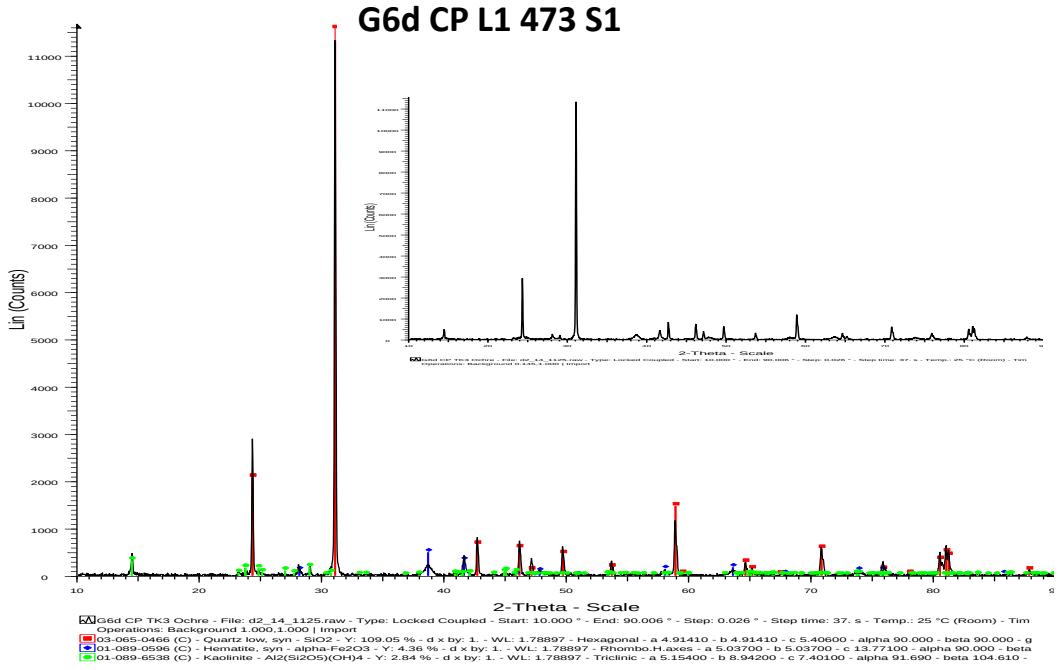
H6c CPA O2 470




H6c CP L16 453
Lin (Counts)
2-Theta - Scale
H6c CP L16 453 - File: d2_14_1137.raw - Type: Locked Coupled - Start: 10.000 ° - End: 90.006 ° - Step: 0.026 ° - Step time: 37. s - Temp.: 25 °C (Room) - Time S
Operations: Background 1.000,1.000 | Import
01-083-2187 (D) - Quartz - alpha-SiO2 - Y: 41.82 % - d x by: 1. - WL: 1.78897 - Hexagonal - a 4.96500 - b 4.96500 - c 5.42400 - alpha 90.000 - beta 90.000 - gam
01-089-0598 (C) - Hematite, syn - alpha-Fe2O3 - Y: 12.92 % - d x by: 1. - WL: 1.78897 - Rhombo.H.axes - a 5.03800 - b 5.03800 - c 13.77600 - alpha 90.000 - bet
03-065-0146 (C) - Gupeiite - Fe3Si - Y: 7.02 % - d x by: 1. - WL: 1.78897 - Cubic - a 5.67000 - b 5.67000 - c 5.67000 - alpha 90.000 - beta 90.000 - gamma 90.000
01-089-6538 (C) - Kaolinite - Al2(Si2O5)(OH)4 - Y: 13.54 % - d x by: 1. - WL: 1.78897 - Triclinic - a 5.15400 - b 8.94200 - c 7.40100 - alpha 91.690 - beta 104.610
01-074-2195 (C) - Goethite, syn - alpha-FeOOD - Y: 25.10 % - d x by: 1. - WL: 1.78897 - Orthorhombic - a 9.95000 - b 3.01000 - c 4.62000 - alpha 90.000 - beta 9
00-048-0957 (I) - Potassium Iron Oxide - K3FeO2 - Y: 18.70 % - d x by: 1. - WL: 1.78897 - Tetragonal - a 6.04200 - b 6.04200 - c 14.02700 - alpha 90.000 - beta 9


G6d CP Roof spalls
Lin (Counts)
2-Theta - Scale
ROOF SPALLS - File: d2_14_2098.raw - Type: Locked Coupled - Start: 10.000 ° - End: 90.006 ° - Step: 0.026 ° - Step time: 37. s - Temp.: 25 °C (Room) - Time St
Operations: Import
01-086-2335 (C) - Calcite, magnesian - (Mg.064Ca.936)(CO3) - Y: 23.11 % - d x by: 1. - WL: 1.78897 - Rhombo.H.axes - a 4.96730 - b 4.96730 - c 16.96310 - alp
01-085-0865 (A) - Quartz - alpha-SiO2 - Y: 14.52 % - d x by: 1. - WL: 1.78897 - Hexagonal - a 4.90000 - b 4.90000 - c 5.40000 - alpha 90.000 - beta 90.000 - gam





Figures D1-D9 PXRD diffraction patterns for some of the CP layer ochre

Appendix E ED-XRF results

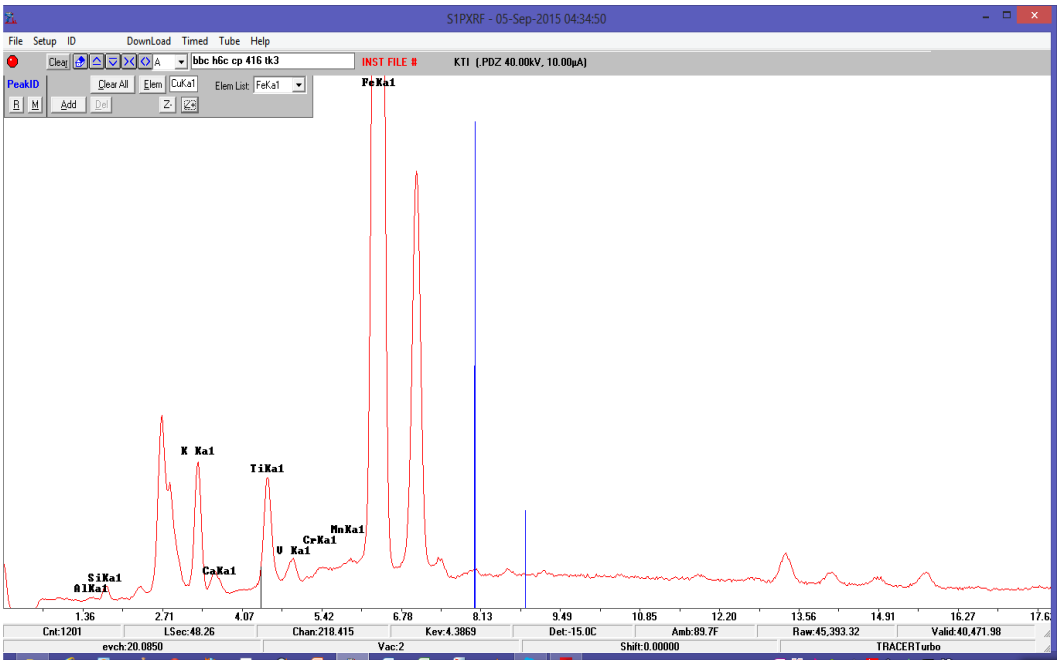


Figure E1 BBC CP H6C L1 416 ED-XRF spectrogram

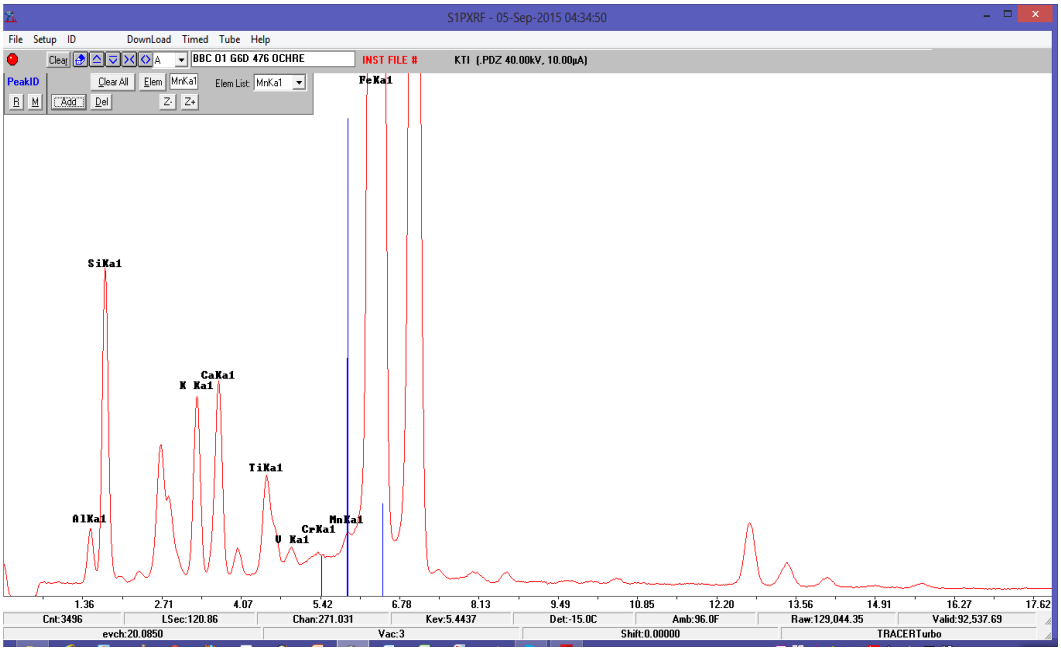


Figure E2 BBC CP G6D O1 476 ED-XRF spectrogram

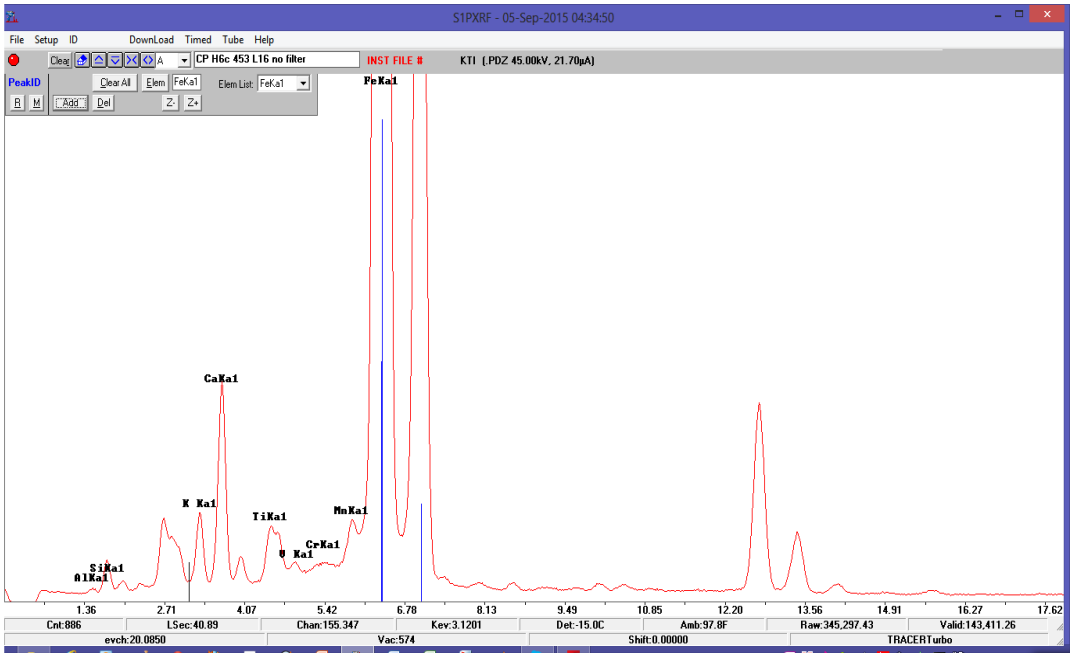


Figure E3 BBC CP H6C L16 453 ED-XRF spectrogram

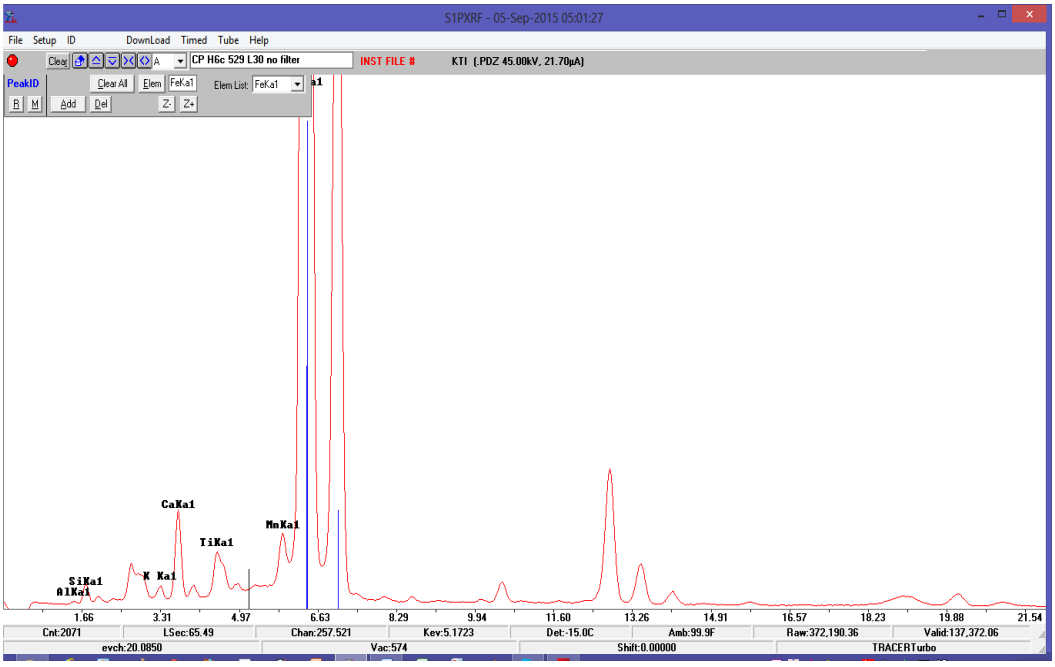


Figure E4 BBC CP H6C L30 529 ED-XRF spectrogram

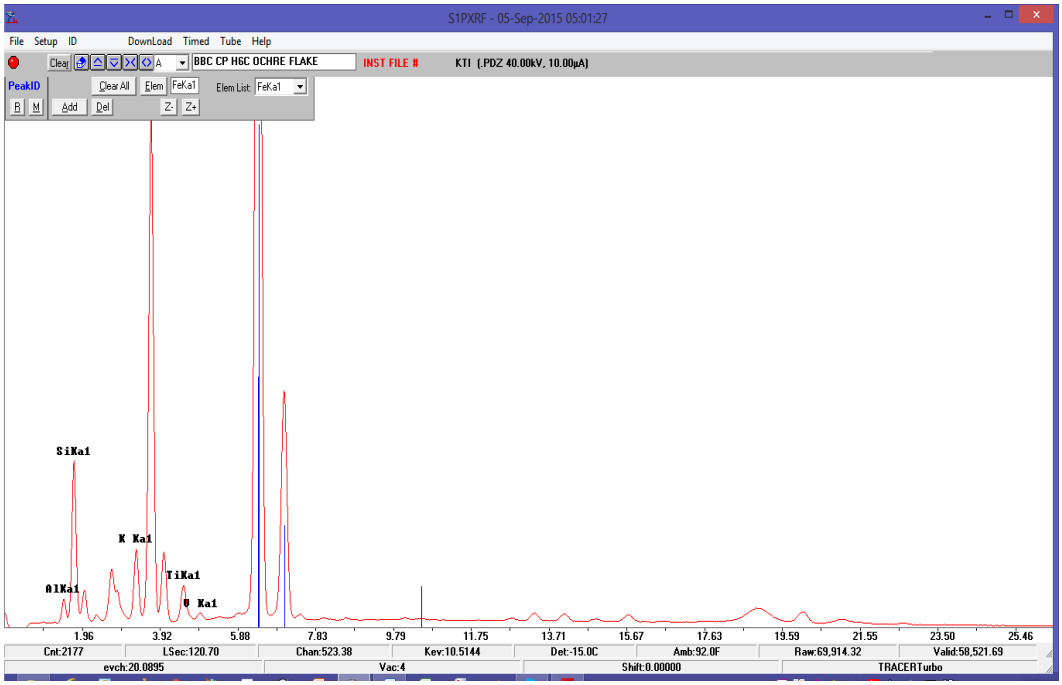


Figure E5 BBC CP H6C OCHRE FLAKE ED-XRF spectrogram

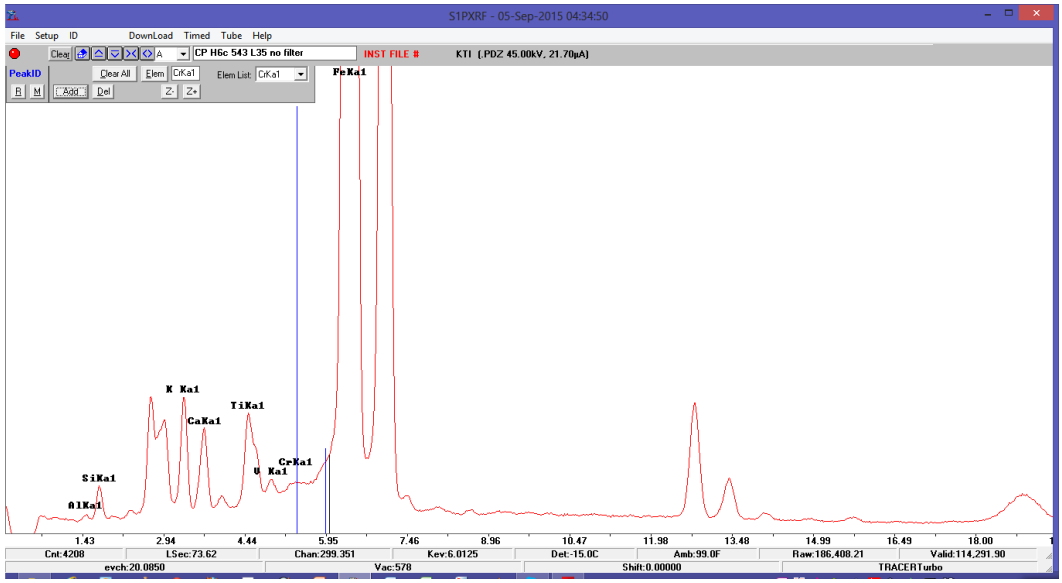


Figure E6 BBC CP H6C L35 534 ED-XRF spectrogram

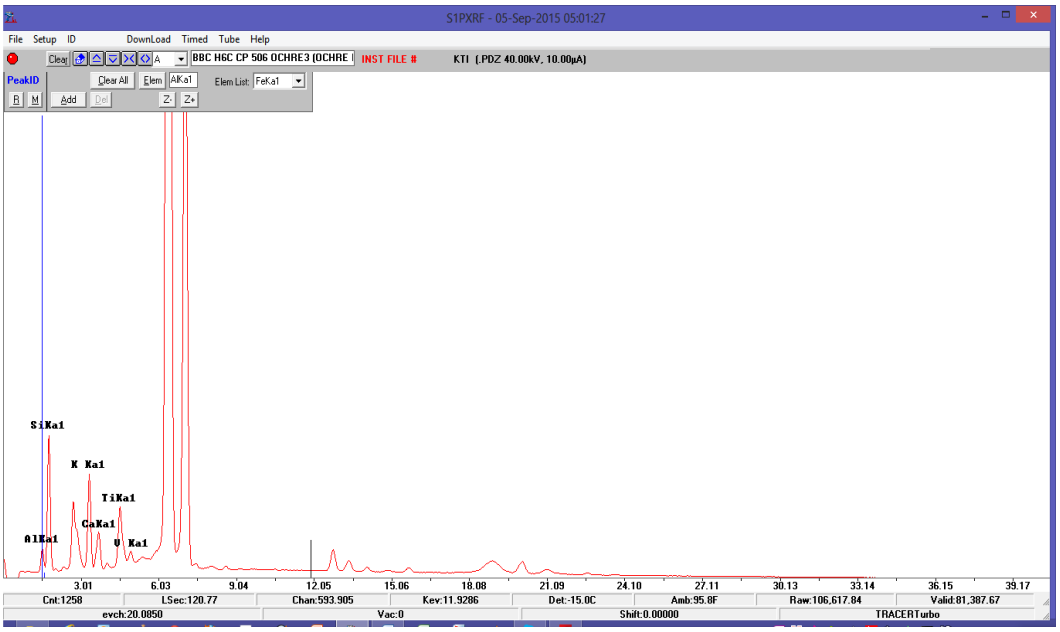


Figure E7 BBC CP H6C 506 ED-XRF spectrogram

Table E1 Fe-normalized and the $\log_{10}$ transformed trace elemental data

Sample name	Log10(V/Fe)	Log10(Cr/Fe)	Log10(Zn/Fe)	Log10(Cu/Fe)	Log(Mn/Fe)	Log10(Zr/Fe)	Log10(Cd/Fe)	Log10(As/Fe)	Log10(Sc/Fe)
BBC H6c CP 506	-3.217	-3.395	-2.966	-4.385	-3.166	-3.537	-4.214	-4.091	-5.303
BBC CP G6D TK3	-3.588	-3.463	-2.940	-3.843	-3.697	-3.396	-4.241	-3.325	-6.843
BBC CP H6C L1 416	-2.407	-2.810	-2.637	-3.228	-2.938	-3.267	-4.772	-3.141	-3.465
BBC CP H6C OCHRE FLAKE	-3.418	-2.723	-3.469	nd	-2.646	-3.276	-4.601	-2.447	nd
BBC CP H6C L30 529	-3.525	-3.959	-2.696	-3.508	-2.978	-4.083	-4.246	-3.146	-5.442
BBC CP H6C L35 534	-3.307	-3.670	-2.949	-4.948	-3.404	-3.925	-4.573	-3.884	-4.554
BBC CP H6C L16 453	-3.345	-3.521	-3.157	-3.325	-2.840	-3.901	-4.299	nd	-4.725

Log10(Sr/Fe)	Log10(Ba/Fe)	Log10(Y/Fe)	Log10(Co/Fe)	Log10(K/Fe)	Log10(Mg/Fe)	Log10(Ti/Fe)	Log10(Al/Fe)	Log10(K/Fe)	Log10(Si/Fe)	Log10(Ca/Fe)
-3.592	-2.844	-3.166	-2.145	-2.684	-2.722	-2.872	-0.724	-1.270	-0.716	-3.342
-3.940	-3.691	-1.856	-2.136	-2.222	-2.312	-3.004	-0.798	-2.069	-0.353	-2.750
-2.750	nd	-0.898	-3.702	-2.063	-1.111	-1.328	0.305	-0.751	0.213	-2.675
-2.960	nd	-2.953	nd	-3.053	-1.975	-3.093	-0.378	nd	-0.205	-2.441
-3.027	nd	-2.357	-4.625	-2.407	-1.670	-1.668	-1.243	-2.615	-0.782	-3.141
-3.624	-2.904	-1.952	nd	-2.724	-2.206	-3.001	-0.756	-1.451	-0.086	-2.420
-3.615	-2.998	-1.949	-4.173	-2.091	-2.044	-2.977	-0.847	-1.646	0.207	-2.560

Table E2 Fe-normalized and the $\log_{10}$ transformed major elemental data

Sample name	Log10(Al/Fe)	Log10(Si/Fe)	Log10(K/Fe)	Log10(Ca/Fe)	Log10(Ti/Fe)	Log10(Cr/Fe)	Log10(Mn/Fe)	Log10(V/Fe)
BBC H6c CP 506	-0.530	-0.148	-1.011	-1.235	-1.756	0.001	-4.200	-3.170
BBC CP G6D TK3	-0.517	-0.126	-0.920	-1.662	-1.634	0.001	-3.517	-3.616
BBC CP H6C L1 416	-0.093	0.343	-0.632	0.059	-1.457	0.001	-2.816	-2.876
BBC CP H6C OCHRE FLAKE	-1.053	-0.859	-0.555	-1.549	-1.129	0.002	-2.310	-2.825
BBC CP H6C L30 529	-0.342	-0.832	-1.865	-1.572	-1.988	0.001	-2.688	-2.747
BBC CP H6C L35 534	-0.581	-1.054	-1.650	-2.074	-2.010	0.001	-2.903	-2.925
BBC CP H6C L16 453	-0.472	-0.964	-1.762	-1.726	-2.030	0.001	-3.328	-2.808

Appendix F GC-MS in organic residue analysis

Table F1 Compounds identified by GC-MS for screened samples

Peak no.	Sample	Name	Weight	R.T. (s)	Area	Library	Similarity	S/N	Noise	Unique Mass
11	H6c CP mastic O1 441 S1	(1,4-Dimethylpent-2-enyl)benzene	174	527.3	120683	mainlib	838	107.52	78.312	118
4	H6c CP mastic O1 441 S1	(1R)-2,6,6-Trimethylbicyclo[3.1.1]hept-2-ene	136	283.6	221839	replib	912	106.33	170.24	93
56	H6c CP mastic O1 441 S1	1,11-Dodecadiene	166	853.6	752090	replib	845	415.24	112.34	59
66	CP H6c L24 520	1,15-Pentadecanediol	244	853.6	470523	mainlib	860	182.33	223.4	95
63	CP H6c L24 520	1,2,4-Thiadiazole-3,5-diamine	116	875.8	282869	mainlib	766	177.44	171.57	74
75	CP H6c L24 520	1,2-15,16-Diepoxyhexadecane	254	1067	5559065	mainlib	712	292.31	434.29	57
57	H6c CP mastic O1 441 S1	1,2-Benzenedicarboxylic acid, butyl 2-ethylhexyl ester	334	767.3	4905500	replib	935	6550.3	57.334	149
44	CP H6c L24 520	1,2-Benzenedicarboxylic acid, butyl 2-methylpropyl ester	278	728.2	258823	mainlib	878	337.64	54.356	149
50	CP H6c L24 520	1,2-Benzenedicarboxylic acid, butyl octyl ester	334	767.2	2850774	replib	827	3987.5	54.356	149
7	CP H6c L24 520	1,4-Benzenedicarboxaldehyde	134	416.3	2285340	replib	715	390.4	84.293	134
48	CP H6c L24 520	1-(Nitromethyl)-cyclohexanol	159	759.7	358221	mainlib	763	214.43	108.8	99
21	H6c CP mastic O1 441 S1	1-Diisopropylsilyloxycyclopentane	200	582.9	506837	mainlib	704	297.95	146.26	89
41	CP H6c L24 520	1-Eicosanol	298	709	16756577	replib	764	539.4	284.49	81
55	H6c CP mastic O1 441 S1	1-Hexene, 3-methyl-6-phenyl-4-(1-phenylethoxy)-	294	749.4	1715225	mainlib	842	591.19	197.73	105
35	CP H6c L24 520	1-Hexene, 3-methyl-6-phenyl-4-(1-	294	706.1	444306	mainlib	859	257.6	168.55	105

		phenylethoxy)-								
74	CP H6c L24 520)	1-Iodo-2-methylundecane	296	882.9	151387	mainlib	777	182.9	76.031	165
86	H6c CP mastic O1 441 S1	1-Iodo-2-methylundecane	296	1102.1	1318286	mainlib	853	194.78	349.85	83
91	CP H6c L24 520	11-Hexadecyn-1-ol	238	1131.7	62610	replib	705	159.68	52.698	137
64	CP H6c L24 520	18-Nonadecen-1-ol	282	905.5	271589	mainlib	725	137.63	130.08	87
48	H6c CP mastic O1 441 S1	2,6-Diisopropylnaphthalene	212	675	179527	mainlib	703	255.45	38.129	197
36	CP H6c L24 520	2,6-Diisopropylnaphthalene	212	652	94450	mainlib	758	195.66	39.44	197
88	H6c CP mastic O1 441 S1	2-Dodecen-1-yl(-)succinic anhydride	266	1108.6	791453	mainlib	777	194.37	349.85	83
99	CP H6c L24 520	2-Dodecen-1-yl(-)succinic anhydride	266	1189.8	483005	mainlib	790	298.92	175.94	95
83	H6c CP mastic O1 441 S1	2-Octylcyclopropene-1-heptanol	266	1064.1	204324	mainlib	799	190.32	106.08	109
8	H6c CP mastic O1 441 S1	3-Hexyn-1-ol	98	416.7	6755464	replib	701	1662	354.56	68
59	CP H6c L24 520	7-Hexadecenal, (Z)-	238	783.2	330323	replib	835	96.273	213.32	82
44	CP H6c L24 520	7-Hexadecenoic acid, methyl ester, (Z)-	268	744.7	228526	mainlib	835	122.57	130.92	59
73	CP H6c L24 520	9,12-Octadecadienoyl chloride, (Z,Z)-	298	953	216974	replib	737	114.76	124.39	129
53	CP H6c L24 520	9-Octadecenal	266	783.2	380889	mainlib	910	112.16	218.4	82
56	CP H6c L24 520	9-Octadecenoic acid (Z)-, methyl ester	296	821.8	4382784	replib	940	2151.4	171.57	74
15	CP H6c L24 520	Benzaldehyde, 2,4-dimethyl-	134	415.5	2875134	mainlib	914	601.09	80.358	134
19	H6c CP mastic O1 441 S1	Benzene, cyclohexyl-	160	474.3	2047985	replib	948	1432.1	107.59	104
8	CP H6c L24 520	Benzene, cyclohexyl-	160	474.4	1121044	replib	949	813.73	98.104	104
49	CP H6c L24 520	Benzenepropanoic acid, 3,5-bis(1,1-dimethylethyl)-4-hydroxy-, methyl ester	292	757	429552	mainlib	795	1275.5	28.681	277
75	CP H6c L24 520	Benzoic acid, 2-methylpropyl ester	178	899.1	767247	replib	866	281.88	215.21	105
88	CP H6c L24 520	Benzoic acid, nonadecyl ester	388	968.3	547566	mainlib	780	510.28	89.403	123
82	CP H6c L24 520	Benzoic acid, octadecyl ester	374	934.4	786792	mainlib	773	606.92	89.403	123

60	H6c CP mastic O1 441 S1	Bicyclo[4.1.0]heptane, 7-butyl-	152	792.5	337512	mainlib	840	114.11	213.32	82
88	CP H6c L24 520	Bis(2-ethylhexyl) phthalate	390	971.5	9620350	replib	925	10996	60.931	149
70	CP H6c L24 520	Butyl benzoate	178	862.6	591608	replib	703	196.61	215.21	105
26	CP H6c L24 520	Butylated Hydroxytoluene	220	566	158422	mainlib	737	367.58	37.132	205
45	CP H6c L24 520	Cholesterol	386	867.6	195058	mainlib	832	134.16	23.531	274
45	H6c CP mastic O1 441 S1	Cholesterol	386	867.6	195058	mainlib	832	134.16	23.531	274
32	CP H6c L24 520	Cyclohexanone	98	759.7	210077	replib	730	111.14	104.37	99
3	H6c CP mastic O1 441 S1	D-Limonene	136	296.3	1922625	replib	923	716.53	198.6	93
11	CP H6c L24 520	Decanoic acid, methyl ester	186	467.7	607016	replib	876	232.16	160.32	74
11	CP H6c L24 520	Decanoic acid, methyl ester	186	467.7	607016	replib	876	232.16	160.32	74
11	CP H6c mastic O1 441 S1	Decanoic acid, methyl ester	186	467.7	607016	replib	876	232.16	160.32	74
78	CP H6c mastic O1 441 S1	Dodecanamide	199	924.9	557453	mainlib	751	321.87	138.53	59
7	CP H6c L24 520	Dodecane	170	397.7	3561825	mainlib	947	127.33	2285.1	57
13	CP H6c L24 520	Dodecane	170	397.6	109405	mainlib	949	239.6	42.683	170
5	H6c CP mastic O1 441 S1	Dodecane	170	397.6	5715374	mainlib	940	188.74	2617.5	57
35	CP H6c L24 520	Dodecane, 1-chloro-	204	670	445270	replib	738	126.11	306.62	91
60	CP H6c L24 520	Dodecanoic acid, methyl ester	214	752.9	795654	replib	761	348.24	186.81	74
72	CP H6c mastic O1 441 S1	Eicosanoic acid	312	892.5	286815	mainlib	574	196.27	110.87	116
10	CP H6c L24 520	Hexadecane	226	441	2064195	replib	886	128.19	1468.6	71
34	H6c CP mastic O1 441 S1	Hexadecane	226	701	1622703	replib	912	169.59	828.68	85
59	CP H6c L24 520	Hexadecanoic acid, methyl ester	270	752.8	592888	replib	765	265.74	172.25	74
59	CP H6c L24 520	Hexadecanoic acid, methyl ester	270	752.8	592888	replib	765	265.74	172.25	74
59	H6c CP mastic O1 441 S1	Hexadecanoic acid, methyl ester	270	752.8	592888	replib	765	265.74	172.25	74
49	CP H6c L24 520	Isopropyl myristate	270	710.2	409071	replib	724	341.99	99.057	102
3	H6c CP mastic O1 441 S1	Limonene	136	296.3	3709316	replib	929	1338.5	216.79	93

61	H6c CP mastic O1 441 S1	Methyl dehydroabietate	314	914.2	86901	replib	799	252.56	27.744	239
61	CP H6c L24 520	Methyl dehydroabietate	314	914.2	86901	replib	799	252.56	27.744	239
59	H6c CP mastic O1 441 S1	Methyl stearate	298	831	12995120	replib	902	6186.8	171.57	74
59	CP H6c L24 520	Methyl stearate	298	831	12995120	replib	902	6186.8	171.57	74
67	CP H6c L24 520	Octadecanoic acid	284	845.4	489498	replib	828	165.38	145.09	59
52	CP H6c L24 520	Pentadecanal-	226	792.3	347946	replib	891	103.88	248.1	82
37	CP H6c L24 520	Pentadecanal-	226	792.1	265868	replib	919	104.64	195.14	82
19	H6c CP mastic O1 441 S1	Pentadecane, 5-methyl-	226	586.7	741986	mainlib	878	187.42	351.51	85
68	CP H6c L24 520	Propylamine	59	862.7	419012	mainlib	800	194.08	146.27	59
7	H6c CP mastic O1 441 S1	Silane, cyclohexyldimethoxymethyl-	188	372.7	828358	mainlib	881	476.57	148.67	105
96	CP H6c L24 520	Silane, trichlorodocosyl-	442	1172.1	87082	mainlib	750	114.98	98.543	133
8	H6c CP mastic O1 441 S1	Silanol, trimethyl-, formate	118	396.5	120791	replib	716	88.726	122.28	75
43	CP H6c L24 520	Silicon tetrafluoride	104	679.4	125326	replib	703	175.01	39.454	196
51	CP H6c L24 520	n-Hexadecanoic acid	256	767.5	17597867	replib	889	3761.5	246.37	73
66	CP H6c L24 520	Tetradecanoic acid	282	836.7	998135	mainlib	918	507.62	78.464	185
66	CP H6c L24 520	Tetradecanoic acid	282	836.7	998135	mainlib	918	507.62	78.464	185
1	H6c CP mastic O1 441 S1	à-Pinene	136	236.7	214016	mainlib	922	105.33	170.24	93
7	H6c CP mastic O1 441 S1	á-Ocimene	136	283.7	512754	mainlib	903	218.09	197.36	93

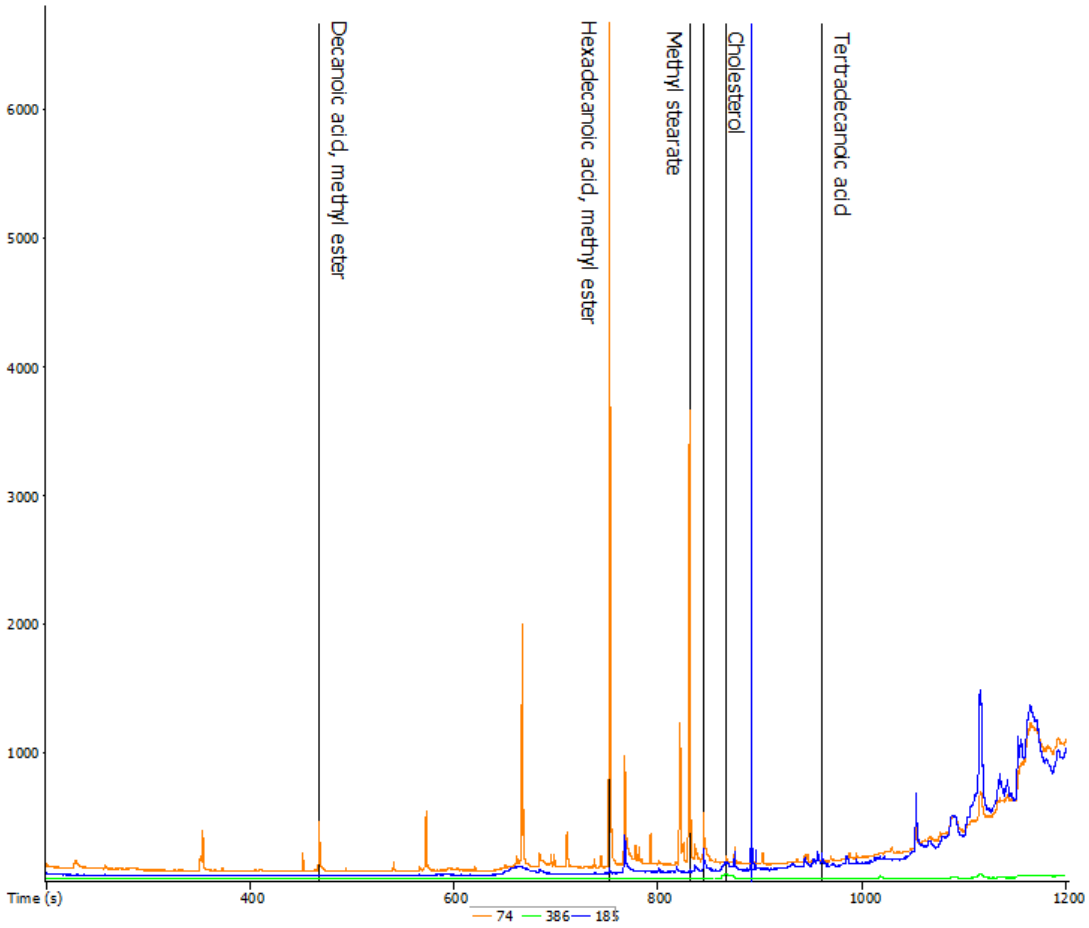


Figure F1 TIC chromatogram for CP H6c L24 520

The chromatogram is expressed according to the total ion current (TIC) of the identified compounds, Decanoic acid methyl acid (186), Hexadecanoic acid methyl ester (74), Methyl stearate (74), Cholesterol (386), Tetradecanoic acid (185)

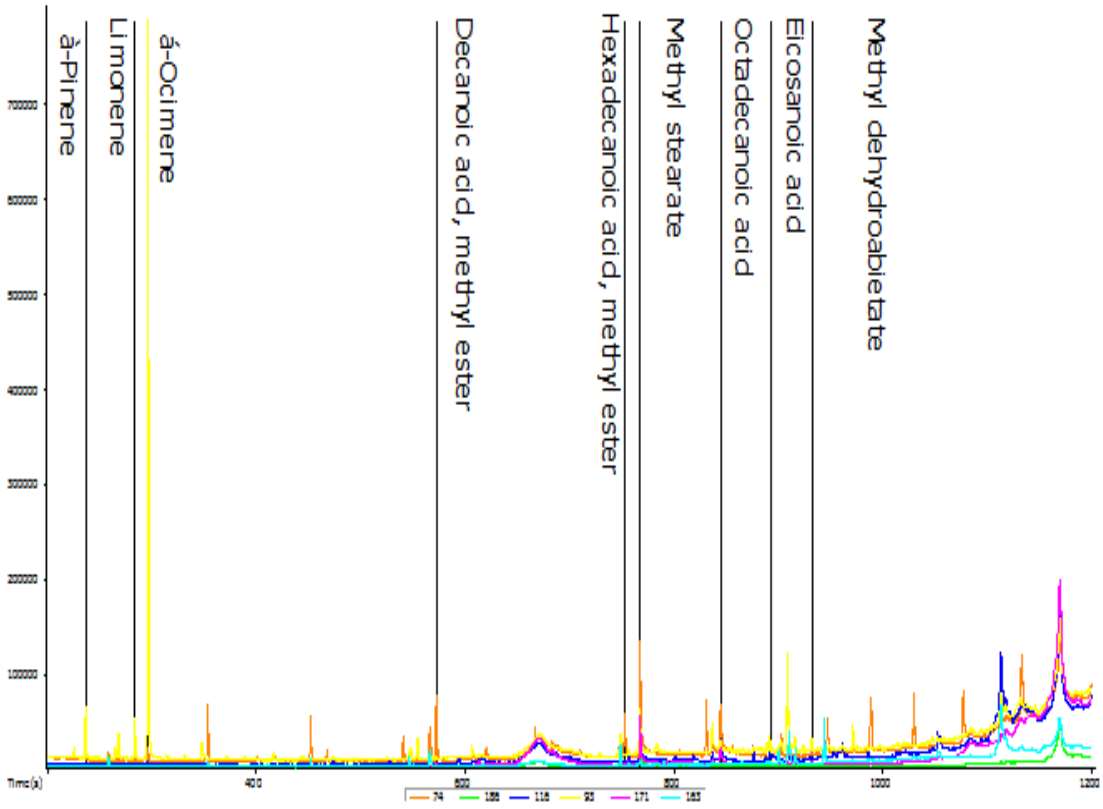


Figure F2 TIC chromatogram for CP H6c mastic O1 441 S1

The chromatogram is expressed according to the total ion current (TIC) of the identified compounds, a-Pinene, Limonene and a-Ocimene (93), Decanoic acid methyl acid (186), Hexadecanoic acid methyl ester (74), Methyl stearate (74), Octadecanoic acid (171), Eicosanoic acid (171), Methyl dehydroabietate (239)